Continuous Transverse Reinforcement – Behavior and Performance

University of Cincinnati
School of Advanced Structures
Bahram M. Shahrooz, PhD, PE, FACI
Herbert L. Bill, PhD, PE, PS
Melody L. Miller
Alyssa M. Doellman

Final Report
January 2, 2014

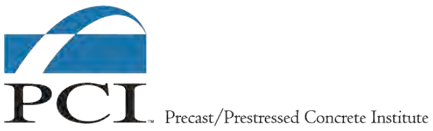

Executive Summary

Recent advancements in automatic steel bar bending machines allow fabrication of "continuous transverse reinforcement" (CTR). The resulting closed stirrups could potentially increase the speed in which transverse reinforcement can be placed, and improve member performance. This system will also satisfy the need for closed stirrups in flexural members in moment-resisting frames intended to resist seismic loading, for members subjected to torsion, or both. The ACI 318 Building Code does not explicitly permit the use of CTR in U.S. design and construction practice, although it is possible to receive approval according to Section 1.4. Such an approval requires sufficient documentation to demonstrate the adequacy of special systems. The documentation typically consists of successful applications or comprehensive analyses and/or test data. The research reported herein was conducted to generate such data and facilitate the use of CTR in construction practice. Ultimately, the research goal is to modify the Code such that CTR is recognized as an acceptable and economical alternative to single-piece stirrups.

Thirty full-scale specimens were designed, tested, and evaluated. The specimens allowed an in-depth study of (a) shear dominant flexural members; (b) members subjected to pure torsion as well as to the combined actions of bending moment, shear, and torsional moment; (c) short columns loaded in compression; and (d) exterior beam-column connections subjected to cyclic loads simulating seismic events. In addition, a number of detailing issues were examined; in particular, splicing of CTR cages, and the differences in how conventional transverse reinforcement and CTR are fabricated. All the specimens were proportioned according to the current Code design provisions and detailing requirements. Each group of specimens included a control specimen using conventional reinforcement.

This research showed that current design provisions and detailing practices are applicable to CTR. In terms of serviceability, strength, ductility, and failure mode, CTR can be used in lieu of conventional transverse reinforcement. The only drawback comes from a scenario when the applied torque is such that torsional cracks are in the same direction as how CTR "spirals".

Based on the research reported herein, the following specific recommendations are made.

- The shear capacity of transverse reinforcement is $V_s = \frac{2A_t f_{yt} d \sin\alpha}{s}$, which can conservatively be taken as $V_s = \frac{1.8A_t f_{yt} d}{s}$. Note that this equation is essentially the same as the current equation ($V_s = \frac{A_v f_{yt} d}{s} = \frac{2A_t f_{yt} d}{s}$).
- To achieve the most favorable capacity and behavior of CTR for shear design, it is recommended that the angled legs of the CTR be placed parallel to the top and bottom faces of a beam. This configuration provides near-vertical stirrup legs coincident wit the shear plane.

- The nominal torsional capacity is $T_n = \frac{A_t f_{yt} A_o \cot\theta\left(1+\sin\alpha\right)}{s}$, which can conservatively be taken as $T_n = \frac{1.9 A_t f_{yt} A_o}{s}\cot\theta$.
- The additional longitudinal reinforcement required to resist tensile forces generated due to torsion can either be computed from current equation $A_l \geq p_h \frac{A_t}{s}\left(\frac{f_{yt}}{f_y}\right)\cot^2\theta$ or from $A_l \geq 2\left(y_0 + x_o \sin\alpha\right)\frac{A_t}{s}\left(\frac{f_{yt}}{f_y}\right)\cot^2\theta$.

- If the direction of the torque is known a priori, e.g., the member is subjected to gravity loads only, CTR has to be placed such that the orientation in which the CTR "spirals" will be in the opposite direction of the diagonal cracks from the applied torque. For cases where the direction of torque could change, the capacity of the member needs to be limited to the torsional cracking capacity (computed based on the current Code) multiplied by strength reduction ϕ = 0.75.

- In lieu of isometric drawings, the plan, side, and cross-sectional views should be used to convey the geometry of CTR.

Acknowledgments

The Charles Pankow Foundation, Prestressed Concrete Institute (PCI), and Concrete Reinforcing Steel Institute (CRSI) Education and Research Foundation provided the funding for this project. A number of companies provided in-kind support; their generosity is sincerely appreciated.

Schnell Reinforcement Procession Equipment supplied the transverse reinforcement;
Contractors Materials Company (CMC) and MMFX Steel Corporation of America provided all the remaining reinforcing bars used in the project;
CMC also provided tremendous assistance and advice in tying the cages, and supplied various items required to fabricate the test specimens;
Tincher's Welding fabricated many of the test fixtures;
Terracon Consultants, Inc. performed material testing; and
Janell Inc., Concrete and Masonry Equipment supplied all the formwork.

Hilltop Basic Concrete supplied the concrete. Their expertise in mix design and proper placement of concrete were extremely helpful. Lehigh University tested the columns.

Mr. Neal Anderson and Mr. Tony Johnson at CRSI are acknowledged and thanked for their advice and assistance at various phases on the project. Mr. David Freedman at CMC was instrumental in obtaining the reinforcing bars, and for ensuring a speedy construction of the test specimens. Mr. Terry Tincher at Tincher's Welding devised a number of creative solutions to overcome numerous challenges encountered in testing of some of the specimens; his creativity was instrumental to successfully complete the project. Dr. Kent Harries at the University of Pittsburgh tested a large number of reinforcing bars; his assistance is greatly appreciated and acknowledged. The research team would like to thank the members of the project advisory panel for their advice and feedbacks.

Table of Contents

List of Tables

List of Figures

Notations

A, B, and, C = Parameters for Ramberg-Osgood function established from a best fit of experimental stress-strain data

A_l = area of longitudinal reinforcement to resist torsion

A_o = gross area enclosed by shear flow path taken as $0.85A_{oh}$

A_{oh} = area enclosed by centerline of the outermost transverse torsional reinforcement

A_{cp} = area enclosed by outside perimeter of member cross section

A_g = gross area of member cross section

A_s = area of longitudinal tension reinforcement

A'_s = area of longitudinal compression reinforcement

A_{sp} = *area of spiral reinforcement*

A_{st} = total area of longitudinal reinforcement

A_t = area of one leg of transverse reinforcement

A_v = total area of shear reinforcement

b_w = beam web width

C_c = concrete cover

D = diameter of confined core

d = effective depth

d_t = diameter of stirrup

d_v = distance between top and bottom longitudinal reinforcement

E_s = modulus of elasticity usually taken as 29,000,000 psi

f_2 = lateral confining pressure

f_c = concrete compressive stress

f'_c = design concrete strength; measured concrete strength at the time of testing

f_{pu} = ultimate tensile strength

f_{sp} = stress in spiral

f_{ss} = steel stress

f_{tr} = stress in column transverse reinforcement

f'_t = concrete tensile strength

f_y = steel yield strength

f'_y = steel yield strength in compression

f_{yt} = yield strength of transverse reinforcement

f_u = tensile strength

H = width of confined core

h = member depth

l_D = length of dogleg

M_n = nominal moment capacity

M_u = ultimate moment

P = axial force

p_{cp} = outside perimeter of member cross section

p_h = perimeter of centerline of outermost torsional transverse reinforcement

r = ratio of compression longitudinal force to tensile longitudinal force

s = spacing of transverse reinforcement

T = torque

T_c = torque resistance provided by concrete

T_{cr} = cracking torque

T_n = nominal torsional resistance

T_s = torque resistance provided by transverse reinforcement

T_u = ultimate torque

V_1, V_2, V_3, V_4 = shear force due to torsion in each leg of transverse reinforcement.

V_c = shear strength provided by concrete

V_n = nominal shear resistance

V_s = shear strength of transverse reinforcement

V_u = ultimate torque

x_o = shorter center-to-center dimension of transverse reinforcement

y_o = longer center-to-center dimension of transverse reinforcement

α = angle between longitudinal reinforcement and inclined transverse reinforcement

ε = strain

ε_f = fracture strain

ε_s = steel axial strain

ϕ = strength reduction factor (0.9 for flexure and 0.75 for shear or torsion)

γ = angle between the axis perpendicular to longitudinal reinforcement and inclined transverse reinforcement

θ = angle between longitudinal reinforcement and diagonal cracks

ρ = longitudinal reinforcement ratio

1. Introduction

1.1 ACI 318 Building Code Provisions

The current shear provisions in the ACI 318 Building Code (2011), referred as the Code hereinafter, allow for shear reinforcement consisting of (a) stirrups perpendicular to the axis of a member; (b) welded wire reinforcement with wires located perpendicular to the axis of a member; or (c) spirals, circular ties, or hoops (Section 11.4.1.1). For nonprestressed members, stirrups or bent-up longitudinal bars with an angle of at least 45^o or 30^o, respectively, are permitted as shear reinforcement. The most common type of transverse reinforcement consists of vertical stirrups with a number of "legs", per (a) above. A spiral wrapping around longitudinal reinforcing bars is another form of transverse reinforcement. Spirals are similar to closed stirrups, but they confine the core more effectively than perimeter stirrups/ties, which can potentially improve ductility and seismic performance. Spirals, which are commonly used in circular columns, are defined in the Code as a continuously wound reinforcement in the form of a cylindrical helix. Spirals are not used in rectangular beams because of the difficulties associated with wrapping circular spirals around longitudinal reinforcing bars in a rectangular section. Hoops can be individual closed ties or a continuously wound tie, where the term "tie" is commonly associated with lateral reinforcement in compression members. A tie is defined as a loop of reinforcing bar or wire enclosing longitudinal reinforcement. The Code permits the use of a continuously wound bar or wire forming a circle, rectangle, or other polygon shape without re-entrant corners.

In seismic applications, some engineers may use continuous hoops even though the Code does not specifically recognize them as a type of shear reinforcement in beams. Recent advancements in automatic steel bar bending machines allow fabrication of "continuous transverse reinforcement" (CTR). The resulting closed stirrups could potentially increase the speed in which transverse reinforcement can be placed, and improve member performance. This system will also satisfy the need for closed stirrups in flexural members in moment-resisting frames intended to resist seismic loading, for members subjected to torsion, or a combination of both. The Code does not explicitly permit the use of CTR, although it is possible to receive approval according to Section 1.4. Such an approval requires sufficient documentations to demonstrate the adequacy of special systems. The documentation typically consists of successful applications or comprehensive analyses and/or test data.

1.2 Overview of Continuous Transverse Reinforcement

Continuous transverse reinforcement (CTR) is an alternative to conventional stirrups, ties, and hoops. This innovative system consists of steel reinforcement that has been robotically prefabricated to form a rectilinear spiral. Designed with specific spacing in a contiguous rectangular loop, such transverse reinforcement is engineered so that it can be condensed, shipped, and untied in the field; the stored energy allows it to spring into place with the desired spacing. Schnell Corporation in Italy, one of several companies that have begun to produce CTR, fabricated the reinforcement used in the project reported herein. However, the resulting findings will not be product specific. Pictured in Figure 1.1(a), one full loop of CTR consists of

some angled and some straight legs. Conventional transverse reinforcement consists solely of straight legs, forming isolated rectangles in independent planes, as shown in Figure 1.1(b).

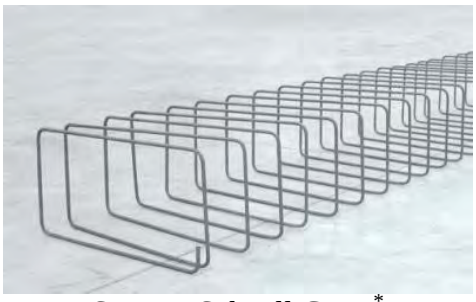

Source: Schnell Corp.*

(a) Continuous

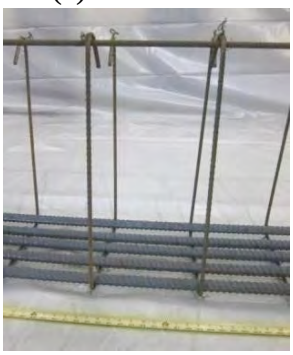

(b) Conventional

Figure 1.1: Examples of continuous and conventional transverse reinforcement

A main advantage of CTR is decreased construction time, which in turn reduces labor costs. The reduction in labor stems from the fact that the reinforcement is shipped in its compressed form (Figure 1.2a) and it springs to the approximate intended spacing once untied at the construction site (Figure 1.2b). Upon expansion to the desired spacing, CTR is tied onto the longitudinal reinforcing bars to form a cage. In contrast, the labor time for a conventional stirrup cage assembly is much longer. The spacing of the conventional stirrups must be measured before each stirrup can be independently tied to the longitudinal reinforcement. Note that it is not necessary to tie CTR at every intersection with the longitudinal reinforcing bars, which would be a significant cost saving by reducing the amount time required to assemble the reinforcing cage.

Other features of CTR are (a) the option for varying the spacing along a segment of continuous transverse reinforcement, (b) a "dogleg" (see Figure 1.2b) on each angled leg to assist with quick expansion when untied, (c) gradually decreasing spacing at the ends to finish with a vertical hoop, and (d) the possibility of bending either No. 3 or No. 4 bars. The reported research will focus on only No. 3 bars for consistency with previous constructions in Italy, and also because the larger energy stored in a No. 4 CTR can pose safety issues when untying the bent reinforcement.

* http://www.schnelltech.com/en/download/PREZENTARE_1_Schnell_Spirex%20_2010.pdf

(a) Compacted form of the stirrup pack prior to shipping

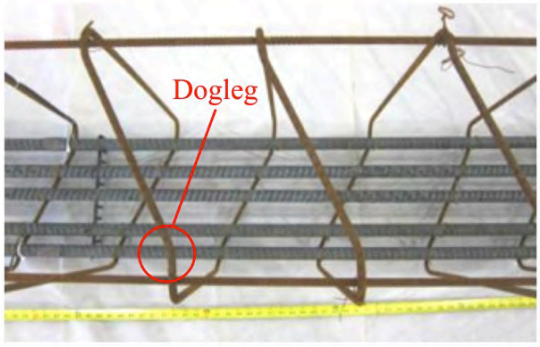

(b) Expanded form (top view)

Figure 1.2: Continuous transverse reinforcement in compressed and expanded forms

Two different types of continuous transverse reinforcement are available. Due to the shape formed when viewed from above (Figure 1.3), they are referred to by Schnell as: (a) M-type, consisting of non-planar vertical legs, and (b) N-type, consisting of planar vertical legs. For the purpose of this research, only non-planar (M-type) continuous transverse reinforcement was tested and compared to equivalent specimens with conventional stirrups. A decision was made to forgo the use of planar reinforcement for this project as a result of the inability to achieve the desired maximum spacing for several test beams. The maximum possible bent angle for CTR is 25 degrees per leg; hence, the non-planar reinforcement, which provides two bent legs for every one bent leg in planar reinforcement, is used more frequently in the field and is the focus of this project. For all types of CTR, the spacing between vertical bars along one side of the beam is equivalent to the spacing of the legs along the other side. For the non-planar continuous transverse reinforcement, however, the vertical legs alternate by half the spacing. As a result, the total area of continuous transverse reinforcement passing through one diagonal crack is equivalent to the total area of conventional stirrups passing through an identical crack.

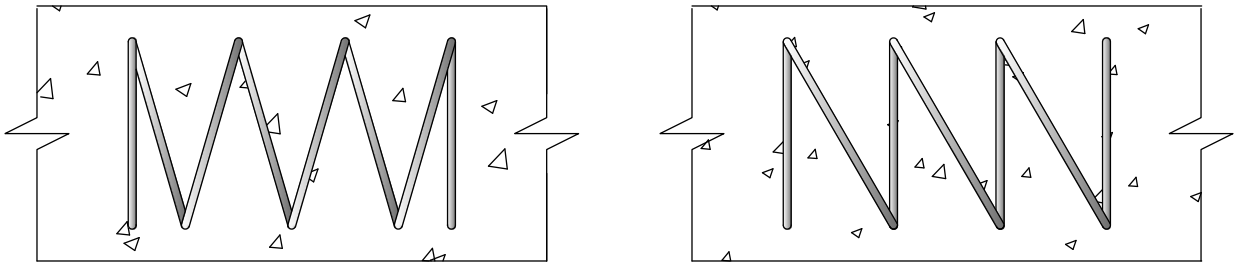

(a) M-Type (Non-planar vertical legs)

(b) N-Type (Planar vertical legs)

Figure 1.3: Plan view of different configurations of continuous transverse reinforcement

The amount of material required to fabricate CTR is less than that for conventional closed stirrups and hoops. The interconnectivity of the CTR reduces the required amount of reinforcing bar needed to fabricate stirrups (see Appendix A). Conventional U-shaped stirrups, on the other hand, require less material than continuous transverse reinforcement. The closed nature of continuous stirrups could increase the confinement of the concrete core, which is expected to benefit the overall performance. Furthermore, the stirrup legs in CTR are inherently developed adequately because they wrap around the longitudinal bars with no hooks in the core.

Visualization of the configuration of CTR could be complex because the top and bottom segments of the continuous transverse reinforcement in a beam are intended to be the angled legs that connect the vertical segments, which in turn provide the primary resistance. In this arrangement, the sides are perpendicular to the horizontal plane, similar to conventional stirrups; the only difference is that the spacing on opposite sides of the beam is offset. As intended, CTR is designed to have angled legs on the top and bottom of the beam while the vertical legs remain perpendicular to the longitudinal steel. This arrangement replicates the configuration of conventional stirrups. Nevertheless, there is the possibility of placing the continuous transverse reinforcement with the angled legs on the sides of the beam, i.e., in the loading plane. In lieu of isometric drawings, the plan, side, and cross-sectional views must be used to convey the geometry of CTR, such as that shown in Figure 1.4. On the other hand, just a side and cross section view are typically sufficient to convey the design details for cases with conventional transverse reinforcement.

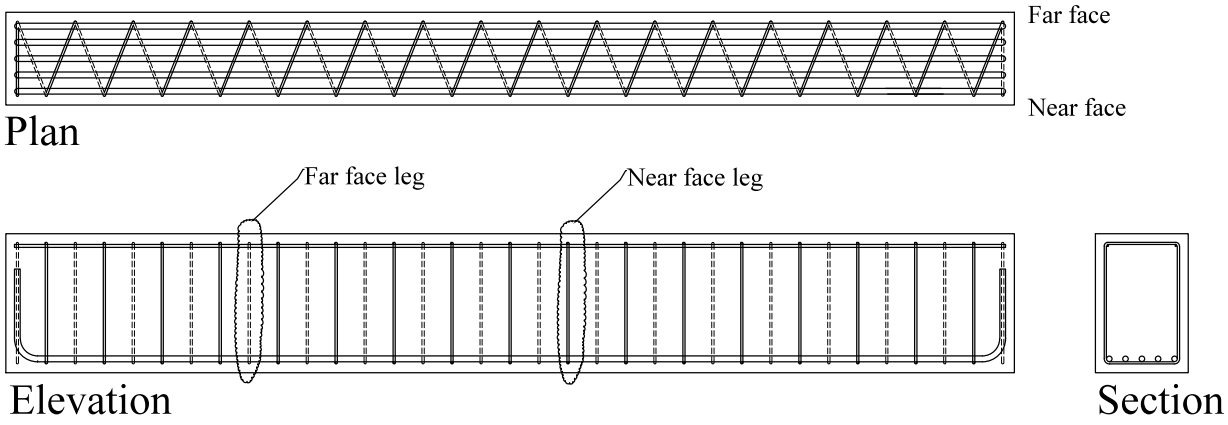

Figure 1.4: Multiple views of continuous transverse reinforcement

1.3 Review of Past Studies

The research presented herein is the first comprehensive study in the United States aimed at evaluating the capacity of continuous transverse reinforcement (CTR). A limited number of studies in Europe have examined this type of reinforcement.

A research project in Italy was focused on CTR produced by Schnell Corporation, which is commercially referred to as Spirex. Cyclic performance of columns with CTR and those with conventional ties was compared (Riva 2009). The test specimen details are shown in Figure 1.5. As illustrated in Figure 1.6, the hysteretic responses of the two columns were rather similar. The test results support the initial hypothesis that columns reinforced with traditional ties and CTR exhibit similar strength and ductility. Although these test columns were not designed according to the ACI Code, the data provide an indication of the expected cyclic performance of columns using CTR.

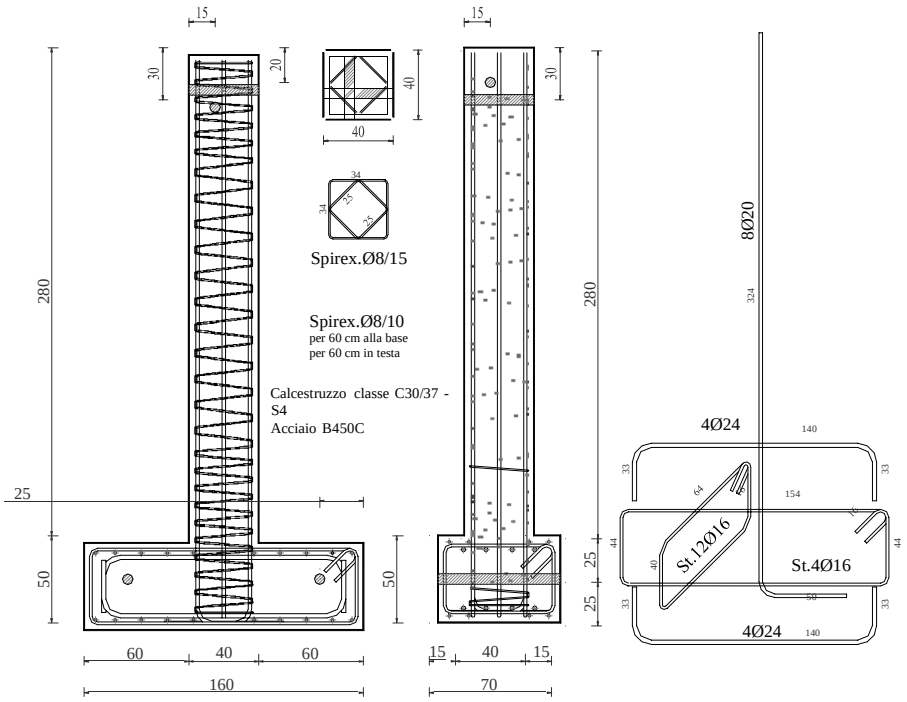

Figure 1.5: Details of test specimens

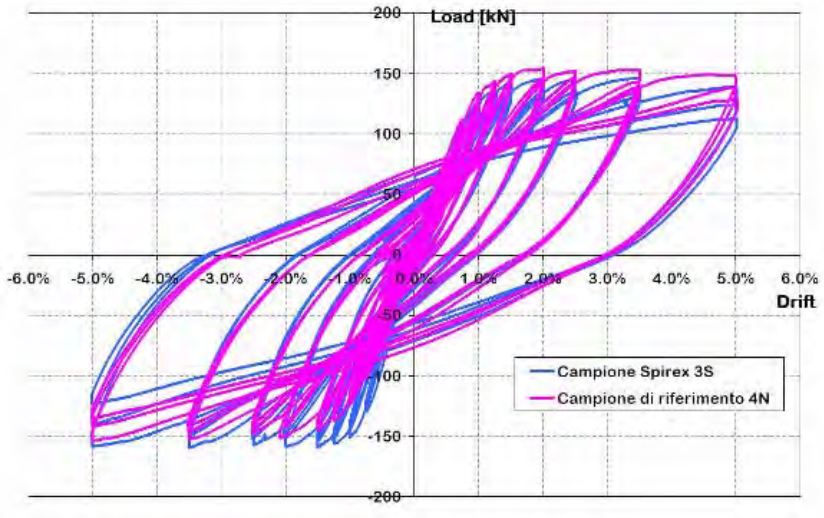

Figure 1.6: Measured hysteretic responses

A research project at the University of Florence (Gianni 2009) examined the shear and flexural capacity of beams reinforced with CTR and conventional stirrups. Two beams of each type of transverse reinforcement were tested under two point loads as illustrated in Figure 1.7. One specimen was designed to fail in shear, whereas the other was designed to have a flexural failure. The two specimens that failed in flexure had identical deflections, but the beam using CTR exhibited a larger shear capacity than the specimen with conventional stirrups. Although the specimens had been designed according to Eurocode 8 specifications, the enhancement offered by CTR would also be expected if ACI specifications had been followed.

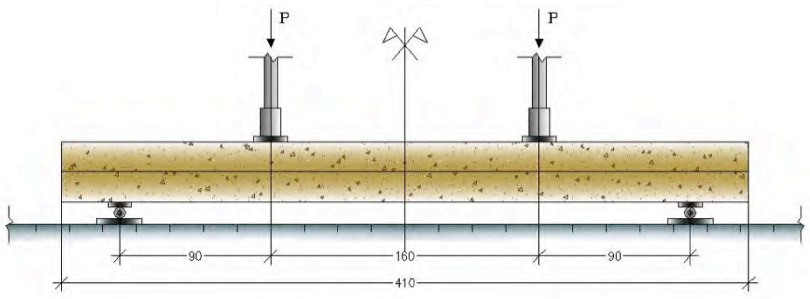

Figure 1.7: Experimental Setup

A study by Chalioris and Karayannis (2013) examined the directional effects of continuous transverse reinforcement (CTR) in beams subjected to pure torque. As seen from Figure 1.8, the torsional capacity is notably influenced by whether the applied torque and resulting angle of twist is in the direction of or opposite to how CTR is "spiraled".

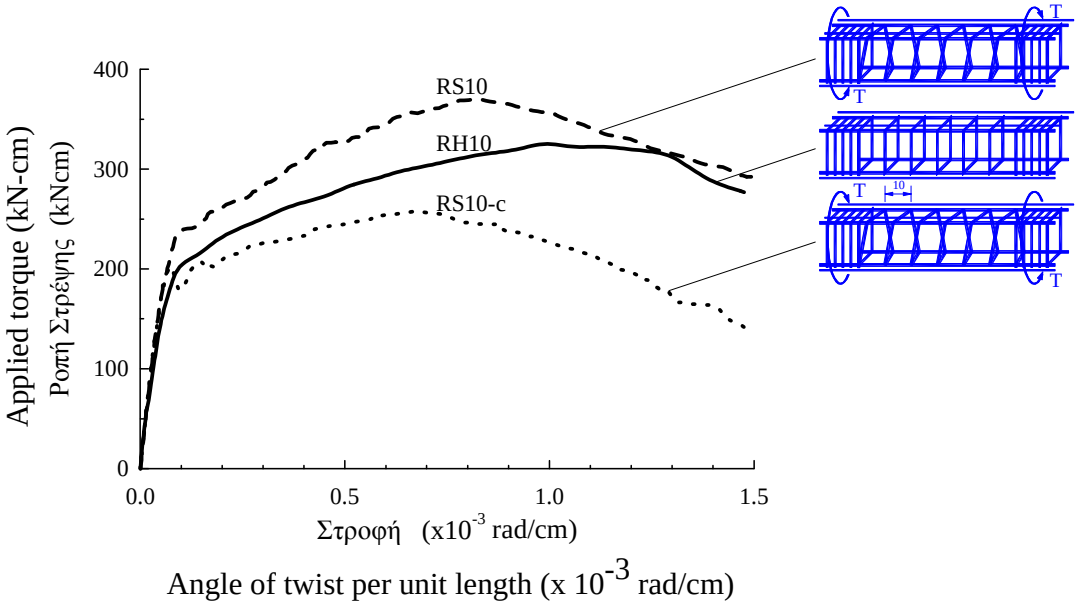

Figure 1.8: Torque vs. angle of twist per length

2. Objectives and Scope

The objectives of the research presented herein are to (a) collect experimental data to demonstrate the capacity and service-level performance of members with continuous transverse reinforcement (CTR); (b) document and compare various failure modes for members using CTR and those with conventional reinforcement; (c) examine the applicability of current design methods, and, (d) if necessary, propose changes so that CTR can be used in structural design.

In order to achieve the stated objectives, a large number of full-scale members and components with continuous transverse reinforcement and conventional reinforcement were designed according to the ACI 318-11 Building Code. The specimens were tested to examine (a) shear capacity of flexural members; (b) potential effects of "doglegs"; (c) pure torsional capacity

of beams; (d) capacity of beams subjected to combined bending moment, shear, and torsion; (d) axial load carrying capacity of short columns; and (e) cyclic response of beam-column connections.

3. Experimental Program

A total of 30 full-scale specimens were fabricated and tested. As described in the following, these specimens represented several structural applications.

3.1 Test Specimens

3.1.1 Shear Specimens

As a first step, the literature from a number of different sources was reviewed to develop the database shown in Appendix B. The database contains 109 specimens, with the following values of longitudinal reinforcement ratio (ρ) and shear-span-to-depth ratio (a/d).

	ρ (%)	a/d
Minimum	0.20	1.00
Maximum	7.50	6.95
Average	2.18	3.44

Using the range of a/d and ρ as a basis, the specimens were selected such that shear failure would precede flexural failure while maintaining a reasonable shear span to depth ratio. After a number of permutations, 24 in. deep x 16 in. wide x 174 in. long beams were selected with a shear-span-to-depth ratio (a/d) of 2.5. The flexural reinforcement consisted of five No. 8, Gr. 100 A1035 reinforcing bars, resulting in reinforcement ratio (ρ) equal to 1.15%. The design goal of reaching the shear capacity prior to flexural capacity was verified through cross-sectional analyses performed by computer program Response 2000 (Bentz 2000), which is based on the modified compression field theory (MCFT). As shown in Figure 3.1, the loading line reaches the shear-moment interaction diagram before developing the flexure capacity, which is 627.7 k-in. for the case shown in this figure.

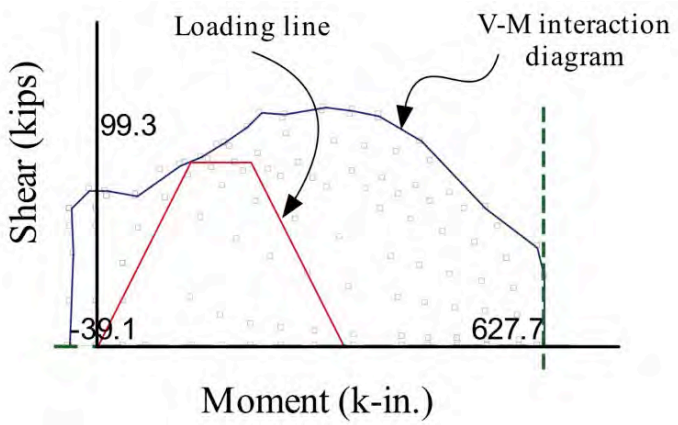

Figure 3.1: Confirmation of shear failure mode

The test specimens in this group consisted of 12 specimens, 6 specimens had 5,000-psi concrete and the remaining 6 beams had 10,000-psi concrete. According to ACI Section 11.4.5, stirrups cannot be spaced larger than $d/4$ or $d/2$ per Eq. 1.

$$s_{max} = d/2 \quad for\ V_s \le 4\sqrt{f_c'}\,b_w d$$
$$s_{max} = d/4 \quad for\ V_s > 4\sqrt{f_c'}\,b_w d \qquad \text{Eq. 1}$$

From a constructability point of view, e.g., to avoid congestion and allow concrete placement, the spacing should not be less than $d/4$. As shown in Table 3.1, the specimens were organized into four groups based on the concrete strength (f'_c) and the spacing of stirrups (s). For each group, a control specimen using conventional U-shaped stirrups was also cast. The location of the angled legs of continuous transverse reinforcement (CTR) was either in the shear plane (i.e., on the sides) or perpendicular to the shear plane (i.e., on the top and bottom faces).

Table 3.1: Shear specimens

	Specimen	Description	Stirrup Spacing	f'_c (psi)
Group 1	S1	Conventional U-shaped stirrups	10 in. ≈ $d/2$	5,000
	S2	CTR with angles on top and bottom	10 in. ≈ $d/2$	5,000
	S3	CTR with angles on side faces	10 in. ≈ $d/2$	5,000
Group 2	S4	Conventional U-shaped stirrups	5 in. ≈ $d/4$	5,000
	S5	CTR with angles on top and bottom	5 in. ≈ $d/4$	5,000
	S6	CTR with angles on side faces	5 in. ≈ $d/4$	5,000
Group 3	S7	Conventional U-shaped stirrups	10 in. ≈ $d/2$	10,000
	S8	CTR with angles on top and bottom	10 in. ≈ $d/2$	10,000
	S9	CTR with angles on side faces	10 in. ≈ $d/2$	10,000
Group 4	S10	Conventional U-shaped stirrups	5 in. ≈ $d/4$	10,000
	S11	CTR with angles on top and bottom	5 in. ≈ $d/4$	10,000
	S12	CTR with angles on side faces	5 in. ≈ $d/4$	10,000

CTR = continuous transverse reinforcement

A representative set of details is provided in Figure 3.2. The complete details for each of the shear specimens can be found in Appendix C. In this appendix, representative photographs of cage fabrication and placement for the shear specimens are also provided.

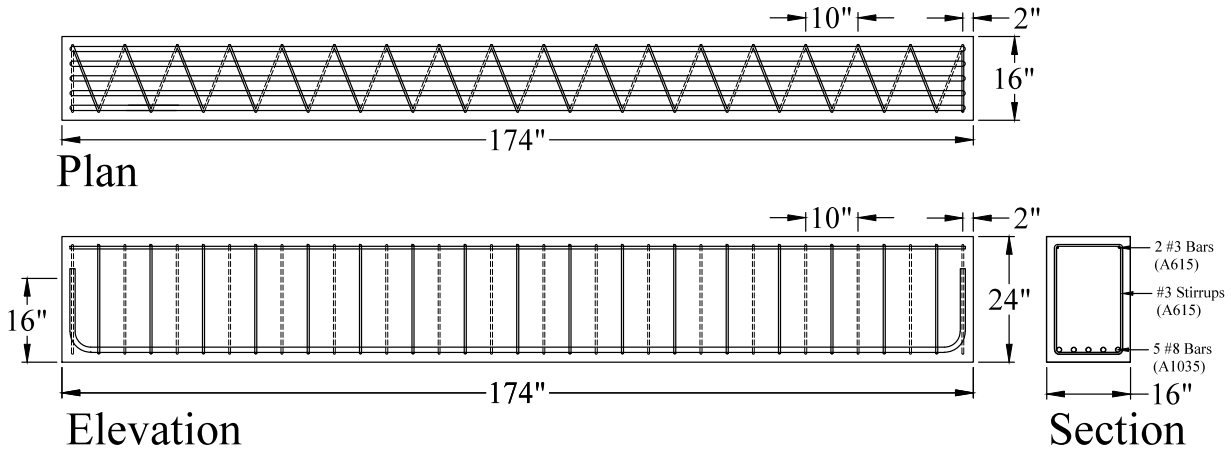

Figure 3.2: Details of specimens S2 and S8

Due to the capabilities of the Spirex machine that bends the continuous transverse reinforcement, the maximum allowable bent angle is 25 degrees. The spacing, the height or width of the transverse reinforcement, and the length of the "dogleg" influence this bent angle. With reference to Figure 3.3, Eq. 2 can easily be derived and used to compute the bent angle (γ in Figure 3.3).

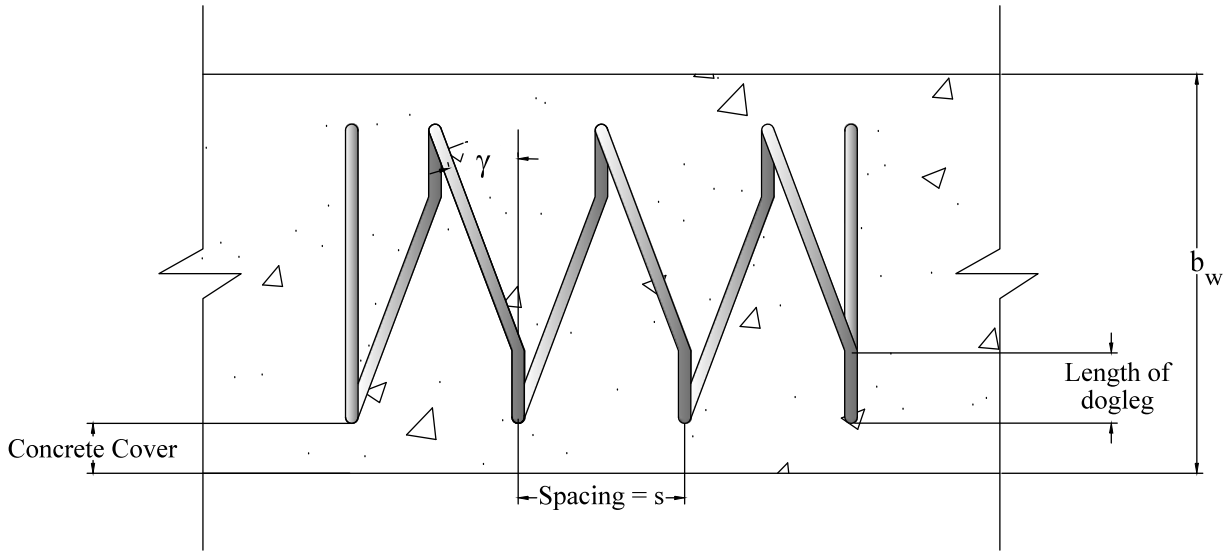

Figure 3.3: Plan view illustrating dogleg and bent angle (γ)

$$\gamma = tan^{-1}\left[\frac{s/2}{b_w - 2\left(C_c + d_t/2\right) - l_D}\right] \qquad \text{Eq. 2}$$

Using Eq. 2, the bent angle was calculated for each specimen. This angle was also measured from the actual cages. As seen from Table 3.2, the actual angles were fairly close to the designed values.

Table 3.2: Measured and designed bent angles

Specimen	*s* (in.)	Angle Location	Designed Angle (deg.)	Measured Angle (deg.)
S2 & S8	10	Top and bottom	24.20	25
S3 & S9		Sides	14.65	15
S5 & S11	5	Top and bottom	12.67	12
S6 & S12		Sides	7.45	7

b_w = 16 in. and h = 24 in. for all specimens.

The specimens were cast in industry standard formwork (see Appendix C), which resulted in slight variations between specimens. Prior to testing, the width, depth, and length at four locations along each specimen were measured. These dimensions were then averaged, and are tabulated in Appendix C.

3.1.2 Spliced Specimen

One specimen was cast in order to evaluate field solutions to potential errors in the fabrication of continuous transverse reinforcement (CTR). This specimen evaluated a scenario where CTR was ordered too long and the CTR needed to be cut to size. Several options were explored to remedy such a scenario.

At the ends of CTR, closed end hoops are provided in order to effectively "close" the reinforcing cage with a traditional hoop with four planar legs. The solution implemented herein involved (a) cutting off the manufactured end hooks, and (b) lap splicing conventional transverse reinforcement to the cut ends. Hence, as shown in Figure 3.4, the spliced region consists of transverse reinforcing bars that are perpendicular to the axis of the member while the continuous transverse reinforcement has angled legs.

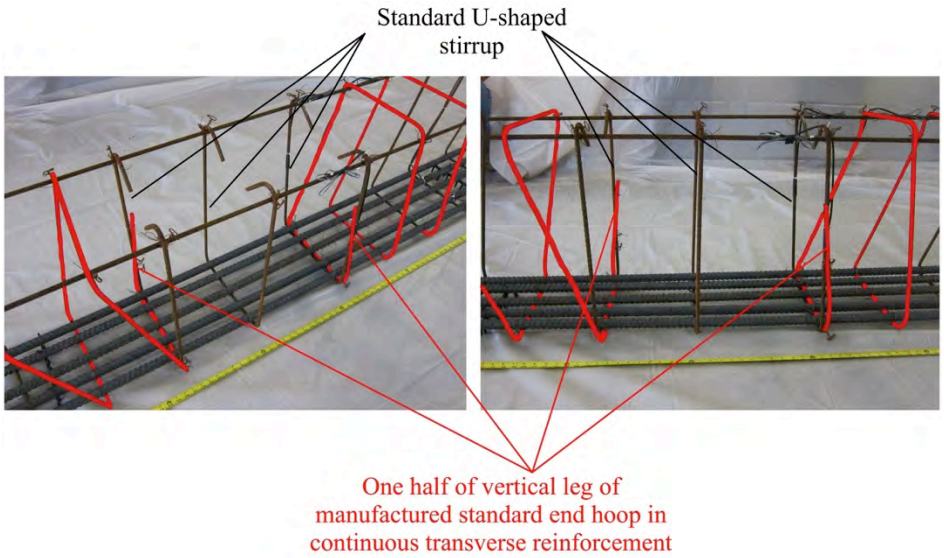

Figure 3.4: Details for splicing two continuous transverse reinforcement cages

The angled legs of the transverse reinforcement were on the sides, i.e., in the shear plane. The details of this specimen are summarized in Appendix D. Similar to the shear specimens, the width, depth, and length at four locations along each specimen were recorded. The average dimensions are tabulated in Appendix D. Representative photographs of the cage work for this specimen are also provided in this appendix.

3.1.3 Pullout Specimen

This specimen examined the potential effects of the "doglegs" or kinks where the bent bar changes angle. This "dogleg" is used in particular by Spirex, and is a necessary part of the bending process to ensure a linear axis of the continuous transverse reinforcement when untied (i.e., the product would not have a visible curve when expanded). To investigate the potential effects of "doglegs" on the development of transverse reinforcement, a series of pullout tests was conducted.

These tests involved applying a tensile load to a portion of the continuous transverse reinforcement (CTR). From a testing point of view, it would be easier to apply the load vertically but the legs of CTR were inclined. To overcome this issue, as shown in Figure 3.5, the angled legs of CTR were cut at two locations (A and B), and the cut bars were rotated as shown in the figure such that the portion to be loaded would be vertical. (In this figure, the portion from the cut at location A would be loaded.) The cage work was stabilized by a number of small diameter bars acting as ties. Using this procedure, two locations with doglegs and two locations with a conventional 90-deg. bend were prepared.

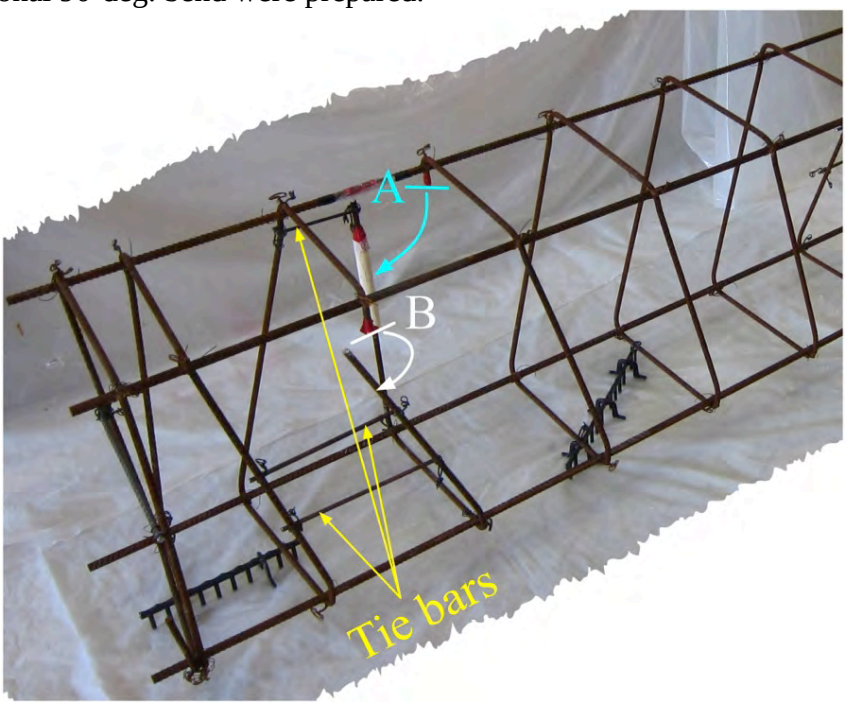

Figure 3.5: Construction of cage for pullout specimens

The cage work was placed inside an available formwork that had been used to construct 16 in. wide by 24 in. deep shear specimens (Section 3.1.2). In order to apply the load, it was necessary to expose a portion of the reinforcing bar. For this purpose, the concrete was placed

only 16 in. deep, i.e., the pullout specimens had a 16 in. x16 in. cross section. Moreover, the upper 5½ in. portion of the bar was debonded in an effort to prevent local cracking at the bar-concrete interface. A small diameter PVC pipe was placed over the bar for this purpose, as seen in Figure 3.5. Hence, the bonded length was 9½ in., corresponding approximately to one half of the total bonded length of CTR in a 24-in. deep beam. The overall length of the pullout specimen was 150 in. The test locations were at least 29 in. apart, as indicated in Table 3.3. The specimen details as well as photographs of the cage work are provided in Appendix E.

Table 3.3: Test locations

Test Number	Location Along Specimen (in.)	Bend Type
1	21	90-deg. hook
2	61	Dogleg
3	90	Dogleg
4	128	90-deg. hook

3.1.4 Specimens Subjected to Pure Torsion

Seven specimens were cast and subjected to pure torsion in order to understand the performance of continuous transverse reinforcement (CTR) used as torsional reinforcement. The test variables were (a) concrete compressive strength; (b) whether the angled legs of CTR are on the top and bottom, or on the two sides; and (c) whether the diagonal cracks formed are in the direction that CTR "spirals" or they are in the opposite direction. For each of the selected concrete strengths (5,000 psi and 10,000 psi), a benchmark specimen using conventional closed stirrups was also cast. The test specimens are shown in Table 3.4. In the "a series" specimens (T1, T2, T3a, T4, and T5a), the diagonal cracks are formed opposite to the "spiral" direction of the CTR, whereas the CTR in T3b and T5b "spirals" in the same direction as the angle of the diagonal cracks. Therefore, as shown schematically in Figure 3.6, the expected diagonal cracks around the specimen would be in the opposite direction of the angled legs of the CTR in the "a" series, but it would be in the same direction for the "b" series. The angled legs in CTR were measured to be 19 degrees from the line perpendicular to the axis of the member.

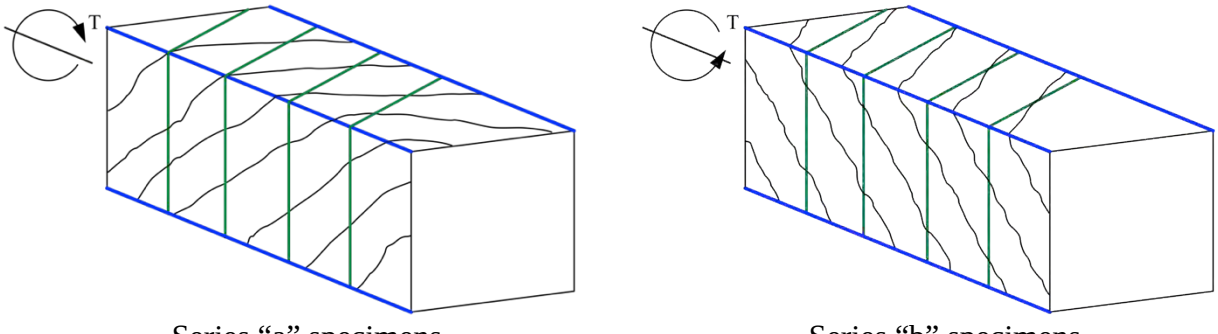

Series "a" specimens Series "b" specimens

Figure 3.6: Cracking and direction of CTR in series "a" and "b" pure torsion specimens

Table 3.4: Specimens subjected to pure torsion

Specimen	Description	f'_c (psi)
T1	Conventional closed stirrups	5,000
T2	CTR with angles on top and bottom	5,000
T3a, T3b	CTR with angles on side faces	5,000
T4	Conventional closed stirrups	10,000
T5a, T5b	CTR with angles on top and bottom	10,000

CTR = continuous transverse reinforcement

In order to use an available test fixture for subjecting the specimens to pure torsion, the dimensions were 12 in. wide x 16 in. deep x 96 in. long. Based on these dimensions, the maximum spacing for transverse reinforcement is 5.3 in. per ACI 318-11 Section 11.5.6.1. The transverse reinforcement was spaced at 5 in. away from the ends, and its spacing was set to 2.5 in. near the ends where the specimen would be engaged in the loading apparatus. A representative set of details for specimens T2, T5a, and T5b is shown in Figure 3.7. The complete sets of drawings as well as photographs of the cage work are provided in Appendix F. This appendix also provides the average values of the width, depth, and length based on four measurements.

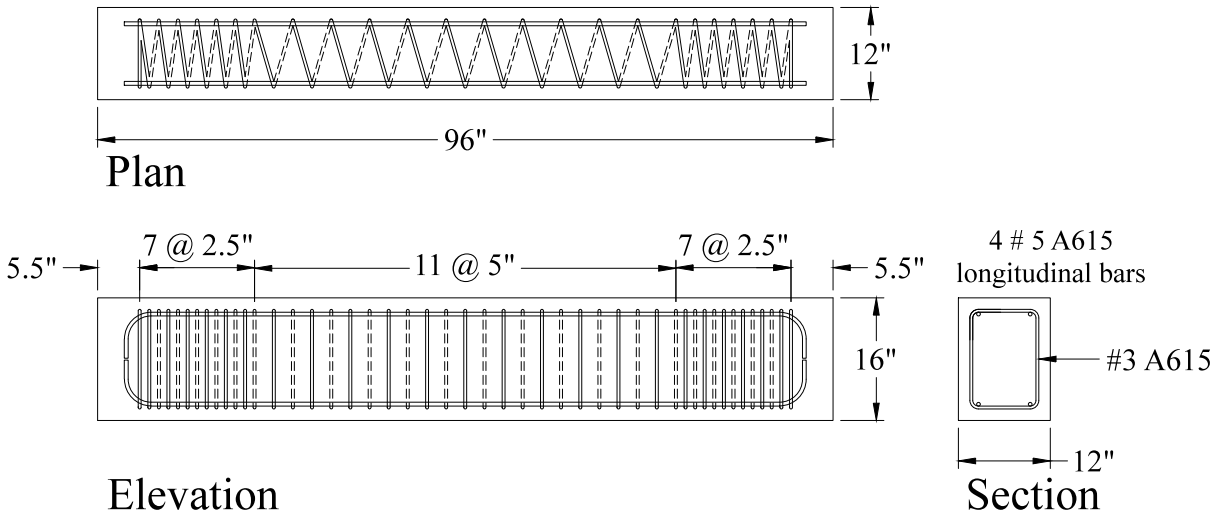

Figure 3.7: Details for specimens T2, T5a, and T5b

3.1.5 Specimens Subjected to Bending Moment, Shear, and Torque

These specimens were intended to simulate spandrel beams subjected to bending, shear, and torsion. To maintain equilibrium, and hence stability of the system, a beam may have to resist a so-called equilibrium torsion (Figure 3.8a). In this case, if the torsional resistance of Beam A is exceeded, the cantilevered canopy will fail because its bending moment cannot be resisted. A member can also be subjected to torsional loading from the bending moment in out-

of-plane members, such as the case shown in Figure 3.8b in which the floor joists framed into the spandrel beam produce torsion. This type of torsion is referred to as compatibility torsion. If the compatibility torsional resistance is exceeded, the transverse members, the floor joists in case of Figure 3.8b, will not fail as long as they have adequate capacity to resist the redistributed moments.

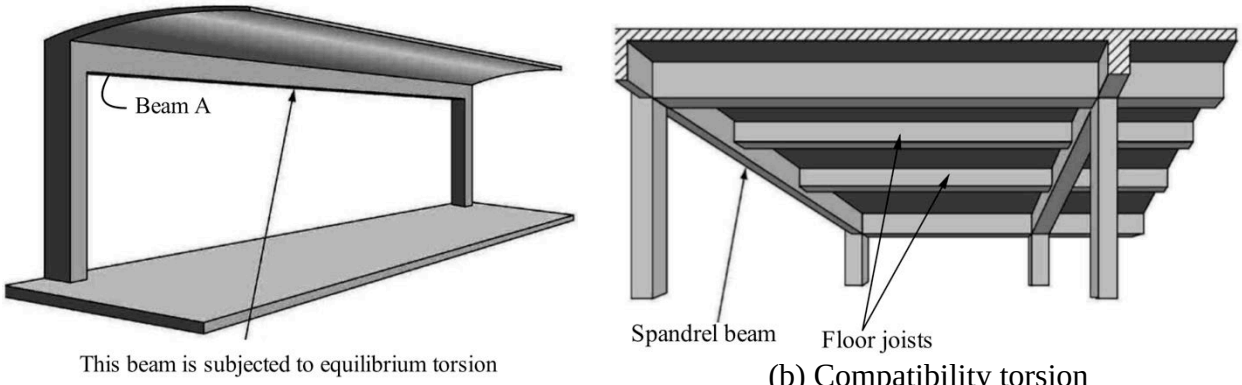

(a) Equilibrium torsion (b) Compatibility torsion

Source: ACI 318-11 (modified)

Figure 3.8: Different types of torsional loading

Regardless of the type of torsion, the member still has to resist bending and shear due to in-plane loads. The test specimens were loaded such that they would be subjected to equilibrium torsion, which is more critical than compatibility torsion.

For consistency with the shear specimens described in Section 3.1.1, the beams were 16 in. wide and 24 in. deep. The beams were 168 in. long. The primary test variables were the type of transverse reinforcement (conventional closed stirrups or continuous transverse reinforcement (CTR)) and whether the angled legs in CTR are in the shear plane or not. For all the specimens, the design concrete compressive strength was 5,000 psi. Three specimens were cast - refer to Table 3.5.

Table 3.5: Specimens subjected to bending moment, shear, and torque

Specimen	Description
TFS1	Conventional U-shaped stirrups
TFS2	CTR with angles on top and bottom
TFS3	CTR with angles on side faces

CTR = continuous transverse reinforcement

Note: A beam identical to TFS2 was also cast to debug the loading apparatus. The results from this test will not, however, be presented herein.

The beams were designed to satisfy all of the applicable design requirements in ACI 318-11, most notably Chapter 9 and 11 provisions. The details for specimen TFS2 are shown in Figure 3.9. The details for all the specimens are illustrated in Appendix G. In this appendix,

representative photographs of the cage fabrication ad layout for all the specimens are also provided. The width, depth, and length at four locations along each specimen were also recorded. The average dimensions are tabulated in Appendix G.

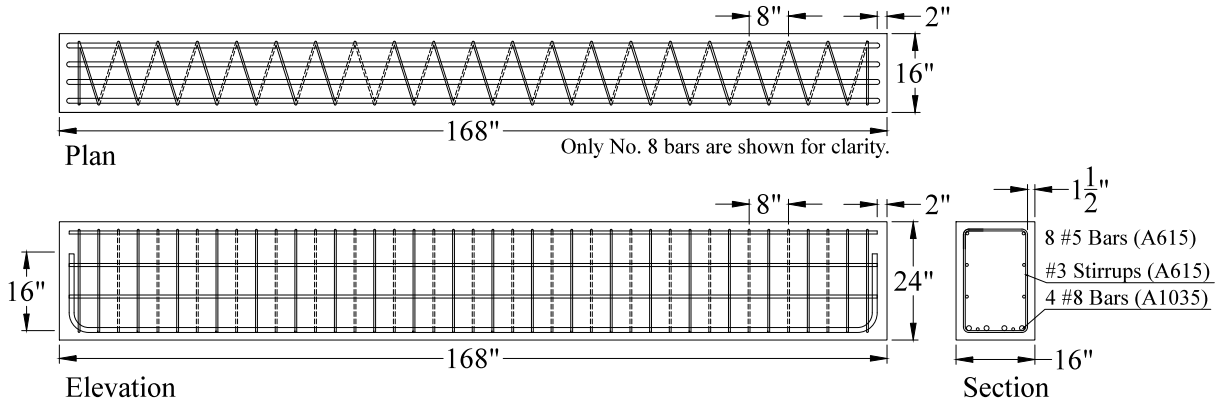

Figure 3.9: Details of specimen TFS2

3.1.6 Stub Columns

Four stub columns were tested to evaluate the axial load carrying capacity of columns with continuous transverse reinforcement (CTR) and those with conventional transverse reinforcement, i.e., either using ties or a spiral. In addition, these specimens were intended to compare the confinement from CTR and conventional transverse reinforcement. Three specimens were square with conventional ties or CTR with two different spacing, and one was a spirally-reinforced circular column. The specimens were sized based on the following criteria:

a. maintain the same axial load capacity,
b. keep the volumetric ratio of the transverse reinforcement as equal as possible,
c. ensure that the specimens could be shipped economically as they were going to be tested offsite,
d. the specimens must perform as short columns, and
e. consider the availability of formwork and ease of construction in the vertical position.

Based on these criteria, 18 in. square columns were selected for three specimens. To keep the cross-sectional areas nearly the same, a 20-in. diameter circular column was selected for the fourth specimen. Eight No. 7 longitudinal A615 reinforcing bars were selected for the square columns, resulting in a longitudinal reinforcement ratio (ρ) equal to 1.48%. Consistent with ACI 318-11 Section 10.9.2, six longitudinal bars were selected for the circular column. To keep the longitudinal reinforcement ratio as close as possible to the value used for the square columns, No. 8 longitudinal bars were used (ρ = 1.51% vs. 1.48% for square columns).

Using the nominal material properties (f'_c = 5,000 psi and f_y = 60,000 psi), the pure axial load capacity was 1884 kips and 1831 kips for the square and circular columns, respectively; both were well within the capacity of the universal testing machine. The column height was selected to be 96”; giving a slender ratio (kl/r) of 18 and 19 for the square and circular columns, respectively. (The value of the radius of gyration, r, was determined according to ACI 318-11

Section 10.10.1.2, and effective length factor, *k*, was taken as 1.) According to ACI 318-11 Section 10.10.1(a), the columns are considered to be short, as the value of *kl/r* is less than 22. The selected height corresponds to 75% of a typical story height, and it was possible to economically cast the specimens in an upright position. Each square column weighed 2,700 lbs. and the weight of the circular column was 2,618 lbs., for a total shipping weight of 10,718 lbs.

As mentioned previously, one of the criteria for proportioning the test specimens was to maintain the same transverse reinforcement volumetric ratio for the specimens with conventional ties and those using continuous transverse reinforcement (CTR). Meeting the requirements of ACI 318-11 Section 7.10.5, the maximum tie spacing was determined to be 14 in. The spacing for CTR was, however, limited to 13.6 in. in order to keep the bent angle below 25 degrees, as shown in Appendix A; but the spacing was established to be approximately 10 in. in order to achieve nearly the same volumetric ratio as that for the specimen with conventional ties. For consistency, the conventional ties were also spaced at 10 in. on center.

The aforementioned values were based on the research team's understanding during the design stage that continuous transverse reinforcement (CTR) for columns would have angled legs on two faces, similar to beams. The actual CTR had angled legs on all four faces. As a result, the spacing could have been as large as 27.3 in. without violating the maximum bent angle of 25 degrees (refer to Appendix A). For this scenario, the volumetric ratio between specimens with conventional ties and CTR could have been kept nearly the same had the spacing been taken as 14 in. Despite this difference, the selected specimens (with transverse reinforcement spaced at 10 in. on center) the measured data will allow an in-depth comparison of the performance of conventional ties and CTR in columns with identical axial load capacities and nearly identical transverse reinforcement volumetric ratios.

According to Section 7.10.4.3 in ACI 318-11, the clear spacing between spirals cannot exceed 3 in. This limit was imposed for the square with CTR to be compared against the circular, spirally reinforced specimen. In order to the keep the transverse reinforcement volumetric ratio the same, the spiral spacing was taken as 2.5 in.

The cross-section and elevation views of the specimens are shown in Figure 3.10. Appendix H provides representative photographs of the cages, as well as formwork.

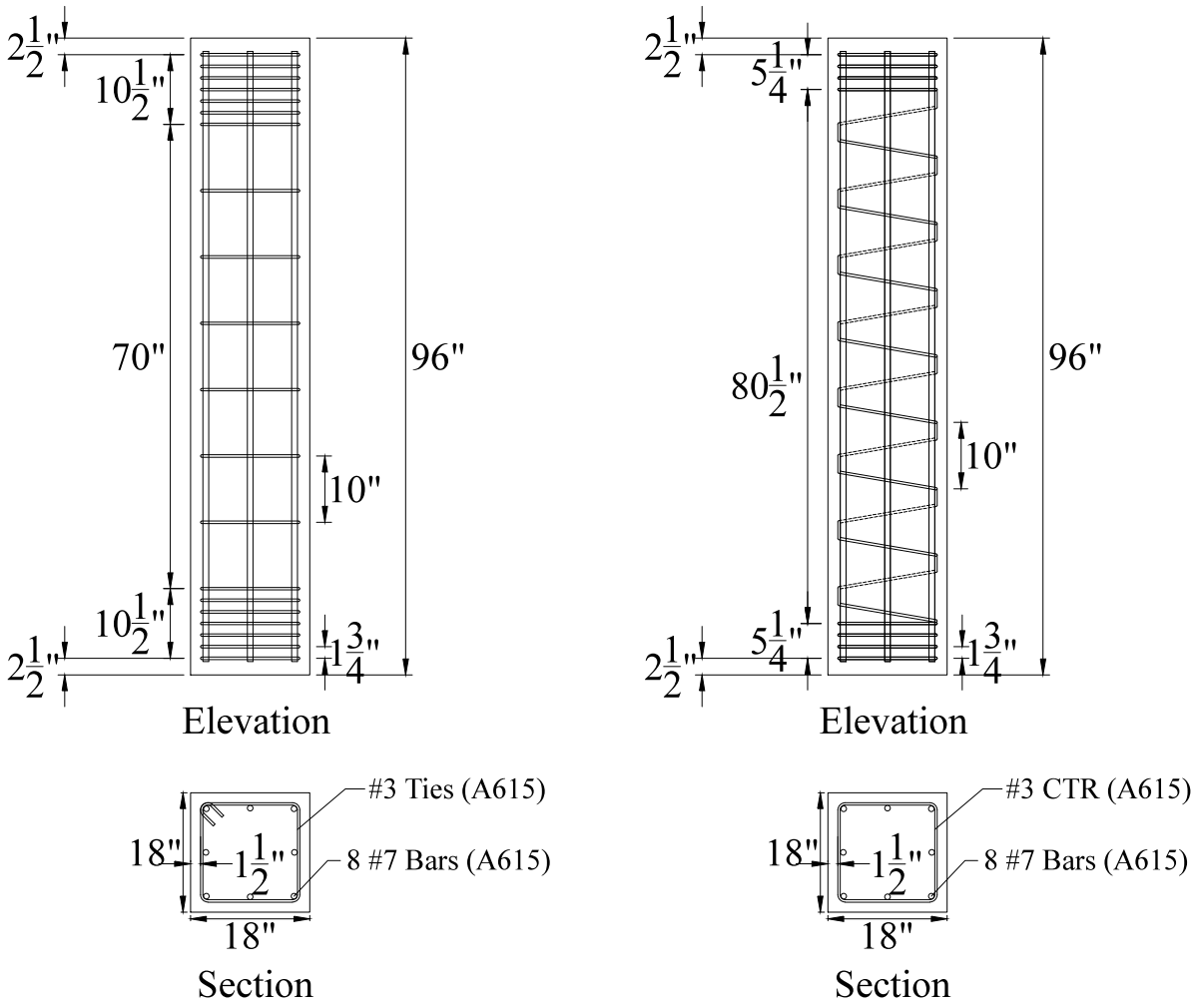

(a) Column C1
Conventional Tie

(b) Column C2
Continuous transverse reinforcement (maximum spacing)

Figure 3.10: Details of column specimens

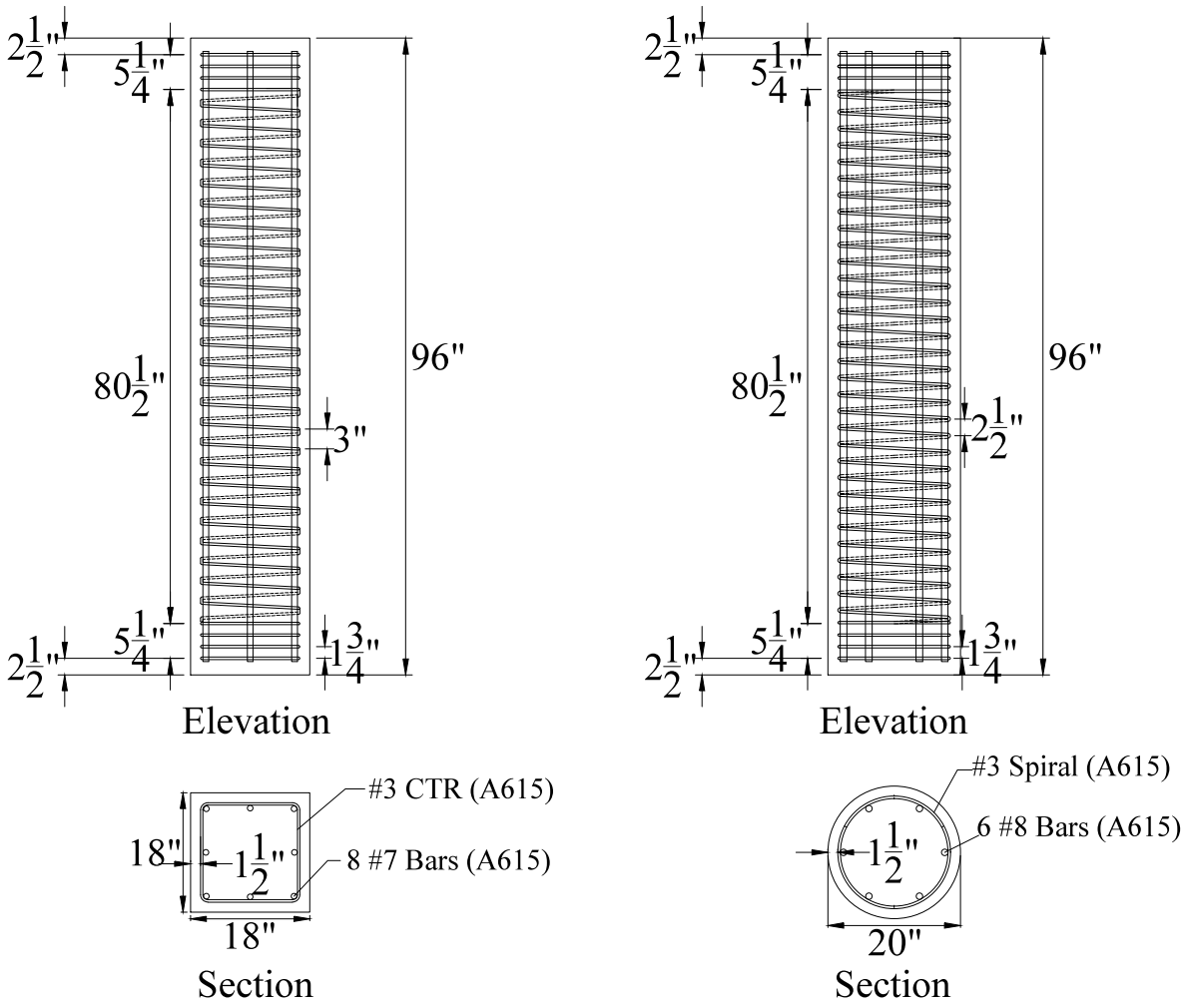

(c) Column C3
Continuous transverse reinforcement (minimum spacing)

(d) Column C4
Conventional spiral

Figure 3.10: Details of column specimens (cont.)

3.1.7 Exterior Beam-Column Connections

Two exterior, full-scale beam-column connections were cast and tested to compare the cyclic performance for cases with conventional seismic ties and those with continuous transverse reinforcement (CTR). Considering past studies (e.g., Wallace 1998) and member sizes encountered in practice, the beams were selected to be 16 in. wide by 24 in. deep, and the columns were 18 in. by 18 in. The beam longitudinal reinforcement consisted of four No. 8 A 615 bars in the top and three No. 8 A615 bars in the bottom. The column was reinforced with eight No. 9 A615 bars distributed uniformly around the perimeter. All the applicable seismic provisions in Chapter 21 of ACI 318-11 were checked as part of detailing of the specimens. Additionally, the joint capacity and details were checked against the ACI Committee 352 recommendations (ACI 352 2010).

The focus of these two specimens was on cyclic behavior of CTR versus conventional seismic ties. Hence, CTR was used in the column and in the expected plastic hinge region in the beam, near the column face. This region was taken as 50 in., corresponding to approximately 2*h* (where *h* is the beam depth), from the face of the column. Note that per ACI Code, the length of plastic hinge region cannot be less than a distance *h* from the critical section, which in this case is the column face.

The details of the two specimens are summarized in Figure 3.11. For construction purposes, both specimens were cast horizontally (refer to Appendix I). Considering that both specimens were cast in a similar fashion, the effects to casting direction, if any, would be nullified between the two specimens. Representative photographs of the cages and formwork are presented in Appendix I.

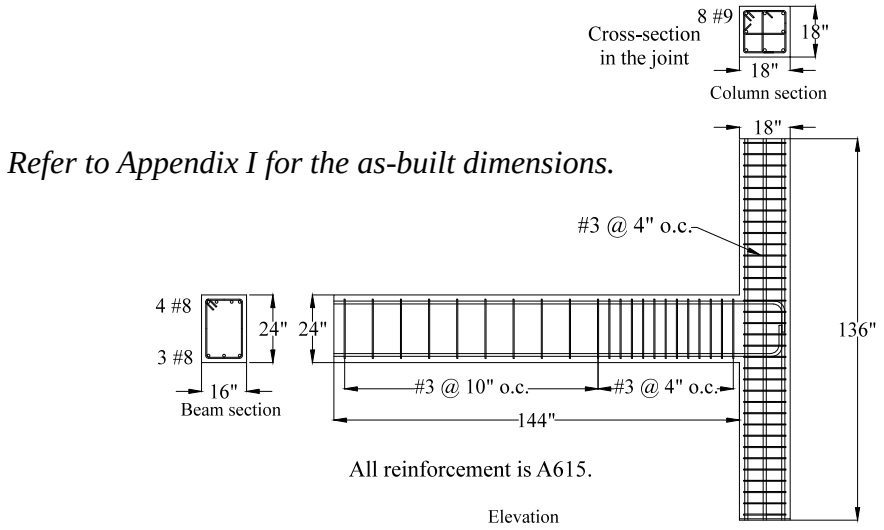

(a) Conventional seismic ties

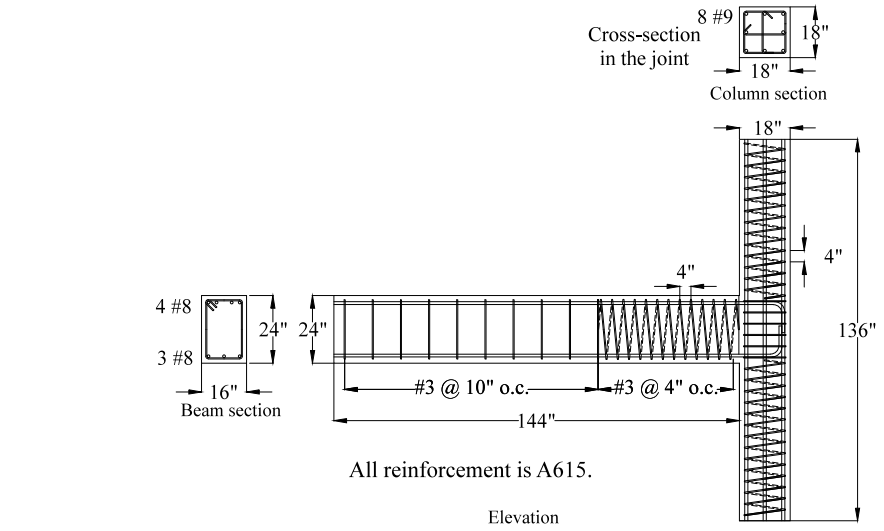

(b) Continuous transverse reinforcement

Figure 3.11: Details of exterior beam-column connections

3.2 Material Properties

As discussed in the previous section, A615 and Grade 100 A1035 reinforcing bars were used at various locations. The basic material properties were documented through testing or based on mill reports. The average values of the yield strength are summarized in Table 3.6. Appendix J provides additional details.

Table 3.6: Average material properties

Bar	f_y (ksi)	f_u (ksi)	ε_f	ASTM
No. 9	70.8	106.6	0.151	A615
No. 8	71.8	110.4	0.163	A615
No. 8	112.0	165.3	0.106	A1035
No. 7	73.7	111.7	0.135	A615
No. 5	72.0	106.6	0.129	A615/A706
No. 3	71.0	103.8	0.128	A615/A706

f_y = yield strength; f_u = tensile strength; E_s = modulus of elasticity; ε_f = fracture strain

The test specimens were cast and tested over a period of ten months. For each batch, compressive strengths at 7 days (occasionally at 9 days or 14 days), 28 days (occasionally at 29 days), and prior to and after testing of a group of similar specimens were obtained. With the exception of the concrete used in the stub columns, tensile strengths (f'_t) at the conclusion of a group of similar specimens were also obtained through split cylinder tests. The average strengths are tabulated in Table 3.7. It is noted that the tensile strength is lower than the expected values computed based on ACI 318-11 equations, i.e., $6.7\sqrt{f'_c}$. The measured properties at all phases of testing are presented in Appendix J. This appendix also summarizes that concrete mix designs.

Table 3.7: Average measured concrete stregths

Test specimen	f'_c (psi)	f'_t	
		psi	$f'_t / \sqrt{f'_c}$
Shear & spliced, 5000 psi	6,208	455	5.8
Torsion, 5000 psi	6,443		5.7
Flexure-shear-torsion, 5000 psi	6,607		5.6
Stub columns, 5000 psi		----	
Beam-column connection, 5000 psi	6,573	387	4.8
Shear, 10000 psi	10,894	573	5.5
Torsion, 10000 psi	10,817		5.5

3.3 Test Setup and Instrumentation

Considering the diversity of the test specimens, a number of different test fixtures had to be employed. The test setup and instrumentation for each type of tests are described in this section.

3.3.1 Specimens Subjected to Shear and Bending Moment

The shear specimens and spliced specimen were tested in three-point bending as shown in Figure 3.12(a), with a center-to-center span of 12 ft. The shear span was 54 in., resulting in a shear span/depth ratio of 2.45. The specimens were supported atop roller supports (Figure 3.12(c)). The load was applied by a 1,200-kip hydraulic ram through a 10 in. x 10 in. steel plate resting on an 8 in. x 10 in. neoprene pad (Figure 3.12(b)). An electric pump was used to manually control the hydraulic ram (Figure 3.12(d)), and load application.

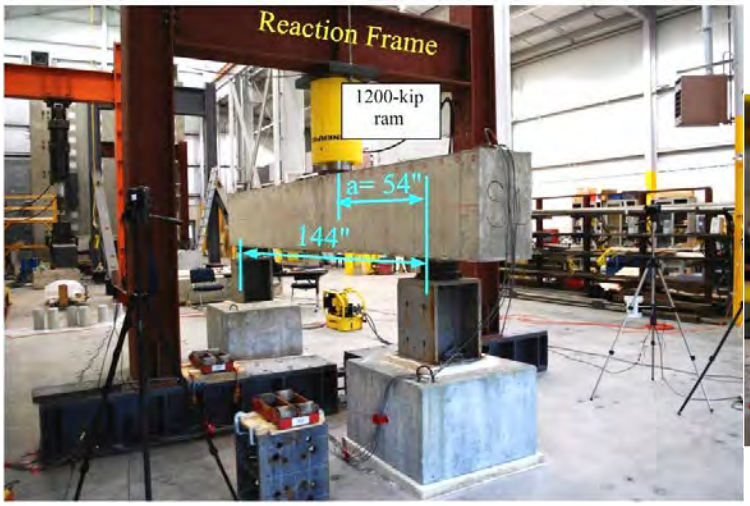

(a) Overall view

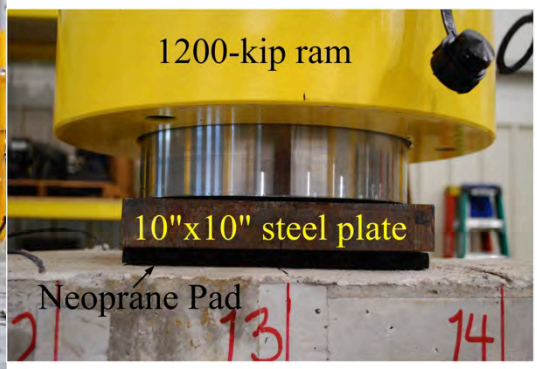

(b) Details at load point

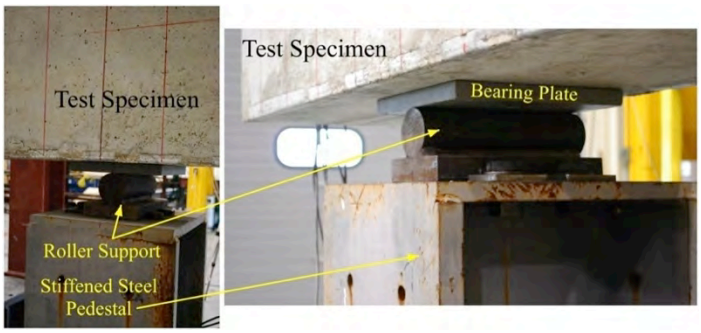

(c) Support Details

(d) Hydraulic system

Figure 3.12: Test setup for shear specimens and splice specimen

A number of 10-mm foil strain gages were bonded to the longitudinal and transverse reinforcement prior to casting the specimens. These gages were intended to predominantly capture the shear response. The locations of these gages are documented in Appendix K. In addition, the applied load was measured through a calibrated pressure transducer (Figure 3.13a),

and the vertical deflection of the beam at the load point was measured using a wire potentiometer (Figure 3.13b). The crack patterns at various load levels were marked and photographed. A crack comparator was also used to measure the crack widths.

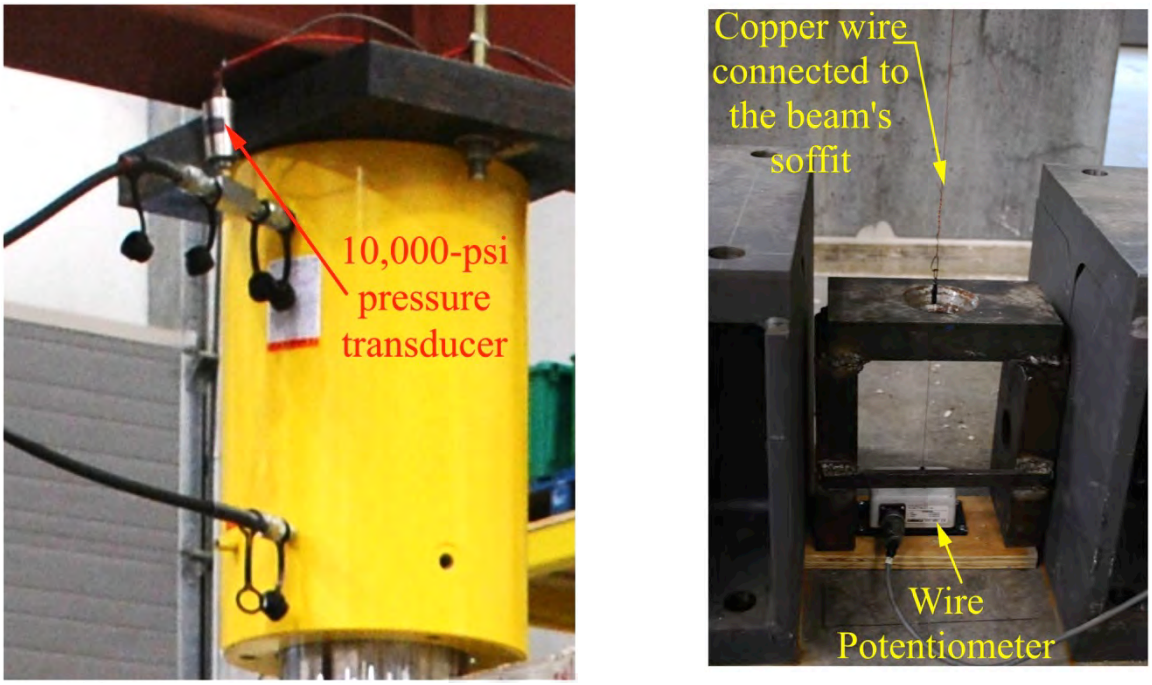

(a) Measurement of load (b) Measurement of deflection

Figure 3.13: External instrumentations

The load was applied monotonically until failure. The load application was stopped at a number of load increments to document the crack patterns and measure the crack widths.

3.3.2 Pullout Specimen

A self-reacting system was used for this series of tests. The system consisted of a number of stiffened channels supported atop the test specimen and a structural beam, as shown in Figure 3.14. The distance between the test bar and the supports of the reaction frame was adequately large, such that the struts forming under the reaction frame would not affect the test results. Using a mechanical coupler, the test bar was connected to a 3/8-in. A193-B7 threaded rod. The mechanical coupler was connected according to the manufacturer's specifications. The rod was, in turn, attached to a 60-kip center hole hydraulic ram that rested on top of the loading beam. The minimum specified yield strength of the threaded rods (125 ksi) was approximately two times larger than the expected yield strength of the test bar (No. 3 Grade 60 reinforcing bar). Hence, inelastic deformations would be concentrated in the test bar.

Three spring-loaded displacement transducers were connected to monitor any potential slip in the mechanical coupler, and displacement of the test bar relative to the concrete surface, see Figure 3.15. In addition, two 10-mm foil strain gages were bonded to the test bar to measure the strain and hence stress in the reinforcing bar.

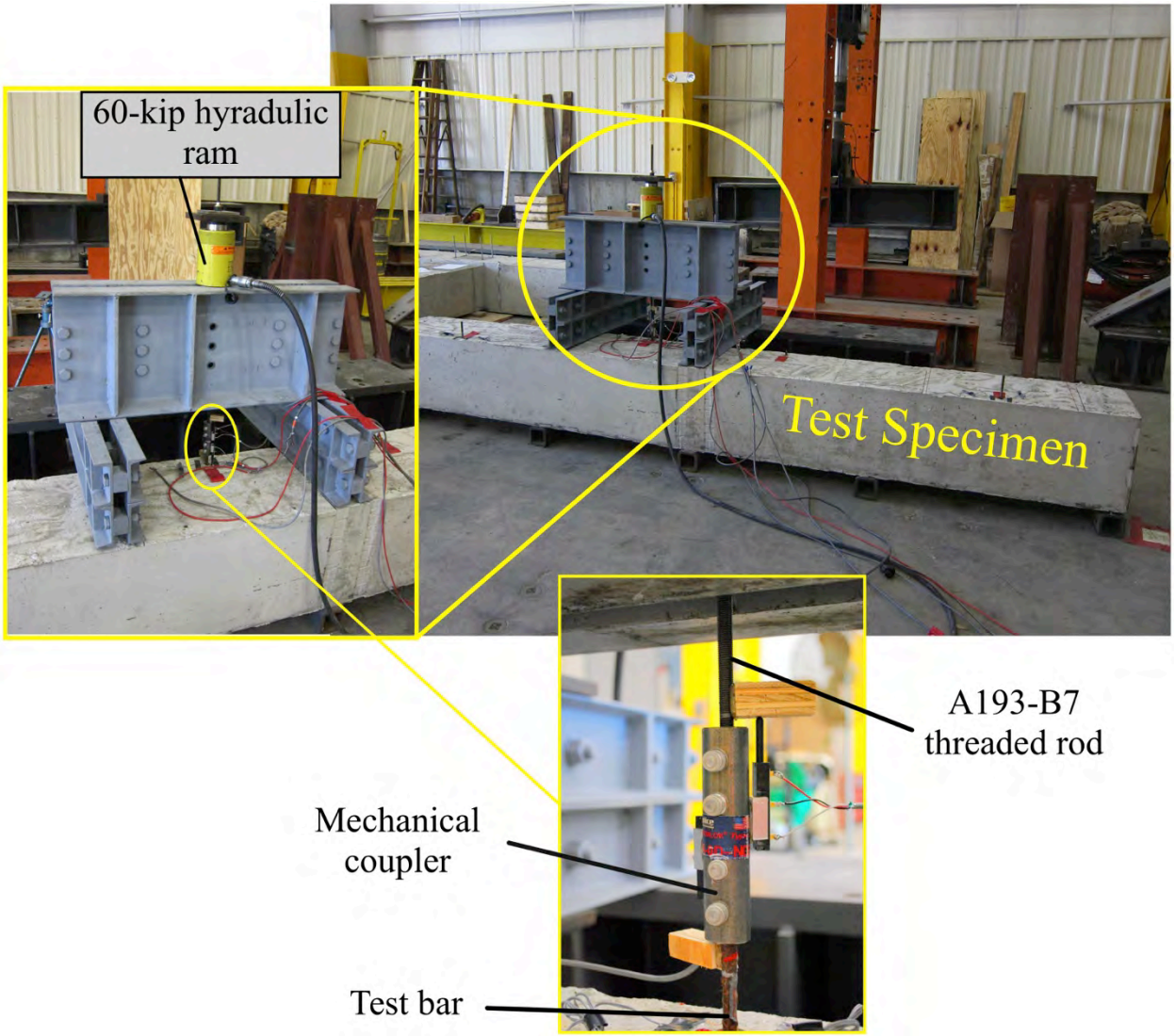

Figure 3.14: Test apparatus for pullout specimens

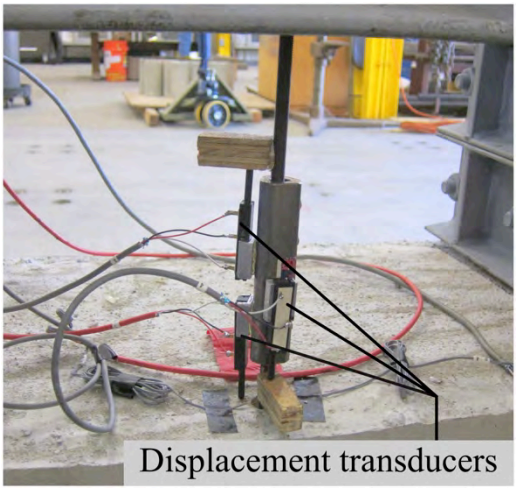

Figure 3.15: Measurement of various displacements

Using a hand operated pump, the load was applied at a relatively constant rate. The test bars were loaded until fracture.

3.3.3 Specimens Subjected to Pure Torsion

In order to apply pure torsion, the specimens were hung from a reaction frame by a pair of double C15x50 members connected through universal joints to moment arms that had been clamped to the specimen (Figure 3.16). One arm was attached to a 60-kip servo-valve controlled actuator, and the other arm was attached to a universal joint by a 1-in. A193-B7 all threaded rod. The latter arm served as the reaction point.

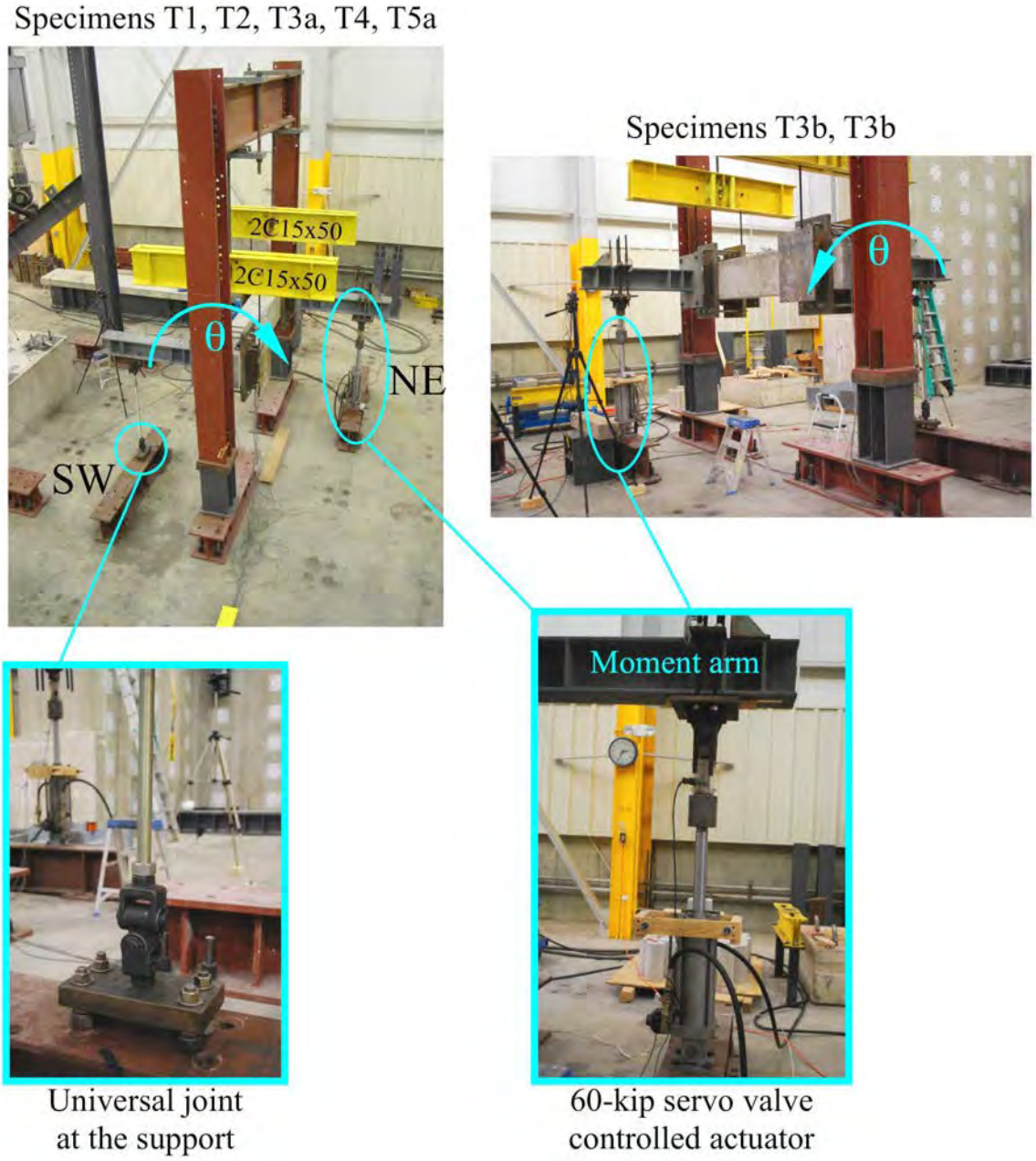

Figure 3.16: Test apparatus for applying pure torsion

As mentioned in Section 3.1.4, two groups of specimens with continuous transverse reinforcement (CTR) were tested. The supported end was on the south end for the specimens using conventional transverse reinforcement and "a" series specimens with CTR, and for "b" series specimens the support was on the north end. As a result, the specimen was twisted clockwise for specimens T1, T2, T3a, T4, T5a; and counterclockwise for specimens T3b and T5b. For the "b" series, the direction of torque was such that the diagonal cracks could potentially not be arrested by the transverse reinforcement, as shown in Figure 3.6(b).

For testing purposes, the actuator was controlled in position-controlled mode, i.e., the moment arm attached to the actuator was lowered in a number of predefined downward displacements. At various displacements, the crack patterns were sketched and photographed for documentation purposes. A crack comparator was also used to measure the crack widths. In addition to measuring the load and displacement of the actuator, strains in transverse and longitudinal reinforcing bars were monitored by a number of bondable 10-mm foil strain gages. The locations of the strain gages for all the specimens are provided in Appendix K.

3.3.4 Specimens Subjected to Flexure, Shear, and Torque

Testing of these specimens proved to be rather challenging. The intent was to examine the performance of conventional and continuous transverse reinforcement (CTR) under the combined actions of bending, shear, and torque such that the respective failure modes would occur simultaneously. After a number of permutations, it was decided to decouple the loading apparatus to apply shear force and bending moment from that used to apply torque. In this manner, it was possible to control the level of shear and bending moment independent of the applied torque.

The test setup is shown in Figure 3.17. A 150-kip servo-valve controlled actuator was placed concentrically along the specimen centerline. This actuator applied the shearing force and bending moment. The load from the actuator was transferred to the beam through a loading "bridge", which was supported on rollers. The distance between each roller and the beam centerline was 7-5/16 in. A double C15x50 was transversely post-tensioned to the beam. On the top of this member, a 120-kip center hole hydraulic ram with an eccentricity of 16 in. with respect to the beam centerline was placed. The beam was subjected to torque by controlling the level of force in this ram. The force in the ram was reacted against the lower portion of the reaction frame, which had been post-tensioned to the strong floor. A 1-in. diameter A193-B7 threaded rod connected the ram to a universal joint, as shown in Figure 3.17.

The specimen was supported atop roller supports in order to resist the shear and bending moment – refer to Figure 3.17. At each end, the beam was restrained against twisting through an assembly consisting of a pair of double C5x9 channels that were clamped onto the beam by high-strength threaded rods. Using high-strength threaded rods, the assembled channels were connected to the reaction wall on the north side; and on the opposite side were connected to a W18x50 stub that had been post-tensioned to the strong floor. Knowing the direction of the applied torque, the threaded rods were positioned such that they would be in tension.

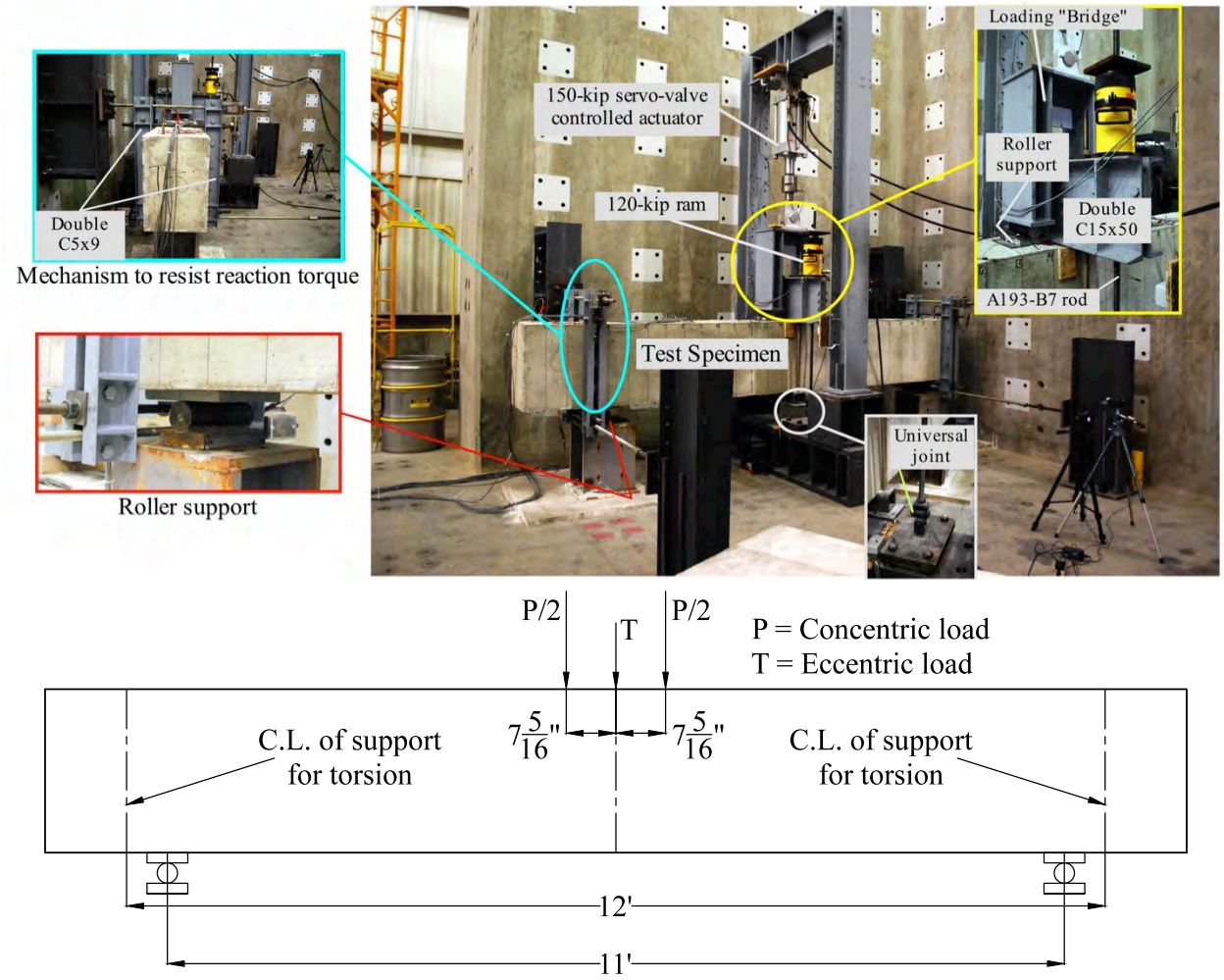

Figure 3.17: Test setup for specimens subjected to bending moment, shear, and torque

In addition to a number of 10-mm foil strain gages bonded to the longitudinal and transverse reinforcing bars, external instruments were installed to monitor various responses. These sensors measured (a) the concentric and eccentric loads (by a load cell and a calibrated pressure transducer, respectively), (b) vertical deflections of the beam at 12 in. on either side of the beam centerline, (c) horizontal and vertical deflection of the beam's south fascia, (d) and the loads in the horizontal threaded rods resisting the applied torque. The latter measurements were used to compute the reaction torques at each support. Figure 3.18 illustrates the primary sensors. The locations of the strain gages are documented in Appendix K.

The concentric and eccentric loads were increased in a number of steps in order to ensure that a particular mode of failure (i.e., flexure, shear, or torsion) would not precede the others. The loading steps consisted of (a) maintaining the eccentric load while increasing the magnitude of the concentric load, and (b) holding the concentric load while increasing the level of eccentric load. This sequence was continued until the conclusion of testing. The complete loading sequence is shown in Figure 3.19. The crack patterns were marked and photographed in order to document the performance at various load levels. A crack comparator was also used to measure the crack widths.

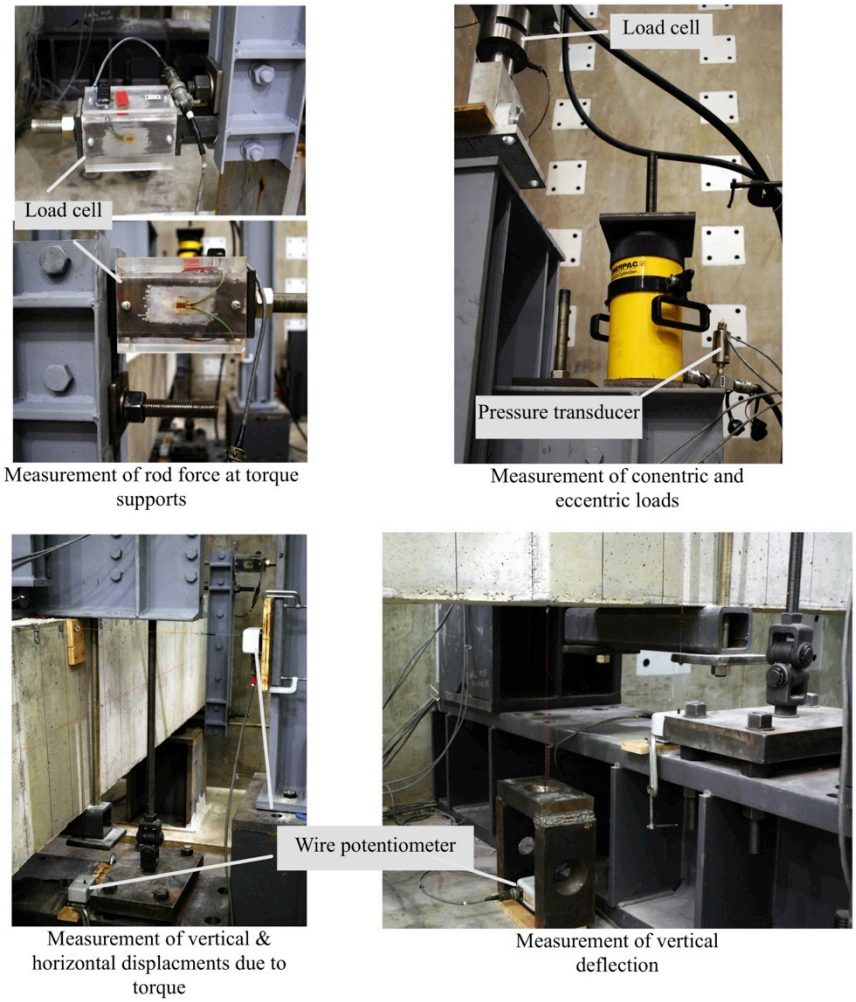

Figure 3.18: Instruments for specimens subjected to bending moment, shear, and torque

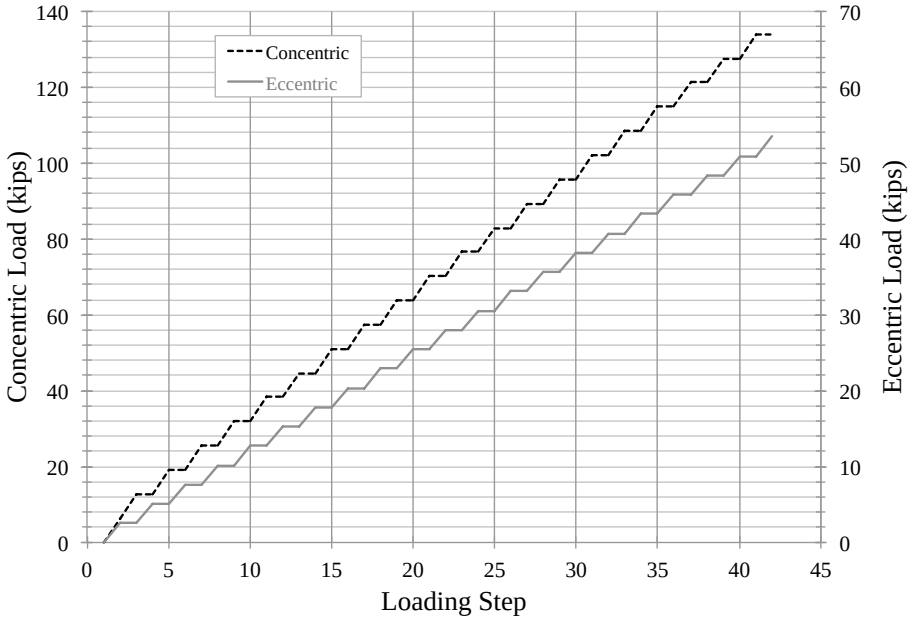

Figure 3.19: Loading sequence

3.3.5 Stub Columns

The stub columns were tested at Fritz Laboratory at Lehigh University using a 5,000,000-pound universal testing machine. The columns were subjected to concentrically applied axial load that was increased monotonically at a rate of approximately 100 kips per minute until failure. The columns were plumbed by hydrostoning the bottom surface on top of a steel plate. The load was distributed by placing a steel plate on the top surface; this plate was also hydrostoned. Two of the stub columns prior to testing are shown in Figure 3.20.

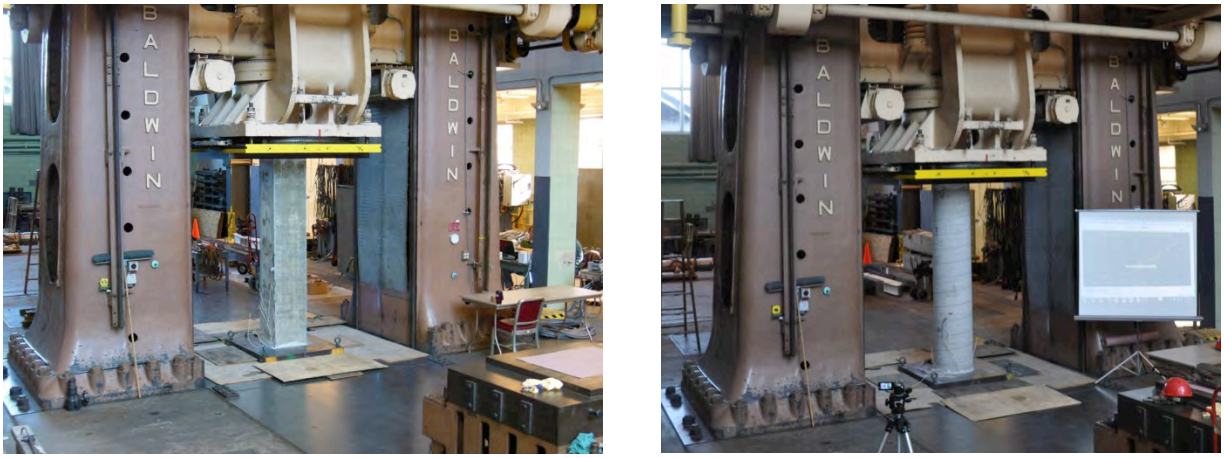

(a) Square specimens (b) Circular specimen

Figure 3.20: Stub columns in universal testing machine

The axial load and column shortening were monitored. In addition, strains in the longitudinal and transverse reinforcing bars, approximately at the midheight, were measured by a number of 10-mm bondable foil strain gages. The locations of the strain gages are summarized in Appendix K.

3.3.6 Exterior Beam-Column Connections

The test setup is shown in Figure 3.21. Three pins were used to support the specimen. The pins represent the inflection points at the midheight of each column and midspan of the beam. A 150-kip servo-valve controlled hydraulic actuator was used to apply the lateral load, which was transferred to the specimen through the pin at the top of the column. The column's bottom pin was bolted to a structural member (W14x159) that had been post-tensioned to the strong floor. A strut with a load cell was attached to the pin at the beam's midspan. This instrumented strut was used to measure the shear in the beam. Knowing the shear force and the applied load, forces in the members could be computed. The dimensions required to calculate the shear force in the beam and the lower half of the column are provided in Figure 3.22.

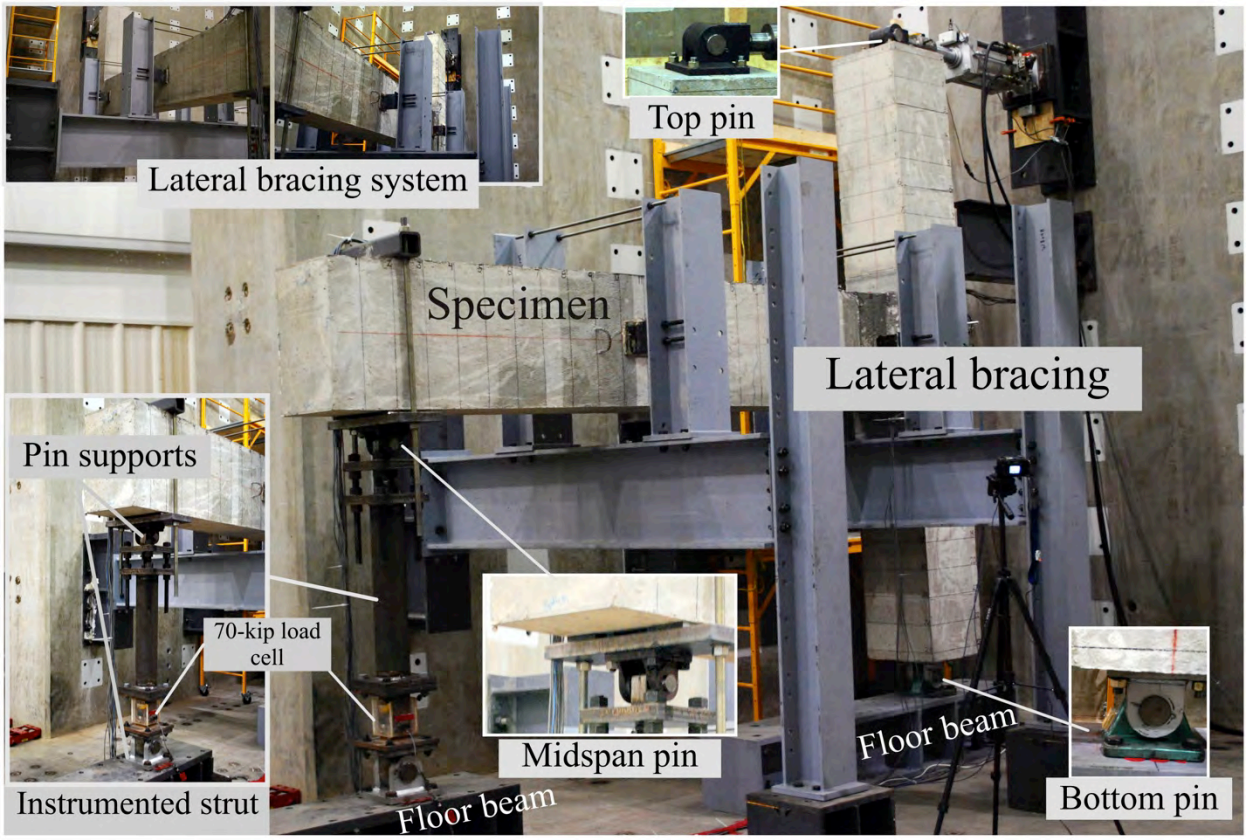

Figure 3.21: Test setup for exterior beam-column connections

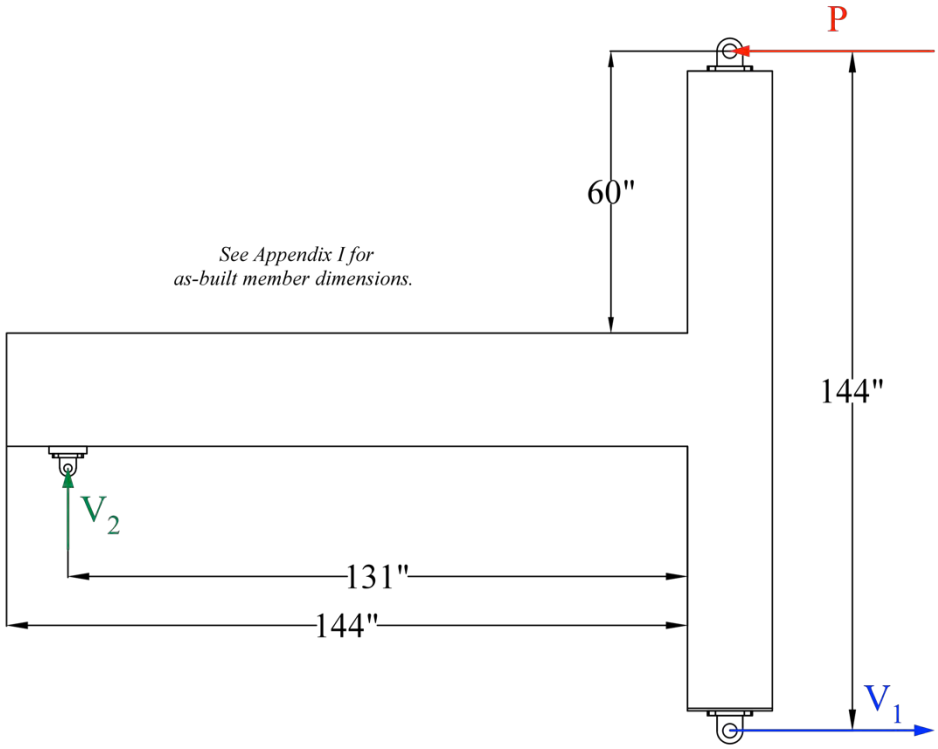

Figure 3.22: Overall dimensions and forces

External and internal sensors were used to capture various responses. The internal sensors were 10-mm foil strain gages bonded to the longitudinal and transverse reinforcing bars at various locations, as summarized in Appendix K. The applied load and lateral displacement were measured by a load cell and wire potentiometer attached to the hydraulic actuator. In addition, the lateral displacement of the column at 5-1/2 in. below the top of the column was monitored. The potential slippage of the floor beams and pin assembly was monitored even though the floor beams (shown in Figure 3.21) had been post-tensioned to the strong floor, and the pin assembly at the bottom of the column had been torqued sufficiently.

As mentioned previously, a load cell was used to measure the force in the strut, which is the beam shearing force. Figure 3.23 illustrates the external sensors. Additionally, the joint shear deformations were determined based on the readings from two spring-loaded displacement transducers placed diagonally in the connection region, refer to Figure 3.24.

The specimens were cyclically loaded by applying displacement cycles shown in Figure 3.25. Up to inter-story drift ratio of 3.25%, two cycles at a given drift ratio were followed by one cycle at smaller drift. Beyond 3.25% drift, the specimen using conventional seismic ties was subjected to one cycle with +3.11% and -4.74% drifts, and the second specimen underwent +/-3.88% and +3.11%/-4.33% drifts. The distance between the column and lateral bracing system did not allow larger drifts. It should, however, be note that the maximum design inter-story drift is 1.5% to 2.5% of the story height depending on the seismic risk category (ASCE 7-10). The specimens were subjected to at least 30% larger drifts.

Similar to the other specimens, loading was paused at predetermined intervals in order to document the crack patterns and measure the crack widths. A crack comparator was also used to measure the crack widths.

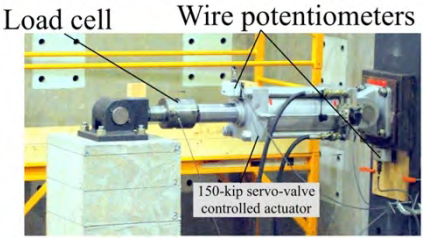

Measurement of lateral force and column lateral displacement

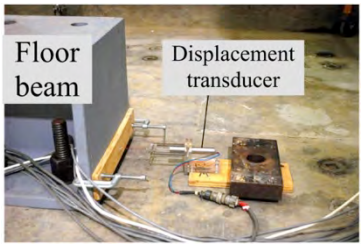

Measurement of slippage of floor beam

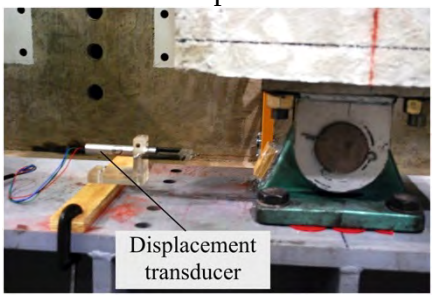

Measurement of slippage of column's bottom pin assembly

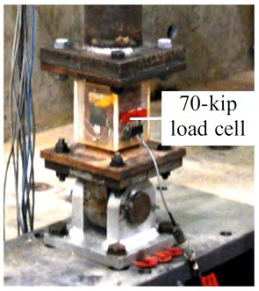

Load cell in the strut

Figure 3.23: Instrumentation for beam-column connections

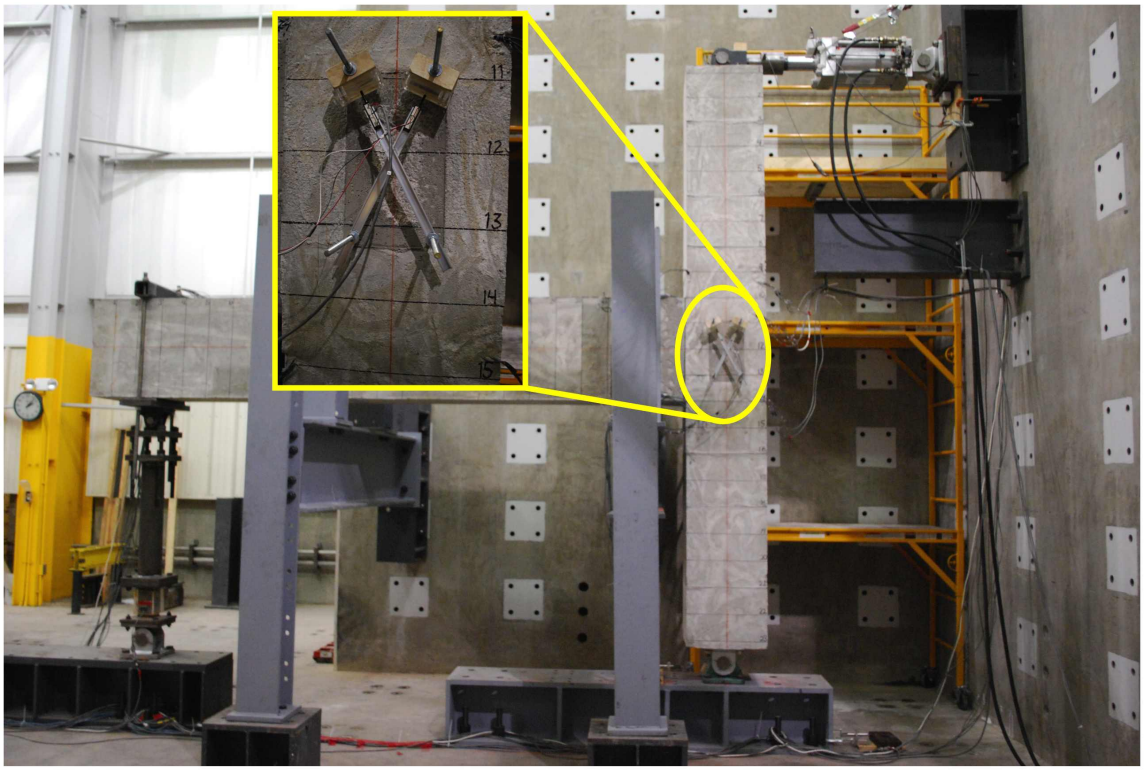

Figure 3.24: Measurement of joint shear deformation

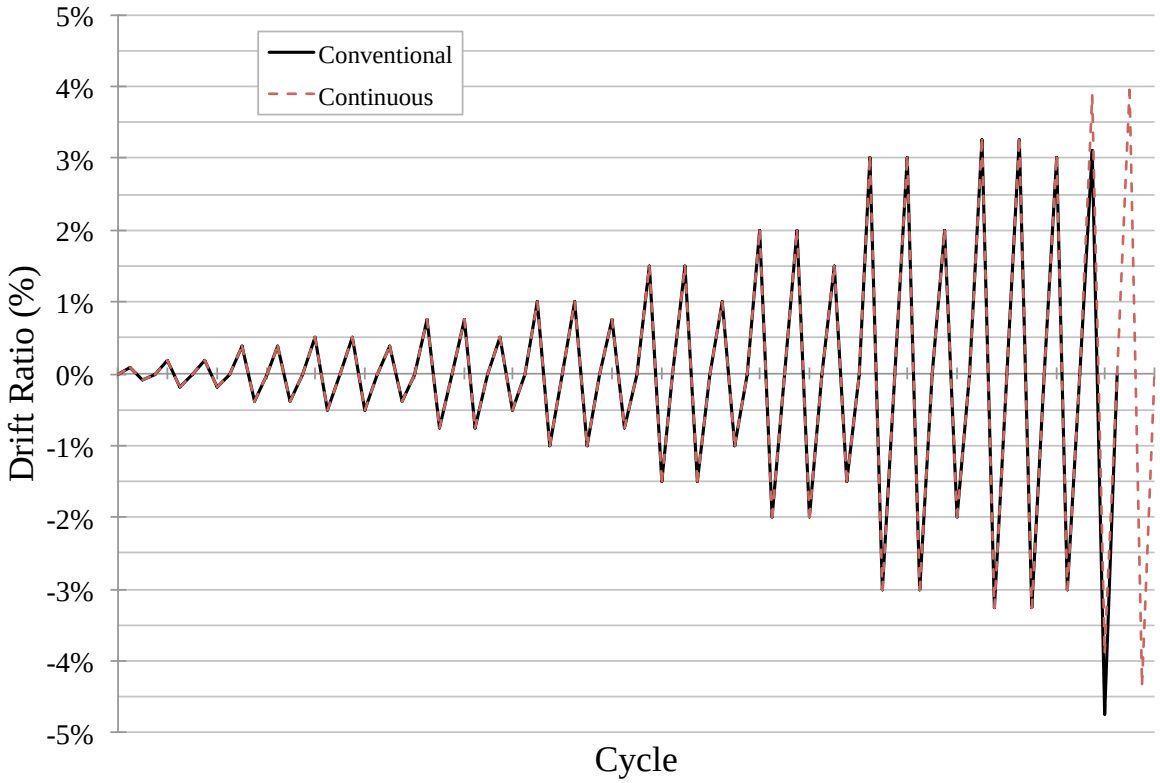

Figure 3.25: Loading protocol

4.0 Test Results and Discussions

A number of metrics are used to evaluate the performance of each of group of specimens. These metrics utilize the visual and measured data. The results are presented and discussed for each group separately in the following sections.

4.1 Shear and Spliced Specimens

4.1.1 Capacity

Using the measured material properties and average as-built dimensions, the capacity of each specimen was computed based on established procedures provided in ACI 318-11. Sample calculations for specimen S2 (using continuous transverse reinforcement (CTR) with angles on top and bottom) and specimen S3 (using CTR with angles on side) are illustrated as follows. The calculated capacities are not reduced by strength reduction ϕ (which is 0.75) in order to compare them against the experimentally obtained capacities.

(a) Specimen S2

$$V_n = V_c + V_s$$

$$V_n = 2\sqrt{f_c'}\, b_w d + \frac{A_v f_{yt} d}{s} \qquad \text{Eq. 3}$$

$$V_n = 2\sqrt{6208} \times 16.1 \times 22.1 + \frac{0.22 \times 71000 \times 22.1}{5}$$

$$V_n = 90663\ lbs = 90.7\ kips$$

$$Left\ reaction = \frac{90''}{(54'' + 90'')} P$$

$$Left\ reaction = V_n = 90.7\ kips$$

$$\therefore P = 145\ kips$$

Due to construction error, the covers to the bottom and top stirrups were 1 1/8" and 1 7/8", respectively, instead of 1 1/2".

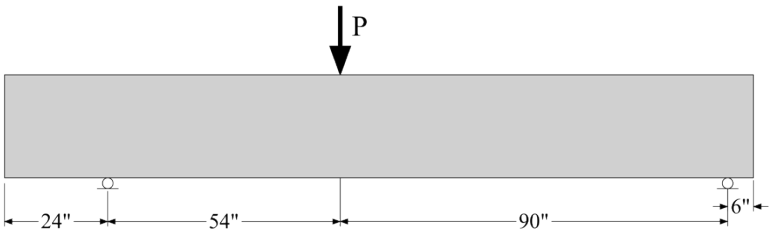

(b) Specimen S3

From Park and Pauly (1975)

$$V_s = \left[\sin\alpha\left(\cot\theta + \cot\alpha\right)\right] A_t f_v \frac{jd}{s}$$

$$Assume\ \theta = 45^o, jd \approx d, f_v = f_{yt}$$

$$V_s = \frac{A_t f_{yt}\left(\sin\alpha + \cos\alpha\right) d}{s}$$

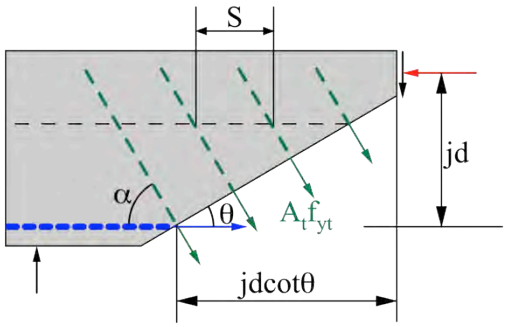

Adopted from MacGregor and White (2009)

On the back face the angle is 180^o - α

$$V_s = \frac{A_t f_{yt}\left[\sin\left(180-\alpha\right)+\cos\left(180-\alpha\right)\right]d}{s}$$

$$V_s = \frac{A_t f_{yt}\left(\sin\alpha-\cos\alpha\right)d}{s}$$

Hence,

$$Total\ V_s = \frac{2A_t f_{yt} d\sin\alpha}{s}$$

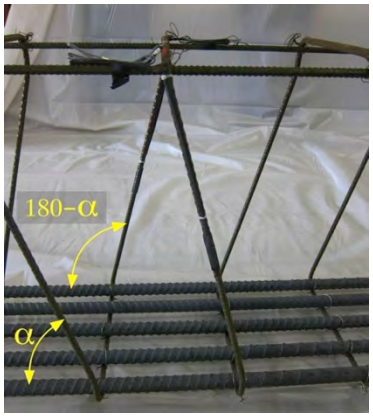

Cage for specimen S3

$$\alpha = 90^o - 15^o = 75^o \quad (see\ Table\ 3.2)$$

$$Total\ V_s = \frac{2A_t f_{yt} d\sin\alpha}{s} = \frac{2\times 0.11\times 71000\times 22.1\times \sin 75^o}{10} = 33344\ lbs$$

$$V_n = 2\sqrt{6208}\times 16.1\times 22.1 + 33344$$

$$V_n = 89487\ lbs = 89.5\ kips$$

$$Left\ reaction = \frac{90''}{\left(54''+90''\right)}P$$

$$Left\ reaction = V_n = 89.5\ kips$$

$$\therefore P = 143\ kips$$

The calculated capacities for all the specimens are summarized in Table 4.1. The maximum load resisted by each specimen is also provided in this table. Based on the data presented in this table, the following observations are made.

- With the exception of specimen S12, the maximum measured load is reduced slightly when the angled legs of CTR are in the vertical shear plane. The most significant drop is for specimen S9, for which the calculated capacity could not be developed (the measured maximum load is 0.96 times the calculated capacity).

  Specimen S9 was the only beam that was cast with concrete from two different trucks, with the bottom 2/3 filled with concrete from the end of one truck and the top 1/3 from the beginning of another truck. There was no time for the first load to set before the remainder of the beam was filled. Although the same mix was delivered in all trucks and the beam was thoroughly vibrated, the upper third of specimen S9 appeared to have more voids. It is possible that the initial load in the second truck had a slightly higher air content and/or water content than the end of the first truck. As a result, the compression zone, where the failure was initiated, could have been slightly weaker resulting in a lower than expected capacity.

- When CTR is used as intended (i.e., the angled legs are on the top and bottom surfaces), the maximum load, on average, is essentially the same as that offered by conventional U-

shaped stirrups. The average ratio of the maximum load in specimens S2, S5, S8, and S11 to that in the corresponding specimens with conventional stirrup is 0.99.

- For group 3 of the specimens (S7, S8, and S9), the maximum load, on average, is 0.90 times the corresponding value for the specimens made with nominal 5,000-psi concrete. In this group of specimens, the transverse reinforcement was spaced at the largest possible value of d/2; hence, the concrete contribution is larger than that for the specimens with d/4 as the spacing of the transverse reinforcement. As discussed in Section 3.2 (Table 3.6), the tensile strength of the selected 10,000-psi mix is lower than the expected value. The relatively large amount of cement (29% of the total weight of the aggregates vs. 18% for the 5,000-psi, refer to Table J.2 in Appendix J) is deemed to have reduced the contribution of aggregate interlock, leading to a lower tensile strength and hence a lower shear capacity. It should, nevertheless, be noted that the measured maximum loads are within the expected scatter of shear strength.

- The maximum load resisted by the spliced specimen was 0.96 times the value in a comparable specimen (S3). This difference is relatively small considering the large variability of shear strength. Hence, the selected technique for splicing continuous transverse reinforcement was apparently successful.

The shear strength of reinforced concrete members can vary significantly. In view of such variability and the values reported in Table 4.1, the continuous transverse reinforcement is deemed to be equivalent to conventional U-shaped stirrups. Moreover, the technique for splicing continuous transverse reinforcement is an effective and simple option.

Table 4.1: Calculated shear capacities and maximum measured loads

Group	Specimen	Calculated Nominal Capacity (kips)	Measured Maximum Load (kips)	Measured / Calculated
1	S1: Conventional	145	218	1.50
	S2: CTR (Angles on top and bottom)	145	200	1.38
	S3: CTR (Angles on sides)	143	192	1.34
2	S4: Conventional	200	236	1.18
	S5: CTR (Angles on top and bottom)	200	251	1.25
	S6: CTR (Angles on sides)	199	228	1.14
3	S7: Conventional	174	193	1.11
	S8: CTR (Angles on top and bottom)	174	194	1.11
	S9: CTR (Angles on sides)	172	165	0.96
4	S10: Conventional	229	259	1.13
	S11: CTR (Angles on top and bottom)	229	255	1.11
	S12: CTR (Angles on sides)	228	274	1.20
	SPL: Spliced CTR (Angles on sides)	143	185	1.29

Note: CTR: continuous transverse reinforcement

4.1.2 Overall Response

The relationships between the applied load and deflection, measured at the load application point, are plotted in Figure 4.1. For each group of specimens, the average value of the nominal capacity computed based on established procedures (tabulated in Table 4.1) is also shown.

Similar to the observations made in the previous section, the calculated nominal capacities (computed based on well-established procedures) could be developed and exceeded except for specimen S9. With the exception of specimen S9, all the comparable specimens with conventional U-shaped stirrups and continuous transverse reinforcement (CTR) exhibit the same stiffness until the peak load, i.e., the load-deflection responses are essentially the same. As indicated in the figure, the change in the stiffness of specimen S9 is attributed to instrumentation problems for this specimen. It is believed that this specimen would also have followed the same load-deflection response as specimens S7 and S8 had there been no issues with the deflection transducer for specimen S9.

For all beam tests in this series, the load dropped rather precipitously after reaching the maximum value, consistent with the brittle nature of shear failure. The percentage of drop from the peak load to the first post-peak value is summarized for each specimen in Table 4.2. For the specimens using 5,000-psi concrete (groups 1 and 2 and the spliced specimen), the specimens using conventional stirrups (S1 and S4) experienced the largest percentage drop. In case of the 10,000-psi specimens (groups 3 and 4), specimens S9 and S12 had the highest drop. As discussed previously, the concrete in the upper one third of specimen S9 appears to have been of a lower quality. The angled legs in specimen S12 were in the shear plane (i.e., on the sides), which is not the detail used in practice. Therefore, the data suggest that continuous transverse reinforcement confines the core more effectively and improves the post-peak shear response.

Table 4.2: Percent drop after the peak load

Group	Specimen	% Drop
1	S1: Conventional	46.2%
	S2: CTR (Angles on top and bottom)	14.0%
	S3: CTR (Angles on sides)	29.1%
2	S4: Conventional	36.9%
	S5: CTR (Angles on top and bottom)	26.6%
	S6: CTR (Angles on sides)	26.2%
3	S7: Conventional	40.9%
	S8: CTR (Angles on top and bottom)	19.4%
	S9: CTR (Angles on sides)	50.2%
4	S10: Conventional	15.6%
	S11: CTR (Angles on top and bottom)	14.1%
	S12: CTR (Angles on sides)	42.7%
	SPL: Spliced CTR (Angles on sides)	22.7%

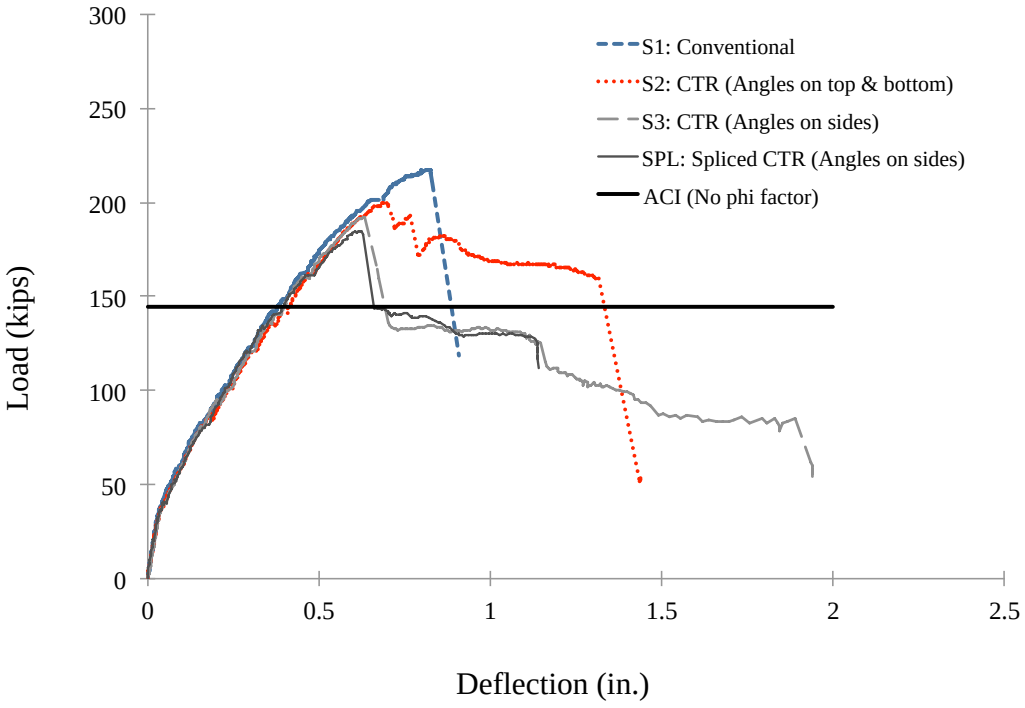

(a) Specimens S1, S2, S3, and spliced specimen (s = 10", f'_c = 5,000 psi)

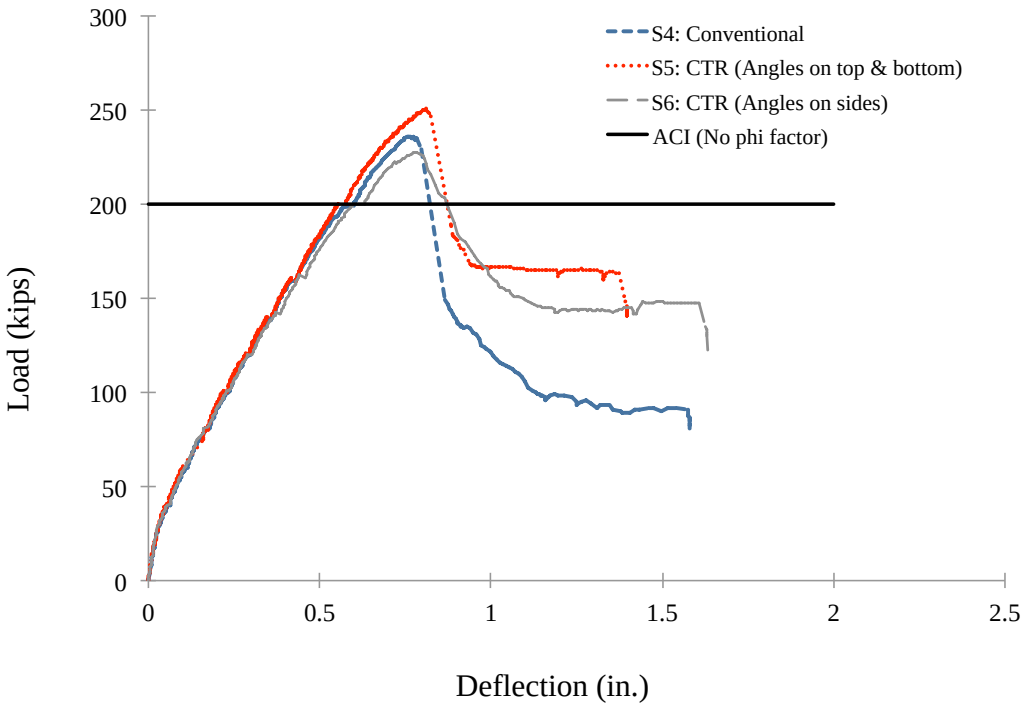

(b) Specimens S4, S5, S6 (s = 5", f'_c = 5,000 psi)

Figure 4.1: Load-deflection relationships
CTR: Continuous transverse reinforcement

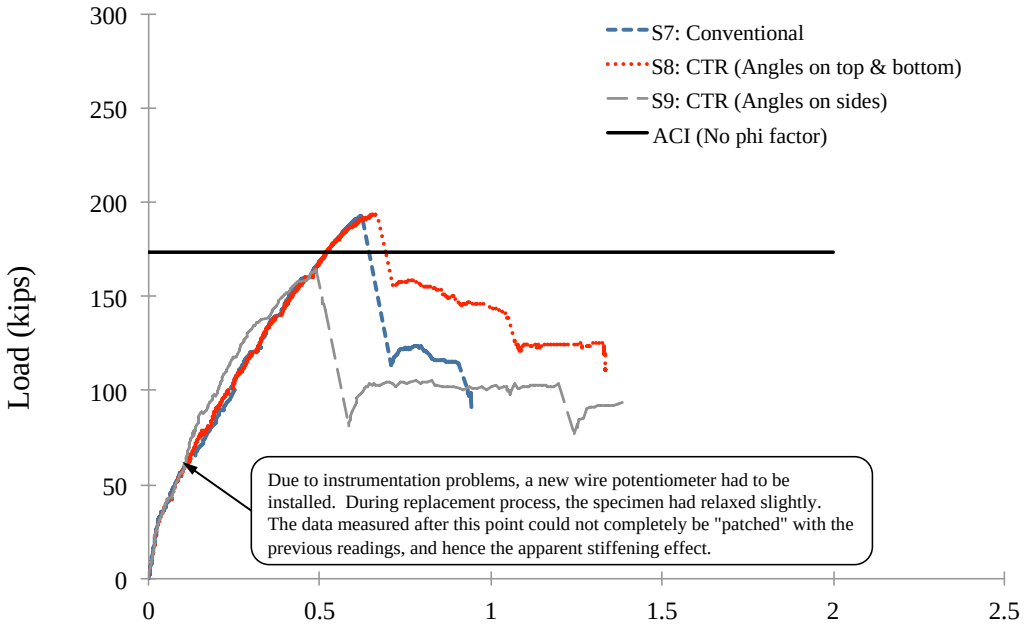

(c) Specimens S7, S8, S9 (s = 10", f'_c = 10,000 psi)

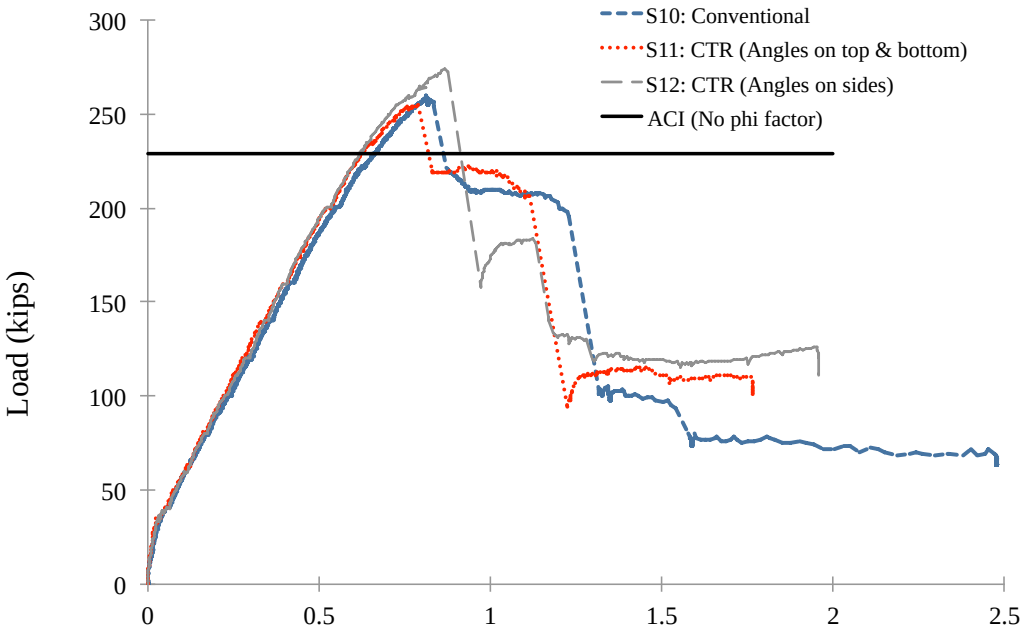

(d) Specimens S10, S11, S12 (s = 5", f'_c = 10,000 psi)

Figure 4.1: Load-deflection relationships (cont.)
CTR: Continuous transverse reinforcement

4.1.3 Failure Mode

The primary failure mode in all the specimens was a combination of diagonal tension and shear compression failure. Furthermore, the contribution of dowel action adding to the shear resistance was evident in all the specimens. Dowel action is defined as the bending of the longitudinal bars spanning a crack opening under direct shear along the cross section of the reinforcement (Huespe et al. 2007)). The failure pattern for specimen S3 shown in Figure 4.2 is a representative illustration of how both specimens with conventional stirrups and continuous transverse reinforcement (CTR) failed.

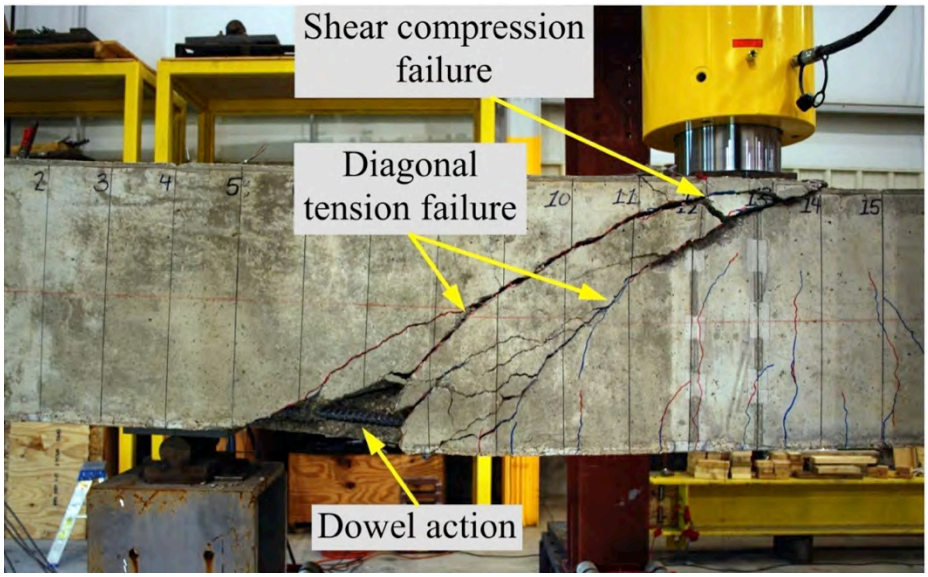

Figure 4.2: Representative failure pattern

After removal of loose concrete in the specimens with CTR, the top stirrup leg was found bowed out upward (see Figure 4.3a). This outward deformation is expected as the top leg acts as anchorage for the vertical legs that resist shear. In the case of conventional U-shaped stirrups, the hooks at the top provide the necessary anchorage. As expected, the small longitudinal top bars, used to hold the cage together, buckled in all the specimens. Moreover, some of the stirrups crossing the diagonal cracks fractured (see Figure 4.3b). Fracture of stirrups is discussed later in Section 4.1.6.

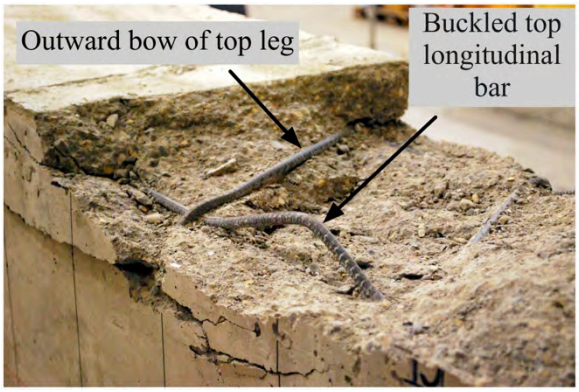

(a) Outward bow and buckling

(b) Fracture

Figure 4.3: Localized damage and failure

4.1.4 Evaluation of Shear Strength from Concrete

The following steps were followed in order to back-calculate the concrete contribution towards shear resistance.

1. The measured stress-strain diagrams for the transverse reinforcement (i.e., No. 3 shown in Appendix J) were consolidated into a single set of values through the use of a Ramberg-Osgood (R-O) (Collins and Mitchell 1991) function shown in Eq. 4.

$$f_{ss} = E_s \varepsilon \left\{ A + \frac{1 - A}{\left[1 + \left(B\varepsilon\right)^c\right]^{1/c}} \right\} \le f_{pu} \qquad \text{Eq. 4}$$

   As shown in Figure 4.4, the R-O function with A = 0.018, B=395, and C=2.9 matches well with two out of the four measured stress-strain diagrams (the other two diagrams were considered outliers and discarded).

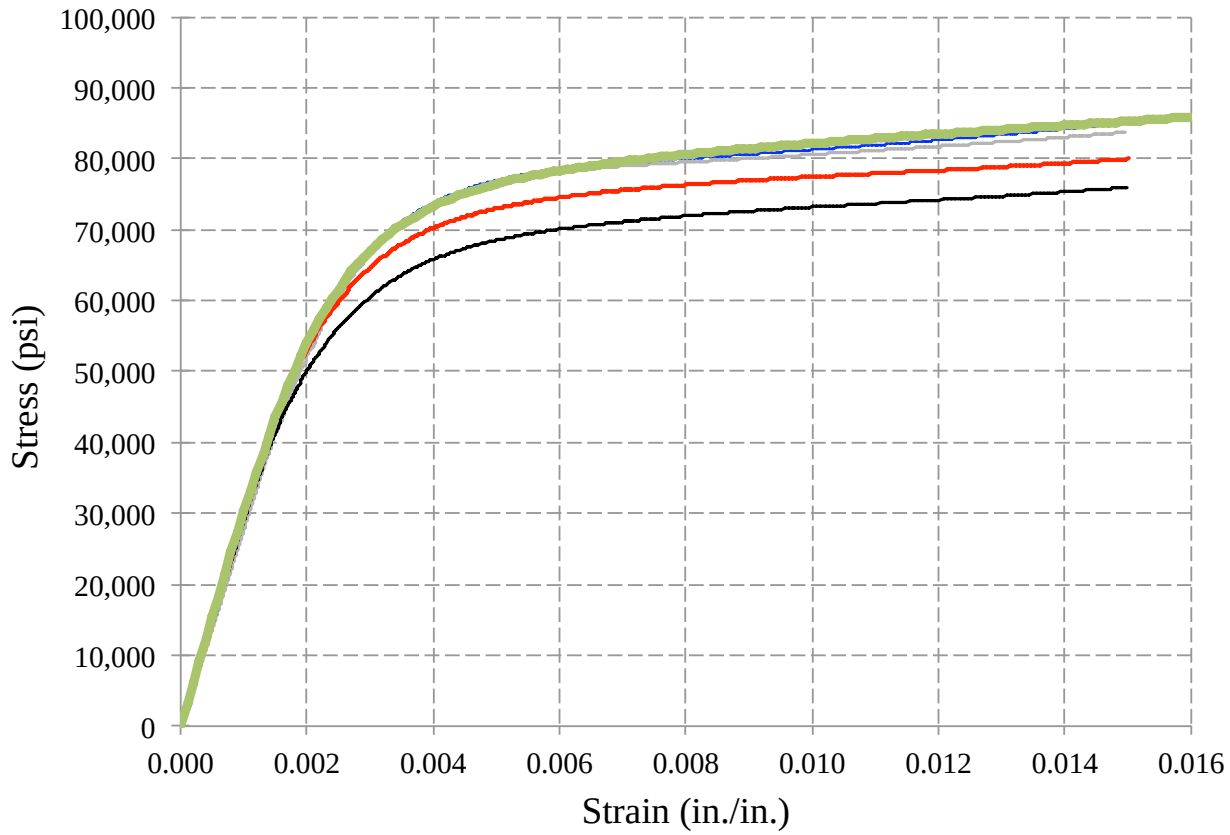

Figure 4.4: Correlation of the measured results by a Ramberg-Osgood function

2. The stress corresponding to a measured value of strain was obtained from the Ramberg-Osgood relationship with the parameters calibrated in step 1.

3. The shear resistance from the transverse reinforcement was obtained from Eq. 5.

$$V_s = \frac{A_v f_v d}{s} \qquad \text{Eq. 5}$$

f_v = stress in transverse reinforcement obtained in step 2

4. Knowing the measured load, the shear force was computed, in particular the shear force in the shorter shear span (a = 54 in.). (The strain gages had been installed in the critical shorter span.)

5. Therefore, $V_c = V - V_s$ where V = shear force computed in step 4 and V_s = shear resistance of transverse reinforcement from step 3.

The shear strength of concrete (V_c) is commonly taken as $2\sqrt{f_c'}b_w d$ although the actual strength is closer to $3.5\sqrt{f_c'}b_w d$. In Section 11.2.2.1 of ACI 318-11, the value of V_c from the more detailed expression is limited to $3.5\sqrt{f_c'}b_w d$. The calculated shear strength provided by concrete, V_c, was normalized with respect to $\sqrt{f_c'}b_w d$. The normalized strength is plotted against the maximum shear force, occurring in the shorter span, in Figure 4.5.

All the specimens exhibit a similar trend. The shear, as expected, is resisted entirely by concrete up to formation of diagonal cracks. Upon cracking, the shear resistance provided by concrete initially dropped but increased again once the transverse reinforcement was fully engaged.

For the specimens made with 5,000-psi concrete (shear specimens S1 to S6 and spliced specimen), the drop in V_c occurs approximately at $1.8\sqrt{f_c'}b_w d$, although there is no significant drop in specimen S5. For specimens S7, S8, S9, which were cast with 10,000-psi concrete and transverse spacing of 10 in., the concrete cracked at approximately $1.6\sqrt{f_c'}b_w d$, which is consistent with a lower than the expected tensile capacity of the 10,000-psi mix. For specimens S10 and S11 with a more tightly spaced transverse reinforcement, diagonal cracking occurred $2.1\sqrt{f_c'}b_w d$. For specimen S12, in which the angled legs were in the shear plane, the drop in V_c occurred at $1.4\sqrt{f_c'}b_w d$, which is the lowest value for all the specimens. As shown in Table 4.3, the concrete shear strength exceeded $2\sqrt{f_c'}b_w d$ in all the specimens with the exception of specimens S7 and S8. No consistent trends could be identified in terms of conventional stirrups versus continuous transverse reinforcement, and both types performed similarly.

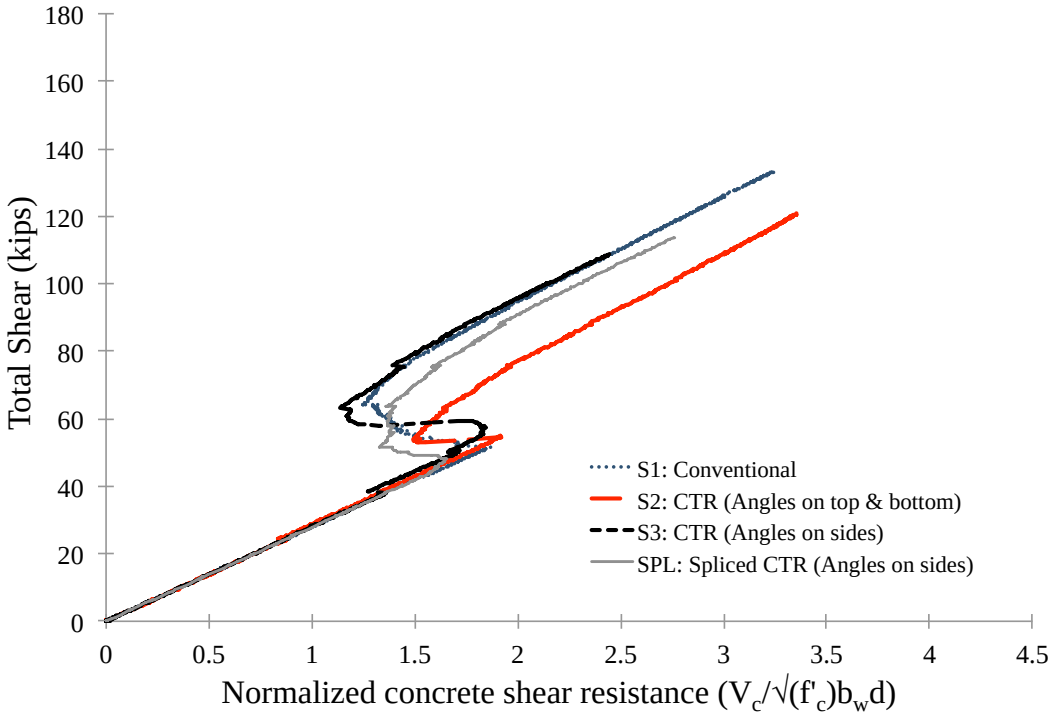

(a) Shear specimens S1, S2, S3, and spliced specimen

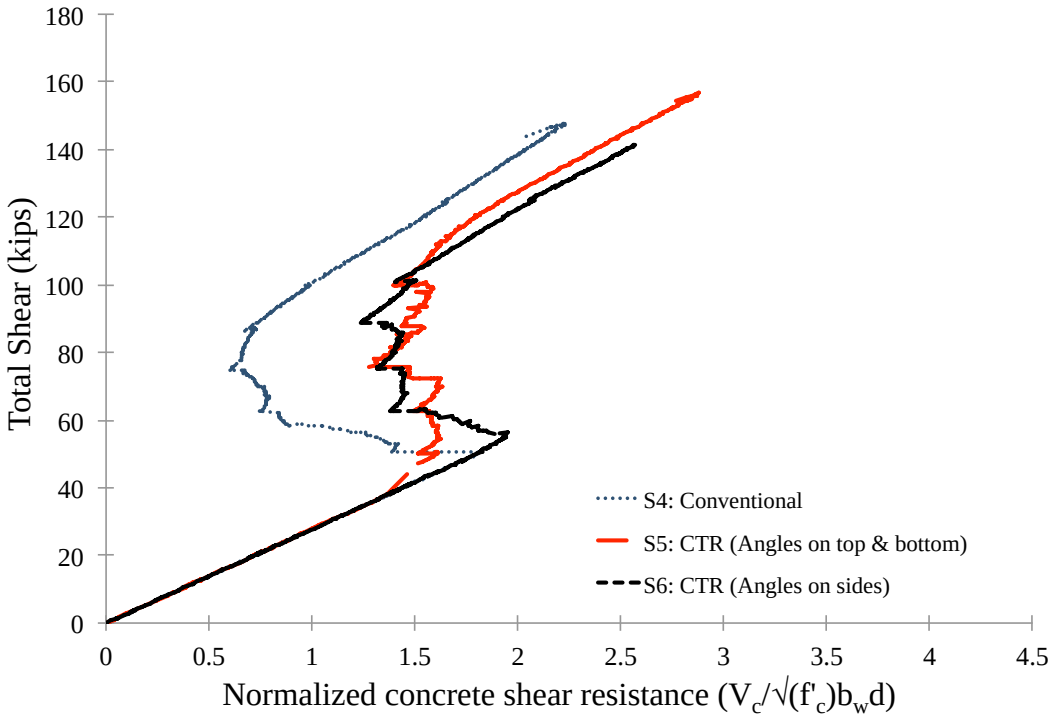

(b) Shear specimens S4, S5, and S6

Figure 4.5: Total shear vs. normalized concrete shear strength
CTR: Continuous transverse reinforcement

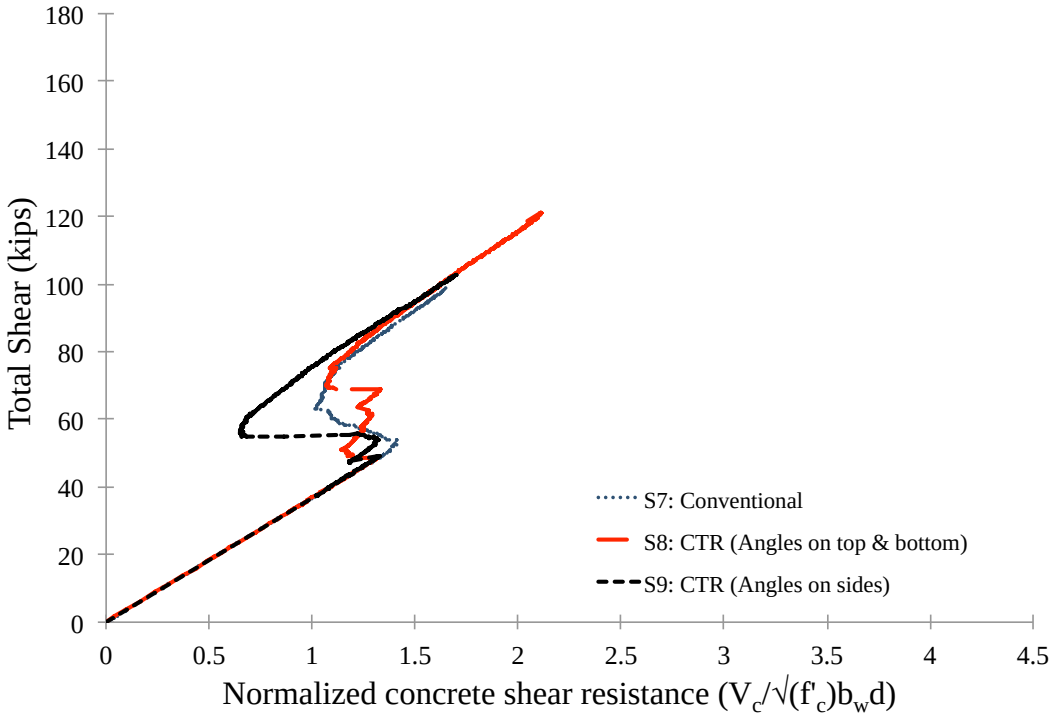

(c) Shear specimens S7, S8, and S9

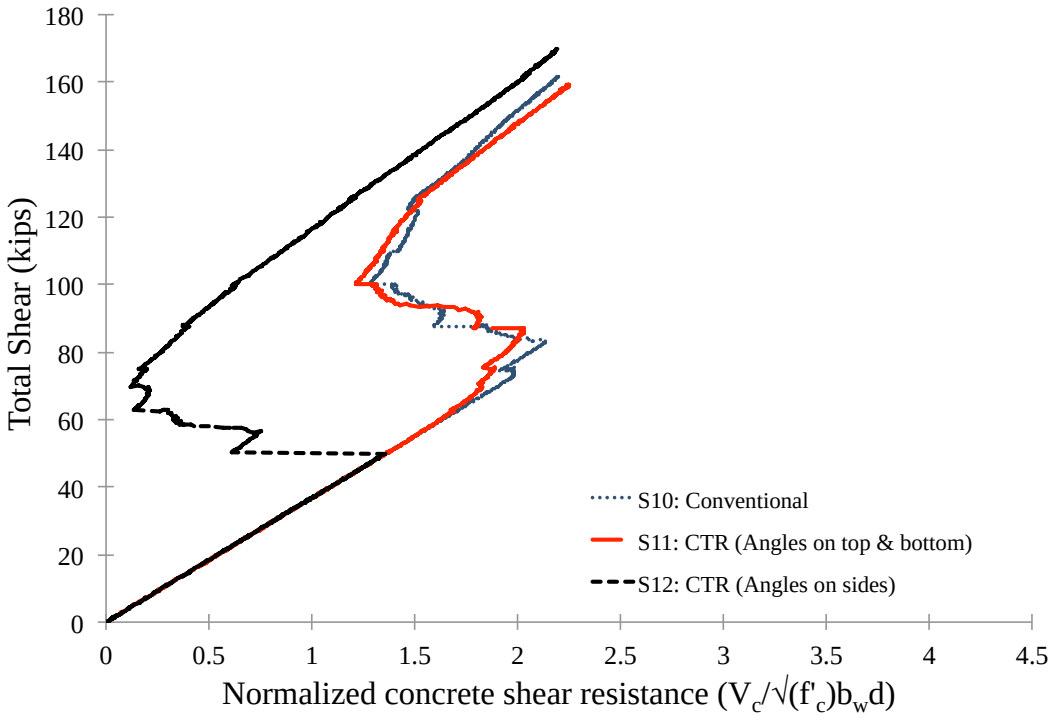

(d) Shear specimens S10, S11, and S12

Figure 4.5: Total shear vs. normalized concrete shear strength (cont.)
CTR: Continuous transverse reinforcement

Table 4.3: Maximum value of normalized V_c

Specimen	$V_c / \sqrt{f_c'} b_w d$
S1: Conventional	3.3
S2: CTR (Angles on top and bottom)	3.4
S3: CTR (Angles on sides)	2.4
S4: Conventional	2.2
S5: CTR (Angles on top and bottom)	2.9
S6: CTR (Angles on sides)	2.6
S7: Conventional	1.7
S8: CTR (Angles on top and bottom)	2.1
S9: CTR (Angles on sides)	1.7
S10: Conventional	2.2
S11: CTR (Angles on top and bottom)	2.2
S12: CTR (Angles on sides)	2.2
SPL: Spliced CTR (Angles on sides)	2.8

4.1.5 Crack Width

The load factors for dead load and live load are 1.2 and 1.6, respectively. A "combined" load factor of 1.5 was assumed in order to determine an approximate value of service load from the maximum measured load. That is, the maximum measured load divided by 1.5 was taken as the service load. An attempt was made to measure the crack widths at service loads obtained based on this assumption. The crack widths were marked and measured on both the front and back faces along the length of the beam. To facilitate the process, 6-in. wide by 12-in. grid lines had been drawn. The crack widths from the two faces were averaged. Note that these values include the effects of both shear and flexural cracks.

The resulting crack widths are plotted in Figure 4.6. The vertical axis for specimens S7, S8, and S9 is plotted at a different scale because of the larger widths in this group. For a group of specimens with comparable details and material properties, there are no discernable differences between the crack widths with the exception of specimen S9, which had continuous transverse reinforcement (CTR) with the angled legs in the shear plane and 10,000-psi concrete. For this specimen, the maximum average crack width is roughly 1.5 times larger than that in comparable specimens S7 and S8. It is important to note that the crack widths for the spliced specimen are comparable to the comparable specimens with either conventional stirrups or CTR. This observation reinforces what has already been concluded regarding the effectiveness of the methodology used to splice two CTR cages. The distribution of cracks along the length is also similar for comparable specimens.

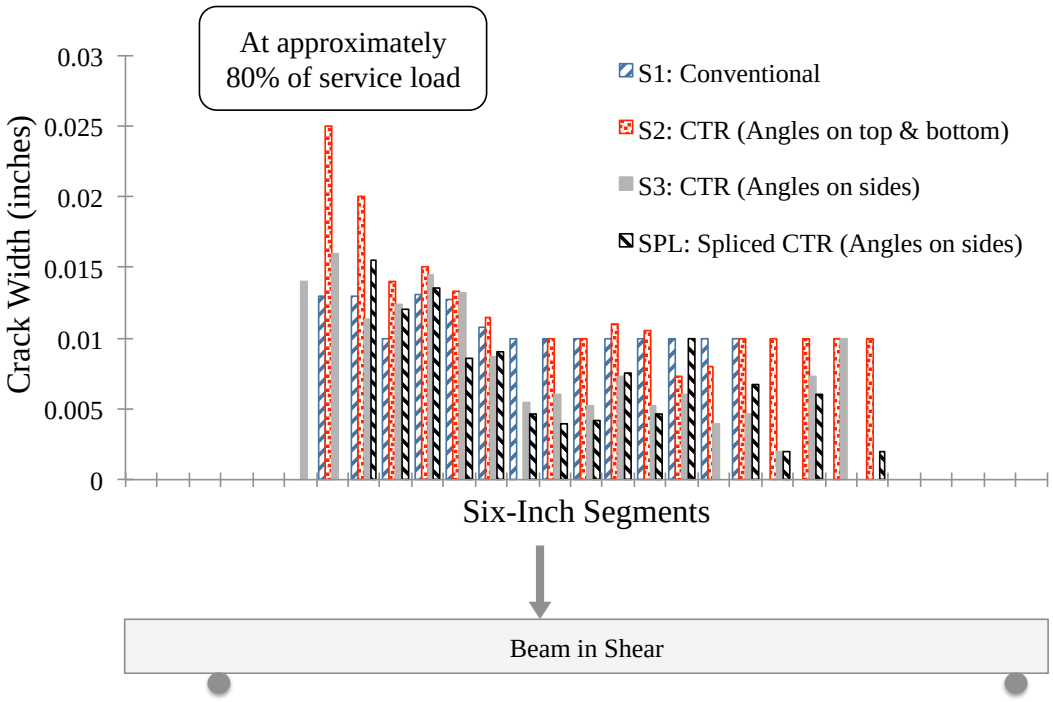

(a) Shear specimens S1, S2, S3, and spliced specimen SPL

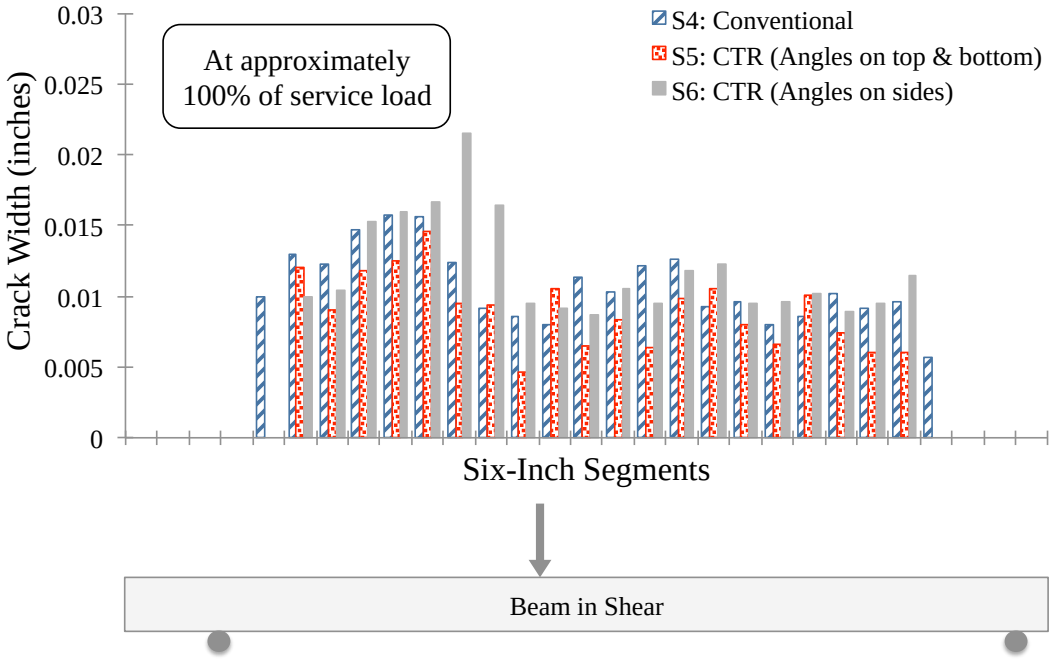

(b) Shear specimens S4, S5, and S6

Figure 4.6: Crack widths
CTR: Continuous transverse reinforcement

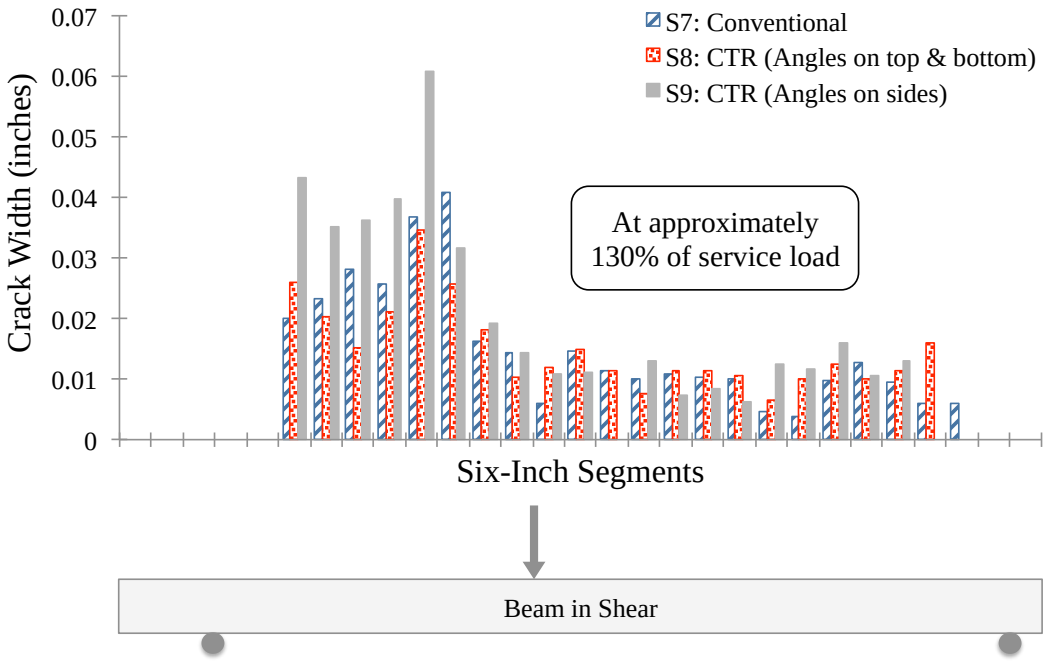

(c) Shear specimens S7, S8, and S9

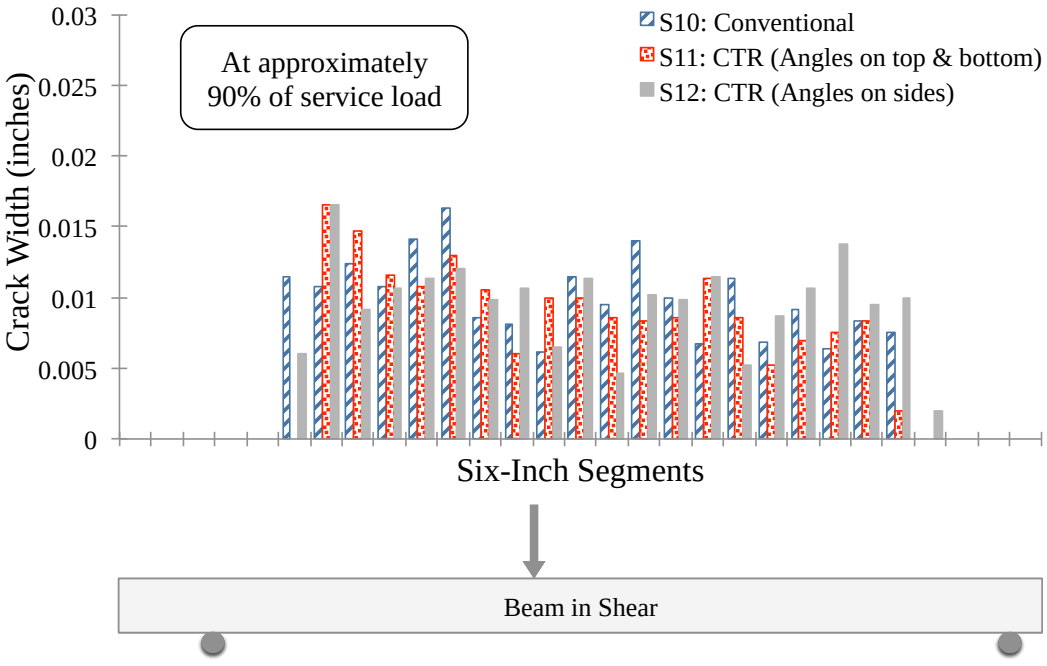

(d) Shear specimens S10, S11, and S12

Figure 4.6: Crack widths (cont.)
CTR: Continuous transverse reinforcement

4.1.6 Influence of Angle of Continuous Transverse Reinforcement

For shear specimens S1, S2, S3, and spliced specimen, the crack patterns at 160 kips are shown in Figure 4.7. This figure depicts a 3-foot section along the span (between grid lines 7 and 12). The actual reinforcement layout is also superimposed on the crack patterns. The crack overlay figures for the remaining specimens are provided in Appendix L.

Between grid lines 7 and 12, four conventional stirrups in specimen S1 cross the diagonal crack; therefore, a total of eight vertical reinforcing bar legs provide shear resistance. For shear specimens S2 and S3 using continuous transverse reinforcement (CTR), nearly seven legs of the transverse reinforcement provide resistance. In the case of the spliced specimen using CTR, five reinforcing bar legs provide shear resistance. For the particular cases shown in Figure 4.7, the vertical resistance of the conventional stirrups is, hence, slightly larger. However, the measured maximum loads (Table 4.1) do not universally support this trend. For specimens with the correct placement of angled legs in CTR (i.e., in the top and bottom), the maximum loads resisted by specimens S2 and S11 are 8% and 2%, respectively, less than their counterparts with conventional stirrups. On the other hand, the maximum loads in specimens S5 and S8 were equal to or larger (by 6%) than comparable beams using conventional U-shaped stirrups.

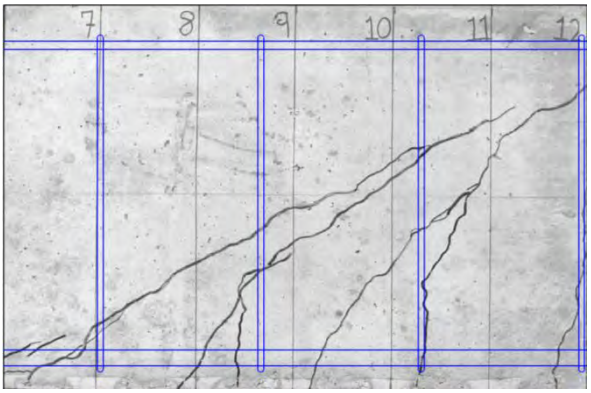

(a) Shear specimen S1
Conventional U-shaped Stirrup

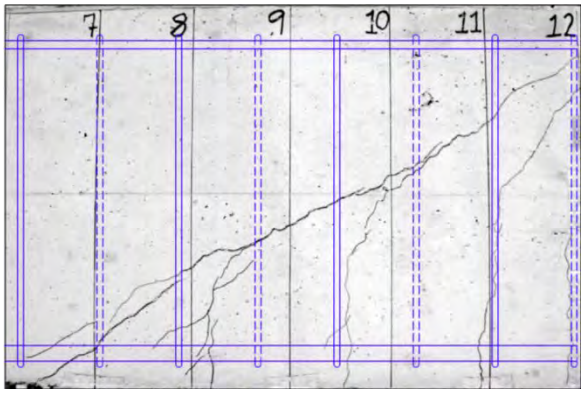

(b) Shear specimen S2
CTR (Angles on top and bottom)

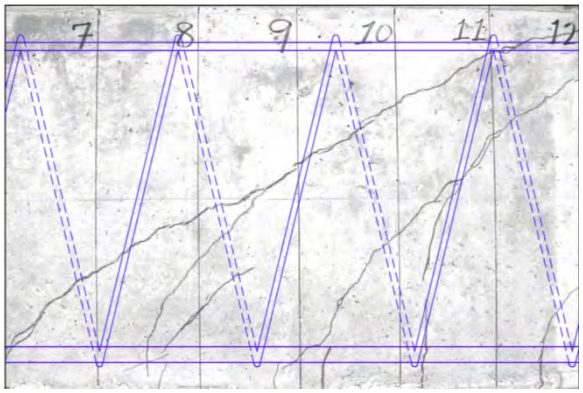

(c) Shear specimen S3
CTR (Angles on sides)

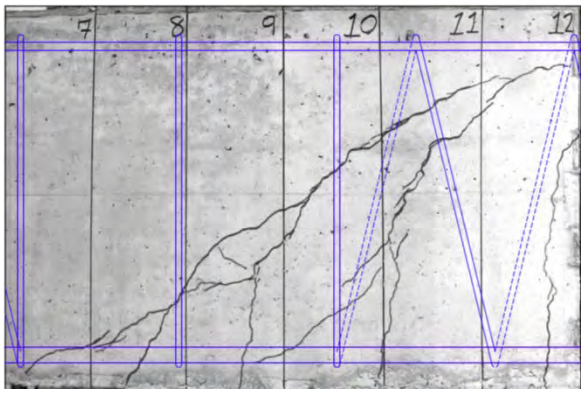

(d) Spliced specimen
CTR (Angles on sides)

Figure 4.7: Crack patterns at 160 kips
CTR: Continuous transverse reinforcement

As discussed in Section 4.1.1, the shear resistance is not the same on the two shear planes if the angled legs in CTR are placed incorrectly, i.e., by being in the vertical surfaces of the beam. This difference could potentially result in a different amount of cracking on the two faces. The average crack widths in specimen S3 on both shear planes are compared in Figure 4.8. The shear resistance of the angled legs on the north face is smaller than the contribution of those located on the south face (refer to Section 4.1.1). The crack widths on the south face are, nevertheless, wider than their counterparts on the north face. Furthermore, the average crack widths on the opposite faces of all the specimens do not indicate a clear trend either, as evident from Table 4.4. In incorrectly installed CTR, the data do not suggest a correlation between the magnitude of crack widths and orientation of the angled legs on the two opposite faces. Note that this issue is irrelevant for properly installed CTR where the angled legs are on the top and bottom faces.

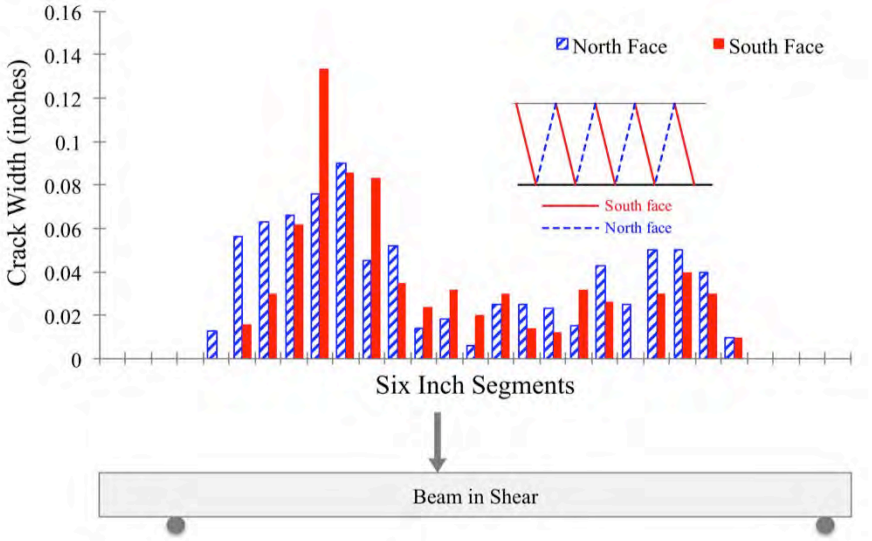

Figure 4.8: Crack widths on different vertical faces

Table 4.4: Average crack widths (in.)

Group	Specimen	South face	North face
1	S1: Conventional	0.019	0.021
	S2: CTR (Angles on top and bottom)	0.026	0.026
	S3: CTR (Angles on sides)	0.022	0.026
2	S4: Conventional	0.042	0.032
	S5: CTR (Angles on top and bottom)	0.032	0.027
	S6: CTR (Angles on sides)	0.034	0.039
3	S7: Convectional	0.052	0.081
	S8: CTR (Angles on top and bottom)	0.061	0.073
	S9: CTR (Angles on sides)	0.106	0.166
4	S10: Conventional	0.028	0.043
	S11: CTR (Angles on top and bottom)	0.032	0.020
	S12: CTR (Angles on sides)	0.030	0.030
	SPL: Spliced CTR (Angles on sides)	0.013	0.025

CTR: continuous transverse reinforcement

The orientation of angled legs in incorrectly installed CTR, however, appears to impact the likelihood for stirrup fracture at or near ultimate loads. In specimens S3 and S6, two diagonal bars fractured; in both cases the fracture occurred on the face where the transverse reinforcement does not provide as much as resistance as the other face. Three out of five fractures in specimen S12 also occurred on the face with a smaller shear resistance. This issue, once again, is not relevant for properly installed CTR.

4.1.7 Summary

In terms of strength, serviceability, and mode of failure, no major differences could be identified between conventional U-shaped stirrups and continuous transverse reinforcement (CTR). The post-failure shear response is improved as a result of confinement from CTR. Well-established procedures can be used for design of beams with CTR. The method implemented to splice CTR cages is simple yet successful.

4.2 Pullout Specimen

As discussed in Section 3.3.2, mechanical couplers were used to transfer the load from a hydraulic jack to the test bars. The measured displacements were inconclusive about whether any slippage occurred within the mechanical coupler. However, the relationships between the applied stress, taken as the applied load divided by the nominal area of two No. 3 reinforcing bar, and strain were sufficient to assess any potential influence of doglegs.

The behavior of a transverse reinforcement with a dogleg may be idealized as shown in Figure 4.9. The "flexibility" of a dogleg may be modeled as a spring with a stiffness of *k*, and the "fixed" support represents the longitudinal bar.

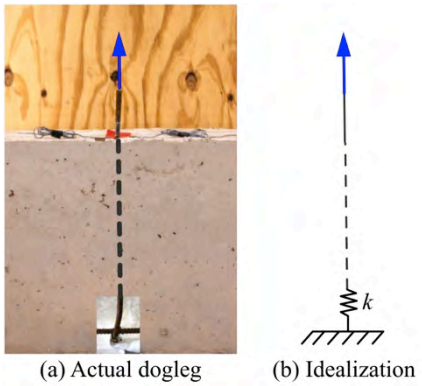

Figure 4.9: Idealization of dogleg

Depending on the value of spring constant, *k*, the stress strain relationships are expected to change as shown in Figure 4.10. If the spring constant is large, the stress-strain relationship of a straight bar (with no dogleg) will be followed. If the dogleg's influence is large, i.e., the value of *k* is small; the stress-strain relationship is different. Initially, the dogleg "straightens" with little resistance while the bar elongates, during which the stress-strain relationship path is from point O to point A, as shown in Figure 4.10. During this stage, the stress that can be developed is less than the corresponding value for the case with no dogleg. The slope of line OA is shallower for

the cases where the influence of the dogleg is more pronounced. At point A, the influence of dogleg is diminished, and any additional elongation is accompanied by a more rapid increase in the stress, i.e., line AB is followed. At point B, the dogleg has "fully straightened" and it no longer influences the behavior, and the stress-strain diagram of the straight bar is followed.

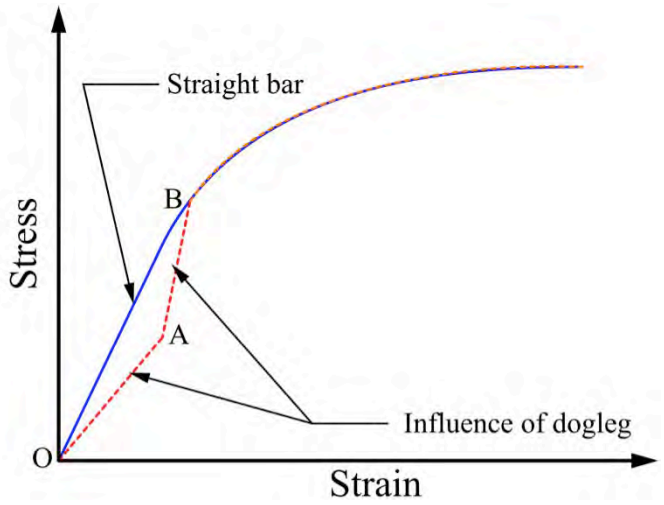

Figure 4.10: Idealization of stress-strain relationships for straight bars and bars with a dogleg

In order to utilize the aforementioned concept, the measured stress-strain relationships for cases with and without a dogleg were compared against the stress-strain diagram based on material testing, as shown in Figure 4.11. In this figure, the diagram from tensile tests is the relationship computed by a Ramberg-Osgood function as discussed in Section 4.1.4.

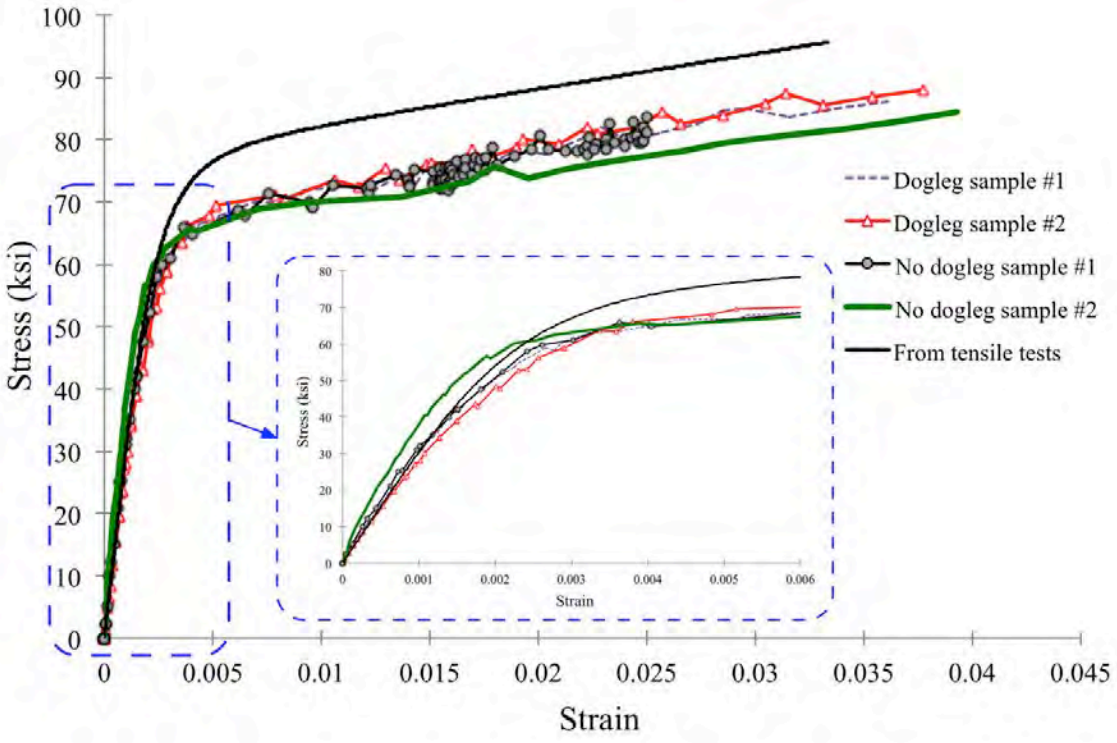

Figure 4.11: Comparison of measured stress-strain diagrams

With the exception of the first test with no dogleg, all the samples were loaded to rupture (Figure 4.12a). The mechanical coupler had not been installed properly for the first test; therefore, the coupler was separated from the reinforcing bar before rupture (Figure 4.12b) but well after the bar had yielded. Therefore, the test results are still valid in terms of assessing the potential influence of doglegs on achieving their yield strength.

(a) Rupture

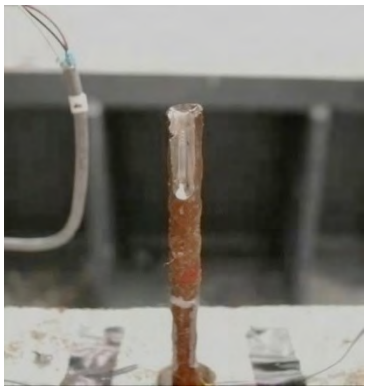

(b) "Block shear" failure due to improper installation of the coupler

Figure 4.12: Failure modes

The measured stress-strain relationships indicate a lower yield strength than that based on material testing. This trend is attributed to the differences in how the strain values were obtained. For material testing, an extensometer with a 2-in. gage length was used, whereas in the pullout tests the strain was measured by a 10-mm (0.39-in.) strain gage. Hence, the stress-strain diagrams in the pullout tests represent a more localized behavior. The cases with a dogleg are similar to those with no dogleg; the differences in the slopes are well within the expected material variability. Moreover, neither of the cases with a dogleg exhibits the behavior depicted in Figure 4.10. Based on the data presented, it is concluded that doglegs do not adversely affect the effectiveness of continuous transverse reinforcement.

4.3 Specimens Subjected to Pure Torque

4.3.1 Capacity

The current ACI 318-11 provides an equation (Eq. 11-21) for computing the torsional capacity of a concrete beam when conventional torsional reinforcement is used, i.e.,

$$T_n = \frac{2A_o A_t f_{yt}}{s}\cot\theta \qquad \text{Eq. 6}$$

Equation 6 was developed based on space truss analogy. A similar equation is derived for cases with continuous transverse reinforcement (CTR), as follows.

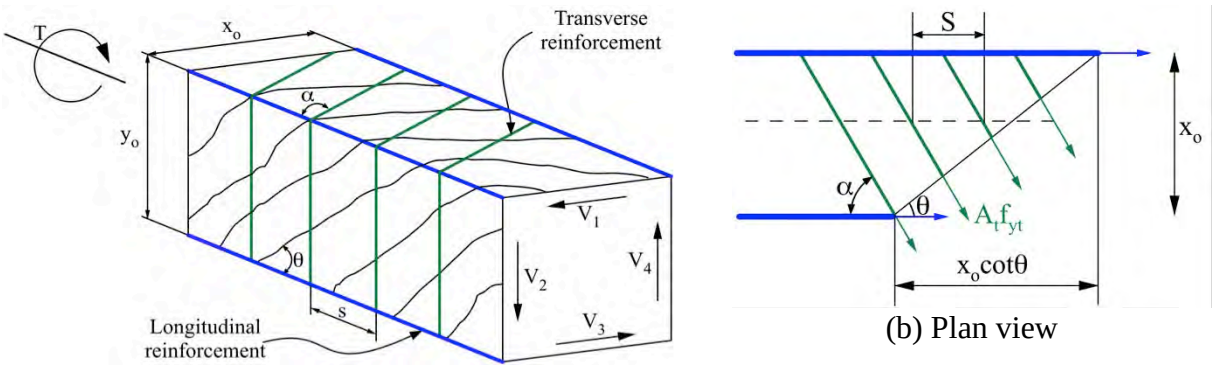

(a) Crack pattern

(b) Plan view

Adopted from Figure R11.5.3.6(a) in ACI 318-11

Figure 4.13: Space truss analogy

$$T_n = V_1\frac{y_o}{2} + V_2\frac{x_o}{2} + V_3\frac{y_o}{2} + V_4\frac{x_o}{2} = V_1\frac{y_o}{2} + V_3\frac{y_o}{2} + V_2 x_o$$

Front & Back Faces:

No. of tranverse reinforing bars crossing diagonal crack $= \dfrac{y_0 \cot\theta}{s}$

$$V_2 = \frac{A_t f_v y_0 \cot\theta}{s}$$

Top face:

$$V_1 = \frac{A_t f_v \left(\cot\theta + \cot\alpha\right) x_o \sin\alpha}{s}$$

Bottom face:

$$V_3 = \frac{A_t f_v \left[\cot\theta + \cot\left(180-\alpha\right)\right] x_o \sin\left(180-\alpha\right)}{s} = \frac{A_t f_v \left(\cot\theta - \cot\alpha\right) x_o \sin\alpha}{s}$$

$$T = \frac{A_t f_v \left(\cot\theta + \cot\alpha\right) x_o \sin\alpha}{s}\frac{y_o}{2} + \frac{A_t f_v \left(\cot\theta - \cot\alpha\right) x_o \sin\alpha}{s}\frac{y_o}{2} + \frac{A_t f_v y_0 \cot\theta}{s} x_o$$

$$T_n = \frac{A_t f_v x_o y_o \cot\theta \sin\alpha}{s} + \frac{A_t f_v x_o y_o \cot\theta}{s}$$

$$\therefore T_n = \frac{A_t f_v x_o y_o \cot\theta \left(1+\sin\alpha\right)}{s} = \frac{A_t f_v A_o \cot\theta \left(1+\sin\alpha\right)}{s}$$

For conventional stirrups, $\alpha = 90^o$. Assuming the stirrups yield, i.e., $f_v = f_{yt}$, the above equation becomes $T_n = \dfrac{2A_t f_v A_o \cot\theta}{s}$, which is the same as Eq. 6 if the transverse reinforcement is assumed to yield, i.e., $f_v = f_{yt}$.

For cases with CTR, the measured angle of the inclined legs (α) was 71^o (or 90^o- 19^o); hence, $T_n = \dfrac{A_t f_{yt}\left(1+\sin 71^o\right) A_o \cot\theta}{s} = \dfrac{1.95 A_t f_v A_o \cot\theta}{s}$, which becomes $T_n = \dfrac{1.95 A_t f_{yt} A_o}{s}$ if the

transverse reinforcement is assumed to yield. Therefore, the following equations can be used to compute the nominal torsional strength.

Conventional stirrups: $T_n = \frac{2A_o A_t f_{yt} \cot\theta}{s}$ Eq. 7(a)

Continuous transverse reinforcement: $T_n = \frac{A_t f_{yt}\left(1+\sin 71^o\right) A_o \cot\theta}{s} = \frac{1.95 A_t f_v A_o \cot\theta}{s}$ Eq. 7(b)

Using the measured material properties and average as-built dimensions, the capacity of each specimen was computed based on Eq. 7(a) and 7(b). The value of θ was taken as 45^o according to Section 11.5.3.6(a) in ACI 318-11.

Conventional stirrups:

$$T_n = \frac{2A_o A_t f_{yt} \cot\theta}{s}$$

Due to construction error, the covers to the bottom and top stirrups were 1.125" and 1.875", respectively, instead of 1.5".

$$x_o = 12.1 - 2\times(1.5 + 0.5\times 3/8) = 11.69\ in.$$

$$y_o = 16 - (1\frac{7}{8} + 0.5\times 3/8) - (1\frac{1}{8} + 0.5\times 3/8) = 12\frac{5}{8}\ in.$$

$$A_o = 0.85 A_{oh} = 0.85\left(x_o \times y_o\right) = 93.3\ in.^2$$

$$A_o = 0.85 A_{oh} = 0.85\left(12\frac{1}{16} - 2\times 1\frac{1}{2} - 2\times\frac{3/8}{2}\right)\left(16 - 2\times 1\frac{1}{2} - 2\times\frac{3/8}{2}\right) = 93.2\ in.^2$$

$$T_n = \frac{2\times 93.3\,in.^2 \times 0.11\,in.\times 71\,ksi\times 1}{5\,in.} = 291\ k-in.$$

Continuous transverse reinforcement:

$$T_n = \frac{1.95 A_o A_t f_{yt}\cot\theta}{s} = \frac{1.95\times 93.3\,in.^2\times 0.11\,in.\times 71\,ksi\times 1}{5\,in.} = 284\ k-in.$$

The maximum measured torque is compared against its calculated capacity in Table 4.5. Due to control issues of the servo-valve controlled actuator, specimen T1 was damaged suddenly at the beginning, and no data are available for this specimen.

The measured torque resisted by specimens T3b, T5b, and T4 is less than the calculated capacity. The inadequacy of specimen T4 is attributed to the high cement content of the 10,000-psi mix that was used. (A similar observation was made for shear specimens.) In case of specimens T3b and T5b, the direction of applied torque was such that the diagonal cracks did not cross the same number of legs of the transverse reinforcement as T3a and T3b. As a result, the capacity of these specimens was less than their "a" series counterpart, approximately 17% for the 5,000-psi specimens and 18% for those with 10,000-psi concrete. However, in comparison to the calculated capacities, the reduction is small (2 to 4%).

The spacing of the transverse reinforcement was 5 in. to meet requirements of ACI 318-11 Section 11.5.6.1 (the spacing is limited to the smaller of $p_h/8$ or 12 in.). It is anticipated that

using a smaller spacing could potentially lessen the impact of the observed directionality effect, although this option poses constructability issues.

In members subjected to pure torsion, diagonal cracks form on all four faces. Therefore, the capacity should not be affected by the location of the angled legs of CTR. This trend is evident by comparing the capacity of specimens T2 (with the angled legs on the top and bottom faces) and T3a (in which the angled legs were on the side faces); their actual capacities are only 3% different. Similarly, the capacities of specimens T3b and T5b are within 2% of each other, even though the angled legs were on different faces. In case of shear loading, as discussed in Section 4.1.1, the capacity is influenced by whether the angled legs are in the shear plane (i.e., the face where diagonal crack form) or not.

Table 4.5: Calculated capacities and maximum measured torques

Specimen	Calculated Nominal Capacity (k-in.)	Measured Maximum Torque (k-in.)	Measured / Calculated
T1: Conventional closed stirrups	291	---	---
T2: CTR with angles on top/bottom (C.W.)	284	326	1.15
T3a: CTR with angles on side (C.W.)	284	337	1.19
T3b: CTR with angles on side (C.C.W.)	284	276	0.97
T4: Standard U-stirrups	291	287	0.99
T5a: CTR with angles on top/bottom (C.W.)	284	345	1.21
T5b: CTR with angles on top/bottom (C.C.W.)	284	282	0.99

CTR: continuous transverse reinforcement

According to Equations 6a or 6b, the nominal torsional capacity is not dependent on the concrete compressive strength. The measured maximum loads indicate a slightly larger capacity when high-strength concrete is used; the maximum load resisted by T5a, which was made a 10,000-psi concrete, is approximately 6% larger than a similar specimen using 5,000-psi concrete, i.e., specimen T2.

4.3.2 Overall Response

The relationships between the applied torque and angle of twist are plotted in Figure 4.14. For comparable 5,000-psi specimens (T2 and T3a), the specimens with angled legs on the top and bottom faces or on the sides exhibit the same stiffness (as indicated by the slope of torque versus angle of twist). This observation further supports the conclusion that the location of the angled legs in CTR used as torsional reinforcement is not significant. Specimen T3b cracked at a smaller torque than the two other specimens; however, the behavior of all three specimens was nearly identical up to cracking. The impact of the direction of torque relative to the orientation of how CTR "spirals" is evident by a smaller cracking torque and a smaller post-peak stiffness of T3b.

In case of the 10,000-psi specimens, the specimen with conventional torsional reinforcement (T4) cracked at a smaller torque than specimen T5a, which had top and bottom

stirrup legs inclined so as to better arrest the diagonal cracks. The behavior of T4 and T5b was similar up to 220 k-in., beyond which specimen T4 maintained capacity better than T5b.

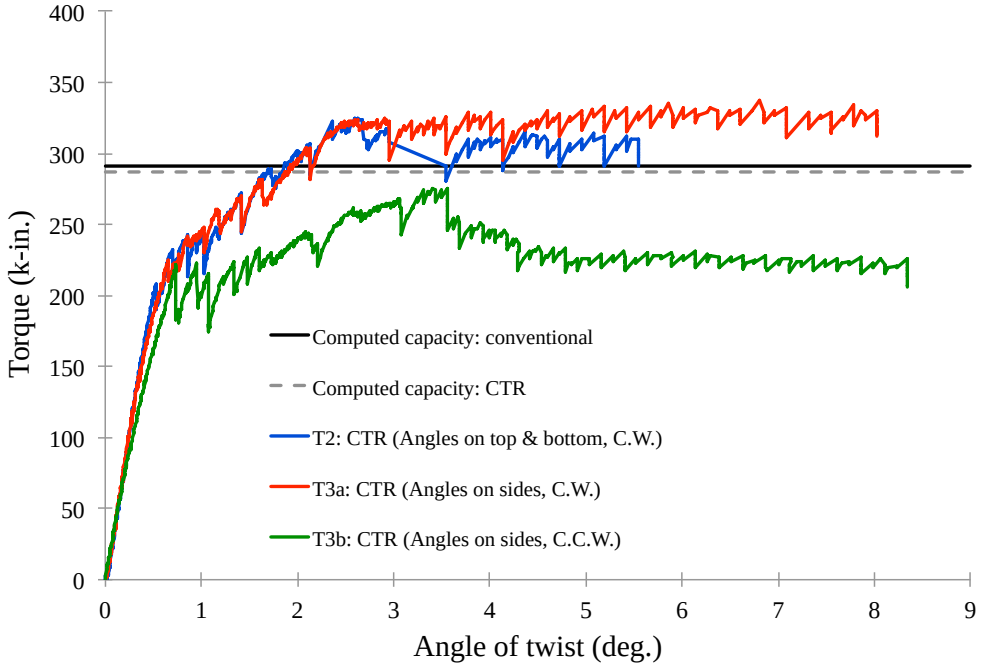

(a) 5000-psi specimens

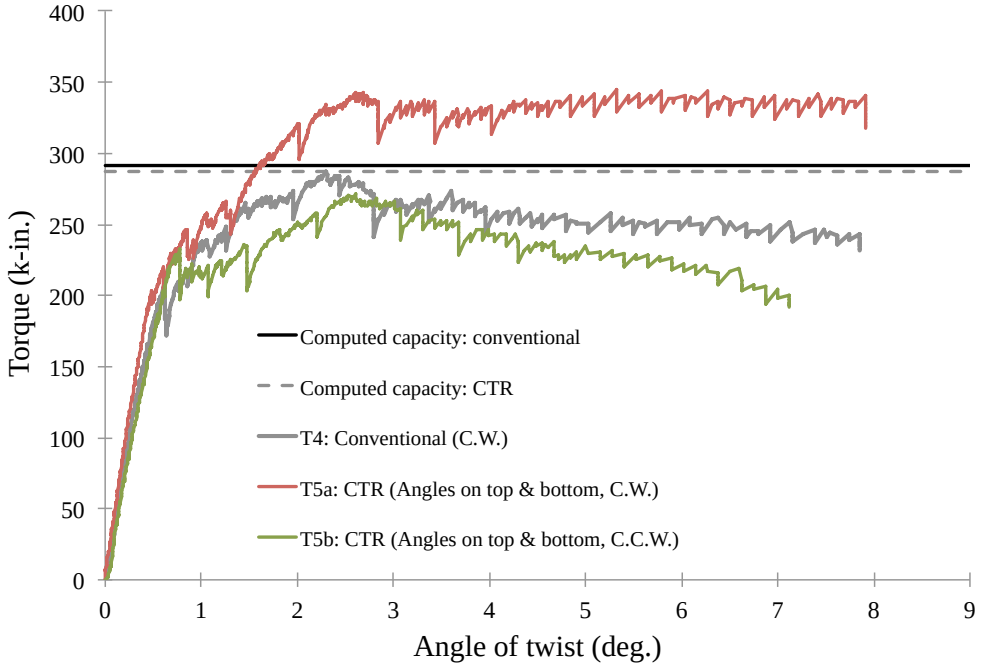

(b) 10,000-psi specimens

Figure 4.14: Measured torque-angle of twist relationships
CTR: Continuous transverse reinforcement

4.3.3 Damage Pattern

At the conclusion of loading, the damage consisted of major cracks spiraling on all four faces, which is expected for pure torsional loading. Cracking in specimens T2 and T3a was not to a level that the concrete cover could be removed. However, large portions of the concrete could easily be chipped in the other specimens due to more significant damage sustained. As explained previously, the tensile capacity of the 10,000-psi specimens is less than the expected value (refer to Table 3.7). As a result, the 10,000-psi specimens experienced significant amount of spalling regardless of the type torsional reinforcement. Representative photographs of damage are provided in Figure 4.15. The importance of the direction of diagonal cracks due to torsion versus the directional angle of the CTR "spiral" becomes evident by comparing the level of damage in T3a and T3b.

(a) Specimen T2

(b) Specimen T3a

(c) Specimen T3b

Figure 4.15: Damage patterns
5,000-psi specimens

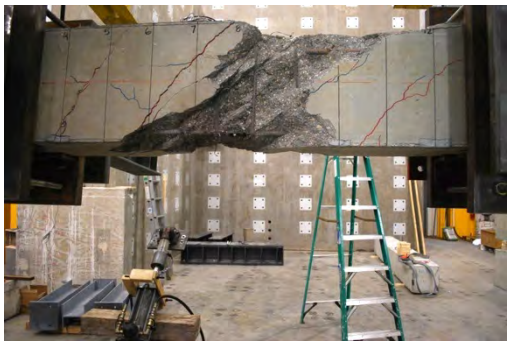


Specimen T4


Specimen T5a


Specimen T5b

Figure 4.15: Damage patterns (cont.)
10,000-psi specimens

4.3.4 Evaluation of Torsional Strength from Concrete

The following steps were followed in order to back-calculate the torsional strength of concrete.

1. Using the same procedure used in Section 4.1.4, a Ramberg-Osgood function was used to represent the measured strain-strain diagrams for the transverse reinforcement.

2. The stress corresponding to a measured value of strain was obtained from the Ramberg-Osgood relationship established in step 1. As shown in Figure 4.16, four strain gages had been bonded to the transverse reinforcement (Top, Bottom, E, and W).

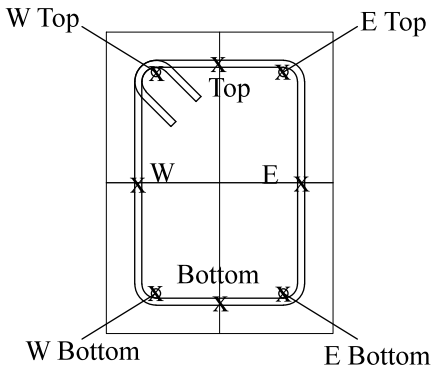

Figure 4.16: Strain gage locations and labels

3. Compute the force in each leg of the transverse reinforcement by multiplying the stresses determined in step 2 by the nominal cross-sectional area of the transverse reinforcement, i.e., compute V_1, V_2, V_3, and V_4 , shown in Figure 4.17

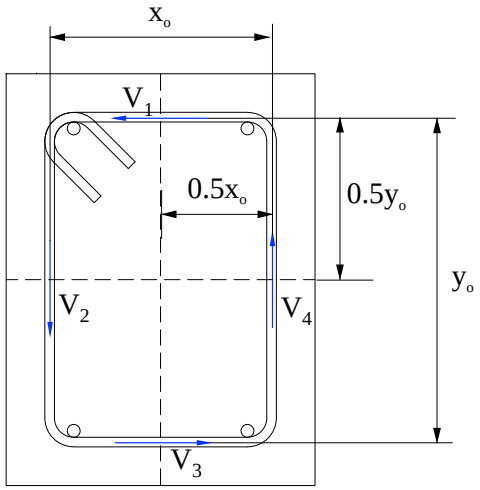

Figure 4.17: Shear flow

4. The shear resistance from the transverse reinforcement was obtained from Eq. 8.

$$T_s = (V_1)\left(\frac{y_0}{2}\right) + (V_2)\left(\frac{x_0}{2}\right) + (V_3)\left(\frac{y_0}{2}\right) + (V_4)\left(\frac{x_0}{2}\right) \qquad \text{Eq. 8}$$

5. Therefore, $T_c = T - T_s$ where T = the applied torque and T_s = torque resistance of transverse reinforcement from step 4. The value of T_c was normalized with respect to $\sqrt{f_c'}\left(\frac{A_{cp}^2}{p_{cp}}\right)$. Per ACI Section 11.5.1(a), the effects of torsional loading can be neglected if the factored torque is less than $\sqrt{f_c'}\left(\frac{A_{cp}^2}{p_{cp}}\right)$; this value corresponds to one quarter of the cracking torque (T_{cr}).

The relationships between the total applied torque and normalized T_c are plotted in Figure 4.18. Up to cracking, the applied torque was resisted entirely by concrete, as expected. Once the specimens cracked, the contribution of concrete dropped and the applied torque was resisted by a combination of the torsional resistance provided by concrete (T_c) and transverse reinforcement (T_s).

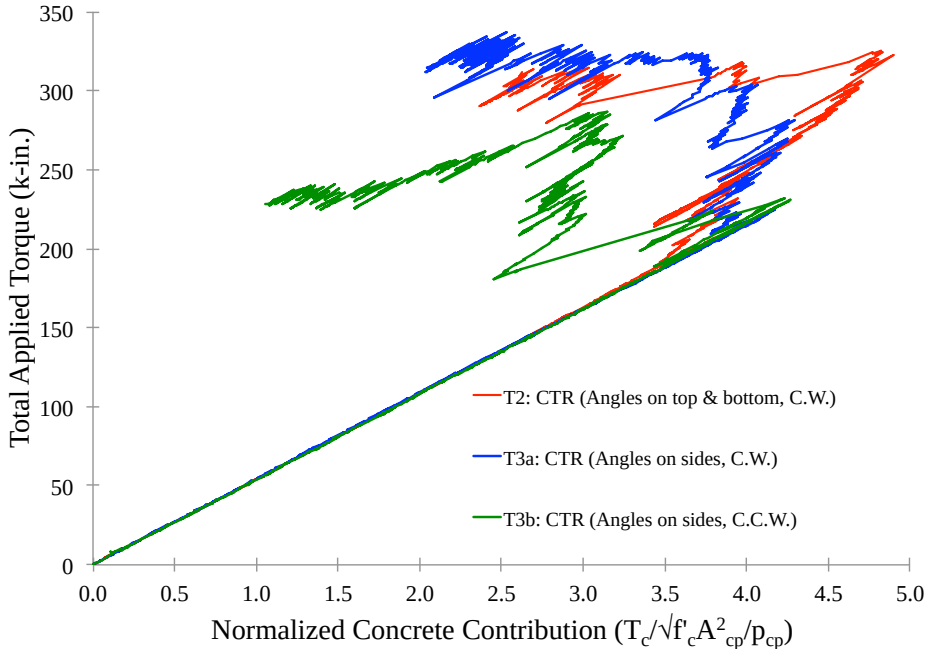

(a) 5,000-psi specimens

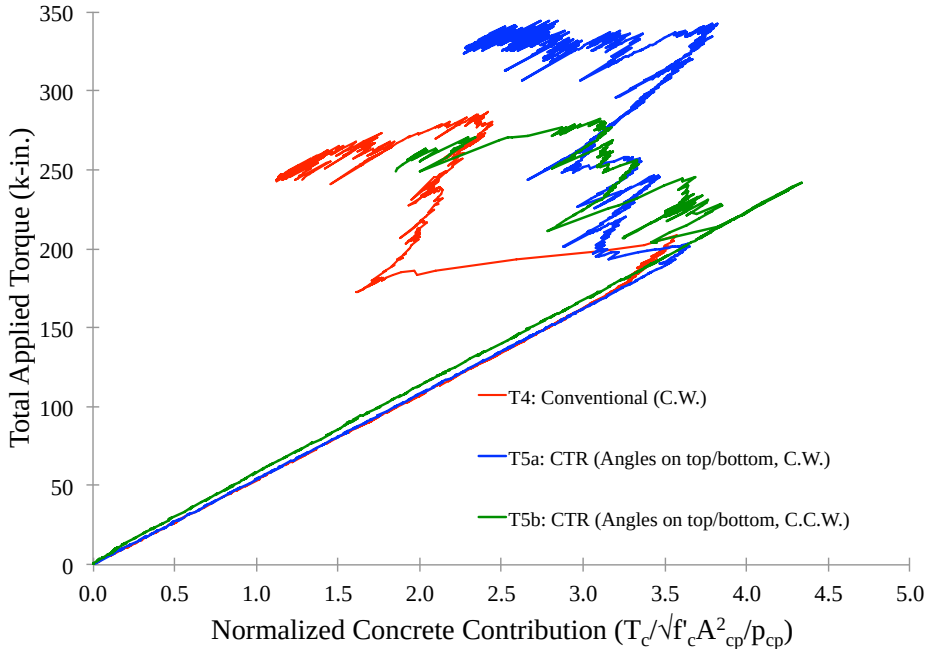

(b) 10,000-psi specimens

Figure 4.18: Applied torque vs. normalized torsional resistance of concrete
CTR: Continuous transverse reinforcement

The maximum and minimum values of normalized value of T_c are summarized in Table 4.6. With the exception of specimens T4 and T5a, the concrete contribution was at least $4.3\sqrt{f_c'}\left(\frac{A_{cp}^2}{p_{cp}}\right)$, i.e., the cracking torque exceeded the expected cracking capacity per ACI 318-11, i.e., $4\sqrt{f_c'}\left(\frac{A_{cp}^2}{p_{cp}}\right)$. The smaller cracking torque for T4 and T5a is attributed to the low tensile capacity of the 10,000-psi mix. For specimens T3b and T5b, the torsional resistance from concrete at the conclusion of testing had dropped significantly more than the corresponding "a" series specimens, i.e., specimens T3a and T5a. The direction of CTR relative to the applied twist did not affect the maximum cracking torque because transverse reinforcement is engaged only after cracking; hence, the details of transverse reinforcement is not relevant prior to cracking.

Table 4.6: Maximum and minimum value of normalized T_c (k-in.)*

Specimen	Maximum	Minimum
T2: CTR (Angles on top and bottom, C.W.)	4.9	2.6
T3a: CTR (Angles on sides, C.W.)	4.3	2.3
T3b: CTR (Angles on sides, C.C.W.)	4.3	1.1
T4: Conventional (C.W.)	3.6	1.3
T5a: CTR (Angles on top and bottom, C.W.)	3.8	2.4
T5b: CTR (Angles on top and bottom, C.C.W.)	4.3	1.9

CTR: continuous transverse reinforcement

*T_c = Tabulated values times $\sqrt{f_c'}\left(\frac{A_{cp}^2}{p_{cp}}\right)$

4.3.5 Evaluation of Longitudinal Force and Reinforcement

As shown in Figure 4.13, diagonal cracks "spiral" around the member. Struts form between these diagonal cracks, which can be assumed to be subjected to identical compressive stresses f_{cd} as shown in Figure 4.19. This figure represents the state of stresses and forces on the vertical faces; a similar free-body diagram can be drawn for the top and bottom faces.

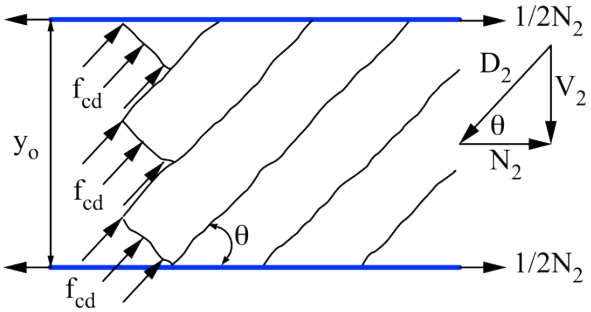

Transverse reinforcement is not shown for clarity.

Figure 4.19: Diagonal struts and compressive stresses due to torsion

From the forces shown in Figure 4.19, $N_2 = V_2 \cot\theta$. Note that the longitudinal force (N_2) is the same for both vertical faces. Similarly, the longitudinal forces on the top and bottom faces are $N_1 = V_1 \cot\theta$ and $N_3 = V_3 \cot\theta$, respectively. (Expressions for V_1, V_2, and V_3 were derived in Section 4.3.1.).

The total longitudinal force is obtained as follows.

$$N = 2N_2 + N_1 + N_3 = \left(2V_2 + V_1 + V_3\right)\cot\theta$$

$$N = \left[2\frac{A_t f_v y_0 \cot\theta}{s} + \frac{A_t f_v \left(\cot\theta + \cot\alpha\right) x_o \sin\alpha}{s} + \frac{A_t f_v \left(\cot\theta - \cot\alpha\right) x_o \sin\alpha}{s}\right]\cot\theta$$

$$N = 2\left(y_0 + x_o \sin\alpha\right)\frac{A_t f_v}{s}\cot^2\theta$$

If the transverse reinforcement is assumed to yield, which is consistent with ACI 318-11, the total longitudinal force becomes $N = 2\left(y_0 + x_o \sin\alpha\right)\frac{A_t f_{yt}}{s}\cot^2\theta$. Longitudinal reinforcement in addition to that for flexure has to be provided to resist N. The required area of additional longitudinal reinforcement is computed from Eq. 9.

$$A_l f_y \geq N$$

$$A_l \geq 2\left(y_0 + x_o \sin\alpha\right)\frac{A_t}{s}\left(\frac{f_{yt}}{f_y}\right)\cot^2\theta \qquad \text{Eq. 9}$$

For conventional transverse reinforcement, $\alpha = 90^o$; hence, Eq. 9 becomes

$A_l \geq 2\left(y_0 + x_o\right)\frac{A_t f_{yt}}{s f_y}\cot^2\theta$ *or* $A_l \geq p_h \frac{A_t}{s}\left(\frac{f_{yt}}{f_y}\right)\cot^2\theta$. This equation is the same as Eq. 11-22 in ACI 318-11.

Based on Eq. 9, the required amount of longitudinal reinforcement was computed for cases with conventional transverse reinforcement and those using continuous transverse reinforcement (CTR).

$$x_o = 12\frac{1}{16} - 2\times 1\frac{1}{2} - 2\times\frac{3/8}{2} = 8\frac{11}{16}$$

$$y_o = 16 - \left(1\frac{7}{8} + \frac{3/8}{2}\right) - \left(1\frac{1}{8} + \frac{3/8}{2}\right) = 12\frac{5}{8}$$

$$p_h = 2(8\frac{11}{16} + 12\frac{5}{8}) = 42\frac{5}{8}$$

Due to construction error, the covers to the bottom and top stirrups were 1 1/8" and 1 7/8", respectively, instead of 1.5".

(a) Conventional

$$A_l \geq 2\left(y_0 + x_o \sin\alpha\right)\frac{A_t}{s}\left(\frac{f_{yt}}{f_y}\right)\cot^2\theta$$

$$\alpha = 90^o \quad \therefore A_l \geq p_h \frac{A_t}{s}\left(\frac{f_{yt}}{f_y}\right)\cot^2\theta$$

$$A_l \geq 42\frac{5}{8}in.\times\frac{0.11\ in.^2}{5\ in.}\times\left(\frac{71\ ksi}{60\ ksi}\right)\times\cot^2\left(45^o\right)$$

$$A_l \geq 1.11\ in.^2$$

(b) CTR

$$A_l \geq 2\left(y_0 + x_o \sin\alpha\right)\frac{A_t}{s}\left(\frac{f_{yt}}{f_y}\right)\cot^2\theta$$

$$A_l \geq 2\left(8\frac{11}{16}in. + (12\frac{5}{8}in.)\sin 71^o\right)\frac{0.11\ in.^2}{5\ in.}\left(\frac{71\ ksi}{60\ ksi}\right)\cot^2 45^o$$

$$A_l \geq 1.07\ in.^2$$

As expected the two values are essentially the same. These values have to be checked against the minimum value of A_l specified in Section 11.5.5.3 of ACI 318-11.

As shown in Appendix K, strain gages had been bonded to each of the longitudinal bars placed to resist longitudinal forces due to torsion. Using the Ramberg-Osgood function described in Section 4.1.4, stresses corresponding to the measured strain data were obtained. The force in each bar is simply the "derived" stress multiplied by the nominal cross sectional area.

In Figure 4.20, the total tensile force due to torsion is plotted versus the applied torque. For a given value of applied torque, the longitudinal forces differ among the comparable specimens. This difference is attributed primarily to local variations in the level of cracking that affect the measured strains and hence the computed bar forces. Despite these differences, the maximum longitudinal forces are fairly close for all the specimens (see Table 4.7). The difference is 15% (between specimens T5b and T4). As calculated above, the required area of longitudinal reinforcing bar is approximately 1.1 in.^{2}; from practical considerations four No. 5 longitudinal bars with a total area of 1.24 in.^{2} had been provided. The available capacity (1.24 in.^{2} x 60 ksi =74 kips) is more than adequate to resist the longitudinal force due to torsion.

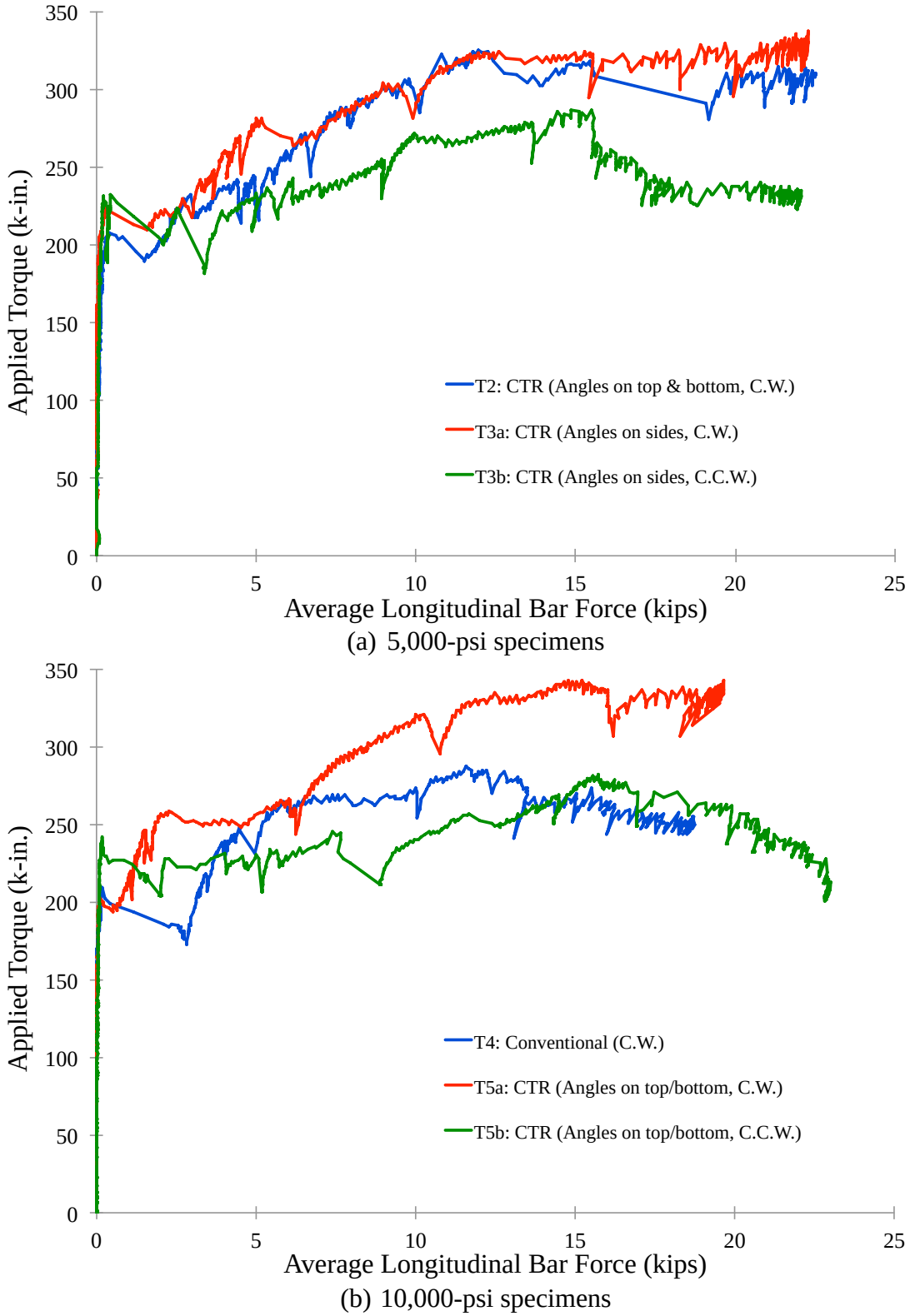

Figure 4.20: Variation of longitudinal force due to torsion
CTR: Continuous transverse reinforcement

Table 4.7: Maximum longitudinal force due to torsion

Specimen	Force (kips)
T1: Conventional closed stirrups	---
T2: CTR with angles on top/bottom (C.W.)	22.5
T3a: CTR with angles on side faces (C.W.)	22.3
T3b: CTR with angles on side faces (C.C.W.)	22.1
T4: Standard U-stirrups	19.5
T5a: CTR with angles on top/bottom (C.W.)	22.2
T5b: CTR with angles on top/bottom (C.C.W.)	23.0

CTR: continuous transverse reinforcement

4.3.6 Crack Width

The crack widths were measured on both vertical faces. Along the length of the beam, 6-in. wide by 8-in. high grid lines had been drawn to facilitate the documentation process. The crack widths from the two faces were averaged. Similar to the shear specimens and spliced specimen (see Section 4.1.5), a "combined" load factor of 1.5 was assumed in order to obtain an approximate value of service level torque from the maximum measured torque. The crack widths at this torque were small and not measurable. Figure 4.21 plots the crack widths at an applied torque equal to 1.5 times the calculated service level torque for the 5,000-psi specimens, and 1.3 times the calculated service level torque for the 10,000-psi specimens.

Although the crack widths within a particular grid line differ among different specimens with comparable details and material properties, there are no discernable differences between the crack widths when considering the entire member. The average of all the crack widths for the entire member was found to be nearly the same in comparable specimens. The crack widths were not influenced by the "spiral" direction of the CTR. The details of transverse reinforcement do not affect the service load behavior because the transverse reinforcement is not fully engaged yet at this stage.

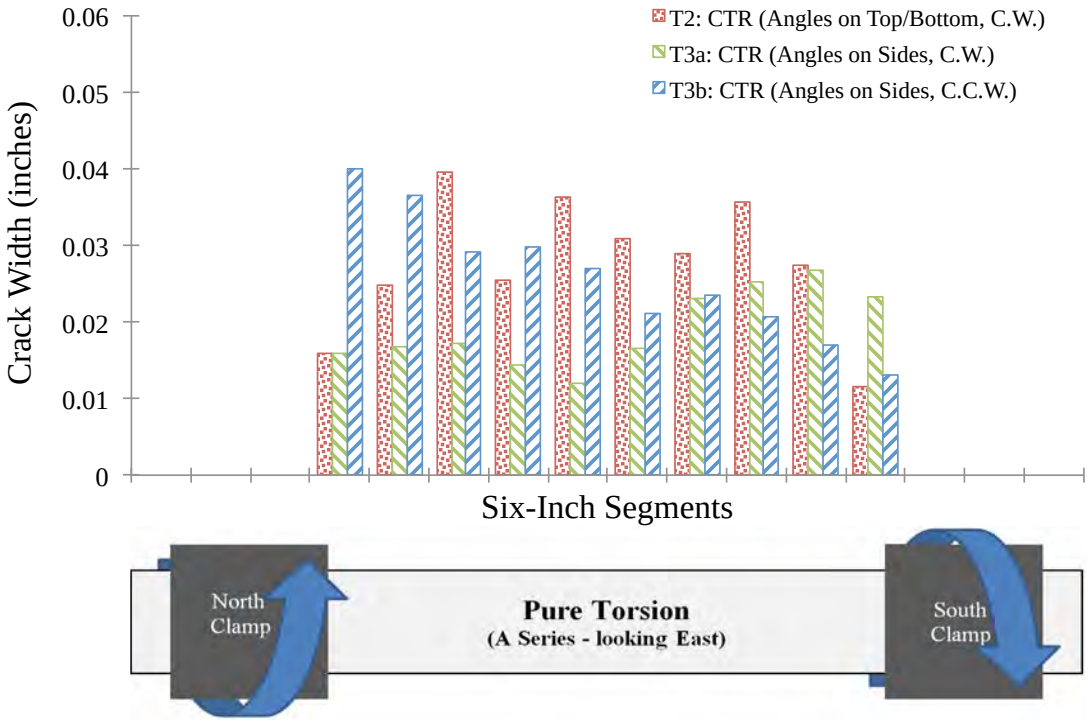

(a) 5,000-psi specimens

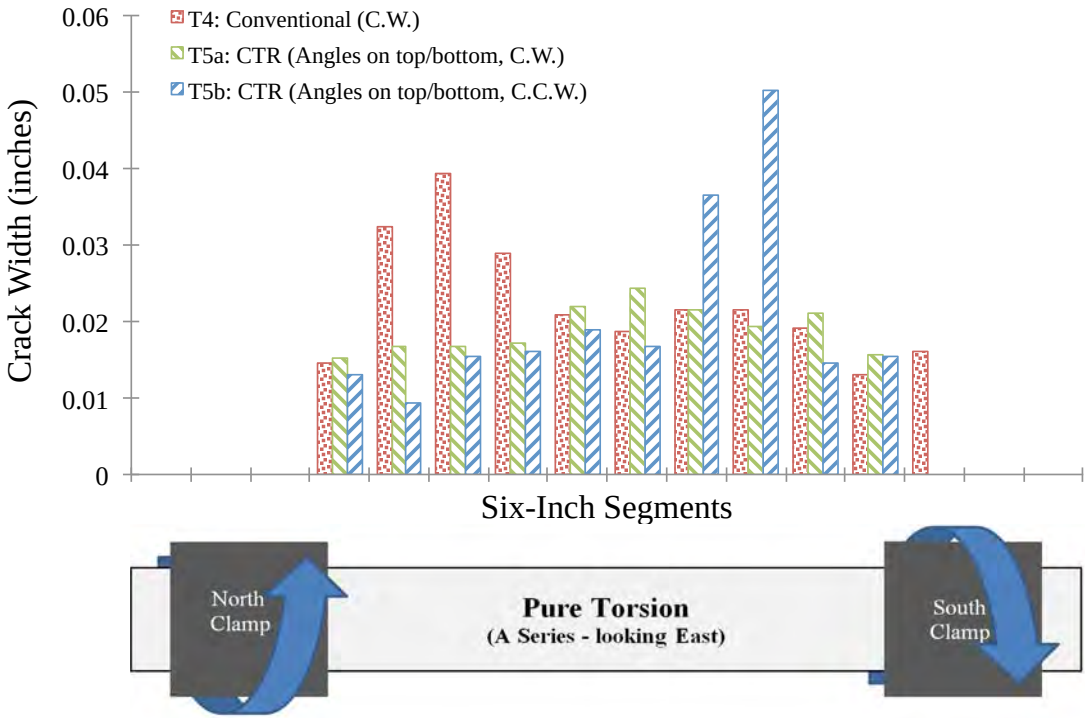

(b) 10,000-psi specimens

Figure 4.21: Crack widths
CTR: Continuous transverse reinforcement

4.3.7 Summary

In terms of serviceability, i.e., crack widths or cracking torque, no major differences were observed for specimens using conventional closed stirrups and those with continuous transverse reinforcement (CTR). The torsional capacity provided by CTR is as good as, if not better than, that from conventional transverse reinforcement. The direction of torque relative to "spiral" of CTR influences the capacity and residual torsional resistance provided by concrete. The performance is negatively affected if the applied torque produces cracks that are in the same direction as how CTR "spirals". It is expected that reducing the spacing between transverse reinforcing bars could, at least partially, mitigate the magnitude of capacity reduction. By reducing the spacing, a larger number of transverse reinforcing bars will cross the diagonal cracks and, hence, the growth of crack widths will be mitigated more effectively. This approach would likely create constructability issues. The amount of longitudinal reinforcement required to resist tensile force generated due to torsional loading can be computed based on existing equations.

4.4 Specimens Subjected to Bending, Shear, and Torque

4.4.1 Overall Response and Capacity

As addressed in Section 3.3.4, a concentric load and an eccentric load were applied in order to subject the specimen to combined effects of flexure, shear, and torsion. Figure 4.22(a) illustrates the relationships between the total applied load (i.e., the sum of the concentric and eccentric loads) and vertical deflection (taken as the average of the two deflections measured at 12 in. on either side of the centerline). Due to incorrect settings in the servo valve controller, the load cell of the concentric actuator could not register values beyond 139 kips even though loads up to 150 kips could have been applied. Therefore, testing of specimen TFS3 was terminated when the concentric load reached 139 kips. The performance of the specimens in terms of flexural and shear behavior is reasonably close with no drastic differences in terms of stiffness and maximum load.

In Figure 4.22(b), the applied torque versus the angle of twist is plotted for each of the specimens. The three specimens had similar torsional responses. Specimen TFS2, which had continuous transverse reinforcement with the angled legs on the top and bottom faces, maintained its torsional rigidity better than the other two specimens. For specimens TFS1 and TFS2, the angle of twist increased even though the applied torque was kept nearly constant at or near the peak torque. At this stage, the flexural-shear capacity had been reached, as reflected by the gradual drop in the load-deflection responses, shown in Figure 4.22(a). The loss of flexural-shear stiffness and strength reduced the torsional rigidity, leading to higher values of angle of twist. Because of this observed behavior, the interaction between flexure, shear, and torsion needs to be taken into account.

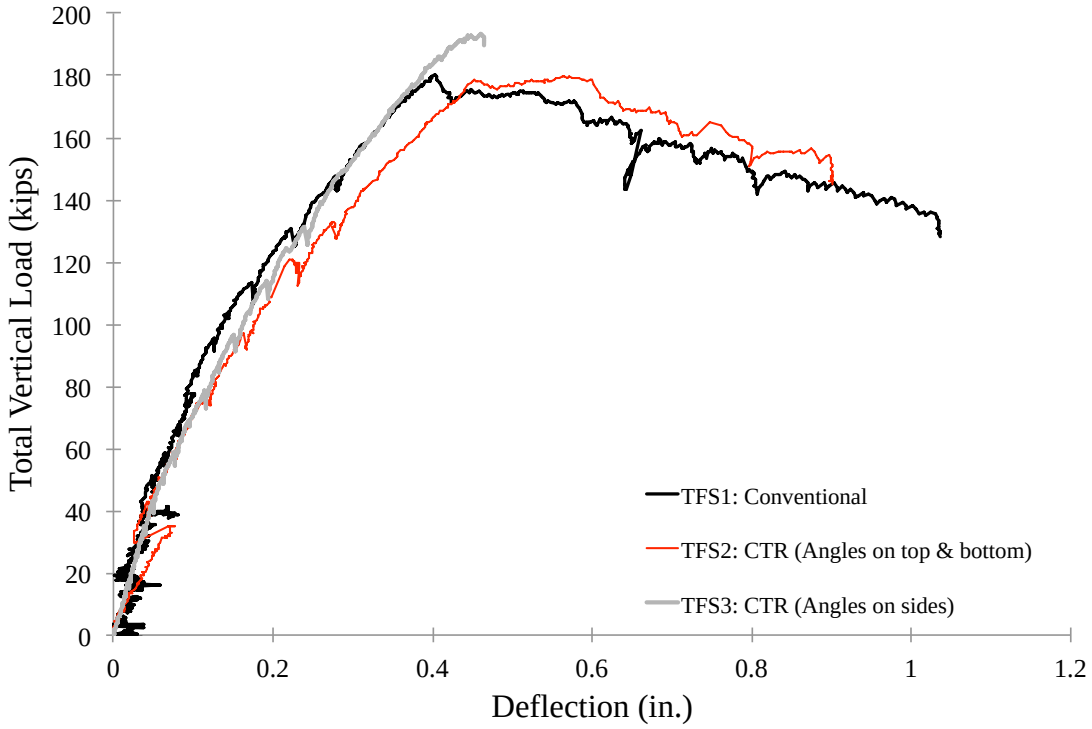

(a) Load vs. deflection

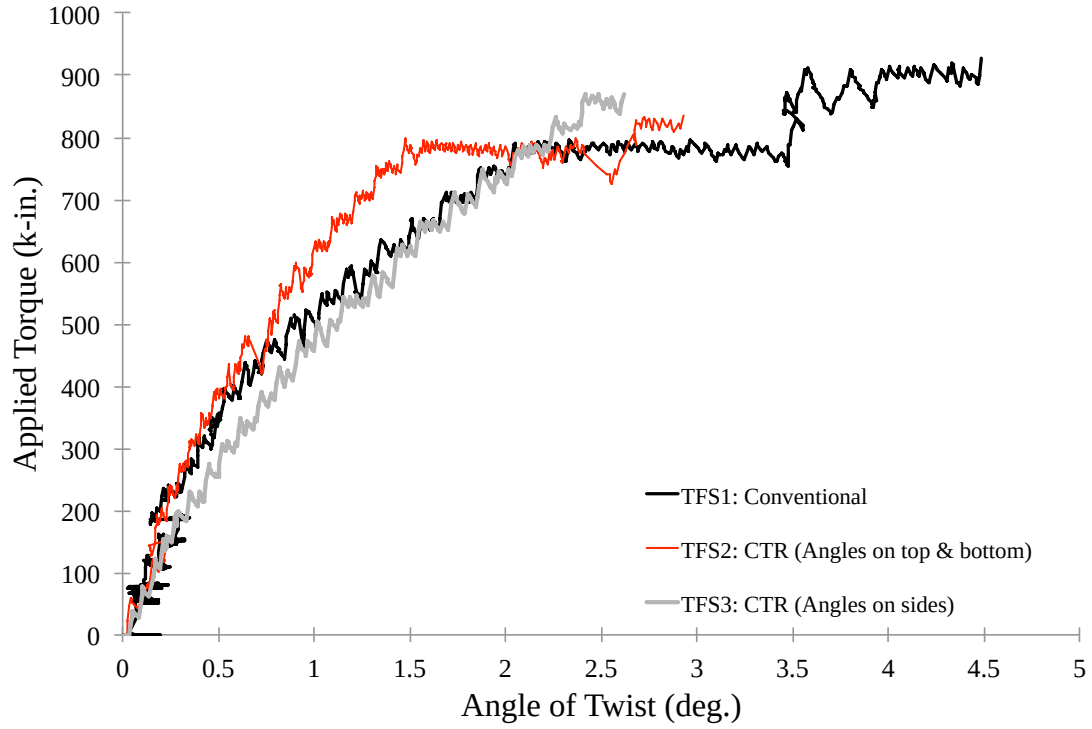

(b) Torque vs. angle of twist

Figure 4.22: Measured global responses
CTR: Continuous transverse reinforcement

The capacity was evaluated by considering the interaction between flexure, shear, and torsion. Non-dimensional interaction relationships proposed by Hsu (1993) were used for this purpose. These relationships model three failure modes, which are modeled by different equations, as indicated in Eq. 10.

- **Mode 1**: The bottom longitudinal reinforcement and transverse reinforcement yield on the side where shear and torsional stresses are additive.

$$\left(\frac{M_u}{\phi M_n}\right)+r\left(\frac{V_u}{\phi V_n}\right)^2+r\left(\frac{T_u}{\phi T_n}\right)^2=1 \qquad \text{Eq. 10(a)}$$

$$\text{where} \quad r=\frac{A_s' f_y'}{A_s f_y}$$

- **Mode 2**: The top longitudinal reinforcement and transverse reinforcement yield on the additive side.

$$-\frac{1}{r}\left(\frac{M_u}{\phi M_n}\right)+\left(\frac{V_u}{\phi V_n}\right)^2+\left(\frac{T_u}{\phi T_n}\right)^2=1 \qquad \text{Eq. 10(b)}$$

- **Mode 3**: The longitudinal and transverse reinforcement on the additive side yield.

$$\left(\frac{V_u}{\phi V_n}\right)^2+\left(\frac{T_u}{\phi T_n}\right)^2+2\left(\frac{V_u\times T_u}{\phi V_n\times\phi T_n}\right)\sqrt{\frac{2d_v}{p_{cp}}}=\frac{1+r}{2} \qquad \text{Eq. 10(c)}$$

The above equations were applied to the specimens. The bottom longitudinal reinforcement consisted of four No. 8 Gr. 100 A1035 reinforcing bars for flexure, and two No. 5 Gr. 60 A615 bars for torsion. The value of f_y for computing r was taken as a weighted average, i.e., $\frac{4\times 0.79\ in.^2\times 112\ ksi+2\times 0.31\ in.^2\times 72\ ksi}{4\times 0.79\ in.^2+2\times 0.31\ in.^2}=105\ ksi$. (The yield strength of No. 8 A1035 and No. 5 A615 reinforcing bars was 102 and 72 ksi, respectively – refer to Table 3.6.) The values of V_n and T_n were computed according to the equations discussed previously in Sections 4.1.1 and 4.3.1. The nominal flexural capacity (M_n) was obtained from basic procedures outlined in the Code.

For specimens TFS1 and TFS2, the maximum concentric load and eccentric load did not occur at the same time. Therefore, the interaction equations were evaluated for two sets of loads, and the larger values were selected. For all the specimens, mode 1 controls as demonstrated in Appendix L. The values of interaction equation are tabulated in Table 4.8; a value of 1.0 or higher indicates failure. The maximum loads in specimens TFS1 and TFS2 were 9% below the expected failure loads. Specimen TFS3 had developed its capacity. The computed values are essentially the same considering the complexities associated with modeling the interaction between flexure, shear, and torsion. In other words, the maximum loads resisted by the

specimens do not suggest any noticeable differences in the capacity of the specimens using conventional and continuous transverse reinforcement.

Table 4.8: Controlling value from interaction equations

Specimen	$\left(\frac{M_u}{\phi M_n}\right)+r\left(\frac{V_u}{\phi V_n}\right)^2+r\left(\frac{T_u}{\phi T_n}\right)^2$
TFS1: Conventional closed stirrups	0.91
TFS2: CTR with angles on top/bottom	0.91
TFS3: CTR with angles on side faces	1.01

CTR = continuous transverse reinforcement

4.4.2 Damage Pattern

Photographs of the specimens at the conclusion of testing are provided in Figure 4.21. In the case of specimen TFS1 (Figure 4.21(a)), the most prominent damage was diagonal tension failure in conjunction with compression failure concentrated on one end of the beam. The damage was similar on the face where the torsional and shear stresses were additive or subtractive. Evidence of damage due to torsion and compression due to flexure is evident on the top surface. As expected, the bars in compression had buckled.

The failure patterns in specimen TFS2 (Figure 4.21(b)) were somewhat different on the two vertical faces. Diagonal tension and compression failure occurred on the face where the shear stresses due to shear force and torsion complemented each other, whereas on the opposite face the damage consisted of compression failure primarily due to flexure and crushing near the supports. The damage due to torsion on the top surface of specimen TFS2 was more pronounced than specimen TFS1.

Specimen TFS3 cracked but did not exhibit any other signs of damage. As shown in Figure 4.21(c), this specimen had experienced diagonal cracks, more notably on the face where shear and torsional stresses were additive. Very limited diagonal cracks due to torsion could be detected on the top surface. Lack of damage in this specimen is not consistent with what the interaction equations indicate, as discussed in the preceding section. This discrepancy could not be explained rationally.

The damage patterns in specimens TFS1 and TFS2 are different. The continuous transverse reinforcement in TFS2 appears to have performed somewhat better by distributing the damage in comparison to the conventional reinforcement in TFS1. Moreover, diagonal tension failure in specimen TFS1 was more pronounced than in specimen TFS2, most likely because the damage was concentrated at one location in TFS1 but it was distributed in TFS2.

(a) Side where shear and torsional effects are subtractive

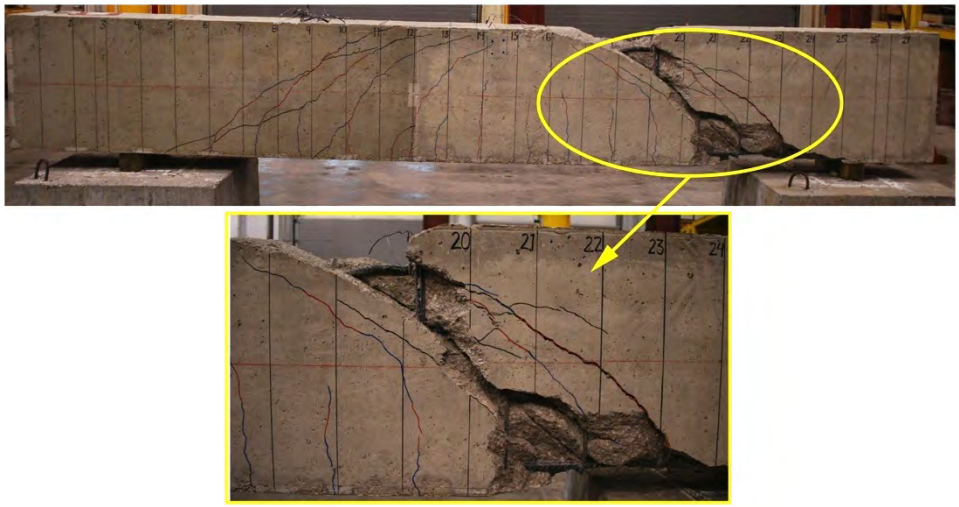

(b) Side where shear and torsional effects are additive

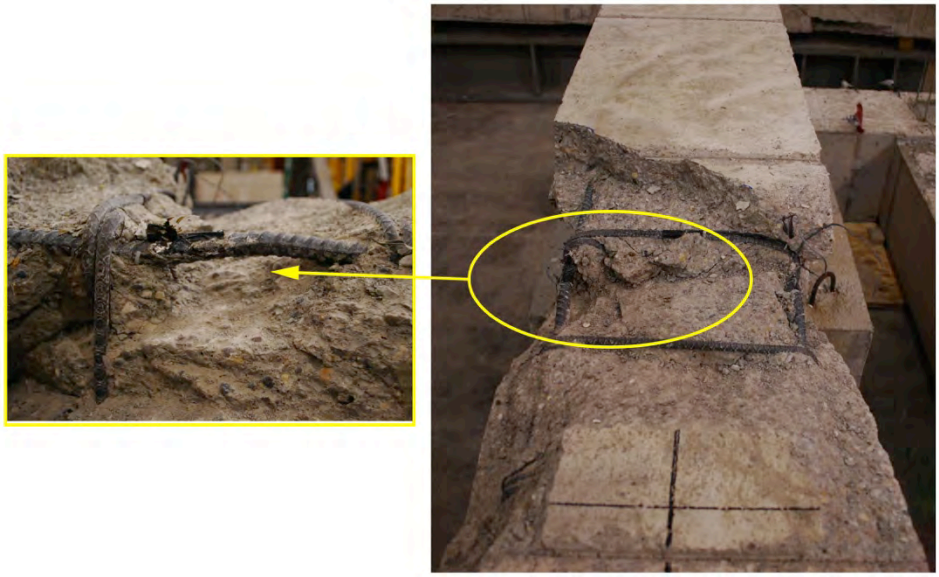

(c) Top view

Figure 4.21(a): Damage patterns for specimen TFS1

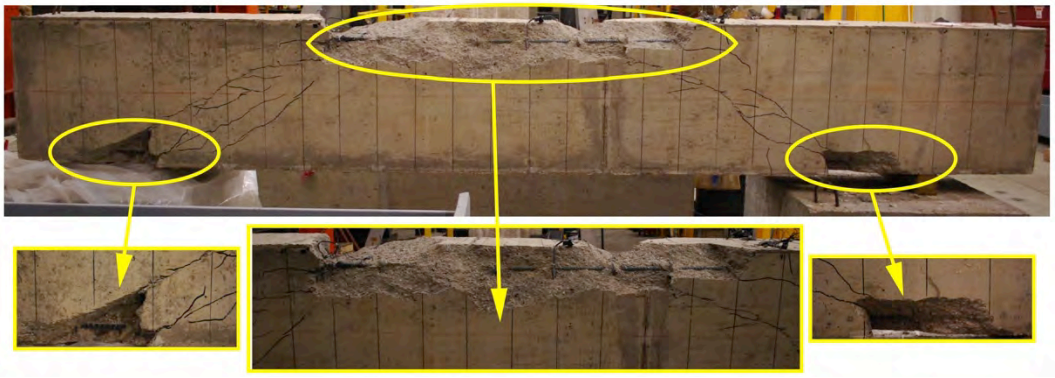

(a) Side where shear and torsional effects are subtractive

(b) Side where shear and torsional effects are additive

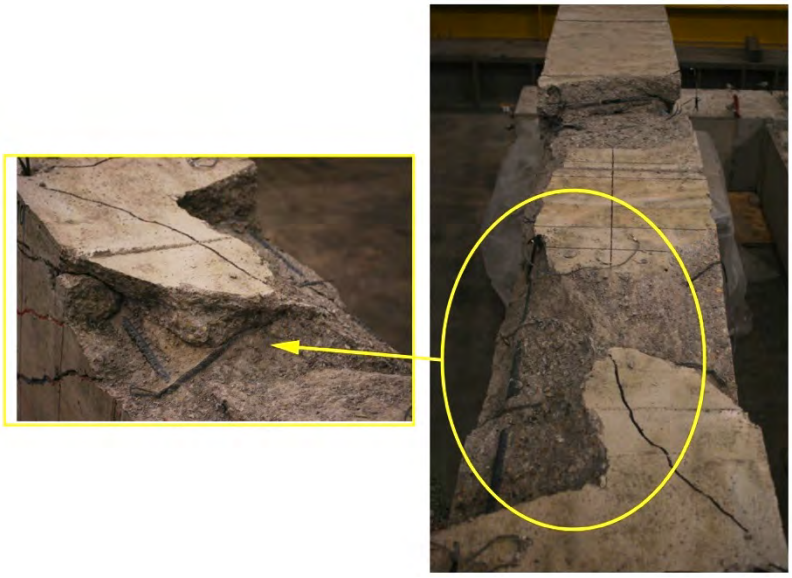

(c) Top view

Figure 4.21(b): Damage patterns for specimen TFS2

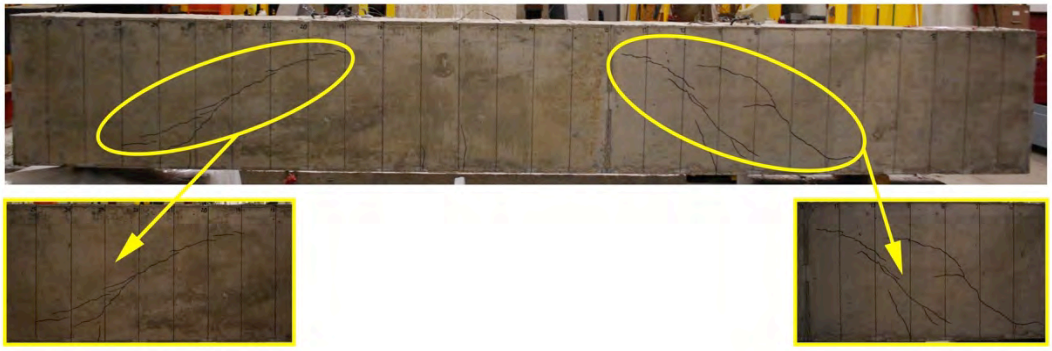

(a) Side where shear and torsional effects are subtractive

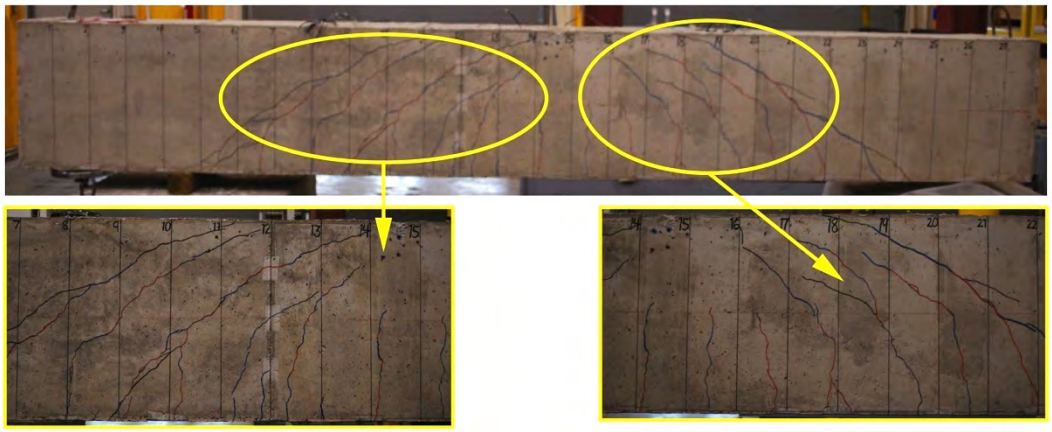

(b) Side where shear and torsional effects are additive

(c) Top view

Figure 4.21(c): Damage patterns for specimen TFS3

4.4.3 Evaluation of Strength from Concrete and Longitudinal Force

This series of specimens was subjected to the combined actions of bending moment, shear, and torsion. Strains due to flexure and torsion were recorded in the reinforcing bars intended to resist longitudinal forces due to torsion. The vertical legs of transverse reinforcement resisted the combined effects of shear and torsion, both of which were included in the corresponding strain gage data. The strain data due to various effects were first separated out, as discussed in Appendix M. The data were, subsequently, used to back-calculate the shear strength provided by concrete, contribution of concrete towards resisting the applied torque, and longitudinal force generated due to torsion. The procedures described in Sections 4.1.4, 4.3.4, and 4.3.5 were followed for this purpose.

As shown in Figure 4.22, the longitudinal force per bar is similar for all the specimens. The maximum longitudinal force (7.6 kips in specimen TFS2) is approximately one third of the available capacity (0.31 in.^{2} x 72 ksi = 22.3 kips).

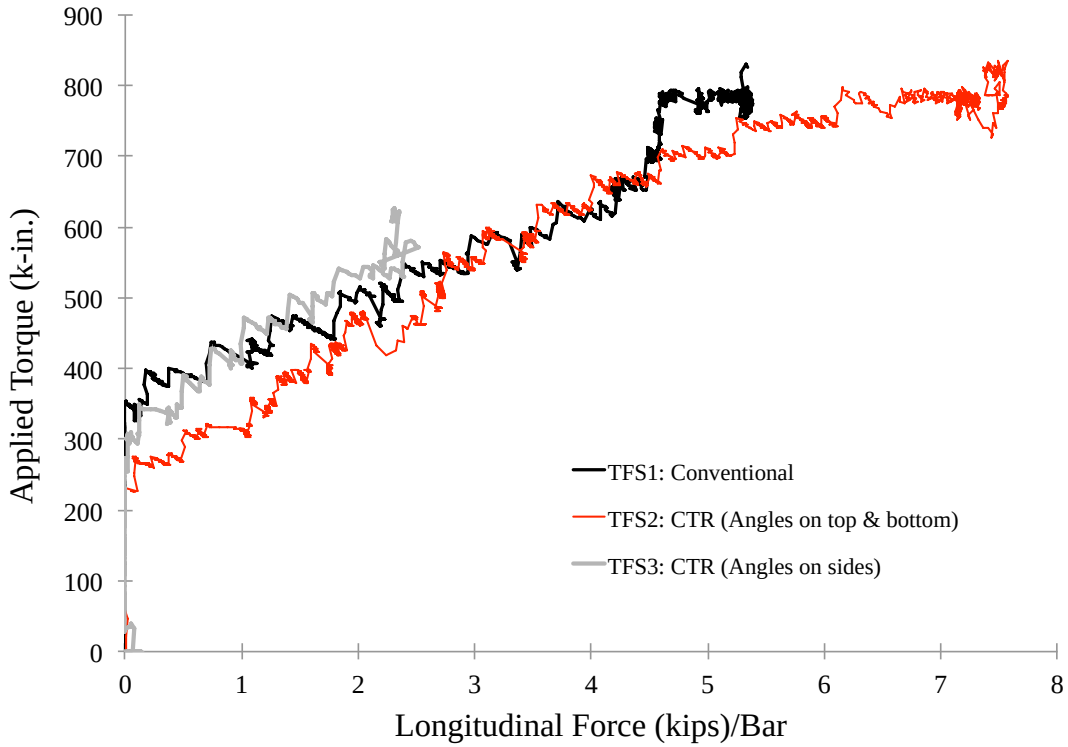

Figure 4.22: Longitudinal force in each No. 5 reinforcing bar due to torque
CTR: Continuous transverse reinforcement

The normalized shear strength provided by concrete versus the shear force (shown in Figure 4.23) is nearly identical for all three specimens. As presented in Figure 4.24, a similar trend is also seen for contribution of concrete towards resisting torsional moment. Note that the torque in this plot is one half of the total applied torque to reflect the value of torque at the locations where the strain gages had been installed (see Figure K.4 in Appendix K).

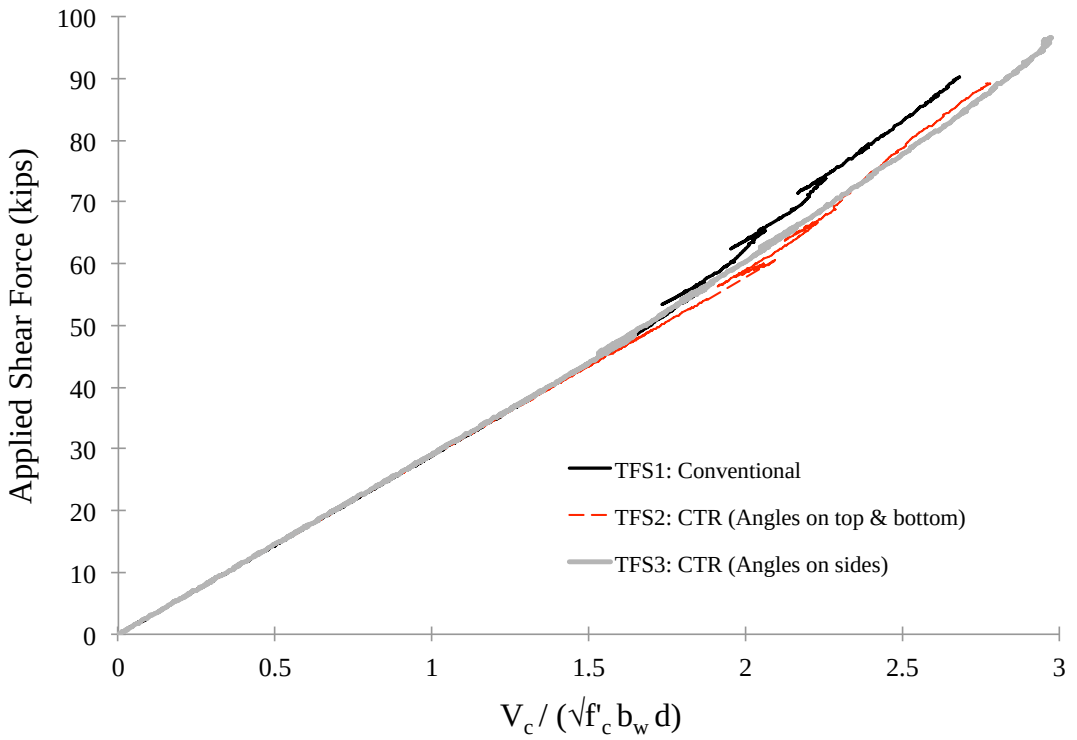

Figure 4.23: Shear force vs. normalized shear strength of concrete
CTR: Continuous transverse reinforcement

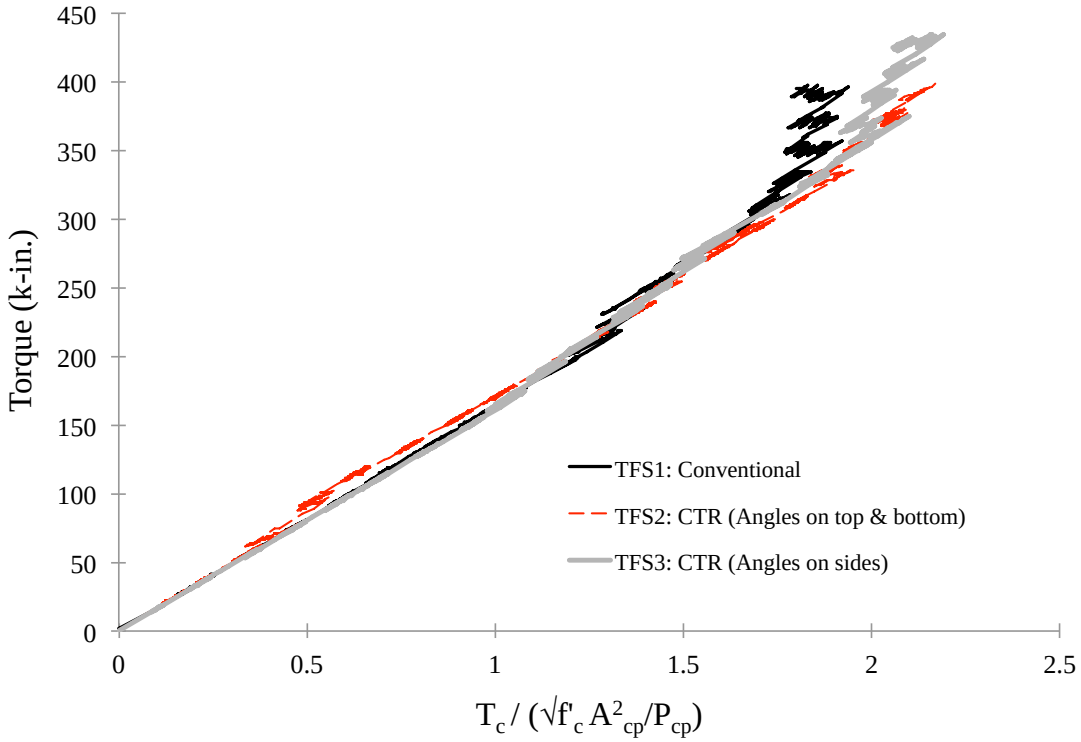

Figure 4.24: Torque vs. normalized torsional strength of concrete
CTR: Continuous transverse reinforcement

4.4.4 Crack width

Figure 4.25 depicts the distribution of crack widths at approximately one half of the maximum measured shear, bending moment, and torsion. The crack widths for the two specimens using continuous transverse reinforcement (CTR) were wider than those in the specimen with conventional transverse reinforcement. This difference cannot be explained, and is in contrast to the similarity of the stiffness in all the specimens (refer to Figure 4.22a).

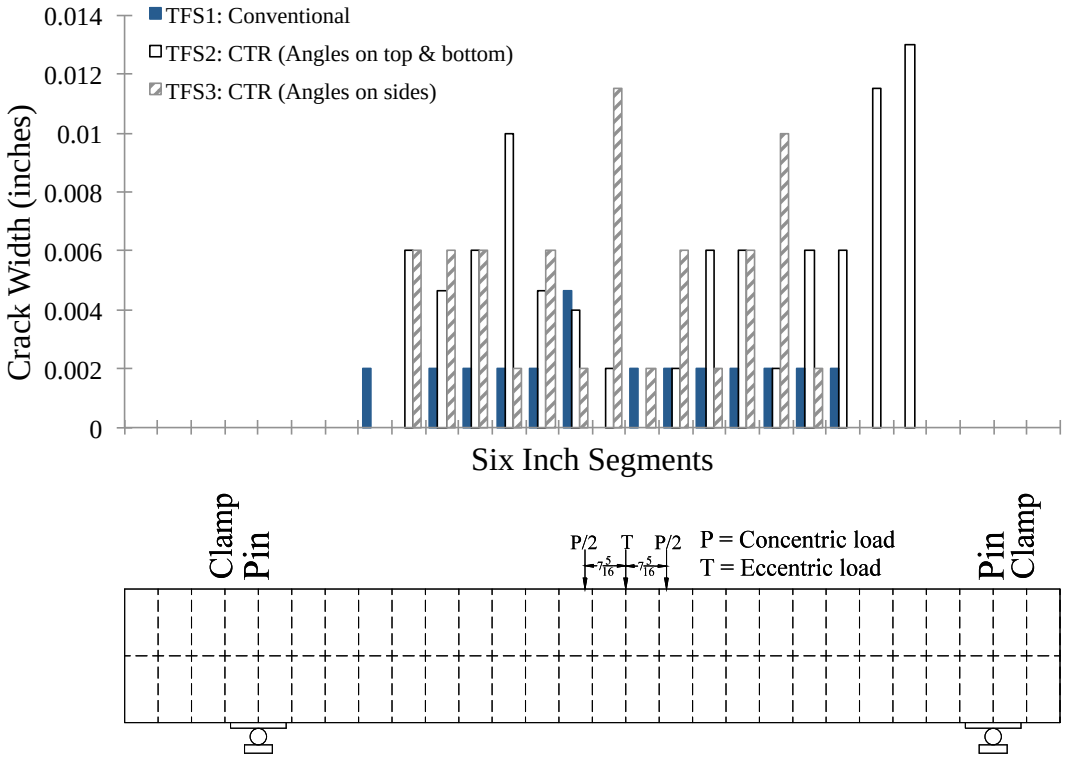

Figure 4.25: Distribution of crack widths along the length
CTR: Continuous transverse reinforcement

4.4.5 Summary

A number of metrics were used to compare various responses of members with conventional and continuous transverse reinforcement. The following observations can be made based on the presented results.

- The stiffness and capacities are similar.
- The contribution of concrete towards resisting shear and torsion is nearly identical.
- The longitudinal force due to torsion is rather close and less than the available capacity.
- The failure modes and crack widths were somewhat different. The level of crack in the specimen using conventional transverse reinforcement was appreciably less than that in the two specimens using continuous transvers reinforcement (CTR).
- The trend of crack widths is not supported by the similarity of the stiffness from the measured load-deflection responses. Damage at the ultimate limit state was concentrated

essentially at one location for the specimen with conventional transverse reinforcement, but it was distributed for the specimen with CTR. (Note that one specimen using CTR had not been damaged at the conclusion of testing.)

- From capacity and detailing points of view, no noticeable differences could be identified between conventional transverse reinforcement and CTR.

4.5 Stub Columns

4.5.1 Capacity

Axial load versus axial shortening, measured over the specimen height, is plotted in Figure 4.26. The axial stiffness (i.e., the slope before initiation of cracking) is consistent for all the specimens. The stiffness up to failure load is nearly the same for all square columns regardless of whether continuous transverse reinforcement (CTR) or conventional ties were used.

At approximately one half of the peak load, the stiffness of specimen C4 (the circular column with conventional spirals) is reduced slightly in comparison to the other specimens. Specimen C4 exhibits a substantial level of post-peak ductility, which is common in spirally reinforced columns. However, the load-carrying capacity of the square columns with conventional ties or continuous transverse reinforcement (CTR) drops suddenly after reaching the peak load.

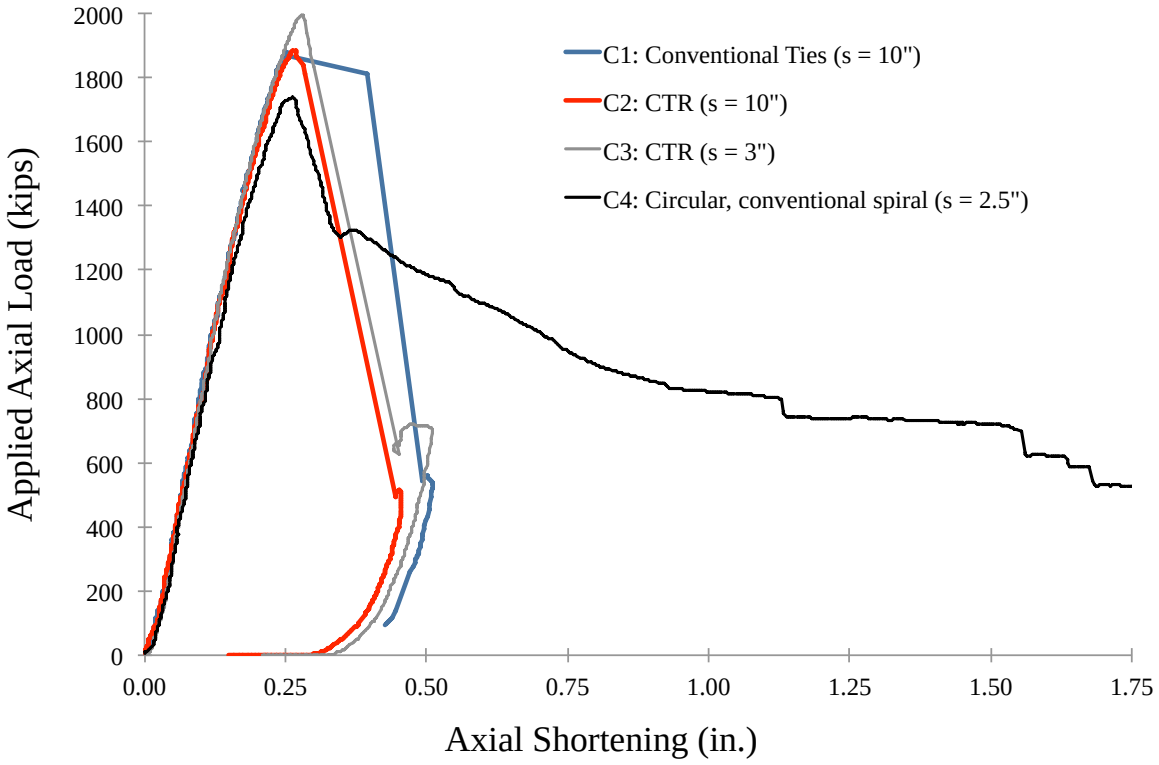

Figure 4.26: Axial load–axial shortening relationships
CTR: Continuous transverse reinforcement

Using the measured material properties, the nominal axial load capacities were computed according to current ACI 318-11 equations. These values are compared against the maximum measured loads in Table 4.9. All the specimens resisted an ultimate load at least 25% higher than the calculated capacity, with specimen C3 achieving the highest test/predicted capacity ratio of 0.34.

Table 4.9: Measured and computed axial load capacities

Specimen	Computed P_n (kips)		Maximum Measured	Measured/
	$0.85 f_c^{'}\left(A_g - A_{st}\right) + f_y A_{st}$	Reduced	P (kips)	Reduced P_n
C1	1756	1493	1881	1.26
C2		1493	1884	1.26
C3		1493	1999	1.34
C4	1709	1367	1740	1.27

Reduced $P_n = 0.85P_n$ or $0.80P_n$ for tied and spiral columns, respectively. The reduction accounts for a minimum eccentricity that is inevitable even in columns subjected to only an axial load.

4.5.2 Confinement

Transverse reinforcement confines the core concrete and improves the overall column ductility. The level of confinement depends on the adequacy of transverse reinforcement to resist passive confinement pressure. The lateral pressure provided in circular cross sections is relatively uniform. On the other hand, in rectangular or square cross sections, the lateral pressure is not uniform, and is concentrated at the stiffer, longitudinal (vertical) bars. Between these bars, the unsupported ties bow or arch outward, as shown schematically in Figure 4.27.

Moreover, the level of confining pressure between transverse reinforcement affects the confinement. For conventional ties that are spaced at discrete elevations, the amount of lateral pressure, and hence the level of confinement, is reduced between the ties. The distribution of lateral pressure at and between ties is compared schematically in Figure 4.27. In case of spiral or continuous transverse reinforcement, the level of confinement is expected to be more uniform than ties.

The level of confinement in various stub columns was evaluated by two different methods. In the first method, the transverse strains measured at column midheight were averaged and converted to stress (f_{tr} or f_{sp} shown in Figure 4.28) by following the procedure described in Section 4.1.4. Assuming a uniform lateral confining stress, the value of f_2 was computed and plotted against the axial stress taken as the applied load divided by the gross cross sectional area (P/A_g), refer to Figure 4.29. Considering that the damage was primarily concentrated near the top, the level of confining stress at the midheight is relatively small. The trend of results is as expected, i.e., (a) spiral reinforcement provides a higher level of confinement, and (b) the value of confining stress increases as the spacing of transverse reinforcement decreases. The efficiency of confinement from CTR is comparable to that from conventional transverse reinforcement.

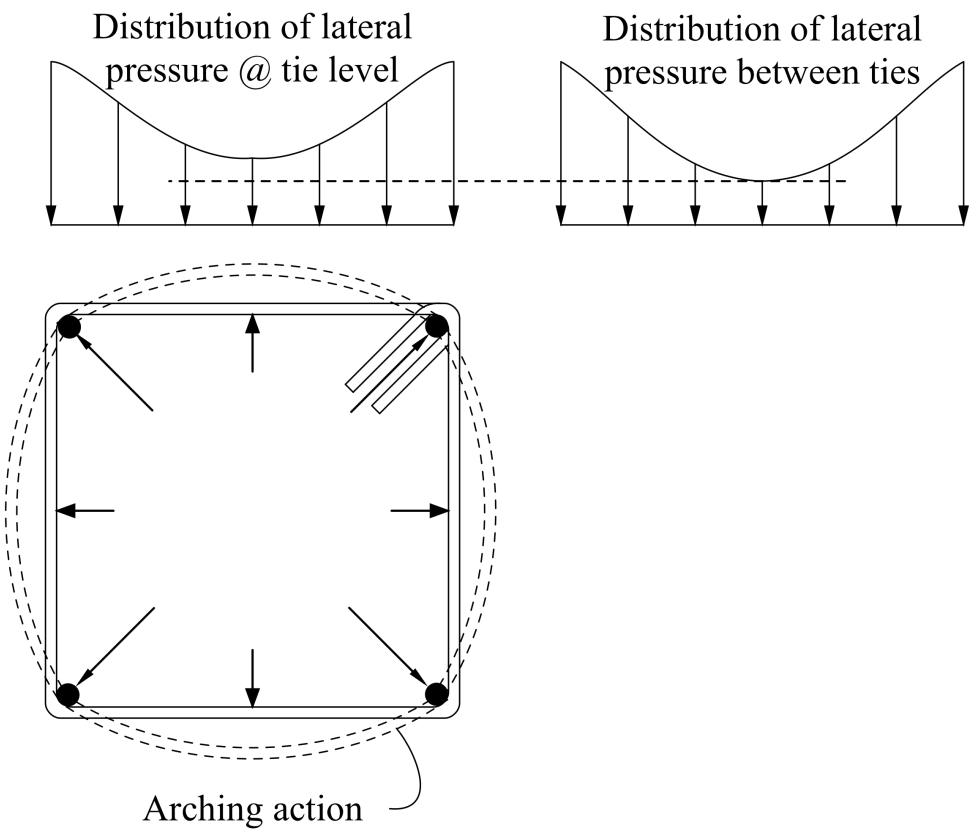

Figure 4.27: Schematic representation of confinement from conventional ties
Adopted from Saatcioglu and Razi (1992)

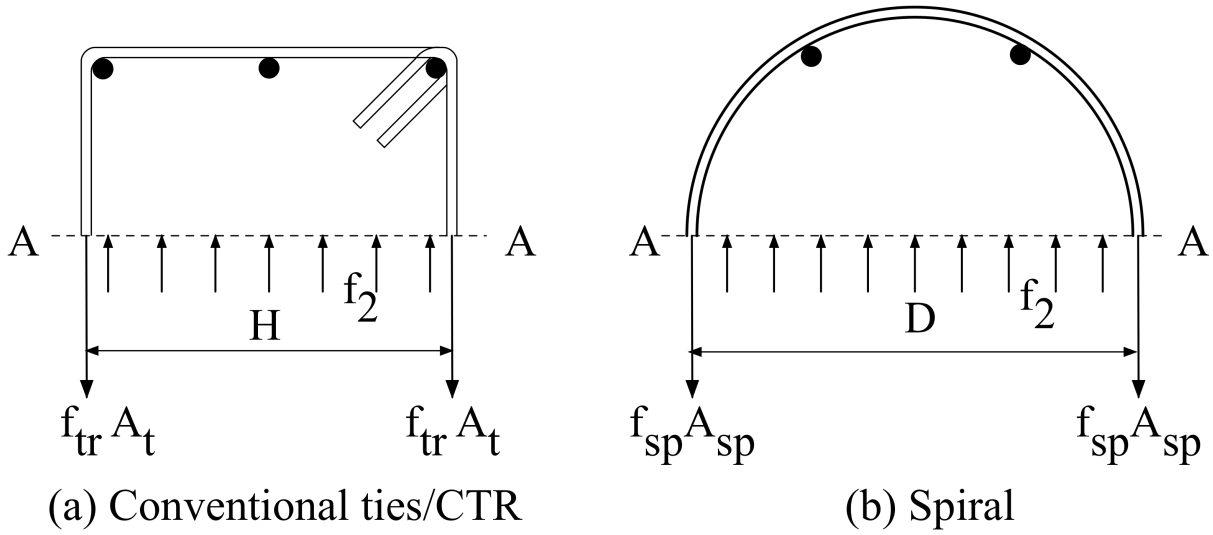

$$(a)\ \sum F = 0;\quad 2 f_{tr} A_t = f_2 sH;\quad f_2 = \frac{2 f_{tr} A_t}{sH} \qquad (b)\ \sum F = 0;\quad 2 f_{sp} A_{sp} = f_2 sD;\quad f_2 = \frac{2 f_{sp} A_{sp}}{sD}$$

Figure 4.28: Calculation of lateral confining pressure

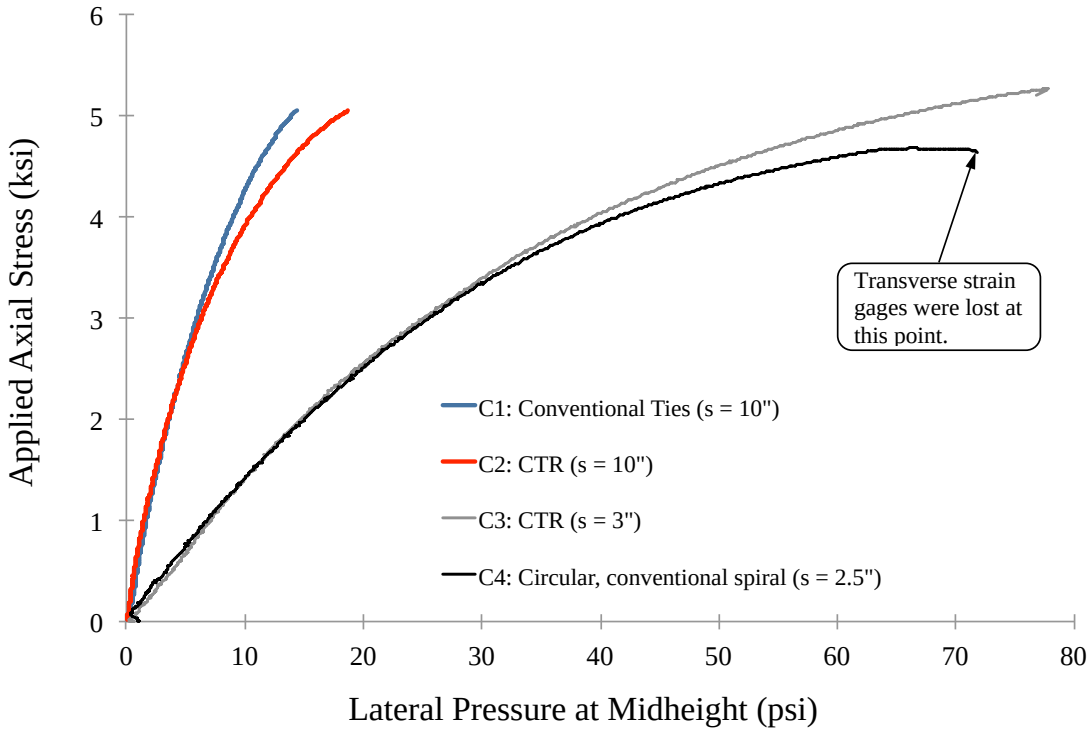

Figure 4.29: Axial stress vs. lateral confining pressure
CTR = continuous transverse reinforcement

In the second method, the strains measured at the midheight of the longitudinal bars were averaged and plotted against concrete axial stress taken as $f_c = \frac{P - A_{st} f_s}{A_g}$, which becomes $f_c = \frac{P - A_{st}\left(E_s \varepsilon_s\right)}{A_g}$ because the longitudinal bars did not yield. In these equations, ε_s is the average strain in the longitudinal bars measured at the midheight. Other researchers have followed a similar procedure (e.g., Moehle and Cavanagh 1985).

The resulting "stress-strain" diagram is illustrated in Figure 4.30. This figure corroborates the observation made from Figure 4.29 in that the level of confinement provided by CTR is comparable to that from conventional types of transverse reinforcement (ties and spirals).

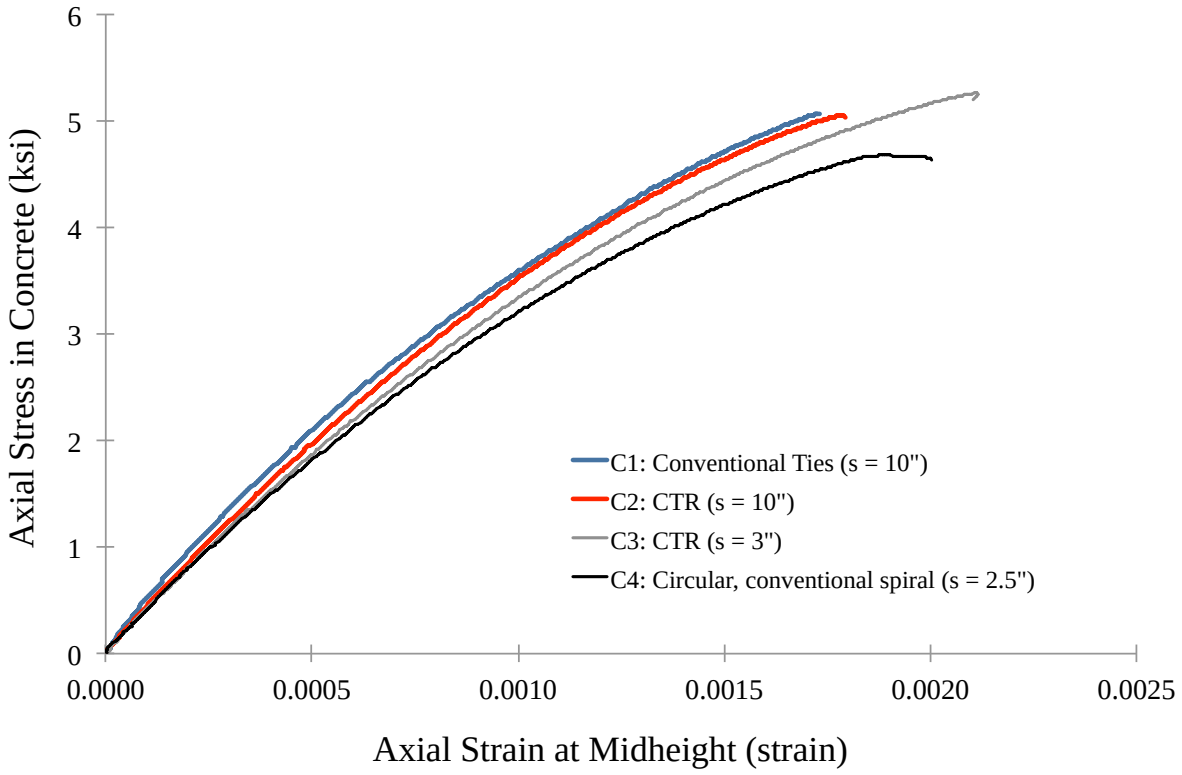

Figure 4.30: Axial stress vs. axial strain
CTR = continuous transverse reinforcement

The brittle failure modes for specimens C1, C2, and C3 are in contrast to the level of confinement from the transverse reinforcement, which was not appreciably different from that in specimen C4. This discrepancy is attributed to localization of failure zones, as discussed in the following section.

4.5.4 Damage Pattern and Failure Mode

At approximately 98 percent of the ultimate load, slight cracking sounds were heard. Shortly afterwards, the columns developed their maximum capacity. With the exception of specimen C3, failure was marked by one of the longitudinal bars buckling between the transverse reinforcement. In the case of specimen C4, the spiral fractured at three locations. Spalling of cover concrete, buckling of longitudinal bar, and fracture of the transverse reinforcement occurred near the top of the column. For each column, the concrete was placed in staged lifts in order to prevent segregation of paste and aggregate. However, the concrete near the top was expected to be slightly weaker than that in the bottom. Concentration of damage near the top is consistent with the expected differences in the concrete quality at the top and bottom. A summary of the failure modes for all the specimens is provided in Figure 4.31.

(a) Specimen C1

(b) Specimen C2

Figure 4.31: Damage patterns and failure modes

(c) Specimen C3

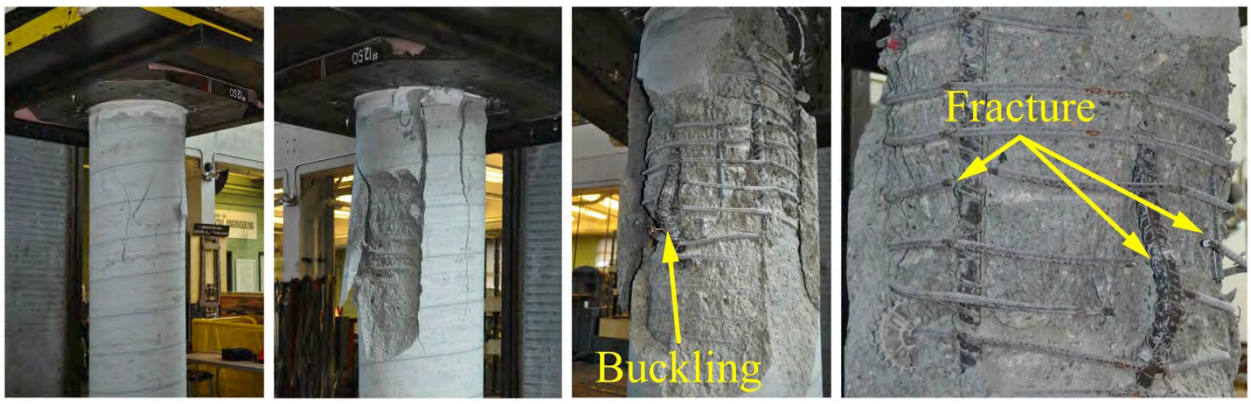

(d) Specimen C4

Figure 4.31: Damage patterns and failure modes (cont.)

4.5.4 Summary

Testing of the reported four stub columns using conventional ties, continuous transverse reinforcement (CTR), or spiral did not reveal any substantial difference in axial load capacity and contribution of transverse reinforcement towards confinement of the core. All the specimens reached and exceeded their expected capacities calculated based on current ACI 318-11 provisions. The mode of failure of the specimens with conventional ties and CTR was brittle, even though the level of confinement was similar.

4.6 Exterior Beam-Column Connections

4.6.1 Global Behavior

Two beam-column joints were tested cyclically to compare relative behavior of CTR and conventional transverse reinforcement. The relationships between the applied load and normalized lateral drift are compared in Figure 4.31. Drift is defined as the applied lateral displacement divided by the unbraced length between the pins at the top and bottom of the column (see Figure 3.21 or 3.22), which represented inflection points in the column. Both of the hysteretic responses are stable and rather similar. Specimen BC2 used continuous transverse reinforcement (CTR) for the full length of the columns and in the beam plastic hinge region. This specimen does not exhibit any signs of reduced load carrying capacity. Despite being subjected to drifts that were at least 30% larger than the maximum design value in current codes, both specimens performed quite well.

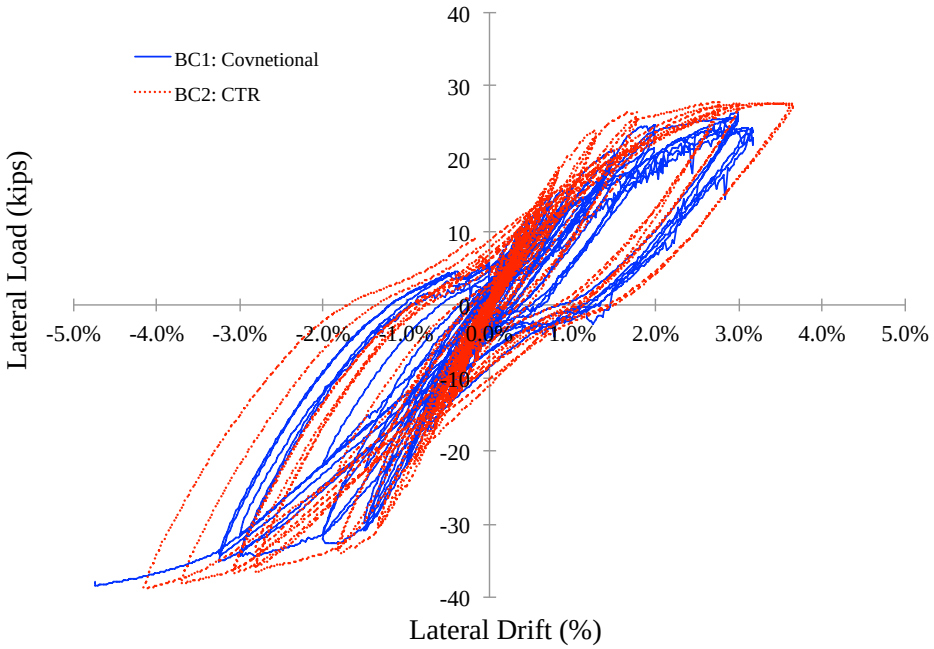

Figure 4.31: Lateral load-lateral drift hysteretic responses
CTR = continuous transverse reinforcement

The performances of the two connections were further evaluated by comparing their energy dissipation characteristics and stiffness degradation. Variation of stiffness as a function of lateral drift is plotted in Figure 4.32. The stiffness in each cycle was taken as the slope of line between the positive and negative peaks, as shown in the figure inset. The rate of stiffness degradation is similar between the two specimens. Moreover, specimen BC2 maintained its global lateral stiffness slightly better than specimen BC1, which had conventional seismic details. For instance, at 1.5% drift, the peak-to-peak stiffness for BC2 was 13 k/in., whereas it was 12 k/in for BC1.

At the conclusion of testing, the stiffness was essentially the same for both specimens. Current seismic design methodologies rely on ensuring that members can adequately dissipate the input seismic energy. The dissipated energy for each cycle was taken as the area under the

lateral load-lateral drift hysteretic loops. The cumulative dissipated energy was obtained by summing the energy per cycle. As evident from Figure 4.33, specimen BC2 dissipated more energy after 1.5% drift. Prior to this point, energy dissipation was slightly more for specimen BC1.

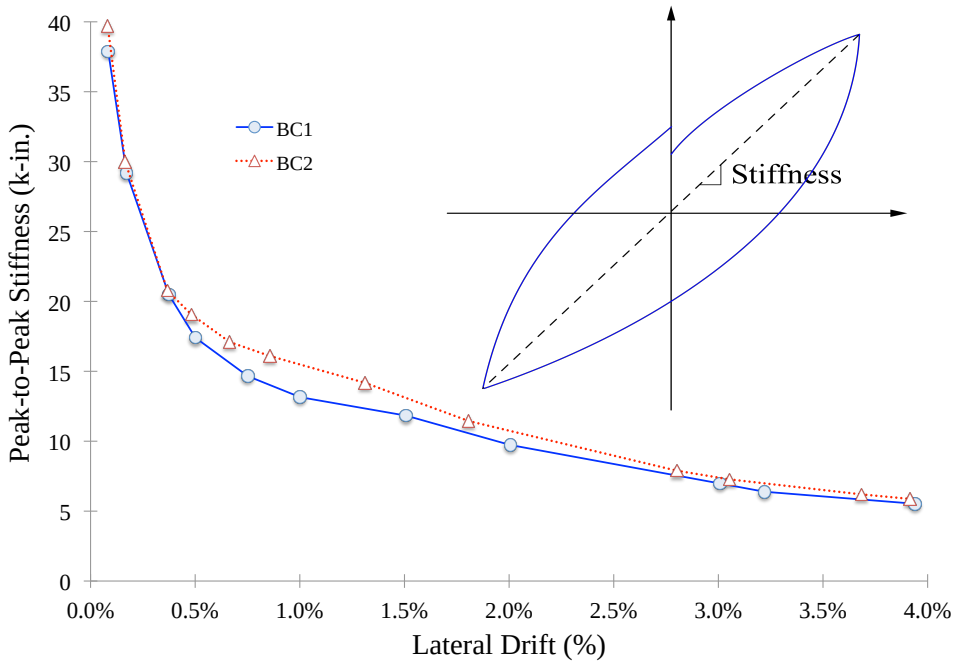

Figure 4.32: Global lateral stiffness degradation as a function of inter-story drift
CTR = continuous transverse reinforcement

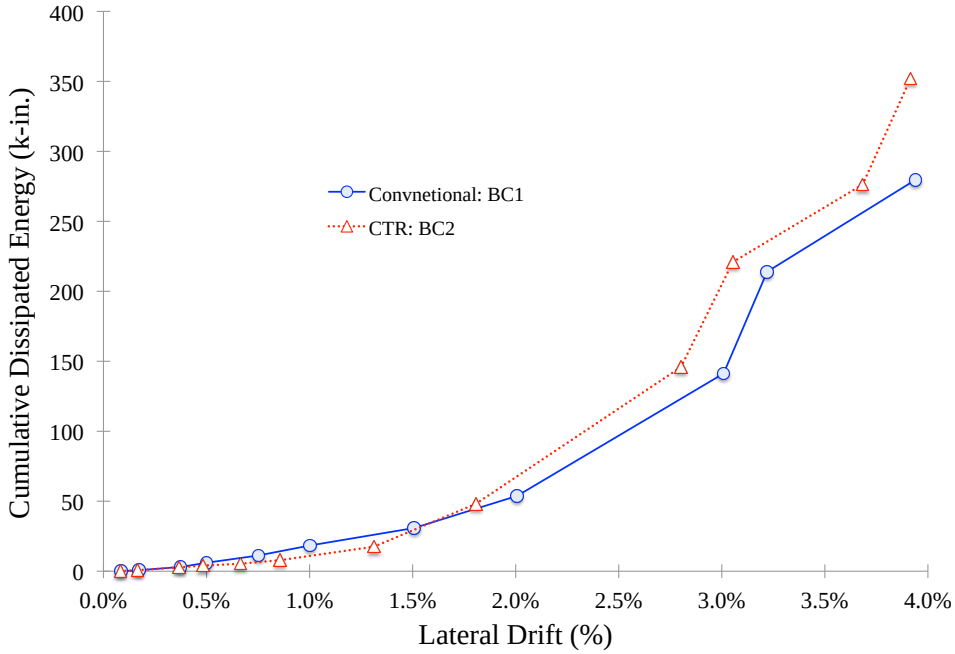

Figure 4.33: Comparison of energy dissipation
CTR = continuous transverse reinforcement

Following the same procedure described in Section 4.3.4, the contribution of concrete towards resisting the beam shear was computed. The beam did not experience major cracking or damage due to shear. This observation is supported from Figure 4.34 that shows the majority of the beam shear was resisted by concrete, and the relationship between the beam shear and resistance of concrete is essentially elastic. The same trend occurred in both specimens.

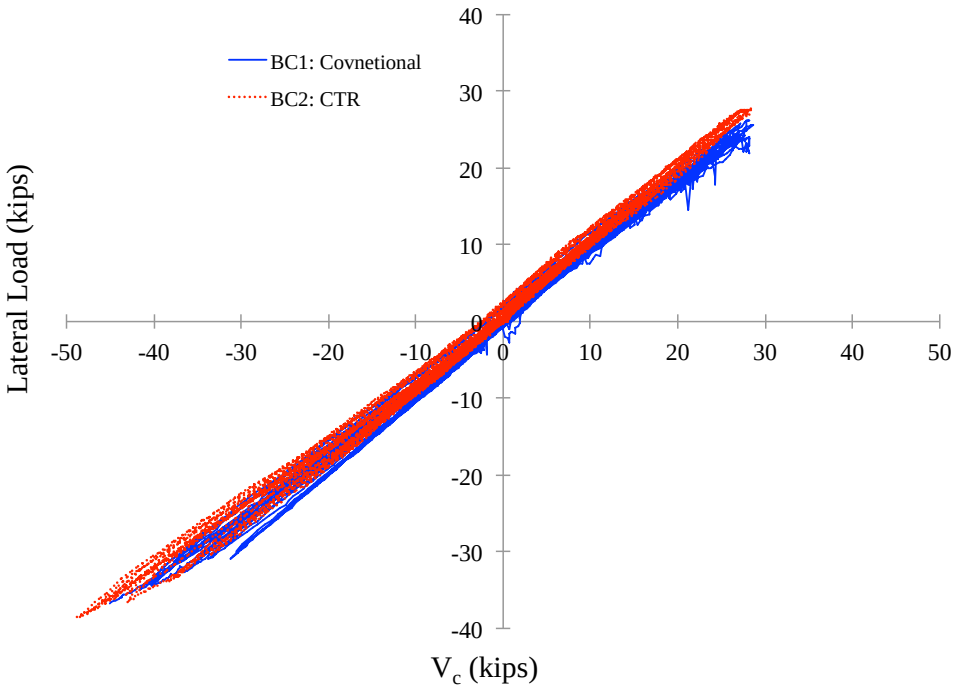

Figure 4.34: Beam shear vs. concrete shear resistance
CTR = continuous transverse reinforcement

4.6.2 Member Response

The measured strains in the longitudinal bars of the beams and columns were used to obtain the curvature from the following relationship.

$$\frac{\varepsilon_{tension\ face} - \varepsilon_{compression\ face}}{distance\ between\ gages}$$

Knowing the applied force and shear force in the beam, the bending moments (in the beam and columns) at the connection face were computed. The moment-curvature relationships are illustrated in Figure 4.35.

Consistent with seismic design philosophy of minimizing inelasticity in the columns, it is evident that the columns in both specimens remained essentially elastic. Using the as-built dimensions and actual material properties, the design flexural capacity of the column (ϕM_n) with no axial load, i.e., the case for the test specimens, is 3617 k-in. This capacity is approximately twice the maximum moment resisted by the columns.

According to ACI 318-11, transverse reinforcement in flexural members of special moment resisting frames is designed for a shear force determined based on developing probable

flexural strength of the member. The probable flexural strength is computed by using $1.25f_y$, where f_y is the specified yield strength. As intended, the beams experienced major inelastic deformations demonstrated by the moment-curvature responses shown in Figure 4.35b. Both specimens had stable hysteretic responses, which is consistent with their energy dissipation capabilities shown in Figure 4.33. The beams in both specimens reached and exceeded the computed probable flexural strength. The ratios of the maximum measured moments to probable flexural capacities are compared in Table 4.10.

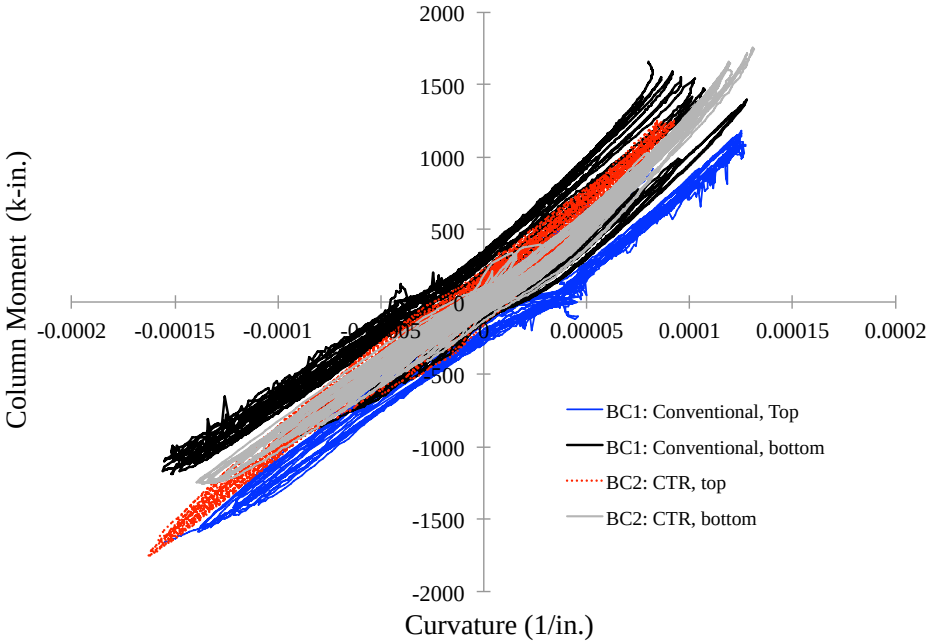

(a) Columns

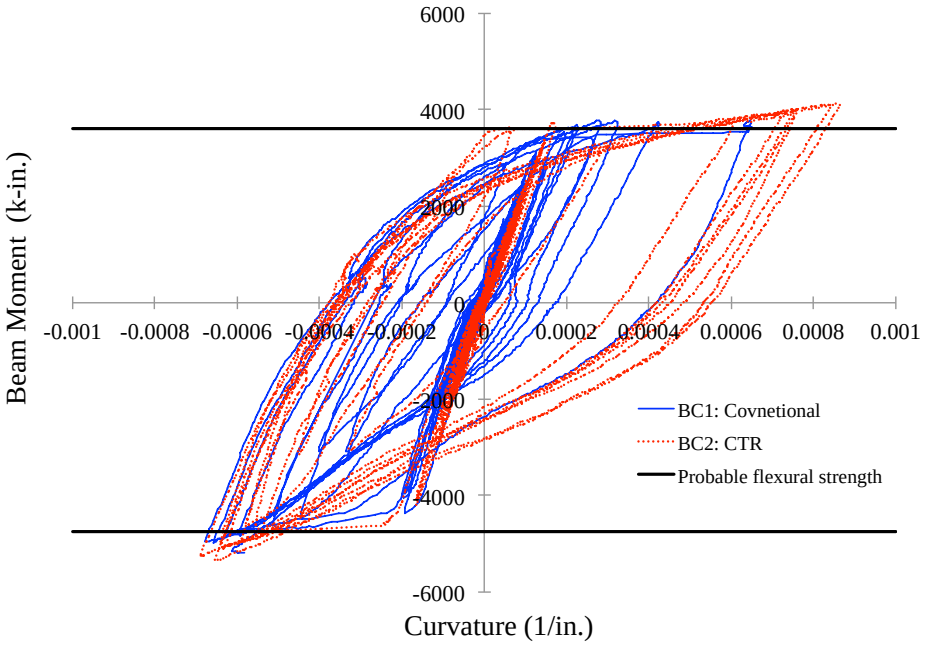

(b) Beam

Figure 4.35: Moment-curvature responses
CTR = continuous transverse reinforcement

Table 4.10: maximum measured moment to probable flexural strength

Specimen	Positive Bending	Negative Bending
BC1: Conventional	1.05	1.14
BC2: CTR	1.14	1.12

CTR = continuous transverse reinforcement

4.6.3 Performance of Joint Region

Using the deformations along the diagonals of the joint region (Figure 3.24), the joint shear angle was computed, as shown in Appendix N. In Figure 4.36, the resulting shear angle is plotted against the applied load, which is the same as the column shear force. The hysteretic response of the joint region is clearly very similar.

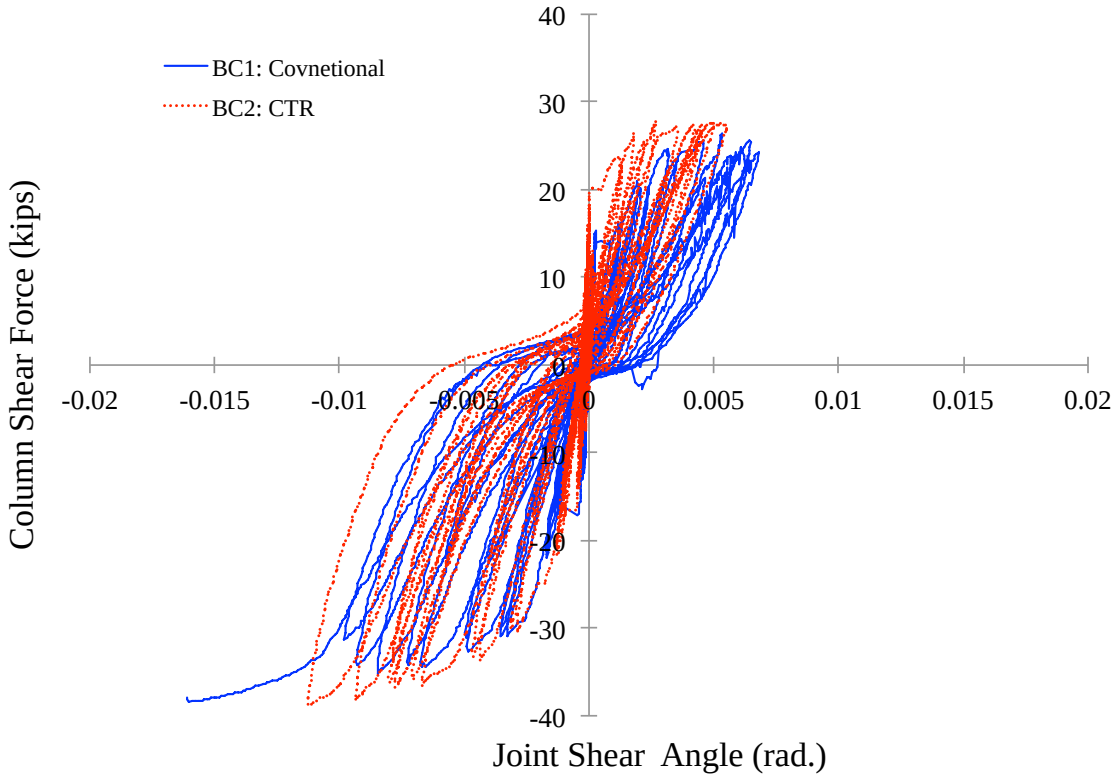

Figure 4.36: Shear angle-column shear
CTR = continuous transverse reinforcement

As shown in Appendix K, strain gages had been bonded to No. 3 transverse reinforcement in the joint region. The measured strains were converted to stresses according to the procedure described in Section 4.1. The transverse reinforcement consisted of a closed tie and a crosstie (Figure 3.11). Therefore, the derived stresses were multiplied by three times the area of a No. 3 reinforcing bar in order to compute the joint shear resisted by steel. The hysteretic relationships between the joint shear force and joint resistance of steel is plotted in Figure 4.37. The performance of the two specimens is nearly identical. The use of continuous

transverse reinforcement in the beam and columns did not affect the performance in the joint region.

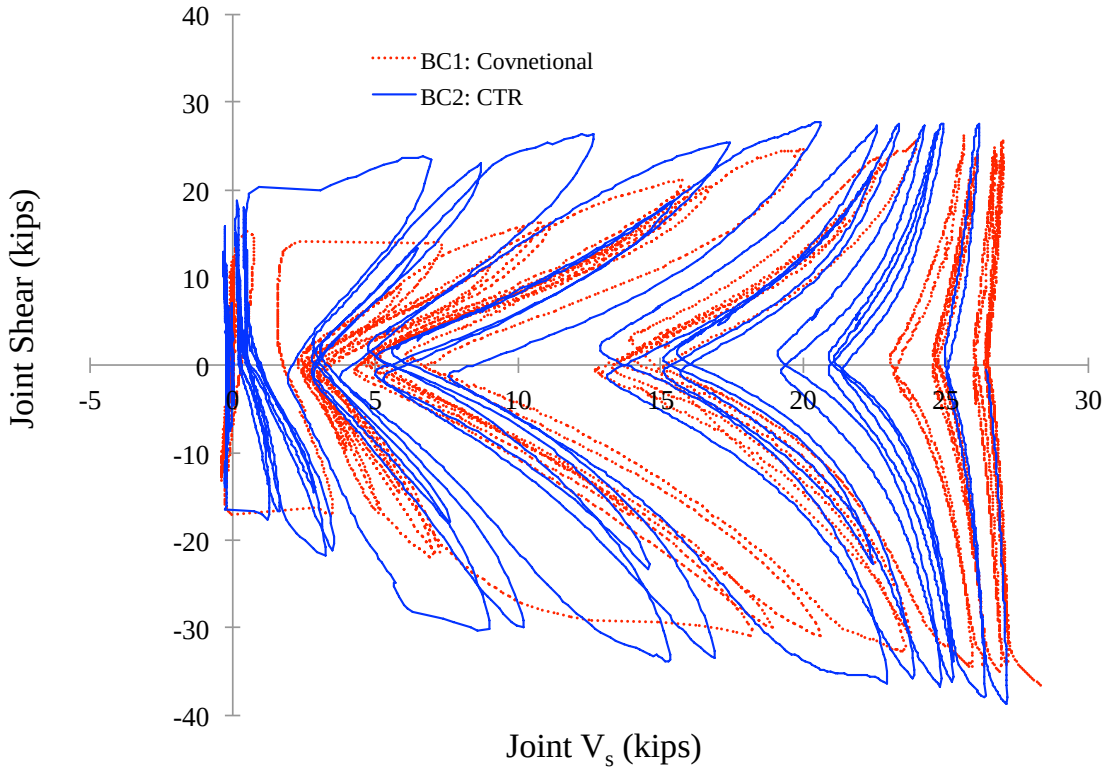

Figure 4.37: Joint shear vs. shear resistance of transverse reinforcement in the joint
CTR = continuous transverse reinforcement

4.6.4 Crack Patterns

The performance of the two specimens from a visual point view was also similar. The patterns at the conclusion of loading are compared in Figure 4.38. The similarity of the two specimens can easily be seen from this figure.

Cracking at beam-column interface

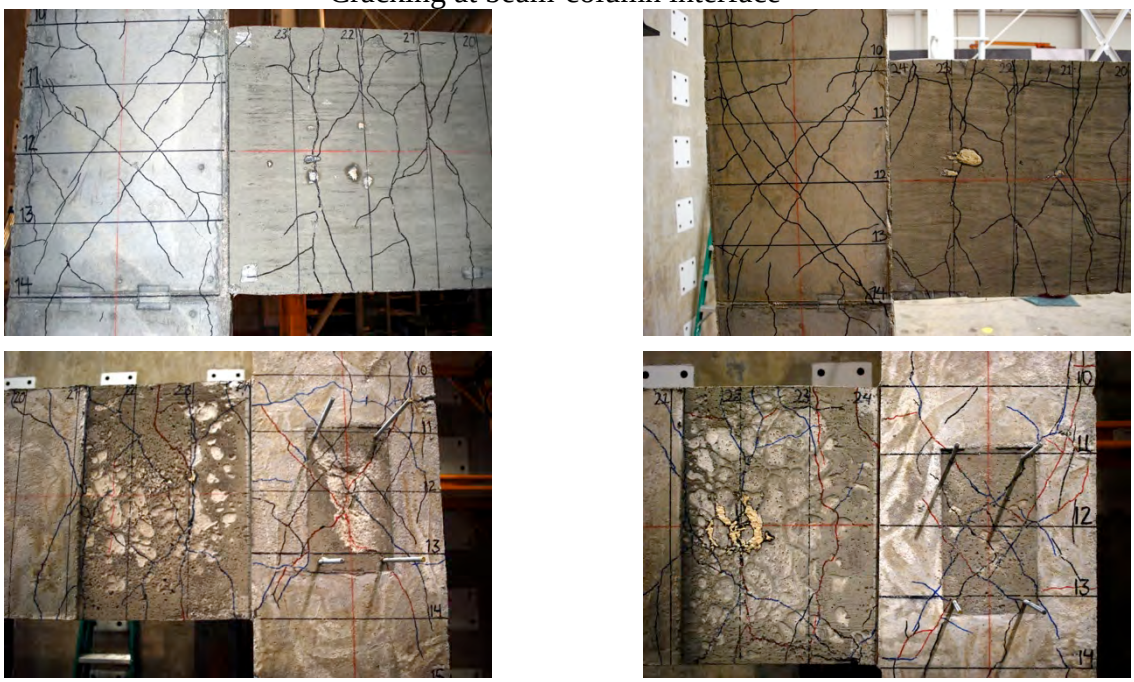

Beam and joint region

(a) Specimen BC1 (conventional) (b) Specimen BC2 (CTR)

Figure 4.38: Crack patterns in the beam-column joint region at the conclusion of testing

4.6.5 Summary

The performances of two exterior beam-column connections subjected to cyclic lateral loading were compared. The overall hysteretic loops, stiffness degradation, energy dissipation, member behavior and strength, response of the connection region, and visual inspection of the crack patterns are not affected by whether conventional seismic ties are used or continuous transverse reinforcement is placed in the beam plastic hinge regions and columns. The available seismic detailing and design procedures are applicable to either type of transverse reinforcement.

5.0 Summary and Recommendations

Continuously wound transverse reinforcement offers a number of advantages over conventional U-shaped stirrups or ties, mainly from the point of view of ease and speed of construction. However, the current ACI 318 Codes does not explicitly permit the application or use of continuous transverse reinforcement (CTR). At this point, approval per ACI 318, Section 1.4 is required in order to use CTR. Nevertheless, such an approval requires demonstration of successful field applications and/or well-documented test/computational data. The research reported herein was conducted to generate such data and facilitate the use of CTR in U.S. design and construction practice. In addition, the research reported herein is aimed at modifying the ACI 318 Code, such that CTR is recognized as an acceptable alternative.

A total of 30 full-scale specimens were designed, tested, and evaluated. The specimens allowed an in-depth study of

(a) shear dominant flexural members;

(b) members subjected to pure torsion as well as to the combined actions of bending moment, shear, and torsional moment;

(c) short columns loaded in compression; and

(d) exterior beam-column connections subjected to cyclic loads simulating seismic events.

In addition, a number of detailing issues were examined; in particular, splicing of CTR cages, and the differences in how conventional transverse reinforcement and CTR are fabricated. All the specimens were proportioned according to the current Code design provisions and detailing requirements. Each group of specimens included a control specimen using conventional reinforcement. Therefore, not only was it possible to experimentally compare CTR versus conventional transverse reinforcement, but also it was possible to evaluate the applicability of current equations to CTR. As needed, changes to the existing design equations were proposed based on the specificities of CTR.

The specimens were evaluated in terms of serviceability, strength, ductility, and failure mode. Based on the synthesis of the data presented in this report, the following conclusions and recommendations are made.

1. Continuous transverse reinforcement provides the same level of shear performance as conventional U-shaped stirrups in terms of crack widths and crack patterns, failure mode, and strength. The post-failure shear response is improved as a result of the enhanced confinement that CTR provides.

2. To achieve the most favorable capacity and behavior of CTR for shear design, it is recommended that the angled legs of the CTR be placed parallel to the top and bottom faces of a beam. This configuration provides near-vertical stirrup legs coincident wit the shear plane.

3. Well-established procedures for shear design are applicable when considering the use of CTR. If the angled legs of CTR are in the shear plane, a condition that is not typical, the following equation is to be used to compute steel shear strength.

   $V_s = \frac{2A_t f_{yt} d \sin\alpha}{s}$ where α is the angle between longitudinal reinforcement and inclined transverse reinforcement.

   Note: The lowest expected value of angle α is $90^o - 25^o = 65^o$. Therefore, the smallest value of V_s is $V_s = \frac{1.8A_t f_{yt} d}{s}$, which is slightly less than $V_s = \frac{A_v f_{yt} d}{s} = \frac{2A_t f_{yt} d}{s}$, i.e., the standard equation for computing steel shear strength.

4. Continuous transverse reinforcement cages can simply and effectively be spliced by first cutting off the manufactured end hooks and then lap splicing conventional stirrups to the cut ends. The specimen in this study that was spliced based on this technique could develop and exceed the calculated nominal capacity.

5. The so-called "dogleg", which is a byproduct of how the selected CTR is fabricated, does not influence the effectiveness of CTR.

6. The crack widths, crack patterns, and cracking torque are essentially the same in specimens using conventional closed stirrups and those using CTR. When using CTR, the torsional capacity is as good as, and in some cases better than that produced from conventional transverse reinforcement. However, the capacity and residual concrete torsional capacity are reduced if the diagonal cracks due to torsion are in the same direction as how CTR "spirals". It is anticipated that the influence of this directional effect would be lessened if the spacing of transverse reinforcement were reduced below the current ACI limit. However, this solution would likely create constructability issues.

   If the direction of the torque is known a priori, e.g., the member is subjected to gravity loads only, CTR has to be placed such that the "spiral" of CTR will be in the opposite direction of how diagonal cracks are formed. For cases where the direction of torque could change, the capacity of the member needs to be limited to the torsional cracking capacity multiplied by strength reduction $\phi = 0.75$, i.e., $4\phi\sqrt{f_c'}\left(\frac{A_{cp}^2}{P_{cp}}\right)$.

   The nominal torsional capacity is $T_n = \frac{A_t f_{yt} A_o \cot\theta\left(1+\sin\alpha\right)}{s}$.

Note: The lowest expected value of angle α is $90^o - 25^o = 65^o$. Therefore, the smallest value of the nominal torsional capacity is $T_n = \frac{1.9 A_t f_{yt} A_o}{s} \cot\theta$, which is slightly less than $T_n = \frac{2 A_o A_t f_{yt}}{s} \cot\theta$, which is in the current Code.

The additional longitudinal reinforcement required to resist longitudinal force due to torsion is computed from $A_l \geq 2\left(y_0 + x_o \sin\alpha\right)\frac{A_t}{s}\left(\frac{f_{yt}}{f_y}\right)\cot^2\theta$. The current equation, i.e., $A_l \geq p_h \frac{A_t}{s}\left(\frac{f_{yt}}{f_y}\right)\cot^2\theta$, can also be used to conservatively determine the required area of steel (A_l).

7. In practice, members are commonly subjected to combined actions of bending moment, shear, and torsional moment. For such a situation, the capacities of members with conventional closed ties and those with CTR are similar. Available interaction equations appear to be adequate for computing the capacity when CTR is used.

8. In terms of axial load capacity and confinement of the core by the transverse reinforcement, no substantial differences could be identified between short columns using conventional ties, CTR, or spiral. Even though the level of confinement was similar in all the columns, the columns with conventional ties and CTR failed in a brittle fashion, whereas the spirally reinforced column did not. The spirally reinforced column also exhibited an excellent post-peak ductility. The current ACI 318 provisions can be used to compute the axial load capacity.

9. Exterior beam-column connections with conventional seismic ties and CTR performed similarly when subjected to cyclic lateral loading. The energy dissipation characteristic of the specimen with CTR was slightly better than the one with conventional seismic ties. The rate of stiffness degradation for the connection using CTR was less than the specimen that had conventional seismic ties. The current seismic design provisions and detailing requirements are sufficient if CTR is used.

10. In lieu of isometric drawings, the plan, side, and cross-sectional views should be used to convey the geometry of CTR.

6.0 Dissemination Plan and Action Items

In order to disseminate the results and findings to the engineering community, two articles will be prepared and submitted for possible publication. One article has already been published in *ACI Concrete International*[1]. The second article will be an in-depth technical paper

[1] Bill H.L., Dolleman A.M., Miller M.L., Shahrooz B.M., "Evaluation of Continuous Transverse Reinforcement," Concrete International, ACI, (35)(11)(2013): 49-55.

for *ACI Structural Journal*. The approved final report will be forwarded to ACI technical committee 445 in order to start the process of changing ACI 318 to allow the use of CTR.

7.0 References

American Concrete Institute (ACI), Committee 318 (2011), "Building Code Requirements for Structural Concrete (ACI 318-11) and Commentary (ACI 318R-11), American Concrete Institute," Farmington Hills, MI, 509 pp.

Bartoli, G. (2009), "Tests on R.C. Beams with 'Spirex' and 'Traditional' Transverse Reinforcement," University of Florence, 7 pp.

Bentz, E.C. (2000), *Response 2000*, http://www.ecf.utoronto.ca/~bentz/home.shtml, accessed June 10, 2013.

Cavanagh, T. and Moehle, J.P. (1985), "Confinement Effectiveness of Crossties in RC", *ASCE Journal of Structural Engineering*, V. 111, No. 10, pp. 2105-2120.

Chalioris, C.E. and Karayannis C.G. (2013), "Experimental Investigation of RC Beams with Rectangular Spiral Reinforcement in Torsion," *Elsevier Engineering Structures*, in press.

Collins, M.P. and Mitchell, D. (1991), "Prestressed Concrete Structures," Prentice Hall, Englewood Cliffs, NJ, 766 pp.

Hsu, T. T. C. (1993), "Unified Theory of Reinforced Concrete," CRC Press, Boca Raton, FL, 313 pp.

Huespe, A. E., Linero S., Dorian L., and Oliver O., Xavier (2007), "A Model of Material Failure for Reinforced Concrete via Continuum Strong Discontinuity Approach and Mixing Theory," *International Center for Numerical Methods in Engineering*; Barcelona, Spain.

Joint ACI-ASCE Committee 352 (2010), "Recommendations for Design of Beam-Column Connections in Monolithic Reinforced Concrete Structures (ACI 352R-02) (Reapproved 2010)," American Concrete Institute, Farmington Hills, MI, 37 pp.

MacGregor, J.G. and Wight, J.K. (2009), "Reinforced Concrete: Mechanics and Design," Fifth Edition, Pearson, Prentice Hall, Upper Saddle River, NJ, 1157 pp.

Park, R. and Paulay, T. (1975), "Reinforced Concrete Structures", Wiley-Interscience Publication, New York, NY, 769 pp.

Riva, P. (2009), "Cyclic Test on Column-Foundations Using Spirex" Stirrups, Research Report, University of Bergamo, Bergamo, Italy, 47 pp.

Saatcioglu, M., Razvi, S.R. (1992), "Strength and Ductility of Confined Concrete," *ASCE Journal of Structural Engineering*, V. 118, No. 6, pp. 1590-1607.

Wallace, J. W., McConnell, S. W., Gupta, P., and Cote, P. A., (1998), "Use of Headed Reinforcement in Beam-Column Joints Subjected to Earthquake Loads," *ACI Structural Journal*, V. 95, No. 5, pp. 590-606.

Appendix A

Required Material for Standard and Continuous Transverse Reinforcement

HOOP CLOSED STIRRUP U-STIRRUP CONTINUOUS

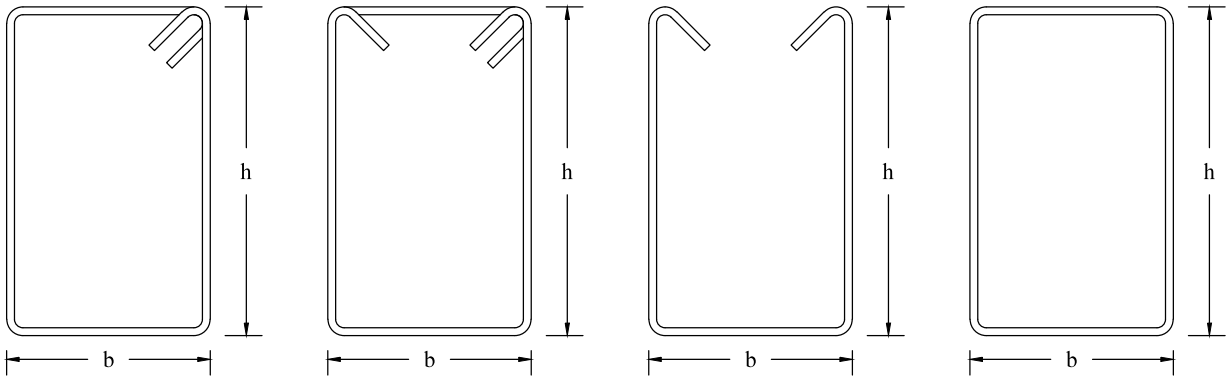

Steel Quantity Comparison

width =	16	in	bar =	# 3	bar
height =	24	in	135° hook length =	4	in
concrete cover =	1.5	in	90° hook length =	4	in
b =	13	in	length of beam =	174	in
h =	21	in	spacing =	10	in
			side cover =	2	in

# of stirrups: 18

HOOP

LENGTH OF STEEL: **114** **ft**

CLOSED STIRRUP

LENGTH OF STEEL: **126** **ft**

U-STIRRUP

LENGTH OF STEEL: **94.5** **ft**

CONTINUOUS

LENGTH OF STEEL: **111.6066** **ft**

PERCENT MORE STEEL: **15.3%**

Appendix B

Shear Database

ACI Stuctural Journal #103-S39	Modeling of Shear Behavior in Reinforced Concrete Beams

Theory: Model developed to determine stress critical elements in Reinforced Concrete. The model was verified with experiemental results.

b (mm)	b (in)	d (mm)	d (in)	ρ (%)	A_s (in^2)	a/d
51	2.01	90	3.54	1.23	0.09	2.25
51	2.01	90	3.54	1.23	0.09	2.25
152	5.98	272	10.71	1.8	1.15	1.50
152	5.98	272	10.71	1.8	1.15	2.00
152	5.98	272	10.71	1.8	1.15	2.50
152	5.98	272	10.71	1.8	1.15	3.50
152	5.98	272	10.71	1.8	1.15	4.50
152	5.98	272	10.71	1.8	1.15	5.50
307	12.09	466	18.35	1.8	3.99	3.92
310	12.20	461	18.15	1.81	4.01	3.97
190	7.48	270	10.63	2.07	1.65	1.00
190	7.48	270	10.63	2.07	1.65	1.50
190	7.48	270	10.63	2.07	1.65	2.30
190	7.48	270	10.63	2.07	1.65	3.50
190	7.48	270	10.63	2.07	1.65	5.50
305	12.01	466	18.35	2.27	5.00	4.90
305	12.01	464	18.27	2.28	5.00	4.93
231	9.09	461	18.15	2.43	4.01	3.95
229	9.02	466	18.35	2.43	4.02	4.91
307	12.09	466	18.35	2.73	6.05	6.91
307	12.09	462	18.19	2.74	6.02	6.90
152	5.98	272	10.71	2.8	1.79	1.00
152	5.98	272	10.71	2.8	1.79	2.00
152	5.98	272	10.71	2.8	1.79	2.50
152	5.98	272	10.71	2.8	1.79	3.00
152	5.98	272	10.71	2.8	1.79	3.50
152	5.98	272	10.71	2.8	1.79	4.00
152	5.98	272	10.71	2.8	1.79	4.50
152	5.98	272	10.71	2.8	1.79	5.50
152	5.98	272	10.71	2.8	1.79	6.00
229	9.02	461	18.15	3.06	5.01	6.95

ACI Stuctural Journal #103-S71	Shear Strength of Reinforced Concrete T-Beams

Theory: The shear resistance of reinforced concrete T-beams with verification from experimental data in other literature.

b (mm)	b (in)	d (mm)	d (in)	ρ (%)	A_s (in^2)	a/d
610	24.02	394	15.51	0.49	1.83	3.93
610	24.02	399	15.71	0.49	1.85	3.88
610	24.02	391	15.39	0.5	1.85	3.96
610	24.02	390	15.35	0.66	2.43	3.97
610	24.02	392	15.43	0.66	2.45	3.96
610	24.02	393	15.47	0.66	2.45	3.94
610	24.02	394	15.51	0.66	2.46	3.92
610	24.02	395	15.55	0.66	2.46	3.92
610	24.02	388	15.28	0.67	2.46	4.00
610	24.02	374	14.72	0.69	2.44	4.14
610	24.02	371	14.61	0.7	2.46	4.18
610	24.02	395	15.55	0.93	3.47	3.92
610	24.02	393	15.47	0.94	3.49	3.94

ACI Stuctural Journal #103-S74	Fiber-Reinforced Polymer Shear Strengthening of Reinforced Concrete Beams: Experimental Study and Analytical Modeling

Experimental: Rectangular Reinforced concrete beams strengthened in shear with externally bonded U-wrapped CFRP. Experiments were designed so that their shear ultimate capacity was reached before flexural failure.

b (mm)	b (in)	d (mm)	d (in)	ρ (%)	A_s (in^2)	a/d
150	5.91	250	9.84	7.50	4.36	3.00

ACI Stuctural Journal #105-S14

Effect of Longitudinal Tensile Reinforcement Ratio and Shear Span-Depth Ratio on Minimum Shear Reinforcement in Beams

Experimental: The effects of longitudinal tensile reinforcement ratio and shear span-depth ratio (a /d) on the minimum shear reinforcement in reinforced concrete beams were examined.

b (mm)	b (in)	d (mm)	d (in)	ρ (%)	A_s (in^2)	a/d
350	13.78	280	11.02	0.93	1.41	3.00
350	13.78	280	11.02	1.4	2.13	3.00
350	13.78	280	11.02	1.4	2.13	4.00
350	13.78	280	11.02	1.4	2.13	5.00
350	13.78	410	16.14	1.79	3.98	3.00
350	13.78	280	11.02	1.86	2.83	3.00
350	13.78	410	16.14	2.24	4.98	2.00
350	13.78	410	16.14	2.24	4.98	3.00
350	13.78	410	16.14	2.24	4.98	4.00
350	13.78	260	10.24	2.79	3.94	3.00
350	13.78	400	15.75	3.21	6.97	3.00
350	13.78	400	15.75	3.21	6.97	3.00
350	13.78	385	15.16	4.76	9.94	3.00

ACI Stuctural Journal #107-S54

Influence of Effective Depth on Shear Strength of Concrete Beams—Experimental Study

Experimental: Tests the hypothesis that the effective depth influences the shear strength of reinforced concrete flexural members with no web reinforcement. Simply supported reinforced concrete beams without shear and skin reinforcement were the test specimens.

b (mm)	b (in)	d (mm)	d (in)	ρ (%)	A_s (in^2)	a/d
305	12.01	232	9.13	1.20	1.32	3.01
408	16.06	529	20.83	1.20	4.01	2.99
305	12.01	681	26.81	1.24	3.99	2.98
306	12.05	530	20.87	1.25	3.14	2.98
203	7.99	233	9.17	1.26	0.92	2.99
306	12.05	822	32.36	1.30	5.07	3.00
508	20.00	684	26.93	1.30	7.00	2.97
613	24.13	822	32.36	1.30	10.15	3.00

ACI Stuctural Journal #107-S57

Maximum Shear Reinforcement of Reinforced Concrete Beams

Experimental: The effects of the shear reinforcement ratio and compressive strength of concrete on the maximum shear reinforcement in RC beams. Beams with various shear reinforcement ratios were tested. Although designed with excessive reinforcement, the beams failed in shear after the yielding of shear reinforcement.

b (mm)	b (in)	d (mm)	d (in)	ρ (%)	A_s (in^2)	a/d
350	13.78	383	15.08	1.44	2.99	3.00
350	13.78	383	15.08	2.4	4.99	3.00
200	7.87	252	9.92	2.55	1.99	3.00
350	13.78	383	15.08	3.35	6.96	3.00
200	7.87	252	9.92	3.82	2.98	3.00
350	13.78	383	15.08	3.83	7.96	3.00
350	13.78	383	15.08	4.79	9.95	3.00
200	7.87	252	9.92	5.1	3.98	3.00
200	7.87	252	9.92	5.54	4.33	3.00
200	7.87	252	9.92	6.92	5.41	3.00

ACI Stuctural Journal #108-S45	Effect of Stirrup Anchorage on Shear Strength of Reinforced Concrete Beams

Experimental: Reinforced concrete sections with varying proper and improper shear reinforcement details were loaded to failure to study the effect of improperly anchored stirrups on the shear strength of reinforced concrete beams. The results suggest that reinforcement anchorage has no significant effect on the shear capacity of a reinforced concrete section.

b (mm)	b (in)	d (mm)	d (in)	ρ (%)	A_s (in^2)	a/d
330	12.99	530	20.87	2.44	6.61	3.00
330	12.99	530	20.87	2.44	6.61	3.00
330	12.99	530	20.87	2.44	6.61	3.00
330	12.99	530	20.87	2.44	6.61	3.00
330	12.99	530	20.87	2.44	6.61	3.00
330	12.99	530	20.87	2.44	6.61	3.00
330	12.99	530	20.87	2.44	6.61	3.00
330	12.99	530	20.87	2.44	6.61	3.00

Appendix C

Details of Shear Specimens

Table C.1: Average as-built dimensions

Specimen	Width (in.)	Depth (in.)	Length (in.)
S1	24 3/16	16 2/16	174
S2	24 2/16	16 2/16	174 2/16
S3	24 3/16	16 3/16	174 2/16
S4	24 1/16	16 1/16	174 2/16
S5	24 2/16	16 3/16	174 6/16
S6	24 1/16	16 2/16	174 2/16
S7	24 1/16	16 2/16	174 7/16
S8	24	16 1/16	174 3/16
S9	24 2/16	16 3/16	174 3/16
S10	24 1/16	16 2/16	174 3/16
S11	24 2/16	16 1/16	174 2/16
S12	24 1/16	16 2/16	174 3/16

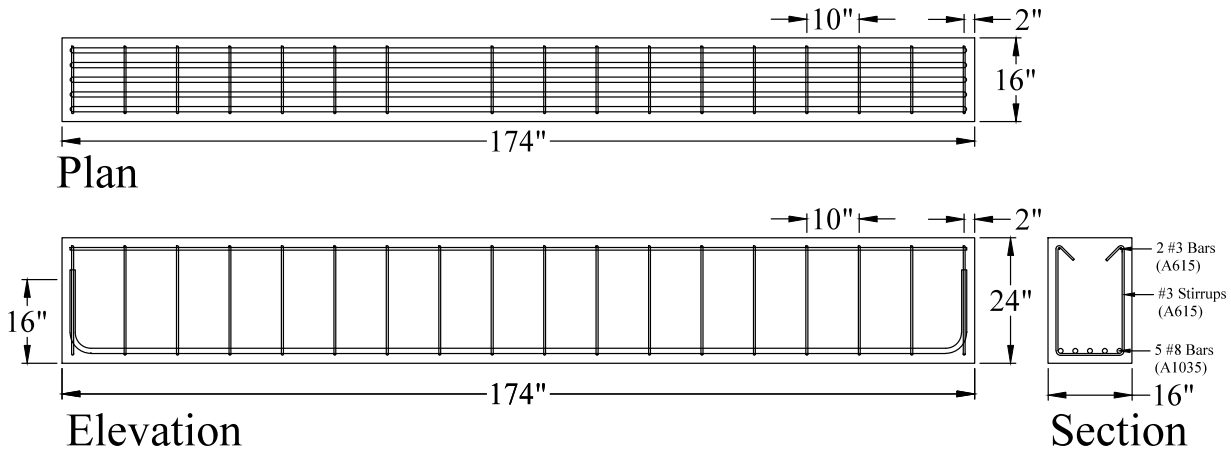

Specimens S1 and S7

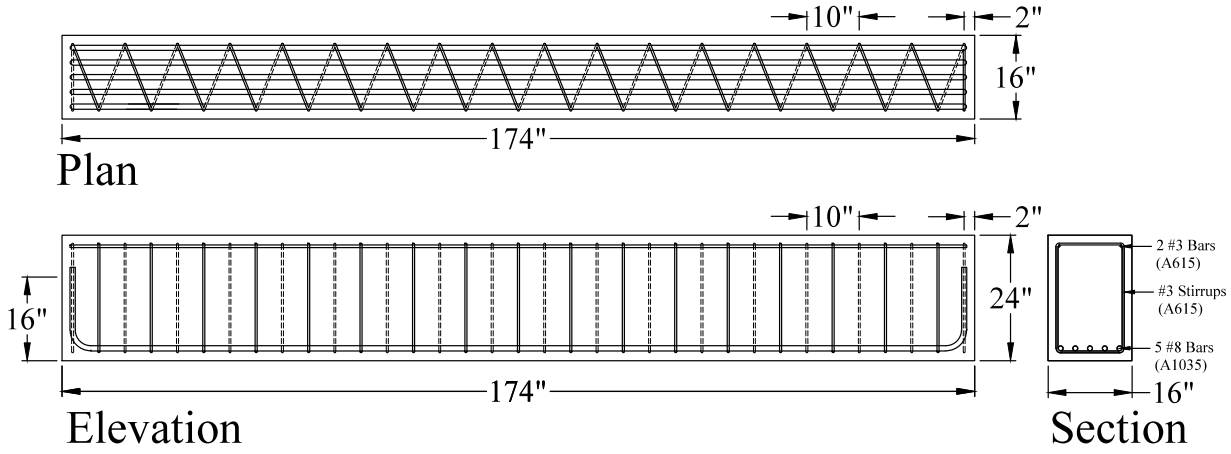

Specimens S2 and S8

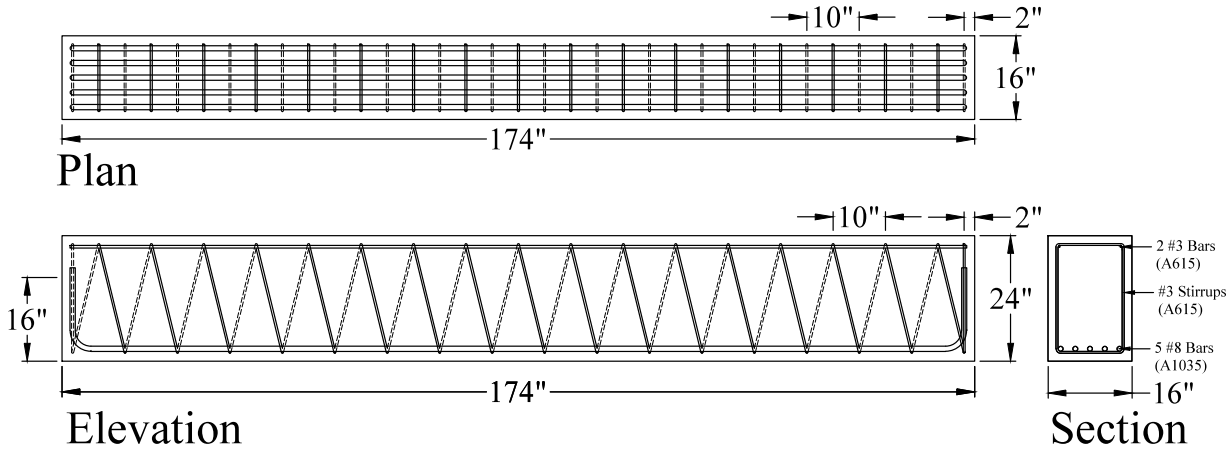

Specimens S3 and S9

Figure C.1: Specimen details

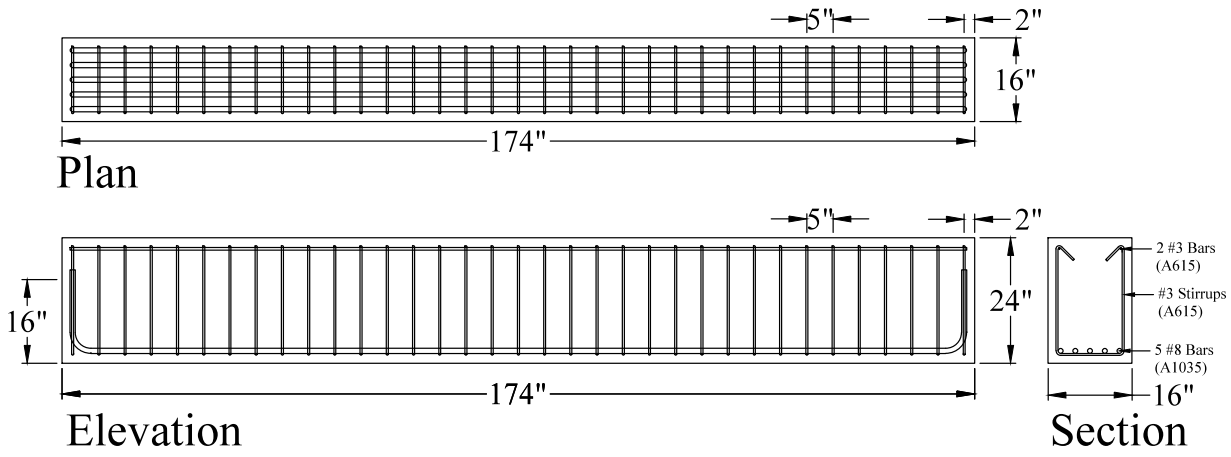

Specimens S4 and S10

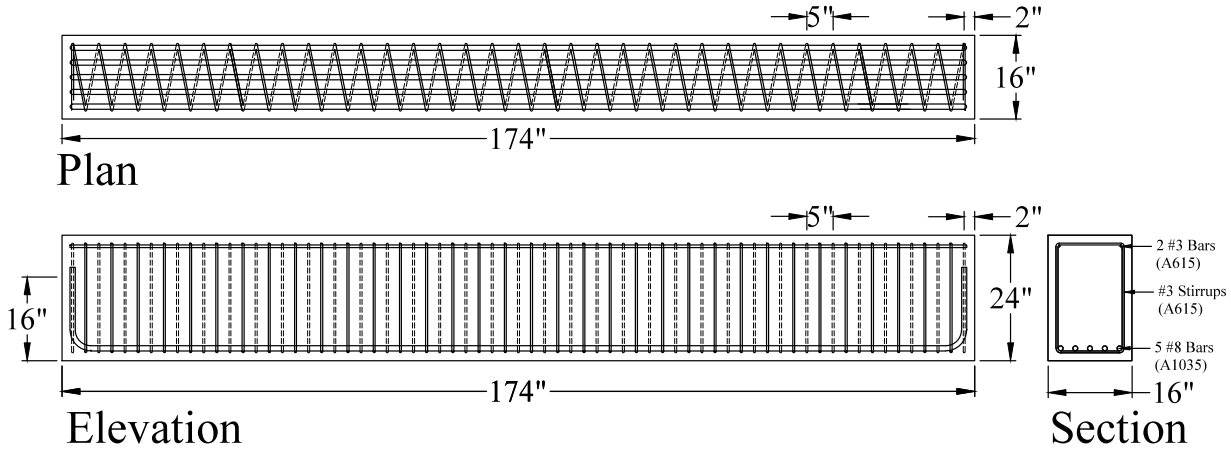

Specimens S5 and S11

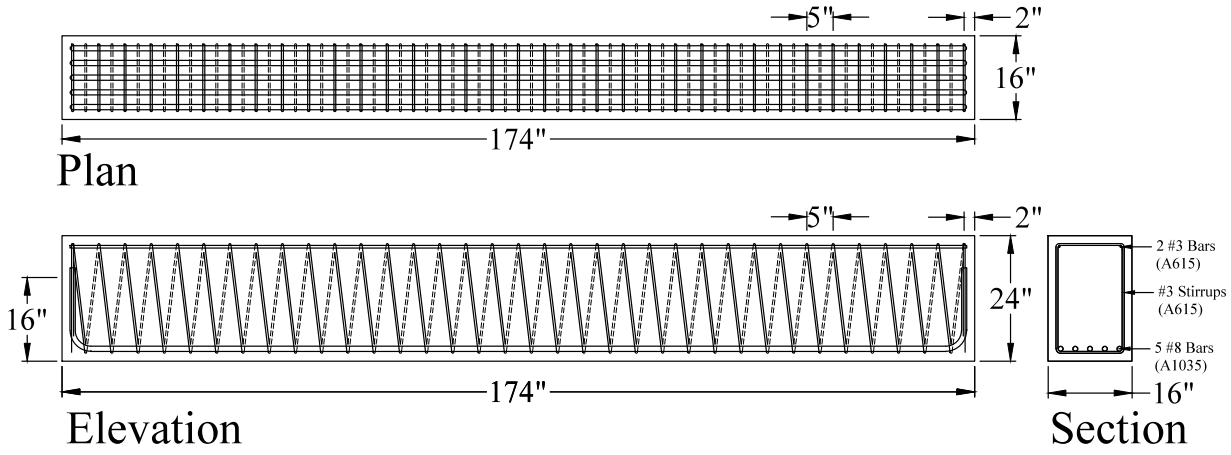

Specimens S6 and S12

Figure C.1: Specimen details (cont.)

(a) Shear specimen S1

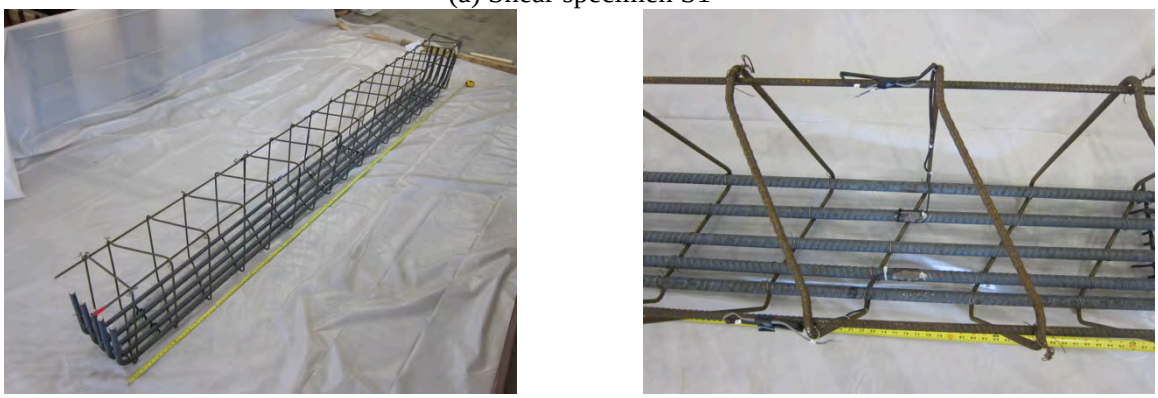

(b) Shear specimen S2

(c) Shear specimen S3

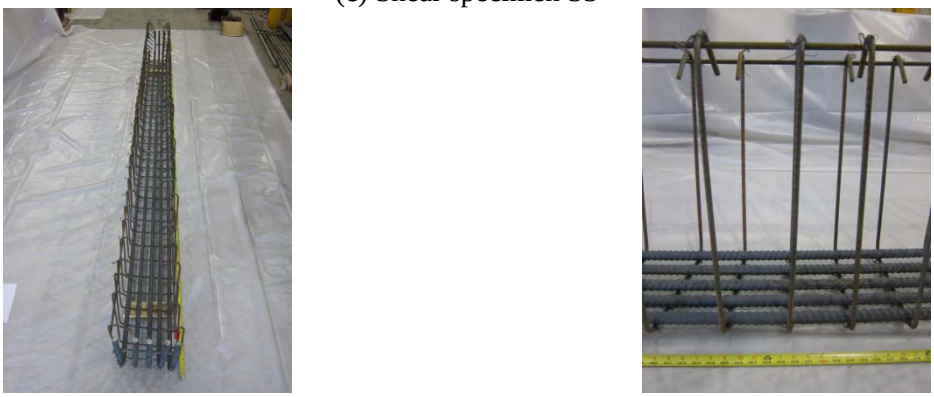

(d) Shear specimen S4

Figure C.2: Cage work

(e) Shear specimen S5

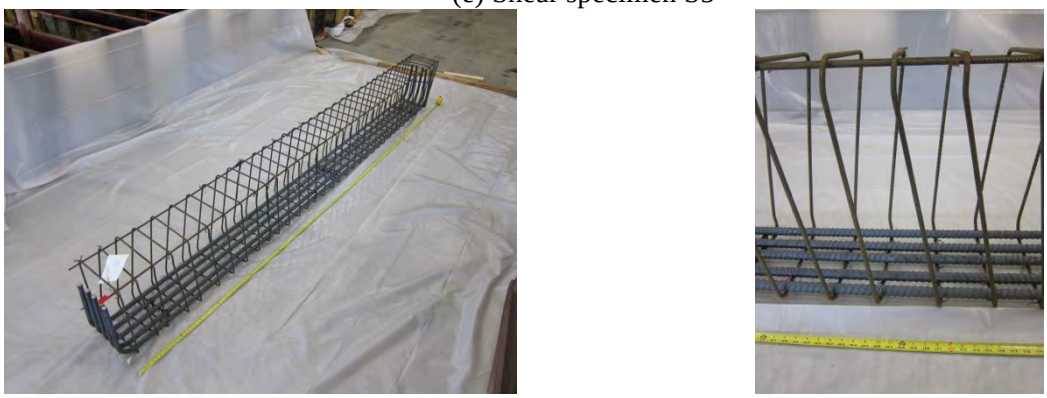

(f) Shear specimen S6

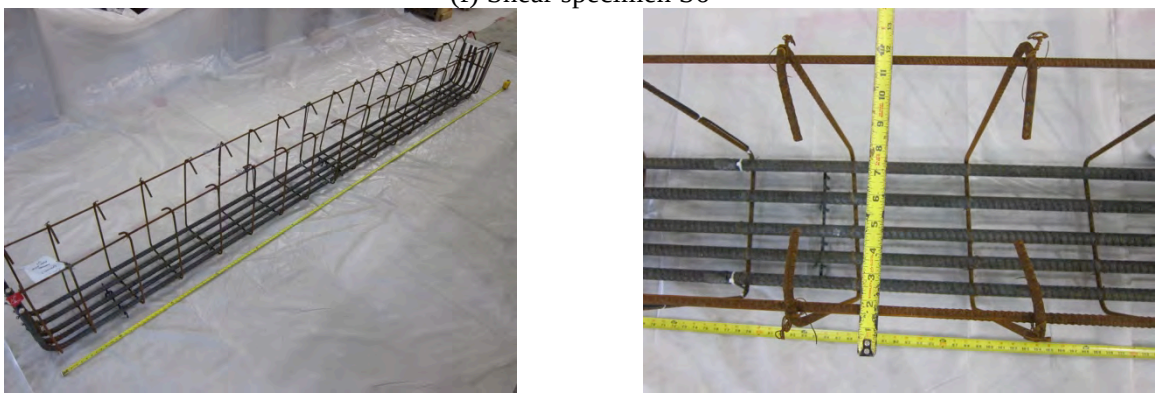

(g) Shear specimen S7

(h) Shear specimen S8

Figure C.2: Cage work (cont.)

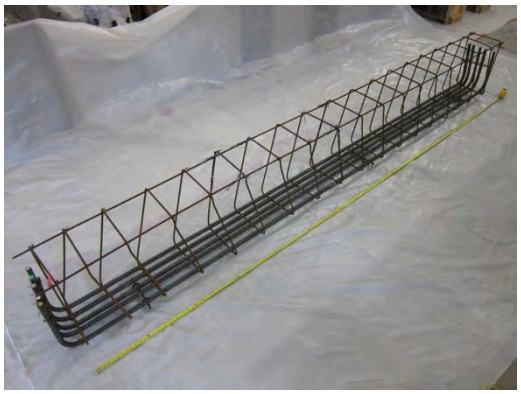
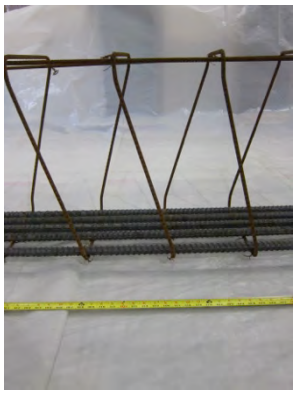

(i) Shear specimen S9

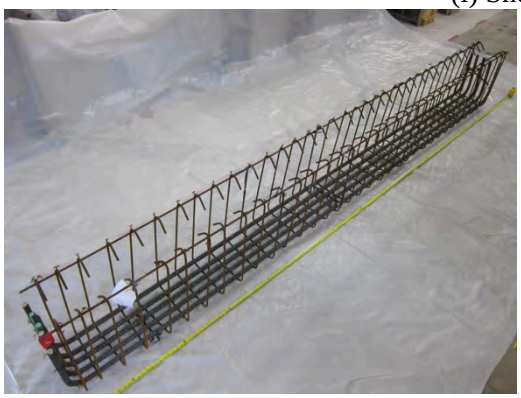
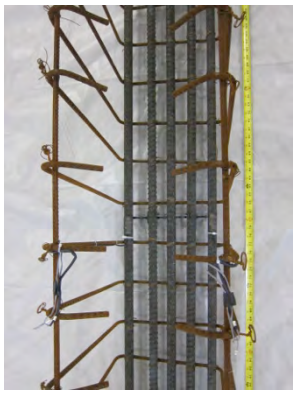

(j) Shear specimen S10


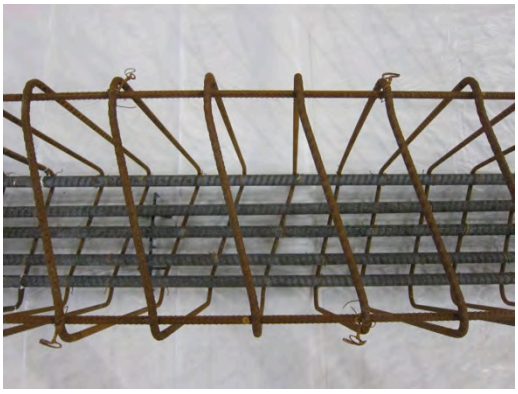

(k) Shear specimen S11


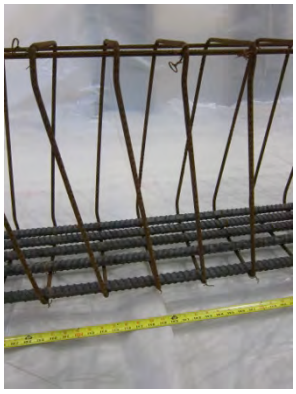

(l) Shear specimen S12

Figure C.2: Cage work (cont.)

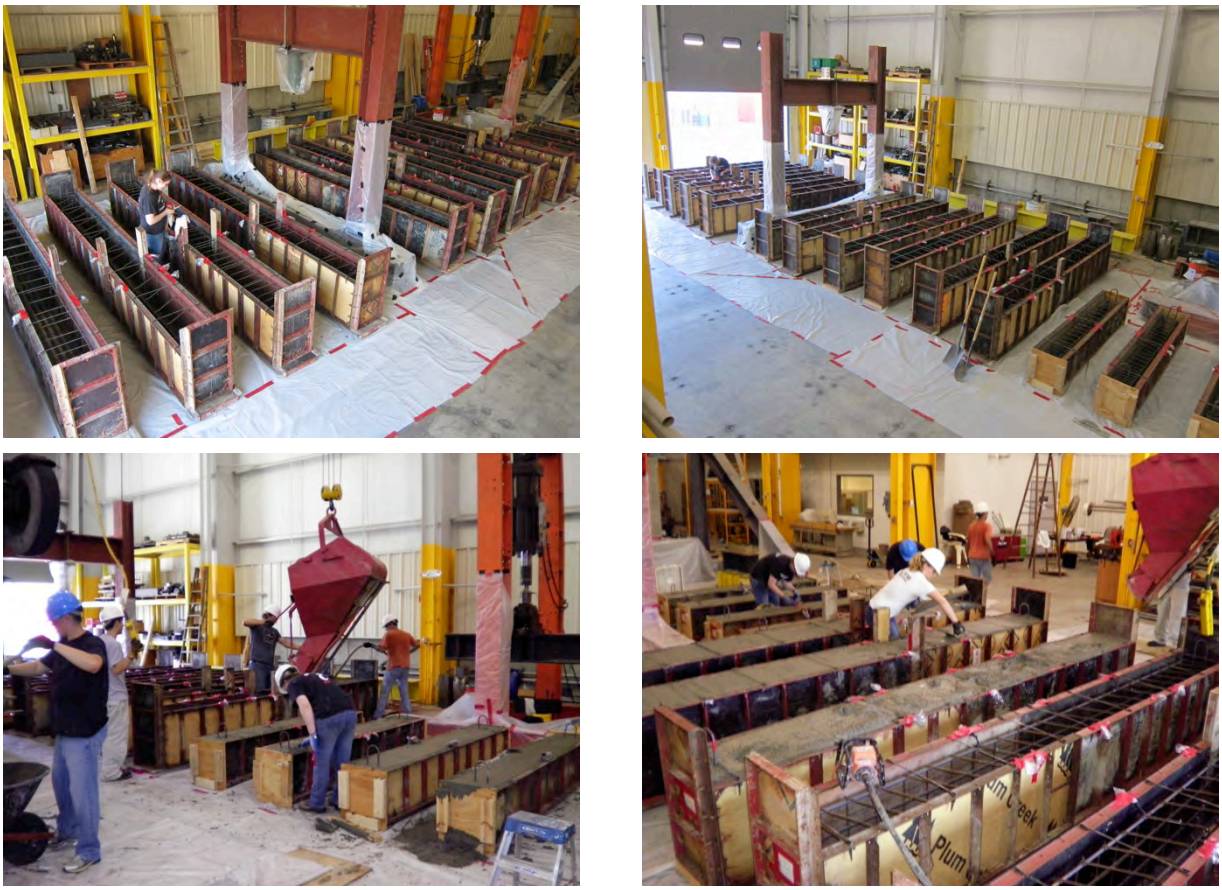

Figure C.3: Formwork

Appendix D

Details of Spliced Shear Specimen

Table D.1: Average as-built dimensions

Specimen	Width (in.)	Depth (in.)	Length (in.)
SPL	24 2/16	16 2/16	174 4/16

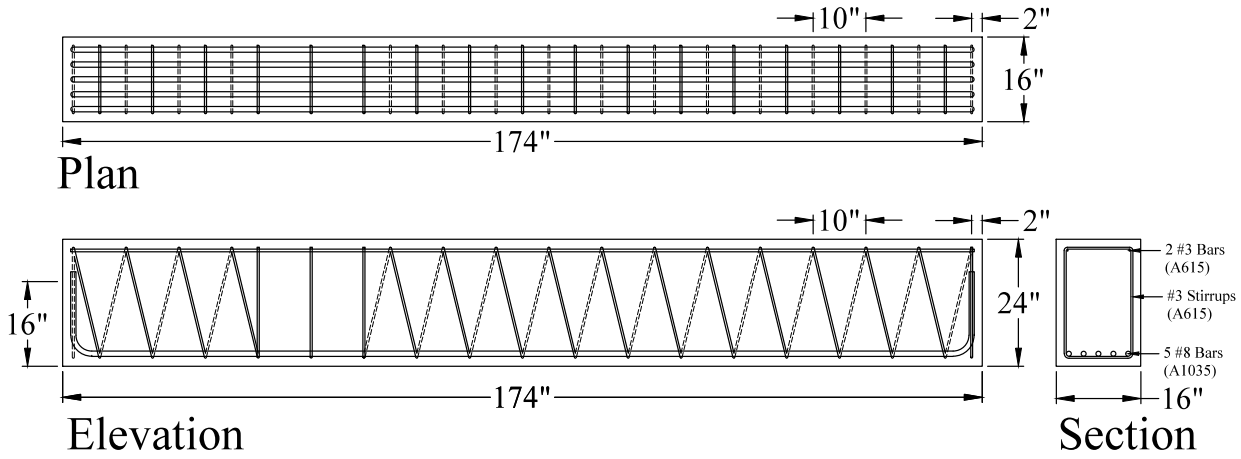

Figure D.1: Specimen details

Figure D.2: Cage work

Appendix E

Details of Pullout Specimen

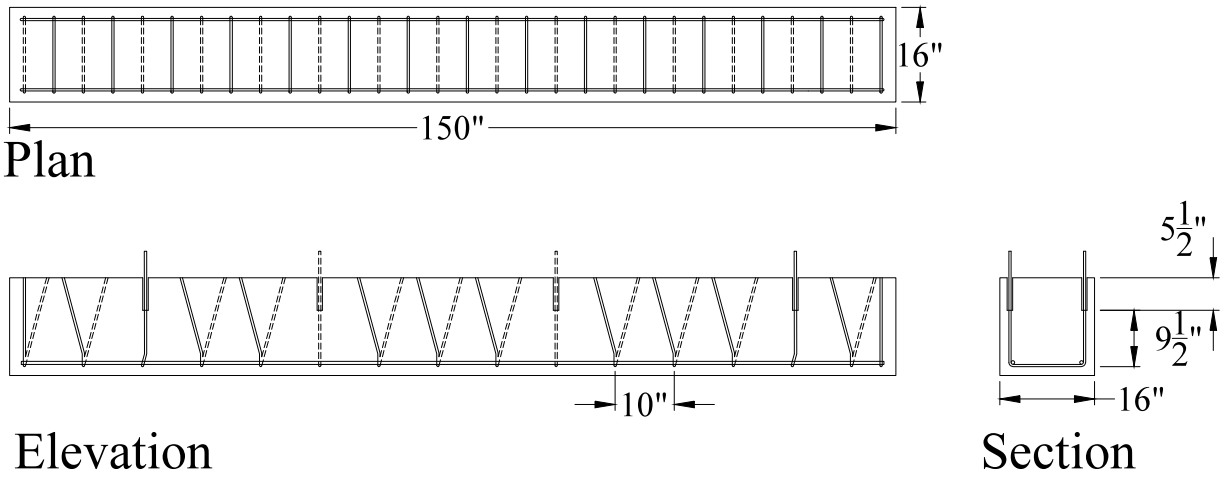

Figure E.1: Specimen details

Figure E.2: Cage work

Appendix F

Details of Pure Torsion Specimens

Table F.1: Average as-built dimensions

Specimen	Width (in.)	Depth (in.)	Length (in.)
T1	---	---	---
T2	12 2/16	16	96
T3A	12 1/16	16 1/16	95 15/16
T3B	12	16	96
T4	12 1/16	16	96
T5A	12 1/16	16	95 15/16
T5B	12 2/16	16	96 1/16

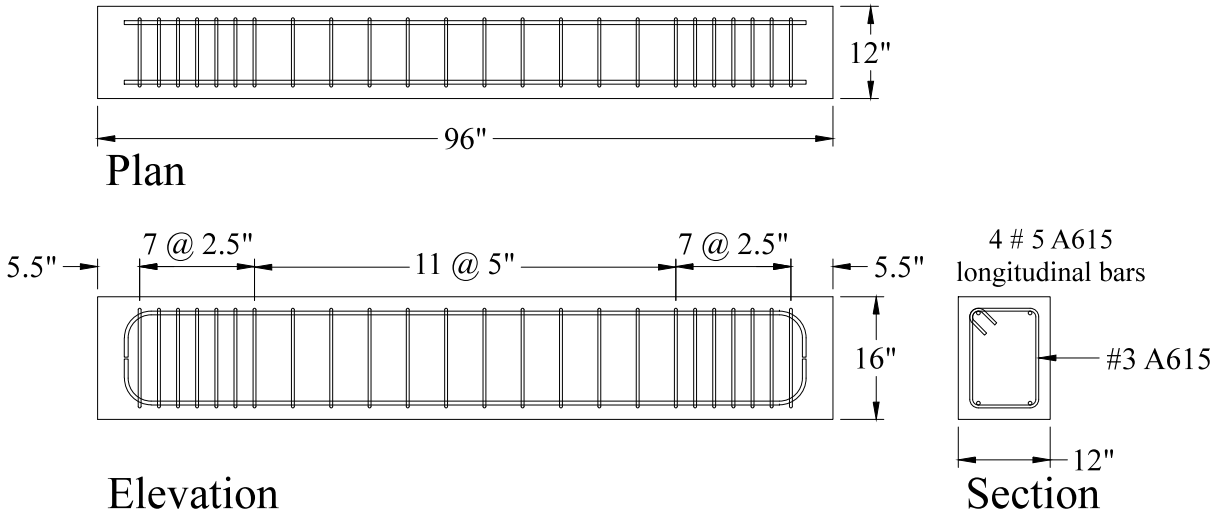

Specimens T1 and T4

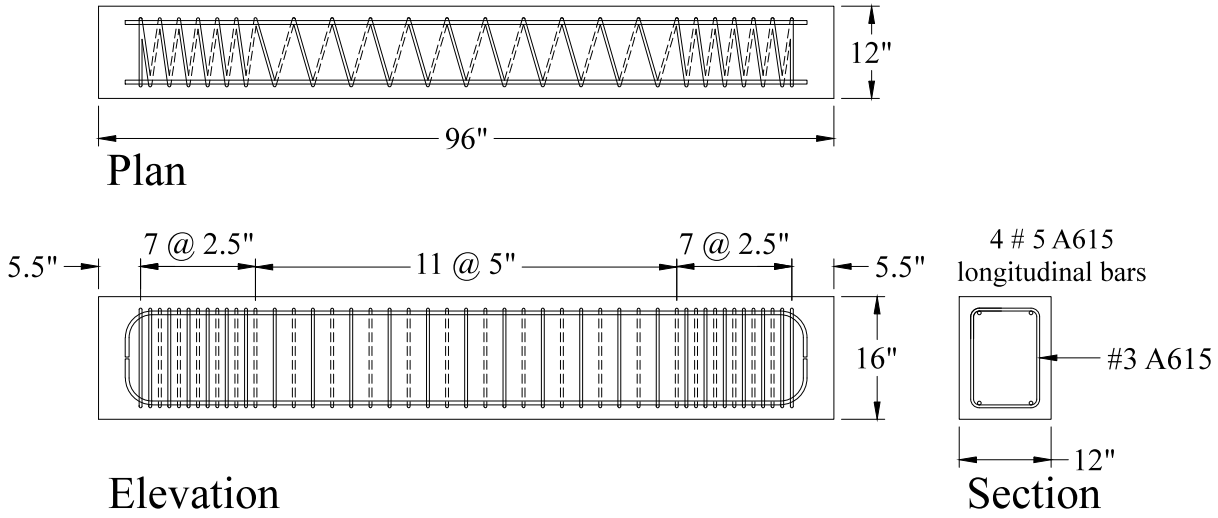

Specimens T2, T5a, and T5b

Figure F.1: Specimen details

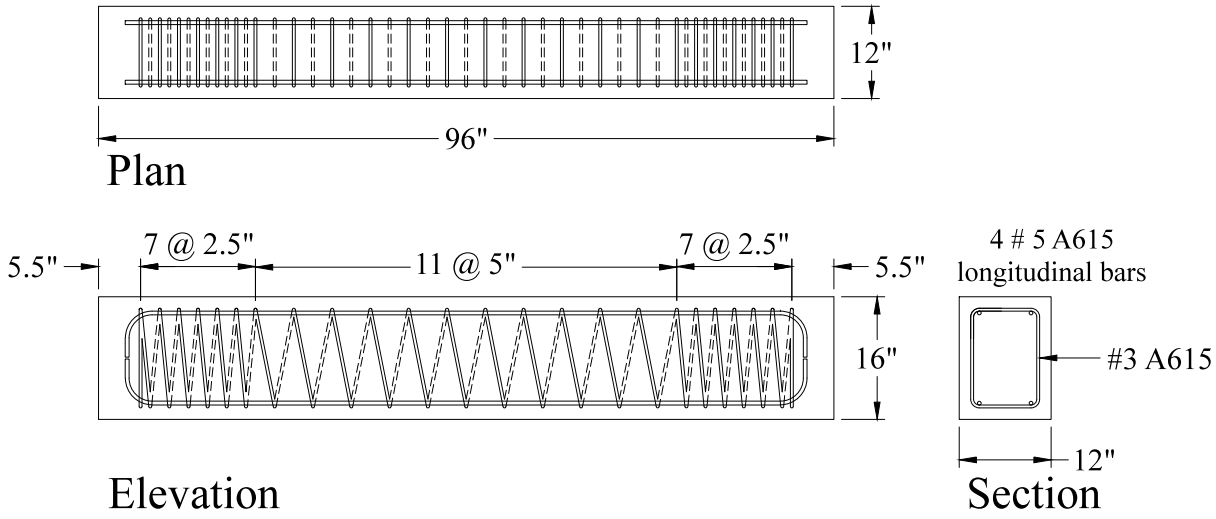

Specimens T3a and T3b

Figure F.1: Specimen details (cont.)

Specimen T1

Specimen T2

Figure F.2: Cage work

Specimens T3a and T3b

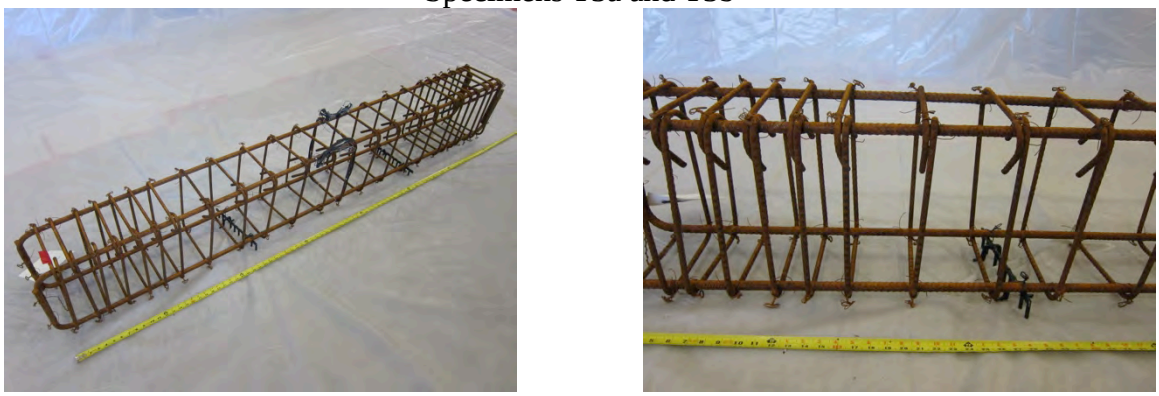

Specimen T4

Specimens T5a and T5b

Figure F.2: Cage work (cont.)

Appendix G

Details of Specimens Subjected to Bending Moment, Shear, and Torsion

Table G.1: Average as-built dimensions

Specimen	Width (in.)	Depth (in.)	Length (in.)
TFS1	16 3/16	24	168 1/16
TFS2	16 2/16	24 1/16	167 15/16
TFS3	16 3/16	24 2/16	168

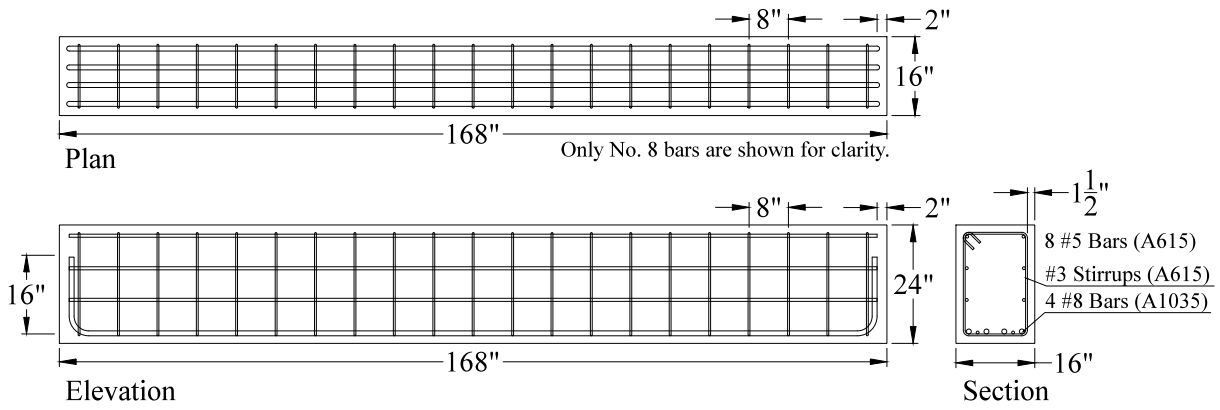

Specimen TFS1

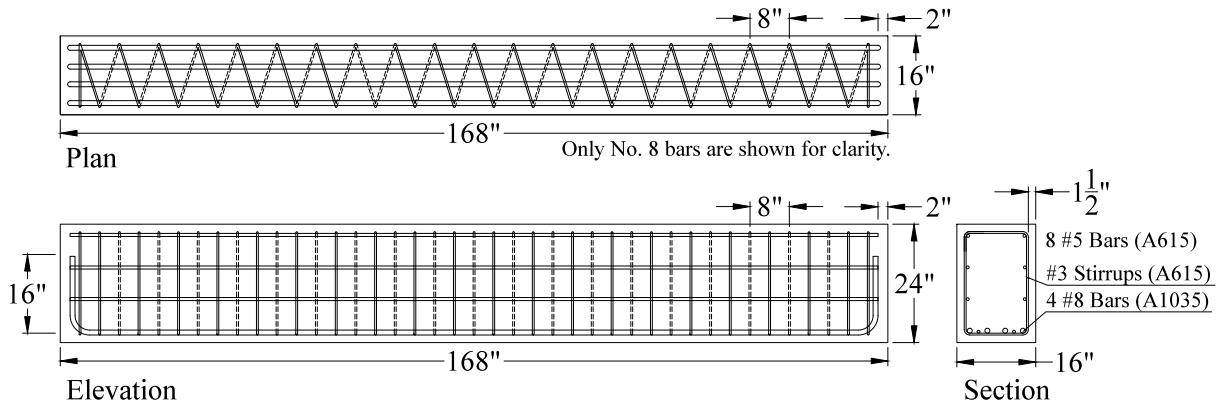

Specimen TFS2

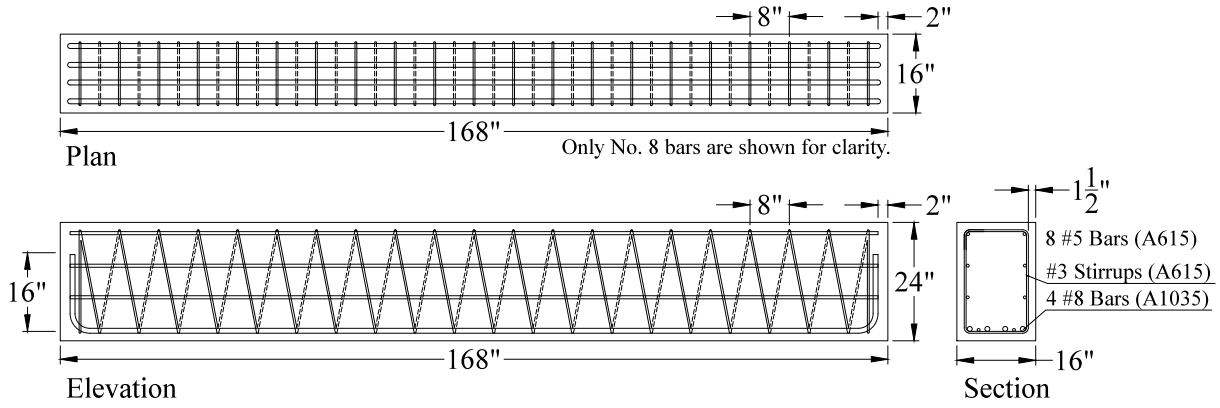

Specimen TFS3

Figure G.1: Specimen details

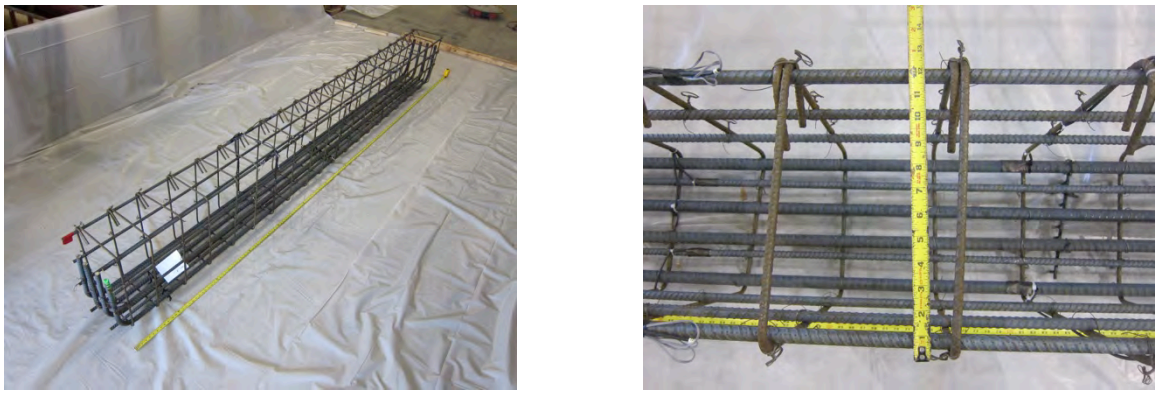

Specimen TFS1

Specimen TFS2

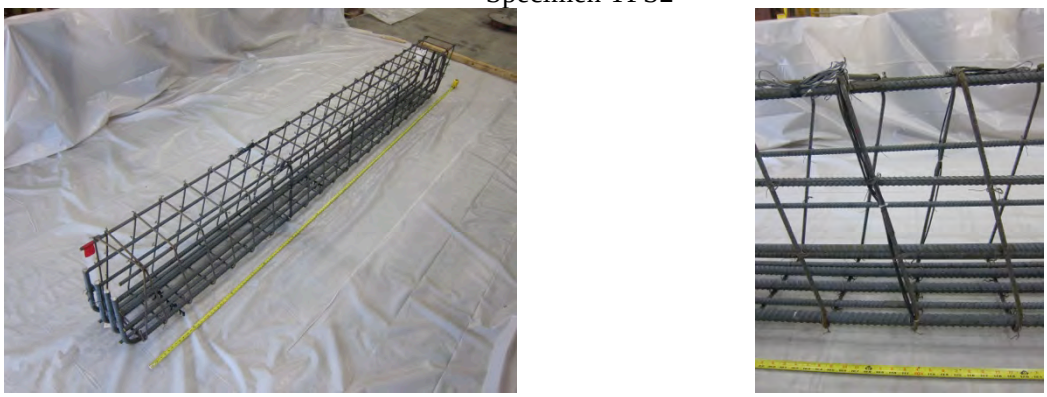

Specimens T3a and T3b

Figure G.2: Cage work

Appendix H

Details of Stub Columns

Volumetric ratio for tied column

$$\rho = \frac{(2a+2h)A_t}{sah}$$

for square columns

$$\therefore \boxed{\rho = \frac{(4h)A_t}{sh^2}}$$

Volumetric ratio for columns with continuous transverse reinforcement

Angles on two faces

$$\rho = \frac{\left[2h+2\sqrt{h^2+(s/2)^2}\right]A_t}{sah}$$

for square columns

a=h

$$\therefore \boxed{\rho = \frac{\left[2h+2\sqrt{h^2+(s/2)^2}\right]A_t}{sh^2}}$$

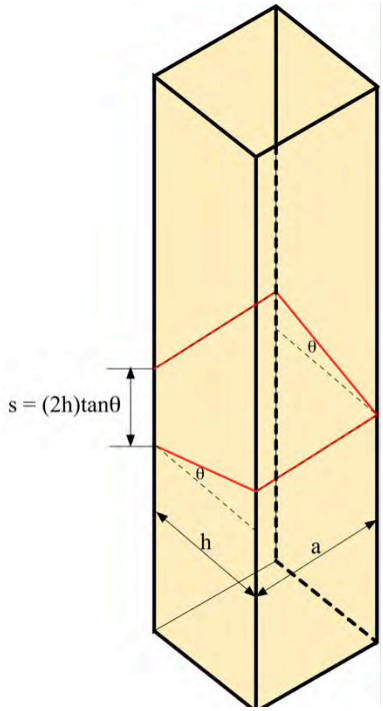

The value of θ is to be kept below 25 degrees.

$$s = 2a\tan\theta = 2h\tan\theta$$

$$h = 18" - 2\left(1.5" + \frac{3/8"}{2}\right) = 14.625"$$

$$\theta \le 25^o$$

$$s \le 13.6"$$

Angles on all four faces

$$\text{Volume of transverse reinforcement} = \left[2\sqrt{h^2 + (h\tan\theta)^2} + 2\sqrt{a^2 + (a\tan\theta)^2}\right] A_t$$

$$\text{Volume of concrete} = ah\left[(2a + 2h)\tan\theta\right]$$

$$\rho = \frac{\left[2\sqrt{h^2 + (h\tan\theta)^2} + 2\sqrt{a^2 + (a\tan\theta)^2}\right] A_t}{ah\left[(2a + 2h)\tan\theta\right]}$$

$$s = (2a + 2h)\tan\theta$$

for square columns

$$a = h$$

$$s = 4a\tan\theta = 4h\tan\theta$$

$$a\tan\theta = h\tan\theta = s/4$$

$$\therefore \boxed{\rho = \frac{\left[4\sqrt{h^2 + (s/4)^2}\right] A_t}{sh^2}}$$

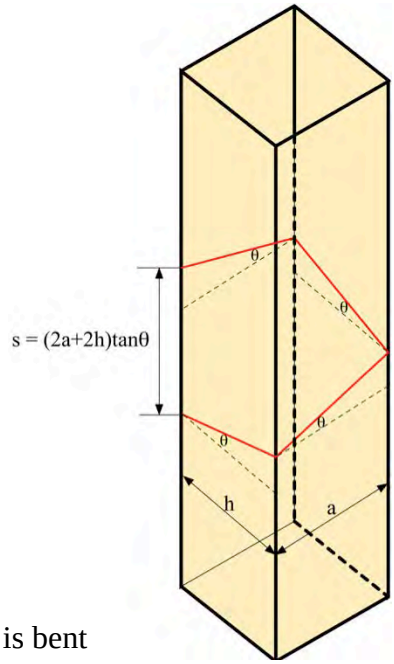

Where

θ= angle at which continuous transverse reinforcement is bent
A_t = area of transverse reinforcement
h = a = core dimensions taken as the center-to-center distance between the horizontal project of the transverse reinforcement
s = spacing of the transverse reinforcement

The value of θ is to be kept below 25 degrees.

$$s = 4a\tan\theta = 4h\tan\theta$$

$$\theta \le 25^o$$

$$s \le 27.3"$$

Column C1

Column C2

Figure H.1: Cage work

Column C3

Column C4

Figure H.1: Cage work (cont.)

Figure H.2: Formwork

Appendix I

Details of Exterior Beam-Column Connections

Table I.1: Average as-built dimensions

Specimen	Beam		Column (in.)
	Width (in.)	Depth (in.)	
BC1	16 3/16	24 1/8	18 1/8
BC2	16 1/8	24 1/16	18 1/8

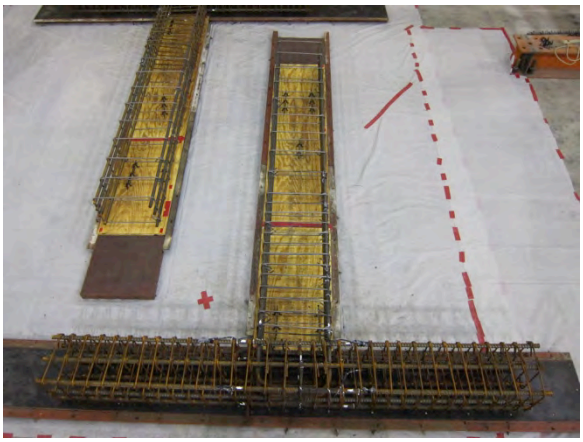

Overall view

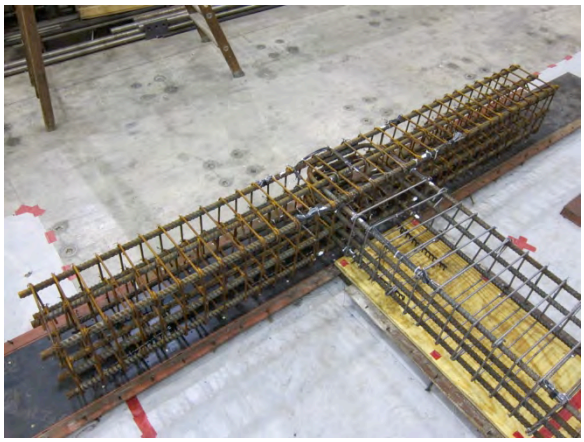

Column and beam

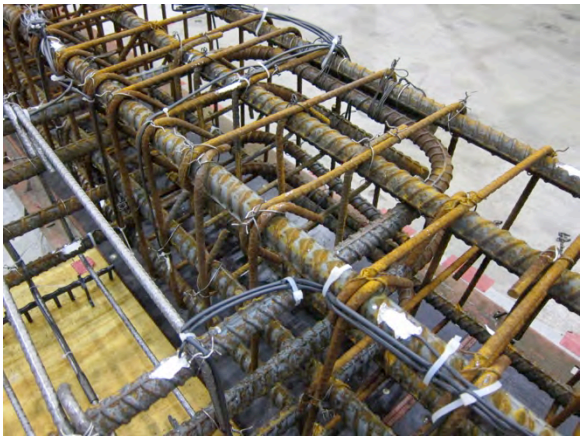

Joint region

Exterior face of joint region

Beam cross section

Column cross section

Beam-Column Connection with Conventional Seismic Ties

Figure I.1: Cage work

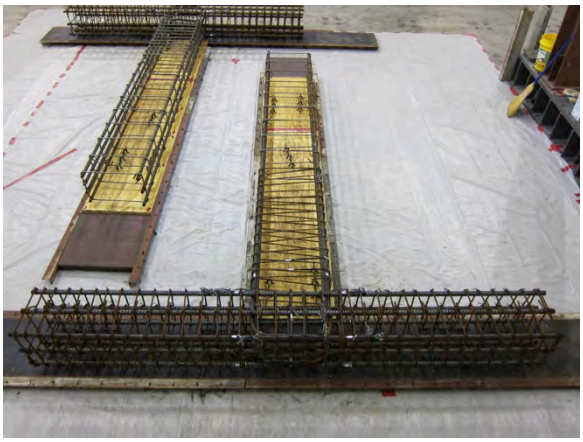

Overall view

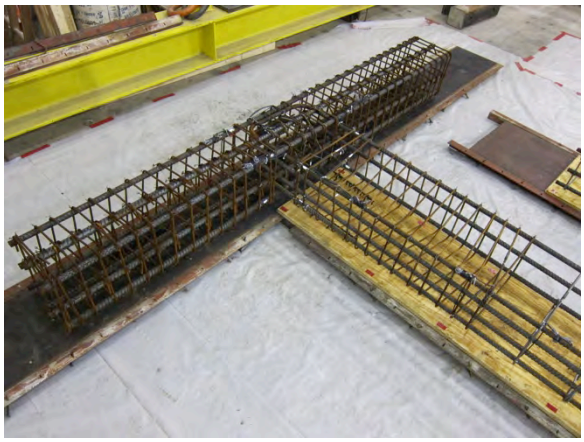

Column and beam

Joint region

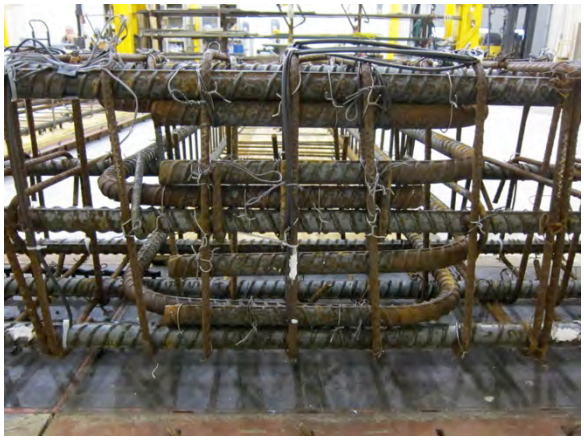

Exterior face of joint region

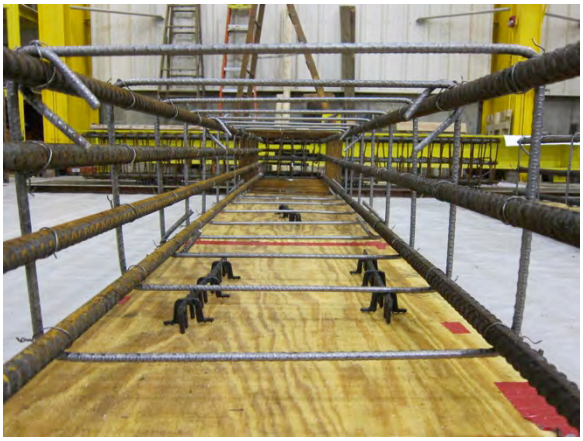

Beam cross section

Column cross section

(b) Beam-Column Connection with Continuous Transverse Reinforcement

Figure I.1: Cage work (cont.)

Detail of hinge assembly at the top and bottom of the column

Detail of rod assembly for measuring the joint shear deformation

Overall view

After placement of concrete

Figure I.2: Formwork

Appendix J

Material Properties and Concrete Mix Design

Table J.1: Material properties of various reinforcing bars

Bar	Sample	f_y (ksi)	E_s (ksi)	f_u (ksi)	ε_f
No. 9 (A615)	Sample 1	48.2*	27438*	87.5*	---
	Sample 2	71.3	29,210	109.6	---
	Mill report	70.7	---	105.3	0.151
		70.5	---	104.8	0.151
	Average	70.8	---	106.6	0.151
	COV	0.6%	---	2.5%	0.0%
No. 8 (A615)	Sample 1	71.4	23,126	113.8	---
	Sample 2	69.4	23,408	111.3	---
	Mill report	71.3	---	108.5	0.163
		75.1	---	112.3	0.163
	Average	71.8	23,267	110.4	0.163
	COV	3.3%	0.9%	2.0%	0.0%
No. 8 (A1035)	Sample 1	92.3[&]	21,823	158.8	---
	Sample 2	96.7[&]	21,704	160.7	---
	Mill report	112**	---	165.3	0.106
	Average	100.3	21,764	161.6	---
	COV	10%	0.4%	2.1%	---
No. 7 (A615)	Sample 1	73.0	25,896	111.6	0.122
	Sample 2	73.6	29,720	111.6	0.095
	Sample 3	73.2	26,993	111.9	0.133
	Mill report	74.6	---	112.0	0.163
		74.3	---	111.4	0.163
	Average	73.7	27,536	111.7	0.135
	COV	0.9%	7.2%	0.2%	21.4%
No. 5 (A615/A706)	Sample 1	73.1	28,436	108.2	0.106
	Sample 2	74.0	26,618	110.2	0.126
	Sample 3	73.2	25,533	108.0	0.104
	Mill report	71.5	---	102.1	0.151
		68.0	---	104.5	0.157
	Average	72.0	26,862	106.6	0.129
	COV	3.4%	5.5%	3.0%	19.1%
No. 3 (A615/A706)	Sample 1	71.3	25,074	105.9	0.076
	Sample 2	69.0	25,433	104.8	0.116
	Sample 3	71.7	26,718	105.6	0.100
	Sample 4	71.5	25,908	105.1	0.155
	Mill report	70.7	---	101.0	0.157
		71.5	---	100.6	0.161
	Average	71.0	25,783	103.8	0.128
	COV	1.4%	2.8%	2.3%	27.8%

* Ignore these values.

& Based on 0.2% offset method

** The yield strength is the average value based on 0.35% EUL (93.98 ksi) and from 0.2% offset method (129.95 ksi).

f_y = yield strength, f_u = tensile strength, E_s = modulus of elasticity, ε_f = fracture strain

Table J.2: Concrete mix designs

Mix	5 ksi		10 ksi	
Provider	Hilltop, Cincinnati		Hilltop, Cincinnati	
Design f'_c (psi)	5,000		10,000	
	Qty	Source	Qty	Source
Portland Cement (lbs/cy)	565	Holcim Ste. Genevieve	825	Lehigh
Fine aggregate (lbs/cy)	1466	Hilltop Patriot	980	Hilltop Patriot
Coarse aggregate (lbs/cy)	1720	Hilltop Patriot	1425	Hilltop Patriot
Mid-size aggregate (lbs/cy)	-	-	430	Hilltop Patriot
Water (lbs/cy)	275	Cincinnati	290	Cincinnati
Silica Fume (lbs/cy)	-	-	67	Master Builders
Pozzolith 80 (oz/cy)	22.6	Master Builders	-	-
Polyheed 1725 (oz/cy)	33.9	Master Builders	-	-
HRWR (oz/cy)	-	-	124.9	GLENIUM 7500
Stabilizer (oz/cy)	-	-	35.7	Delvo
w/c ratio	0.49		0.33	
Unit weight (lbs/cf)	149.1		148.8	
Slump (in.)	7.5		8.00	
Air content (%)	1.5		1.5	

Table J.3: Measured concrete compressive strength

Test Specimens	Age (days)	Testing phase	f'_c (psi)	Average f'_c (psi)
Shear, Torsion, Flexure-Shear-Torsion (FST) 5 ksi	9	----	5,290 5,180 4,780 4,740 4,830 4,940	4,960
	28	----	5,900 5,990 5,990	5,960
	44	Before testing shear specimens	6,440 5,830 6,100	6,123
	72	After testing shear specimens	6,260 6,410 6,210	6,293
	107	Before testing torsion specimens	6,760 6,200 6,370	6,443
	170	Before testing FST specimens	6,330 6,640 6,210	6,393
	212	After testing FST specimens	6,840 7,080 6,590 6,560	6,768
Shear, Torsion 10 ksi	7	----	9,330 9,140 8,910 9,830 9,830 10,050	9,515
	29	----	10,710 11,030 11,170 11,800	11,178
	57	Before testing shear specimens	8,670 11,360 11,880	10,637
	84	After testing shear specimens	11,320 11,240	11,280
	102	Before testing torsion specimens	10,520 10,490 11,440	10,817

Table J.3: Measured concrete compressive strength

Test Specimens	Age (days)	Testing phase	f'_c (psi)	Average f'_c (psi)
Stub columns 5 ksi	14	----	4,980 4,950 4,950	4,960
	28	----	5,320 5,440 5,410	5,390
	97	Before testing stub columns	4,760 5,450 5,300	5,170
Beam-column (BC) connections 5 ksi	7	----	4,980 4,720 4,340	4,680
	28	----	5,810 5,020 5,230	5,353
	103	Before testing BC connections	6,940 6,430 6,350	6,573

Table J.4: Measured concrete tensile strength

Test Specimens	Age (days)	f'_t (psi)	Average f'_t (psi)
Shear, Torsion, Flexure-Shear-Torsion (FST) 5 ksi	112	430 440 480 470	455
Shear, Torsion 10 ksi	112	550 540 540 600 560 645	573
Beam-column connections 5 ksi	107	415 375 370	387

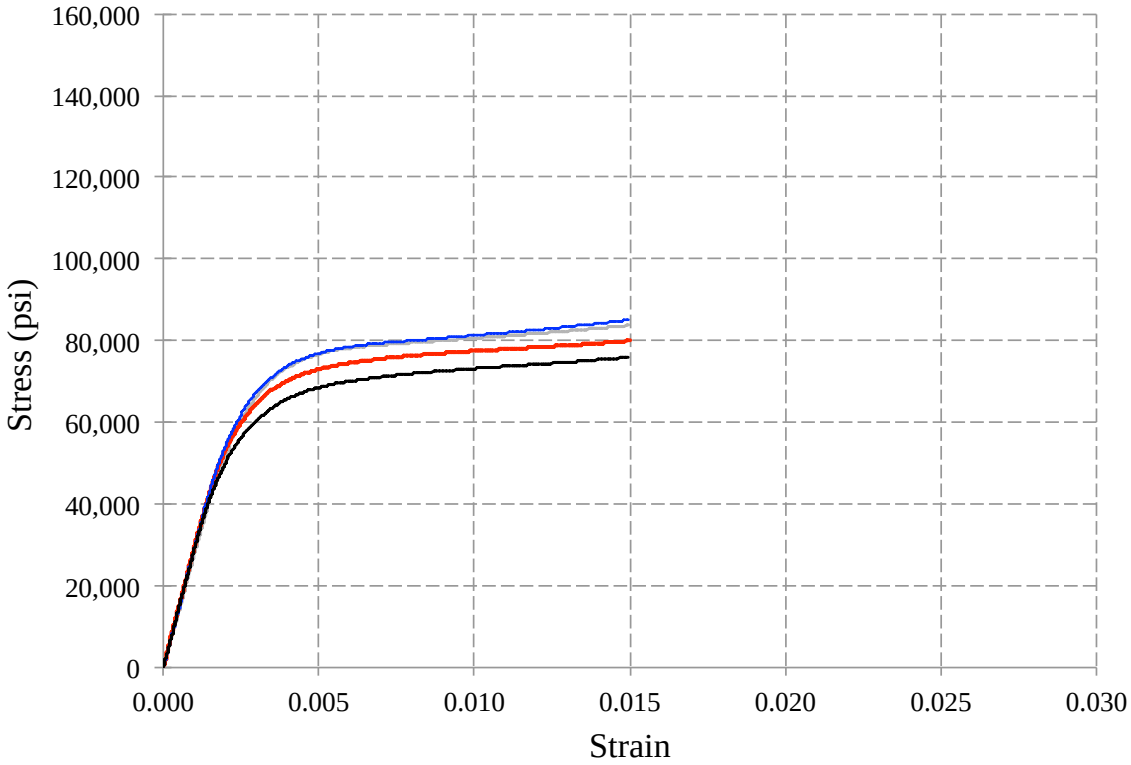

(a) No. 3 (A615/A706) reinforcing bars

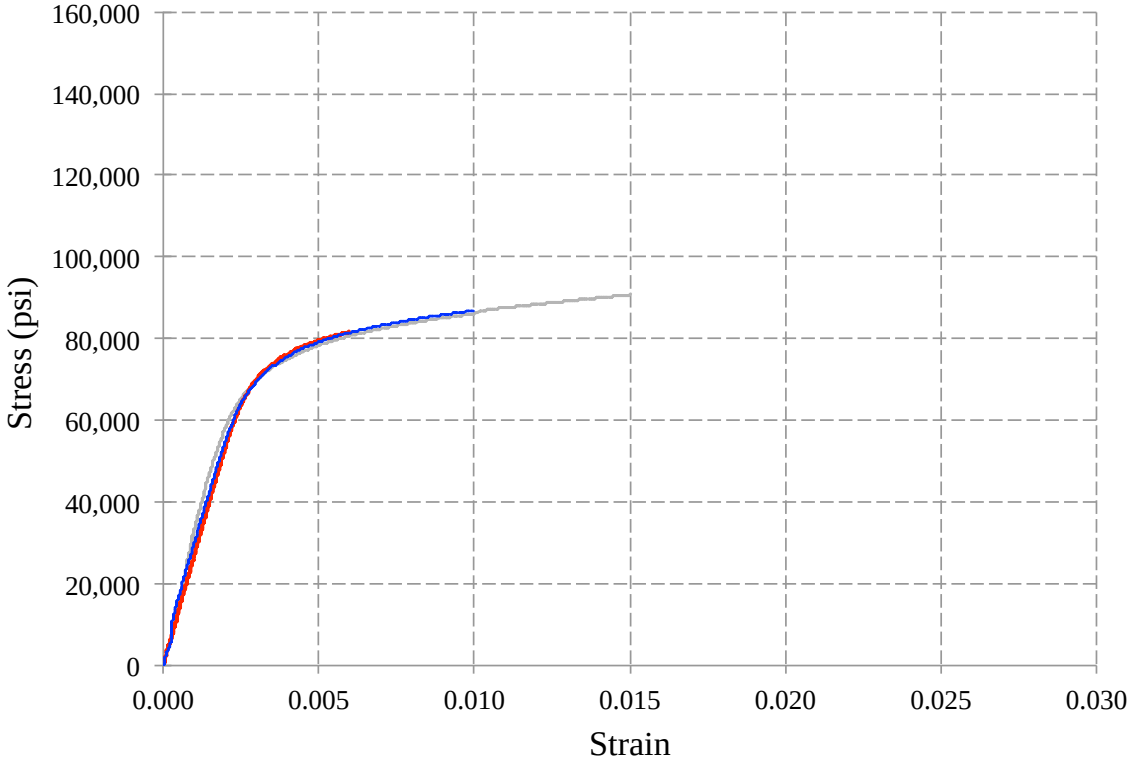

(b) No. 5 (A615/A706) reinforcing bars

Figure J.1: Measured Stress-Strain Diagrams

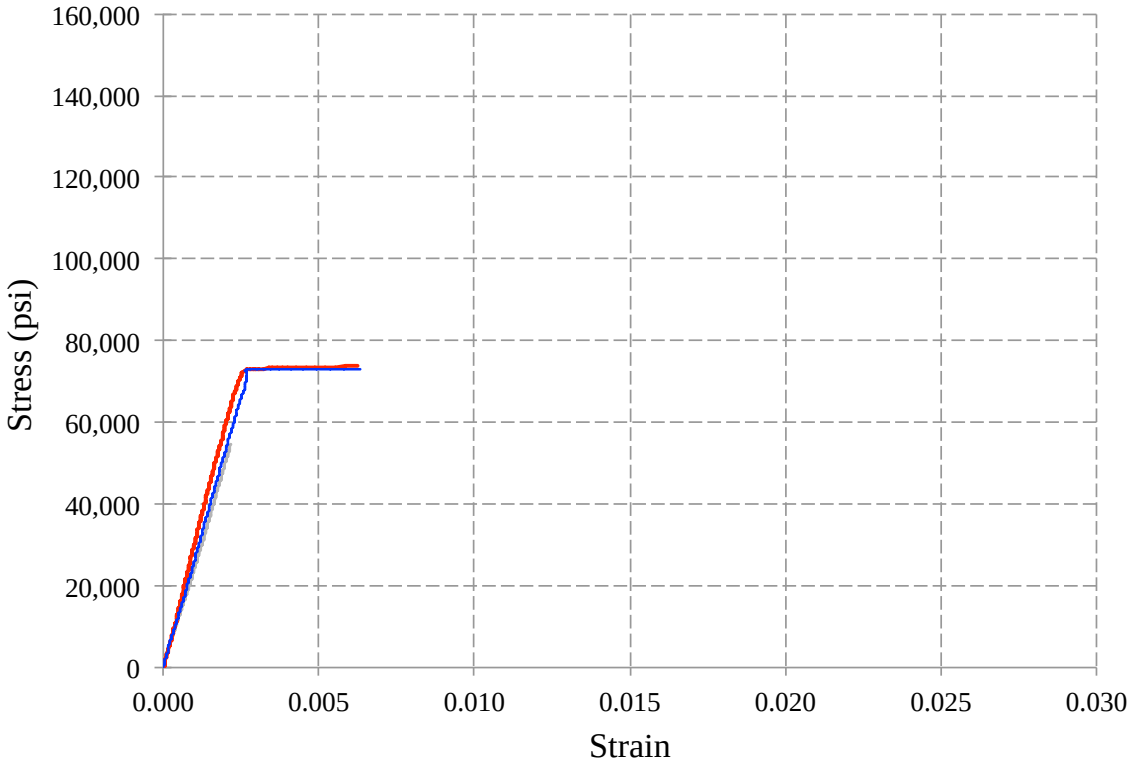

(c) No. 7 (A615) Reinforcing bars

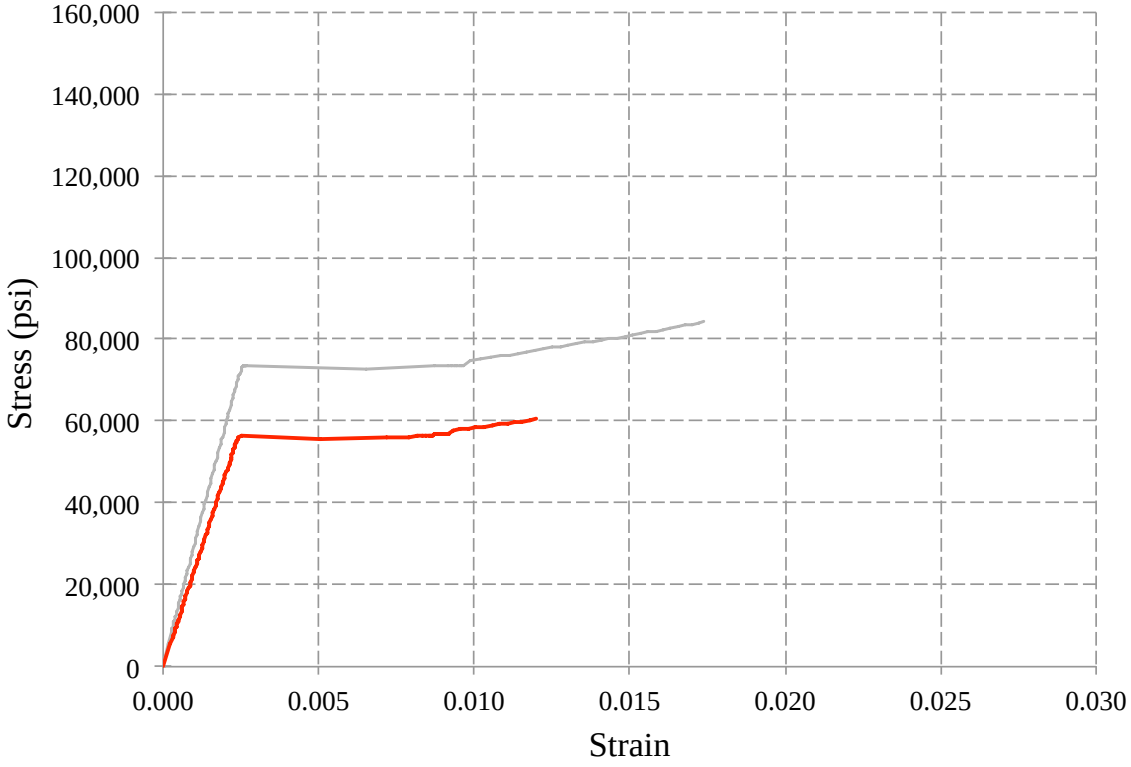

(d) No. 8 (A615) Reinforcing bars

Figure J.1: Measured Stress-Strain Diagrams (cont.)

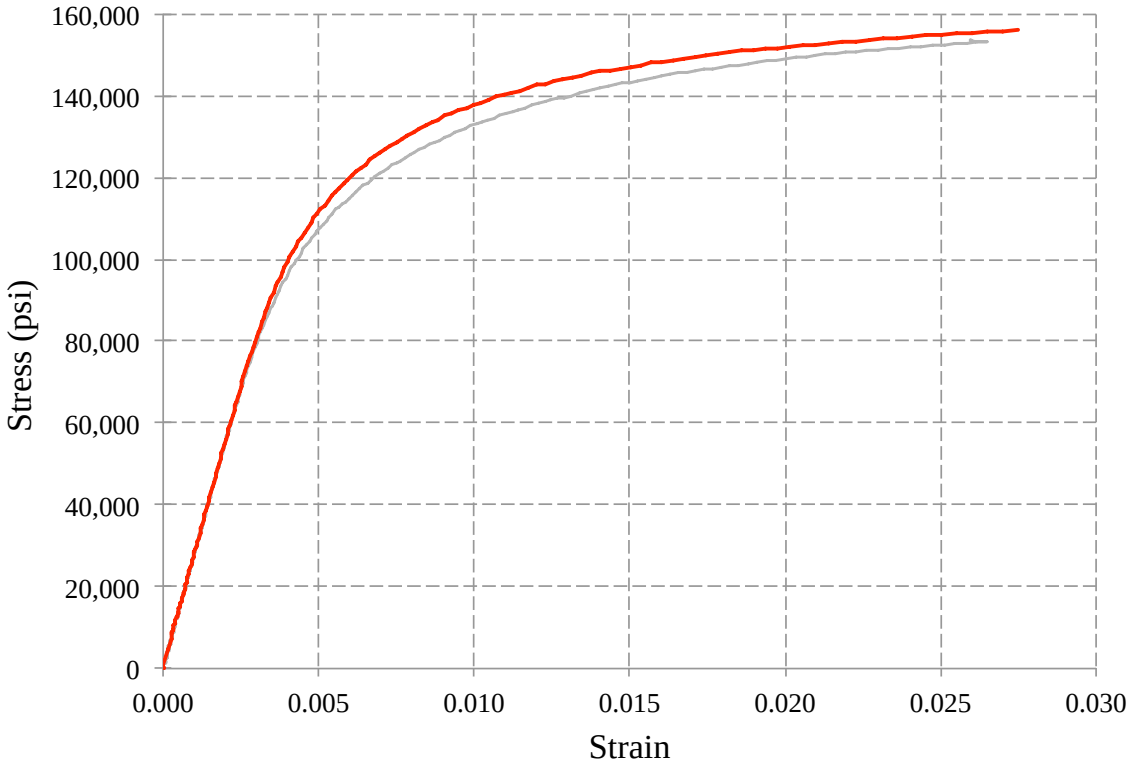

(e) No. 8 (A1035) Reinforcing bars

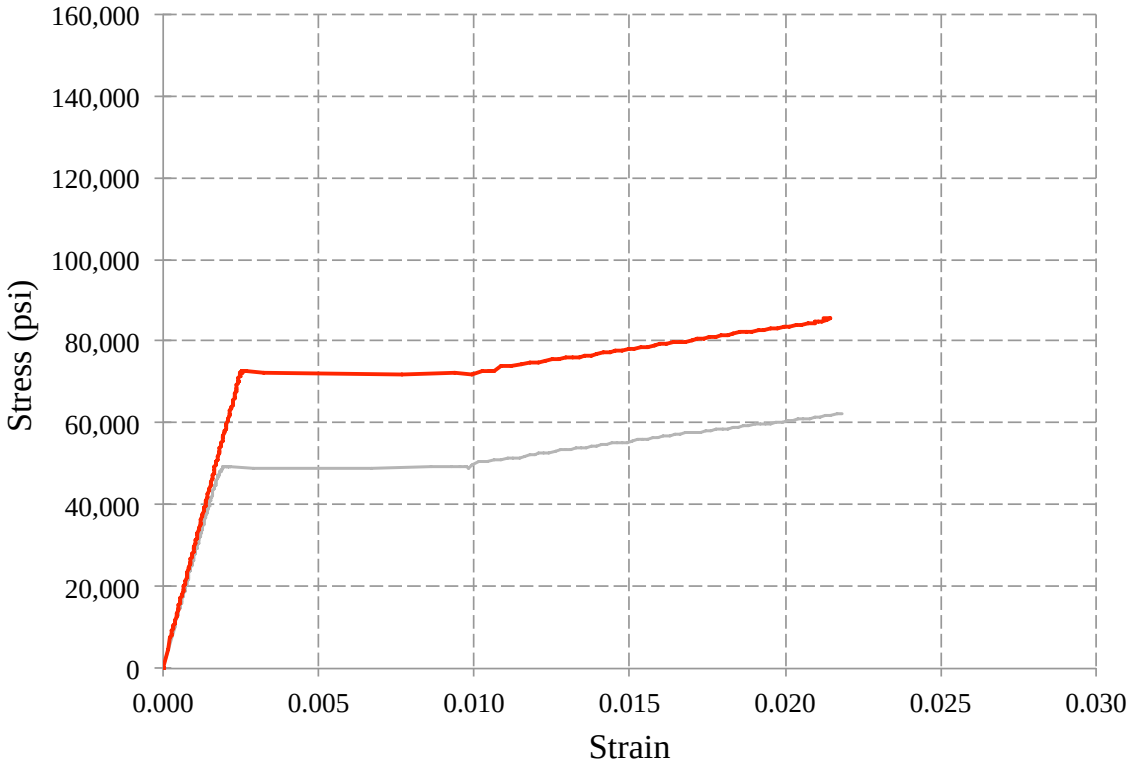

(f) No. 9 (A615) Reinforcing bars

Figure J.1: Measured Stress-Strain Diagrams (cont.)

Appendix K

Location of Strain Gages

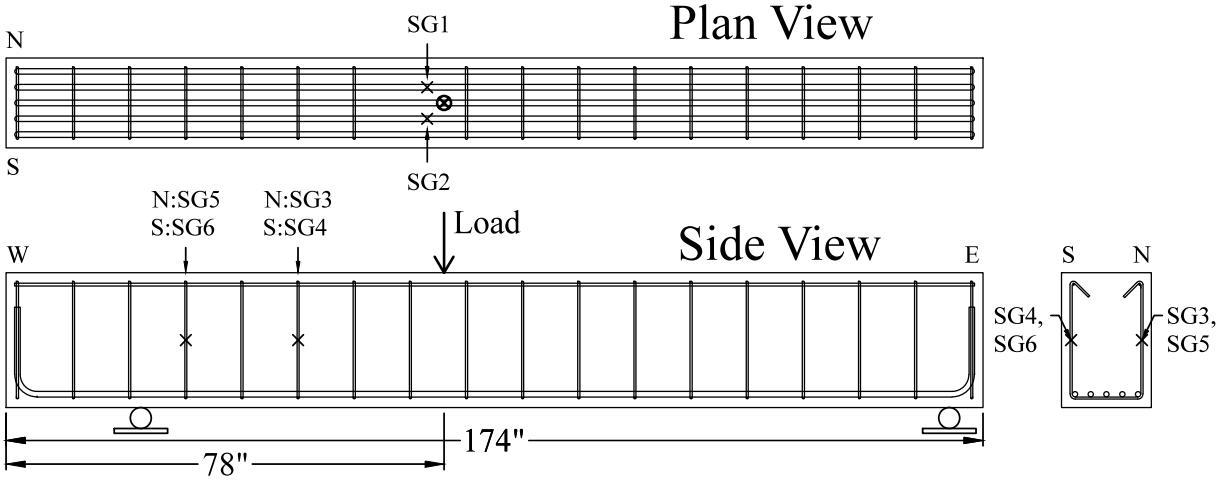

SG1	SG2	SG3	SG4	SG5	SG6
74	75	52	52	32	33

(a) Shear Specimen S1

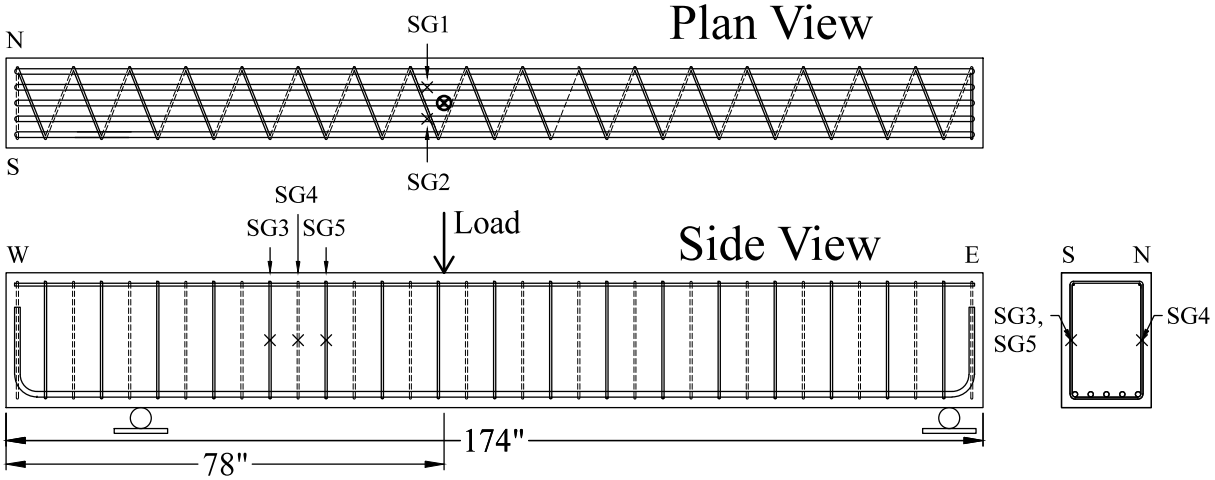

SG1	SG2	SG3	SG4
76	76	44	49

(b) Shear Specimen S2

Figure K.1: Location of strain gages in shear specimens

Note: All the distances are in inches, and are from the west end.

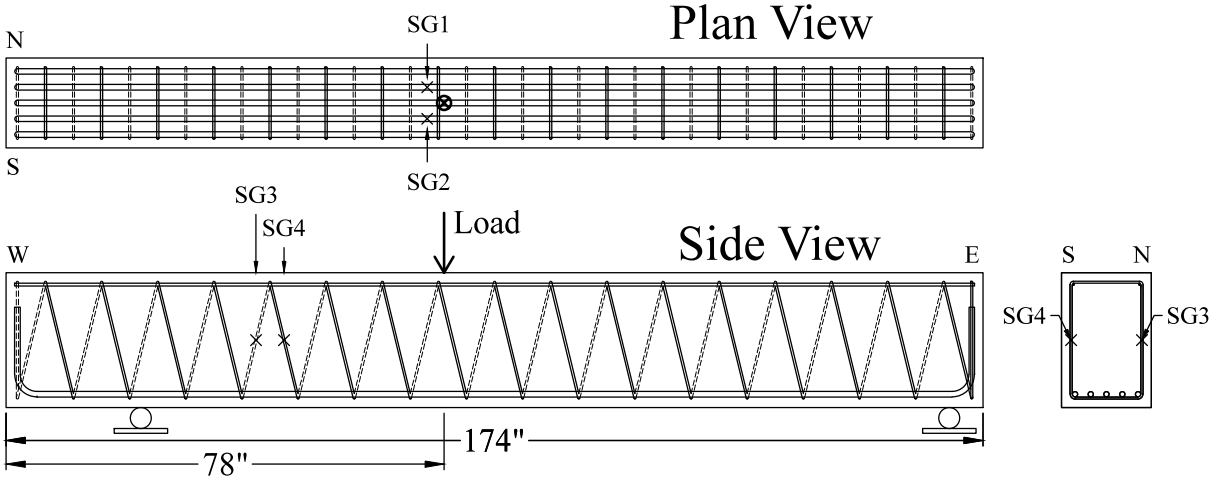

SG1	SG2	SG3	SG4
77	77	48	53

(c) Shear Specimen S3

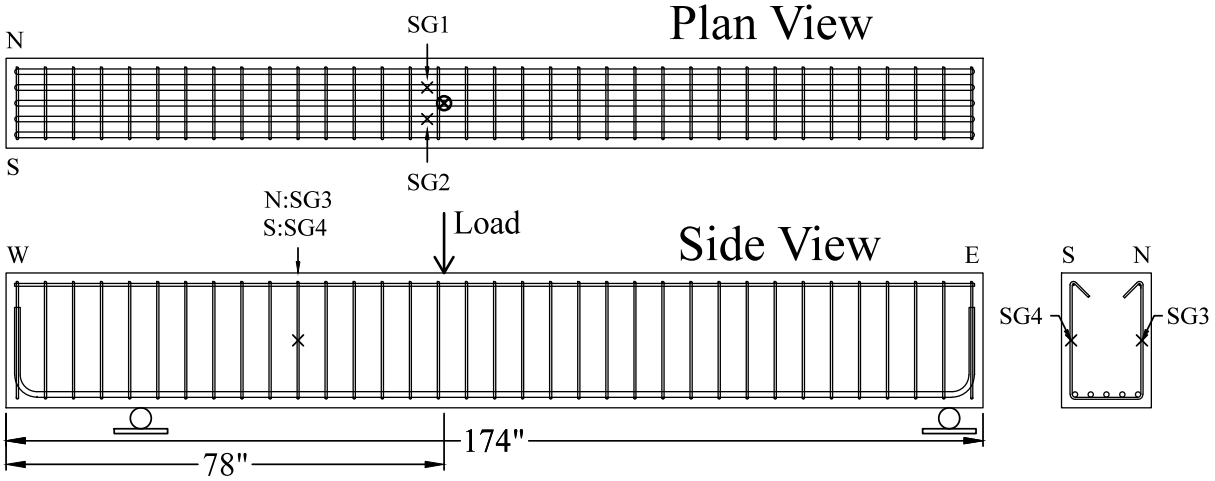

SG1	SG2	SG3	SG4
79	79	51	50

(d) Shear Specimen S4

Figure K.1: Location of strain gages in shear specimens (cont.)

Note: All the distances are in inches, and are from the west end.

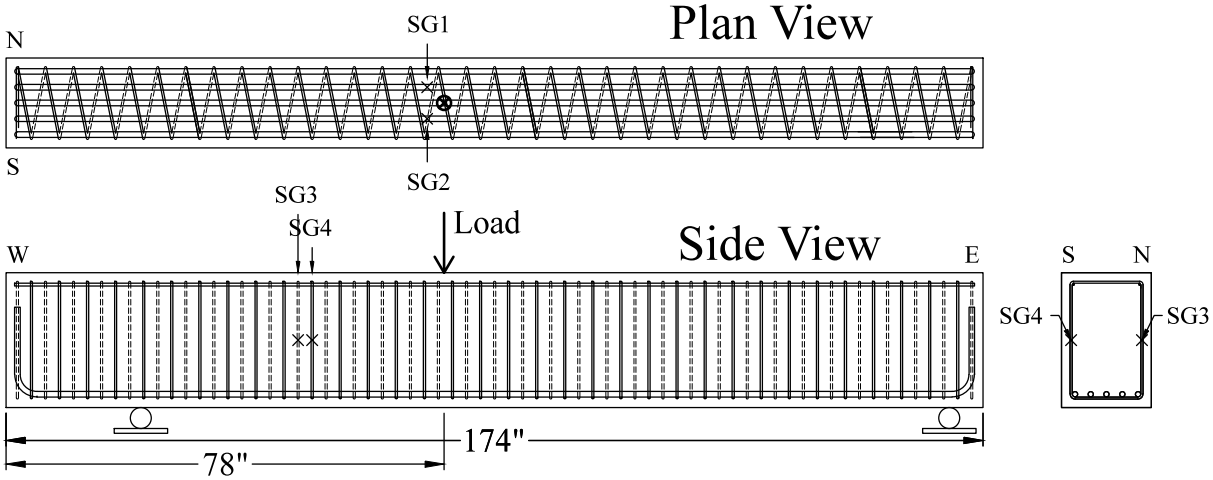

SG1	SG2	SG3	SG4
79	79	50	52

(e) Shear Specimen S5

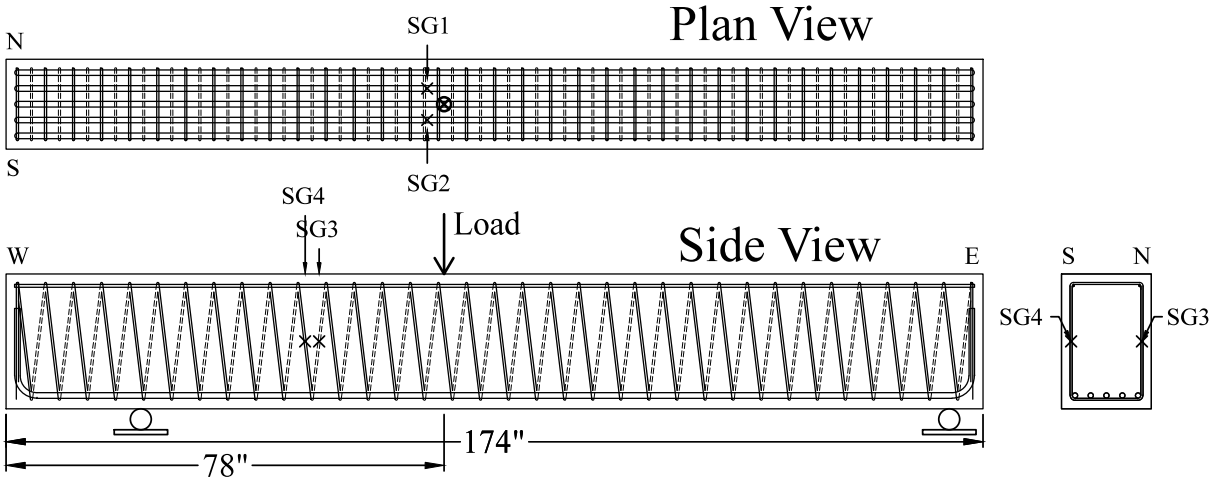

SG1	SG2	SG3	SG4
78	78	52	50

(f) Shear Specimen S6

Figure K.1: Location of strain gages in shear specimens (cont.)

Note: All the distances are in inches, and are from the west end.

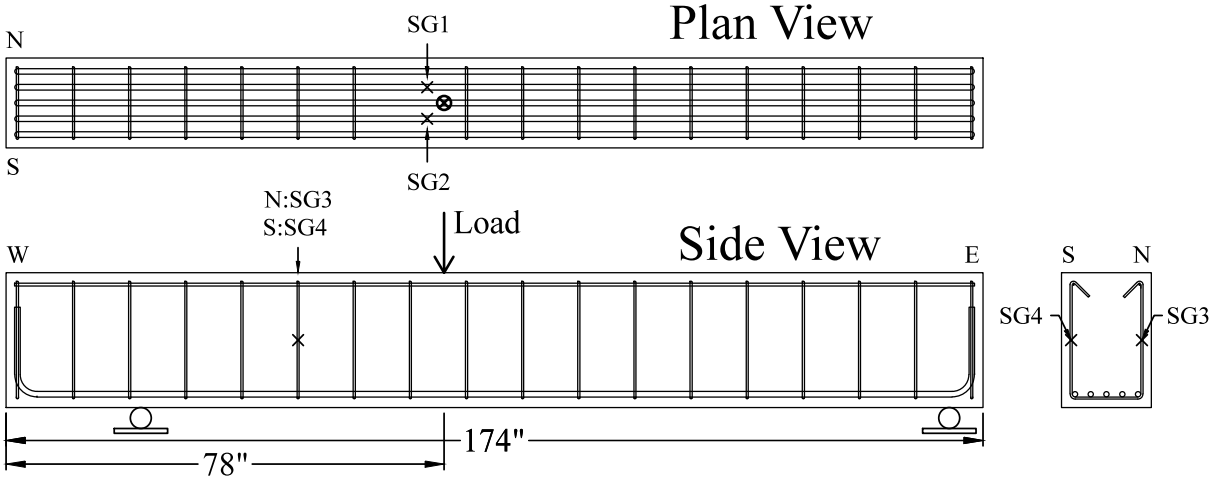

SG1	SG2	SG3	SG4
80	80	52	52

(g) Shear Specimen S7

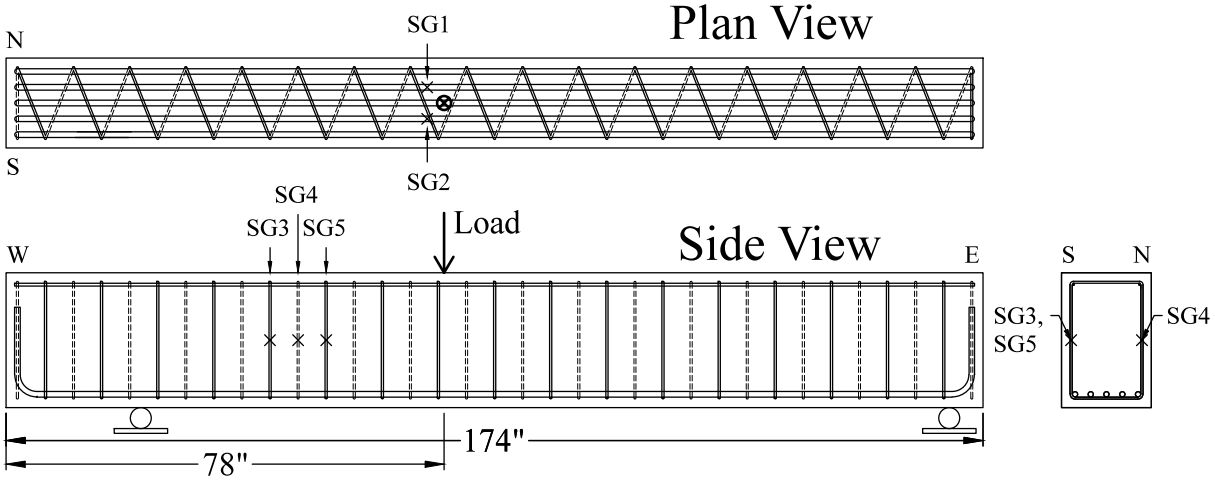

SG1	SG2	SG3	SG4	SG5
80	80	48	52	57

(h) Shear Specimen S8

Figure K.1: Location of strain gages in shear specimens (cont.)

Note: All the distances are in inches, and are from the west end.

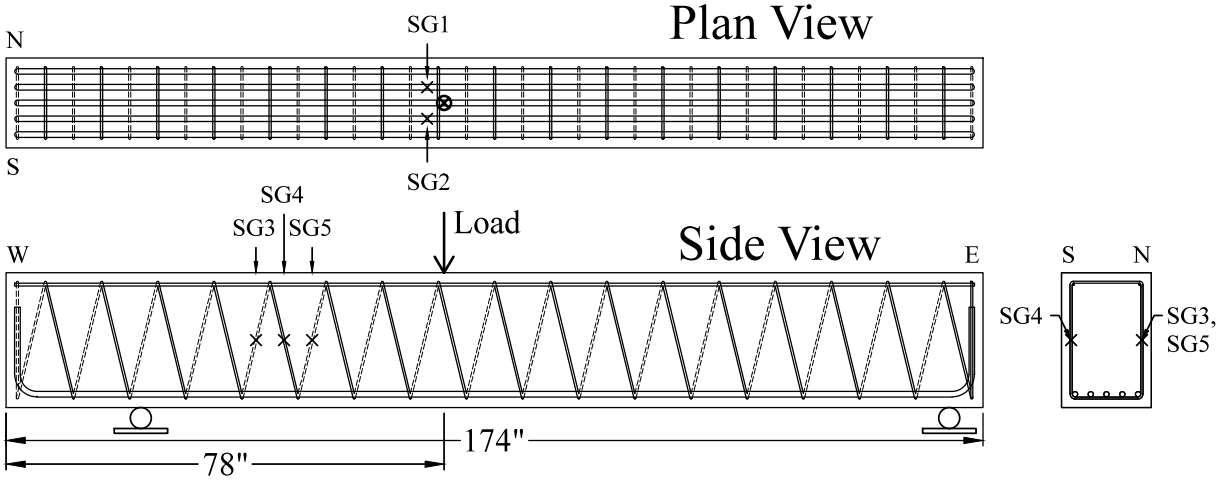

SG1	SG2	SG3	SG4	SG5
80	80	48	51	57

(i) Shear Specimen S9

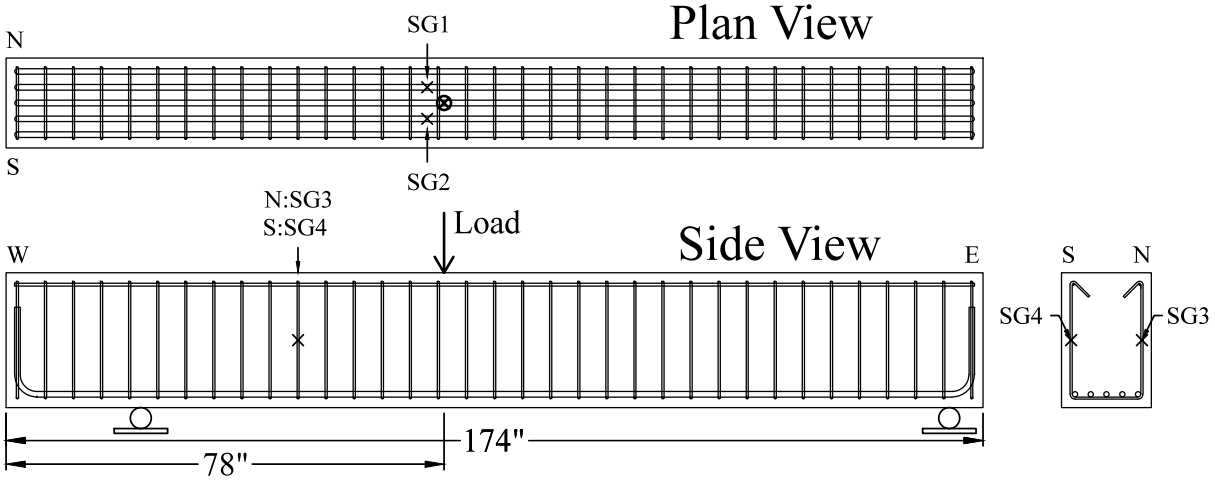

SG1	SG2	SG3	SG4
79	80	54	53

(j) Shear Specimen S10

Figure K.1: Location of strain gages in shear specimens (cont.)

Note: All the distances are in inches, and are from the west end.

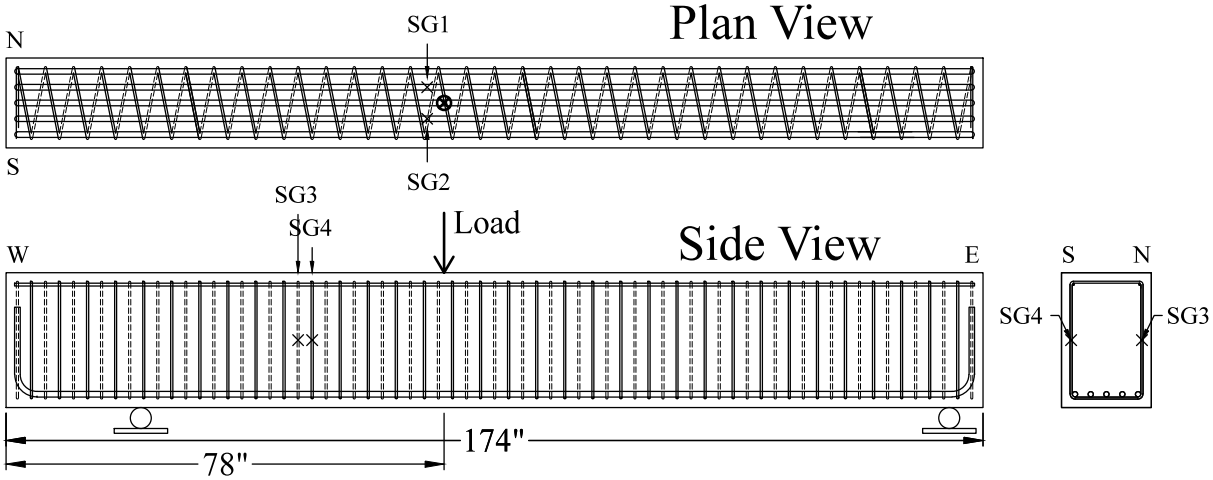

SG1	SG2	SG3	SG4
80	80	49	52

(k) Shear Specimen S11

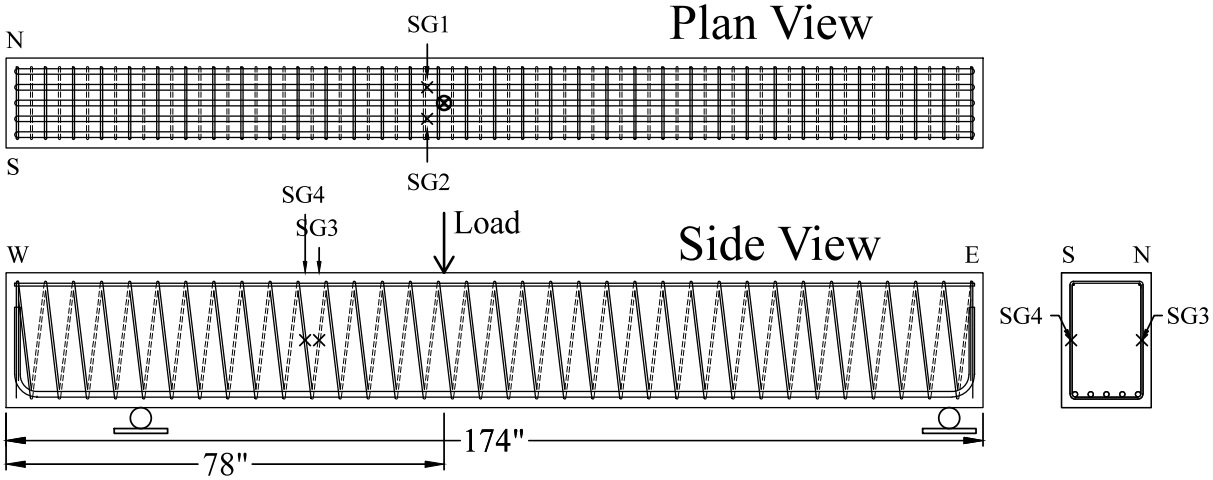

SG1	SG2	SG3	SG4
80	80	55	52

(l) Shear Specimen S12

Figure K.1: Location of strain gages in shear specimens (cont.)

Note: All the distances are in inches, and are from the west end.

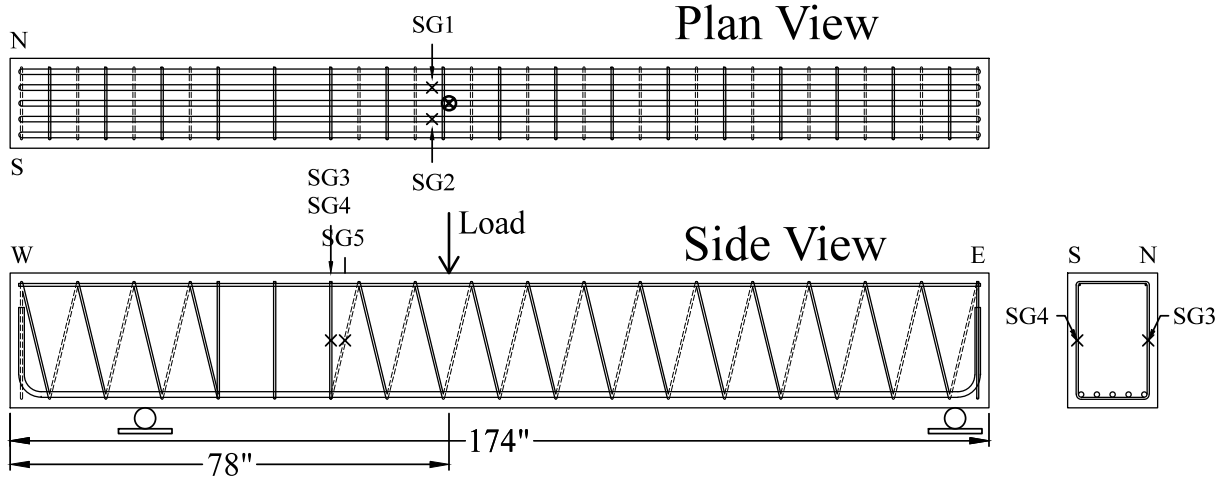

SG1	SG2	SG3	SG4	SG5
79	79	51	56	56

Figure K.2: Location of strain gages in spliced shear specimen

Note: All the distances are in inches, and are from the west end.

Specimen	Label							
	Longitudinal bars				Transverse reinforcement			
	W top	E top	W bottom	E bottom	Top	W	E	Bottom
T1	48	48.25	48.5	48.75	50.5	51	51.5	51.5
T2	50.25	49.25	50	49	50.5	49	51.25	48.25
T3a	48	48	46.75	46.75	46.25	49.25	47.25	48.25
T3b	48.5	48.5	46.25	46.5	46.5	49.5	47.5	48.5
T4	49	49	49	49	50.5	51	50	50.5
T5a	48.5	48	48.5	48	48.5	47.5	49	46.5
T5b	47	46.5	47	46.5	47	45.5	48	45

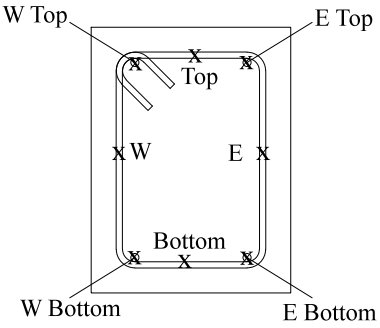

T1, T4

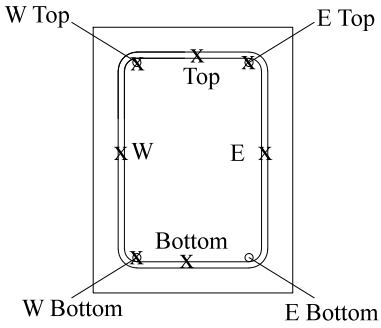

T2, T5a&b, T3a&b

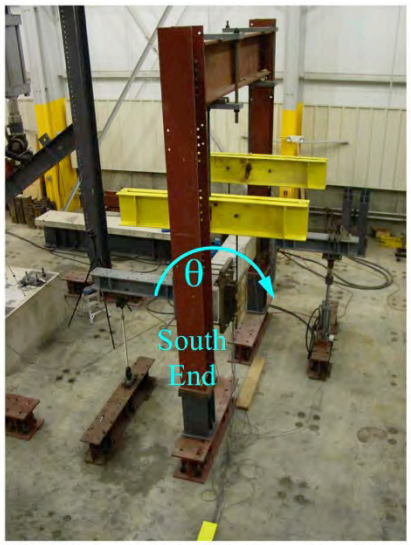

Specimens T1, T2, T3a, T4, T5a

Specimens T3b, T3b

Figure K.3: Location of strain gages in specimens subjected to pure torsion

Note: All the distances are in inches, and are from the south end.

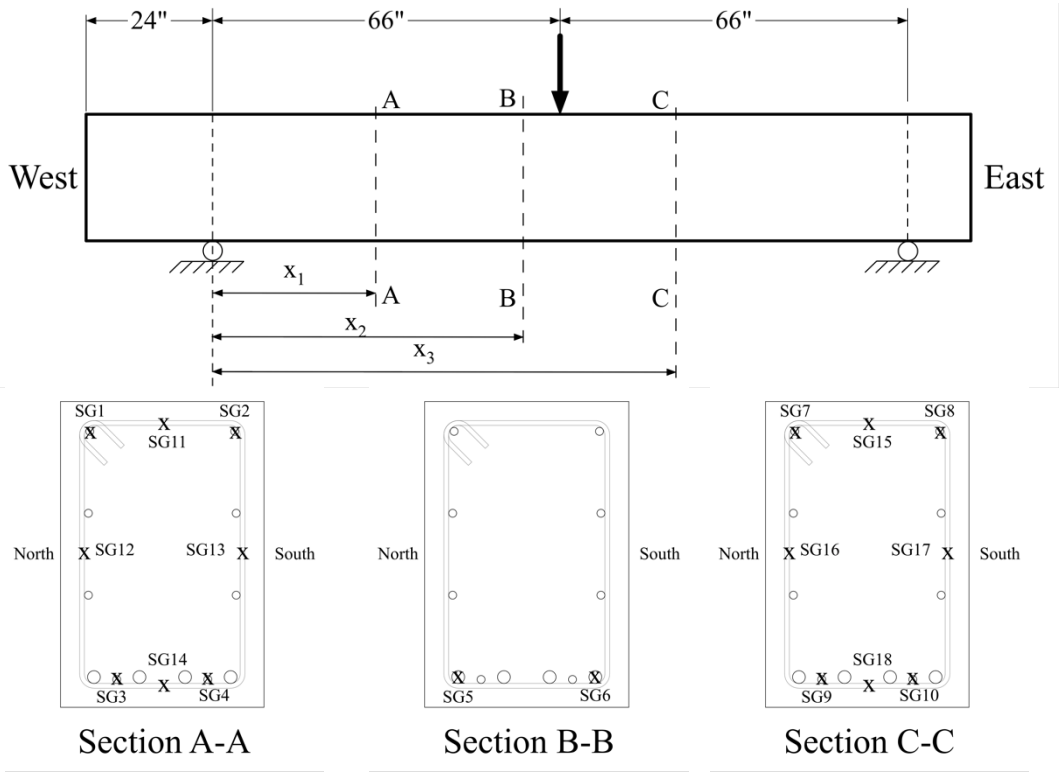

(a) TFS1

Label	x1 (in.)	x2 (in.)	x3 (in.)
SG1	31.0	---	---
SG2	31.5	---	---
SG3	31.0	---	---
SG4	31.0	---	---
SG5	---	58.5	---
SG6	---	59.0	---
SG7	---	---	89.0
SG8	---	---	88.5
SG9	---	---	88.0
SG10	---	---	88.0
SG11	27.5	---	---
SG12	27.5	---	---
SG13	27.5	---	---
SG14	27.5	---	---
SG15	---	---	91.0
SG16	---	---	91.0
SG17	---	---	91.0
SG18	---	---	91.0

Figure K.4: Location of strain gages in specimens subjected to bending moment, shear, and torque – Specimen TFS1

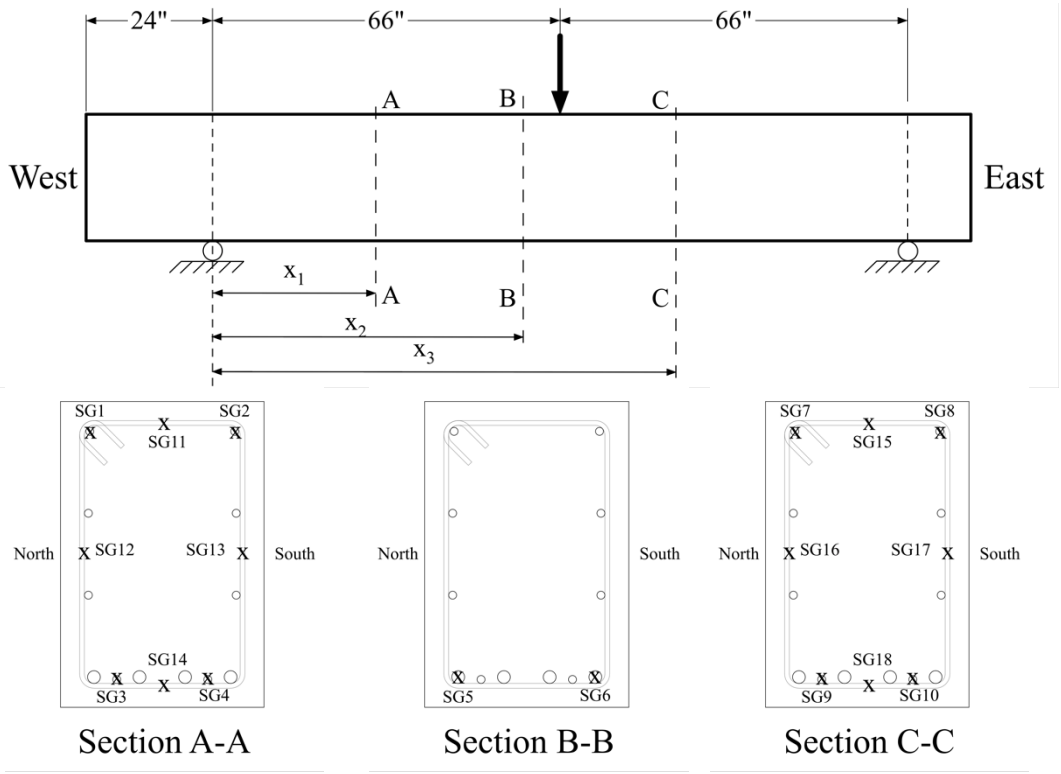

(b) TFS2a

Label	x1 (in.)	x2 (in.)	x3 (in.)
SG1	32.5	---	---
SG2	31.5	---	---
SG3	31.5	---	---
SG4	31.0	---	---
SG5	---	60.5	---
SG6	---	59.5	---
SG7	---	---	89.0
SG8	---	---	90.0
SG9	---	---	89.0
SG10	---	---	88.5
SG11	31.0	---	---
SG12	29.0	---	---
SG13	25.0	---	---
SG14	26.5	---	---
SG15	---	---	94.0
SG16	---	---	92.5
SG17	---	---	97.0
SG18	---	---	90.5

Figure K.4: Location of strain gages in specimens subjected to bending moment, shear, and torque (cont.)

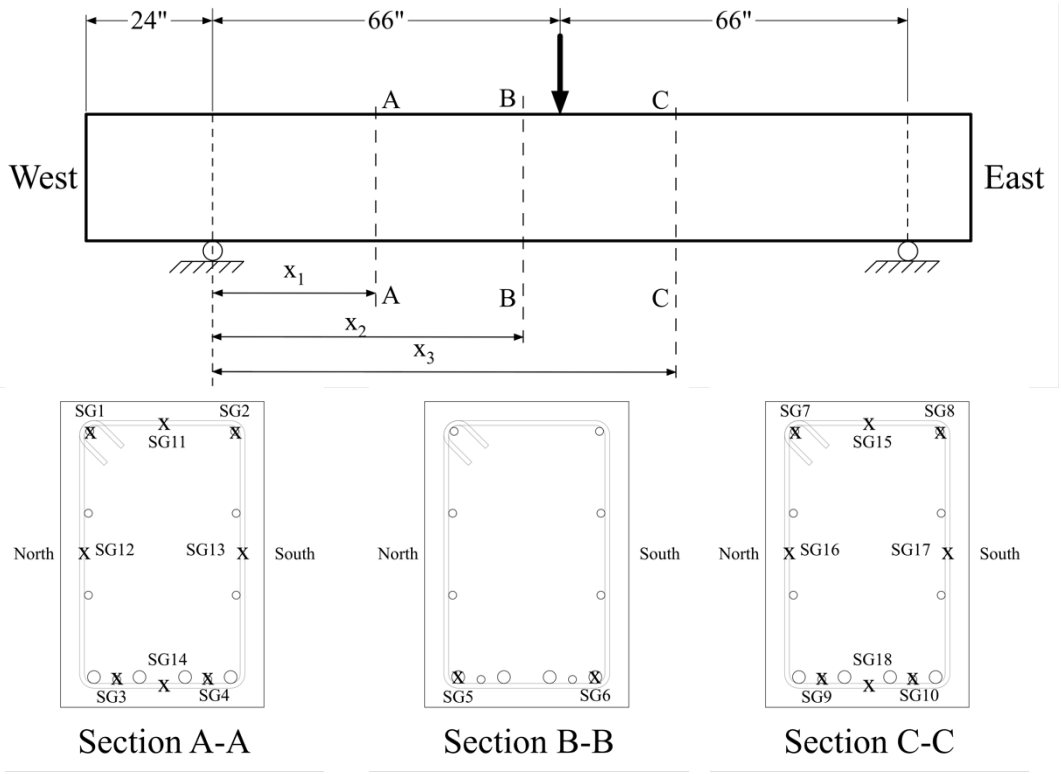

(c) TFS3

Label	x1 (in.)	x2 (in.)	x3 (in.)
SG1	31.0	---	---
SG2	31.0	---	---
SG3	32.0	---	---
SG4	32.0	---	---
SG5	---	59.5	---
SG6	---	60.0	---
SG7	---	---	89.0
SG8	---	---	88.5
SG9	---	---	89.0
SG10	---	---	89.0
SG11	27.0	---	---
SG12	25.5	---	---
SG13	29.0	---	---
SG14	30.5	---	---
SG15	---	---	94.5
SG16	---	---	93.5
SG17	---	---	89.5
SG18	---	---	91.0

Figure K.4: Location of strain gages in specimens subjected to bending moment, shear, and torque (cont.)

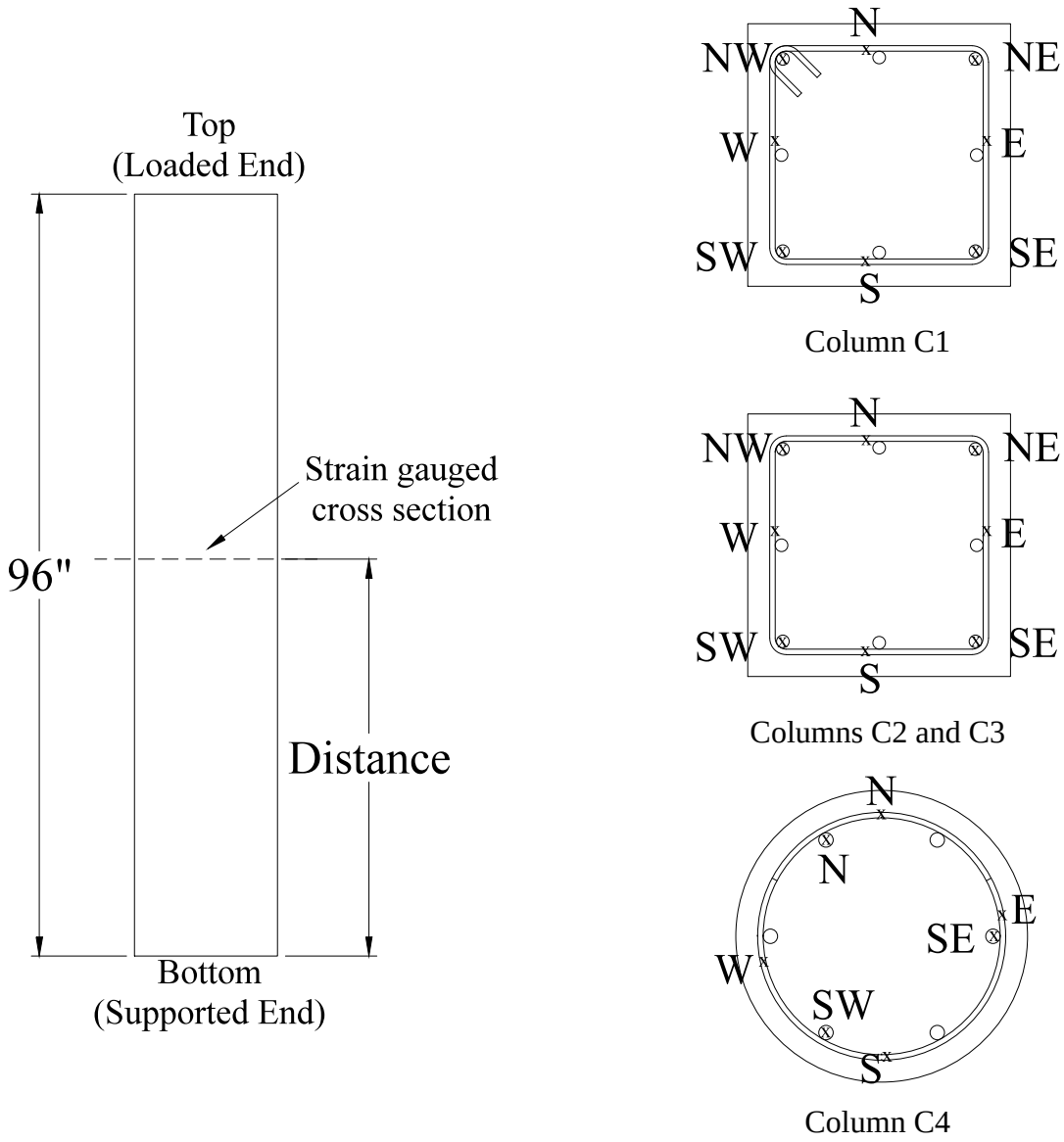

Specimen	Label								
	Longitudinal bars					Transverse reinforcement			
	N	NE	NW	SE	SW	N	E	S	W
C1	---	47.5	47.5	47.5	47.5	44	44	43.5	43.5
C2	---	48	48	47	48	51.5	49	47	44.5
C3	---	48	48	49	49	46.5	48.5	48	47
C4	48.25	---	---	46.75	48.25	47.25	48	47.25	49.5

Figure K.5: Location of strain gages in stub columns

Note: All the distances are in inches, and are from the bottom.

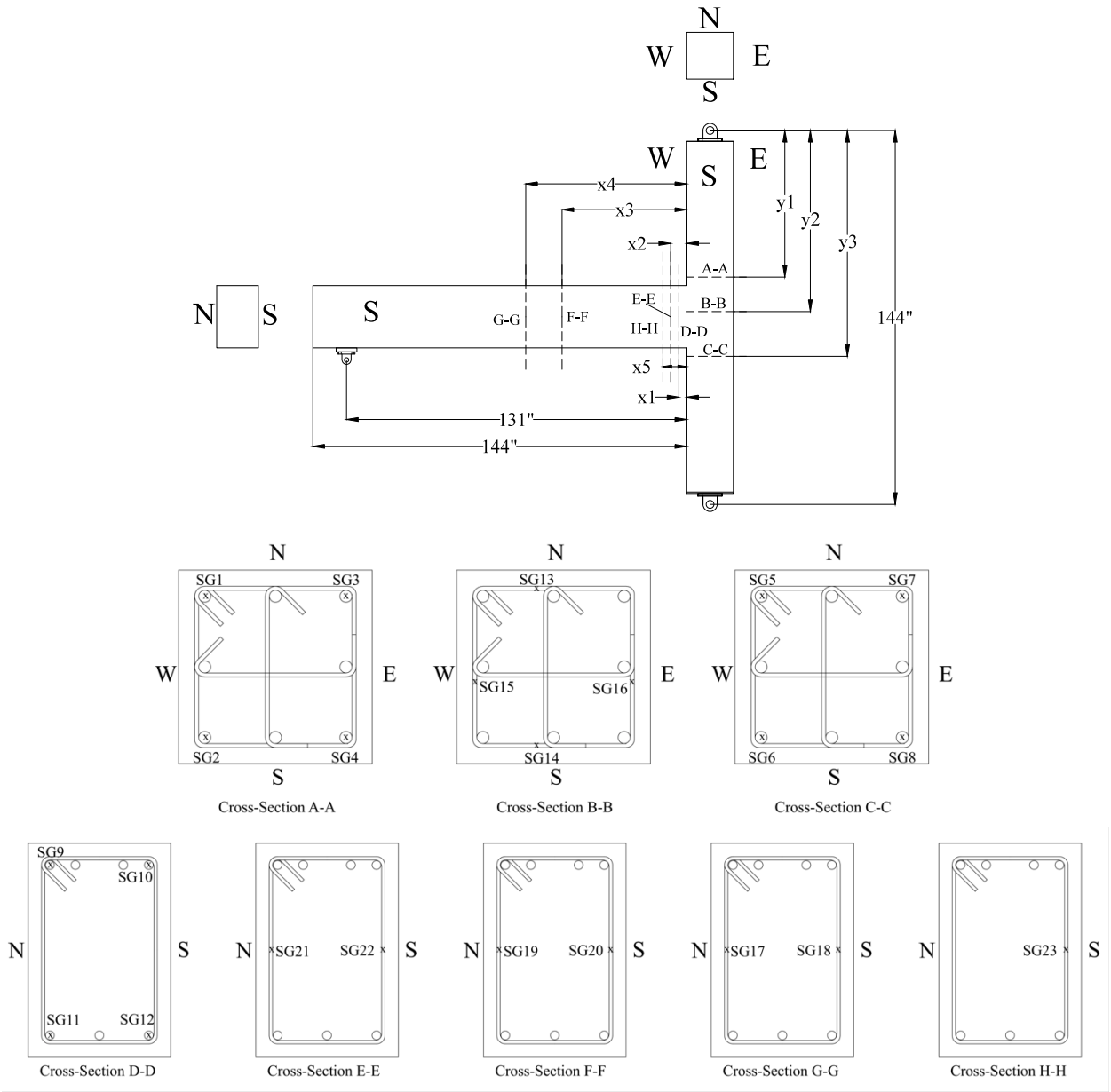

Section	Label	Dimension	BC1	BC2
A-A	SG1	y1	58	57 1/4
	SG2		57 3/4	58 3/4
	SG3		57 1/4	57 1/2
	SG4		57 3/4	58 3/4
B-B	SG13	y2	70 3/4	72 1/4
	SG14		70 3/8	72 1/4
	SG15		71	72 1/2
	SG16		70 3/8	72 1/4
C-C	SG5	y3	86 3/4	85 1/2
	SG6		86 1/4	86
	SG7		86	85 1/2
	SG8		86	85 3/4

Section	Label	Dimension	BC1	BC2
D-D	SG9	x1	2 1/4	4 1/2
	SG10		3 1/4	4 1/2
	SG11		2 1/2	3 3/4
	SG12		3 1/4	3 3/4
E-E	SG21	x2	5 3/4	7 1/2
	SG22		6 1/2	5 1/2
F-F	SG19	x3	45 3/4	47 1/4
	SG20		46 1/4	48 1/4
G-G	SG17	x4	60	60 1/8
	SG18		60	60 1/8
H-H	SG23	x5	----	9 1/4

Figure K.6: Location of strain gages in beam-column connections
Note: All the distances are in inches.

Appendix L

Flexure-Shear-Interaction Equations

Measured yield strength of bottom reinforcement: f'_y = 112 ksi

Measured yield strength of top reinforcement: f'_y = 72 ksi

Average measured concrete compression strength; f'_c = 6607 psi

Weighted average yield strength of bottom longitudinal reinforcement

$$f_y = \frac{4 \times 0.79\ in.^2 \times 112\ ksi + 2 \times 0.31\ in.^2 \times 72\ ksi}{4 \times 0.79\ in.^2 + 2 \times 0.31\ in.^2} = 105.4\ ksi$$

Measured yield strength of top reinforcement: f'_y = 72 ksi

Bottom longitudinal reinforcement: 4 No. 8, A_s = 4x0.79 in.^{2} = 3.16 in.^{2}

Top longitudinal reinforcement: 2 No. 5, A'_s = 2x0.31 in.^{2} = 0.62 in.^{2}

$$r = \frac{A'_s f'_y}{A_s f_y} = \frac{0.62 \times 72}{3.16 \times 105.4} = 0.112$$

Average measured b_w for all specimens = 16.17 in.

Average measured h for all specimens = 24.78 in.

Due to construction error, the covers to the bottom and top stirrups were 1.125" and 1.875", respectively, instead of 1.5".

d = 22.78 in.

d_v= 20.59 in.

$C = T$

$$0.85 f'_c a b_w = A_s f_y; \quad a = \frac{3.16 \times 112}{0.85 \times 6.607 \times 16.17} = 3.897\ in.$$

$$\phi Mn = A_s f_y \left(d - a/2\right) = 1 \times 3.16 \times 112 \left(22.78 - 3.897/2\right) = 7373\ k-in.$$

$$x_o = 16.17 - 2 \times (1.5 + 0.5 \times 3/8) = 12.79\ in.$$

$$y_o = 24.78 - (1.875 + 0.5 \times 3/8) - (1.125 + 0.5 \times 3/8) = 21.41\ in.$$

$$A_o = 0.85 A_{oh} = 0.85 \left(x_o \times y_o\right) = 232.75\ in.^2$$

Mode 1:

$$\left(\frac{M_u}{\phi M_n}\right) + r\left(\frac{V_u}{\phi V_n}\right)^2 + r\left(\frac{T_u}{\phi T_n}\right)^2 = 1$$

$$where \quad r = \frac{A'_s f'_y}{A_s f_y}$$

Mode 2:

$$-\frac{1}{r}\left(\frac{M_u}{\phi M_n}\right) + \left(\frac{V_u}{\phi V_n}\right)^2 + \left(\frac{T_u}{\phi T_n}\right)^2 = 1$$

Mode 3:

$$\left(\frac{V_u}{\phi V_n}\right)^2 + \left(\frac{T_u}{\phi T_n}\right)^2 + 2\left(\frac{V_u \times T_u}{\phi V_n \times \phi T_n}\right)\sqrt{\frac{2d_v}{P_{cp}}} = \frac{1+r}{2}$$

Specimen TFS1 (Conventional transverse reinforcement)

$$T_n = \frac{2A_o A_t f_{yt} \cot\theta}{s}$$

$$T_n = \frac{2 \times 232.75\,in.^2 \times 0.11\,in. \times 71\,ksi \times 1}{8\,in.} = 454\ k-in.$$

$$\phi T_n = 454\ k-in.$$

$$V_n = V_c + V_s$$

$$V_n = 2\sqrt{f_c'}\, b_w d + \frac{A_v f_{yt} d}{s}$$

$$V_n = 2\sqrt{6607} \times 16.17 \times 22.78 + \frac{0.22 \times 71000 \times 22.78}{8} = 104360\ lbs.$$

$$\phi V_n = 104360\ lbs. = 104\ kips$$

Case	M_u (k-in.)	V_u (kips)	T_u (k-in.)	Mode 1		Mode 2		Mode 3	
				Value	Limit	Value	Limit	Value	Limit
Max. M & V	5474	90.2	397	0.91	1	-5.12	1	2.58	4.96
Max. T	4566	74.2	464	0.78	1	-3.98	1	2.58	4.96

Specimen TFS2 (Continuous transverse reinforcement with angles on top & bottom)

$$T_n = \frac{2A_o A_t f_{yt} \cot\theta}{s}$$

$$T_n = \frac{2 \times 232.75\,in.^2 \times 0.11\,in. \times 71\,ksi \times 1}{8\,in.} = 454\ k-in.$$

$$\phi T_n = 454\ k-in.$$

$$V_n = V_c + V_s$$

$$V_n = 2\sqrt{f_c'}\, b_w d + \frac{A_v f_{yt} d}{s}$$

$$V_n = 2\sqrt{6607} \times 16.17 \times 22.78 + \frac{0.22 \times 71000 \times 22.78}{8} = 104360\ lbs.$$

$$\phi V_n = 104360\ lbs. = 104\ kips$$

Case	M_u (k-in.)	V_u (kips)	T_u (k-in.)	Mode 1		Mode 2		Mode 3	
				Value	Limit	Value	Limit	Value	Limit
Max. M & V	5462	90.0	390	0.91	1	-5.13	1	2.53	4.96
Max. T	4740	77.5	417	0.80	1	-4.34	1	2.36	4.96

Specimen TFS3 (Continuous transverse reinforcement with angles on the sides)

From Section 4.3.1

$$T_n = \frac{A_t f_y \left(1+\sin\alpha\right) A_o \cot\theta}{s} = \frac{0.11\times 71\times\left(1+\sin 71\right)\times 232.75\times\cot 45}{8} = 442\ k-in.$$

$$\phi T_n = 442\ k-in.$$

From Section 4.1.1 $V_s = \frac{2A_v f_{yt} d \sin\alpha}{s}$

$$V_s = \frac{2\times 0.11\times 71\times 22.78\times \sin 71}{8}$$

$$V_s = 42.1\ kips$$

$$V_c = 2\sqrt{f_c'}\, b_w d = 2\sqrt{6607}\times 16.17\times 22.78 = 59882\ lbs. = 59.9\ kips$$

$$\phi V_n = 59.9 + 42.1 = 102\ kips$$

Case	M_u (k-in.)	V_u (kips)	T_u (k-in.)	Mode 1		Mode 2		Mode 3	
				Value	Limit	Value	Limit	Value	Limit
Max. M, V, & T	5876	96.7	435	1.01	1	-5.25	1	3.22	4.96

Appendix M

Manipulation of Strain Gage Data for Specimens Subjected to Bending Moment, Shear, and Torsion

As shown in Figure K.4 in Appendix K, 18 strain gages had been bonded to the longitudinal and transverse reinforcing bars. Eight No. 5 longitudinal bars were provided to resist the longitudinal force due to torsion; however, these bars were also subjected to bending moment. The bending component in the bottom two No. 5 longitudinal bars was taken out according to Eq. M.1. The strain data from the top two No. 5 longitudinal bars were ignored because these bars were in compression generated by bending moment. In retrospect, strain gages should have been bonded to the middle four No. 5 longitudinal bars. The vertical legs of transverse reinforcement resist the combined effects of shear and torsion. To separate out the strain due to shear and torsion, the formulation shown in Eq. M.2 was followed. Note that strain in the horizontal legs of the transverse reinforcement is predominately due to torsion.

Average longitudinal strain due to torsion in No. 5 bars at section A-A

$$\left(\frac{SG3+SG4}{2}\right)-\left(\frac{x_1}{x_2}\right)\left(\frac{SG5+SG6}{2}\right)$$

Average longitudinal strain due to torsion in No. 5 bars at section C-C

$$\left(\frac{SG9+SG10}{2}\right)-\left(\frac{L-x_3}{x_2}\right)\left(\frac{SG5+SG6}{2}\right)$$ Eq. M.1

SG3, *SG4*, *SG5*, *SG6*, *SG9*, and *SG10* are the strain readings at the location of these strain gages. Dimensions x_1, x_2, x_3, and L are shown in Figure 4.22.

Average strain due to shear in transverse reinforcement at section A-A

$$\left(\frac{SG12+SG13}{2}\right)$$

Average strain due to shear in transverse reinforcement at section C-C

$$\left(\frac{SG16+SG17}{2}\right)$$

Average strain due to torsion in the vertical leg of transverse reinforcement at section A-A Eq. M.2

$$\left(\frac{SG13-SG12}{2}\right)$$

Average strain due to shear in transverse reinforcement at section C-C

$$\left(\frac{SG17-SG16}{2}\right)$$

SG12, *SG13*, *SG16*, and *SG17* are the strain readings at the location of these strain gages.

Appendix N

Calculation of Joint Shear Angle

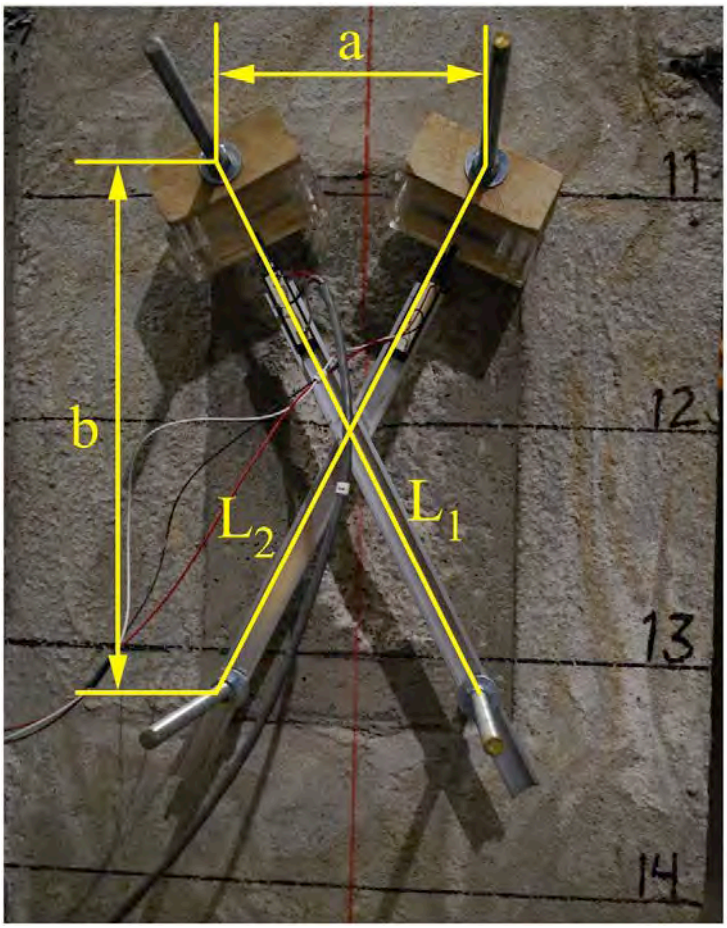

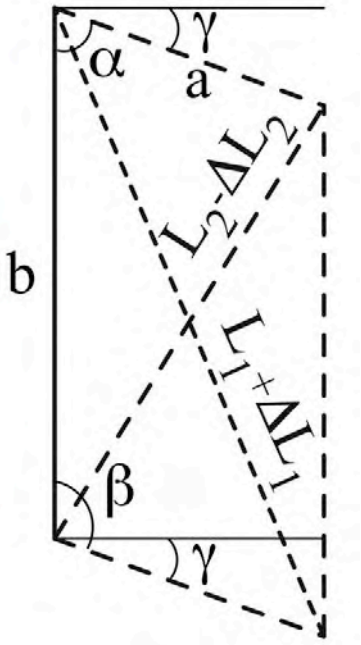

Apply the law of cosines.

$$\left(L_1+\Delta L_1\right)^2 = a^2+b^2-2ab\cos\beta$$

$$\cos\beta = \frac{\left(\Delta L_1\right)^2+2L_1\Delta L_1}{-2ab};\quad \beta = a\cos\left[\frac{\left(\Delta L_1\right)^2+2L_1\Delta L_1}{-2ab}\right]$$

$$\left(L_2-\Delta L_2\right)^2 = a^2+b^2-2ab\cos\alpha$$

$$\cos\alpha = \frac{\left(\Delta L_2\right)^2+2L_2\Delta L_2}{-2ab};\quad \alpha = a\cos\left[\frac{\left(\Delta L_2\right)^2+2L_2\Delta L_2}{-2ab}\right]$$

$$\textit{Average shear angle} = \frac{\beta-\alpha}{2}$$